Identifying proteins that preferentially bind ATP- over ADP-F-actin

Sophie Claydon

BSc (Hons)

Thesis submitted in fulfilment of the requirements for the Degree of Doctor of Philosophy

February 2024

Cancer Research UK – Scotland Institute

University of Glasgow

Abstract

The cytoskeleton is a dynamic network of proteins that grants cells internal organisation, structure and mobility. This gives cells the ability to participate in all manner of physiological processes, such as immune response, growth and development. However, the same genes and proteins that control these processes can also be altered and participate in pathological events such as cancer and metastasis. The actin cytoskeleton is responsible for the formation of cellular protrusions that allow cells to migrate. The process that gives rise to these protrusions is the polymerisation of actin into its filamentous form, F-actin. This is a highly dynamic process that involves regulation by many other proteins and some degree of self-regulation. Actin monomers incorporated into the polarised filament are ATP bound. Upon polymerisation, actin intrinsic hydrolytic activity gives rise to differing states of nucleotide bound conformations throughout the actin filament. Certain proteins are known to bind the aged, ADP-bound portion of F-actin, and contribute to negative regulation for example by promoting depolymerisation. Similarly, we hypothesise that some proteins would preferentially bind the ATP-bound portion of F-actin and be involved in positive regulation of polymerisation.

To investigate this, we optimised a methodology for creating F-actin filaments that mimic the ATP-bound portion using non-hydrolysable analogues of ATP, and constructed affinity chromatography columns that were used to isolate specific interactors. Subsequent mass spectrometry revealed a pool of proteins that preferentially bind ATP-bound over ADP-bound F-actin. One of the identified hits, Eps8, was employed to explore the mechanism of ATP-F-actin binding. Combining molecular biology cloning techniques and super resolution microscopy, we identified Eps8's SH3 domain as the main regulator of this interaction. Many of the proteins identified as preferentially binding ATP-F-actin contain SH3 domains, suggesting a more generalised role of this domain in the binding to ATP-actin, either directly or indirectly. SH3 domains are known to interact with proline rich sequences. Recent work from our lab has shown the importance of the polyproline domains of members of the WAVE regulatory complex on the formation of actin protrusions. Based on these combined data, we hypothesise that the SH3/polyproline domain interaction could constitute an axis for the recruitment of different proteins involved in actin polymerisation to

the site of ATP-F-actin, generating a positive feedback loop of polymerisation. More work, for example using purified proteins and binding assays, is needed to determine the exact method of ATP-F-actin binding, the role it has in positive regulation of polymerisation and its biological relevance.

Table of Contents

List of Tables

List of Figures

Acknowledgement

I would like to thank Robert for giving me the opportunity to undertake my PhD in the Insall lab. It's been a crazy journey, but I have gained so much confidence as a scientist. I used to be afraid of experiments without a tried and tested protocol, but now composing, optimising, and validating a protocol is part of the fun! I would also like to thank Laura, for chats about my mass spec data and valuable insights and feedback during my lab meetings. To all the members of R2 and R6 over my years here too, thank you for all the scientific discussions and fun! Honourable mentions as follows, in alphabetic order of course…

Amelie, How to make the perfect fresh bread, a qualitative study to test on PhD students, *The Journal of Excellent Scientific Guidance*

Amelie! Thank you for being a great friend and an amazing source of knowledge and advice. I always really valued your opinion of my project and could ask for advice on any idea or protocol. I will always remember those sandwiches in Prague! Thank you for recreating the perfect bread each year for my birthday!

Clelia, High maintenance PhD students and how to handle them, *The Journal of RUBBISH!!*

Clelia, my first R6 friend! I've always admired and looked up to you. For your scientific integrity and for your kind soul – you were such a good friend and comfort to me at the start of my PhD journey. The healthy cubicle was never the same after you left!

James, What to do when you are a post doc and still can't prepare DNA gels, *The Journal of Good Music Taste*

Even though you arrived later in my PhD you were still one of the best people I met here! You were a lot of fun and I love chatting about music and games with you. Also, if I did something stupid in the lab, you had usually done something more stupid so I felt better.

Jammie, Three drops and how they can solve all your problems, *The Great Whisky Journal*

Jammie!!!! I had so much fun with you, and you also taught me a lot. You pretended you never wanted to help but you are very kind and did it anyway. I learned a lot with you and laughed a lot, especially away at conferences or by pranking you.

Nikki, Behind the line man; a lesson in darts and life, *The Royal Journal*

Your majesty, what can I say! Thank you so much for everything. You have helped me so much, not just with the PhD but with life. You are an amazing scientist, a fountain of knowledge and most importantly an incredible and kind person. We have had so much fun over the years and still do, I've gained a best friend for life. Now lets go bird watching and you can tell me to stay behind the line in the bird hide too.

Peggy, How many sweets can a PhD student eat; a quantitative study, *The Journal of Flowers in Hair*

I don't think I was spoiled by anyone more than you Peggy! You are the best at giving gifts and treats and always knowing how to make me smile. I loved sitting next to you even though I was probably annoying you with my heater. Thank you for always providing me with advice and being patient with me and my silly questions about cloning. You are an amazing friend and I request that you leave the lab at a normal hour to come and celebrate with me!

Pete, How to know everything about molecular cloning in the world that has ever existed ever, *The Journal of Good Teaching*

Pete, I would not have survived cloning without you! I think you are an incredible teacher and you taught me so many skills that will stay with me throughout my scientific career. Always willing to listen and give advice, and not just about science as you were encouraging me to keep up with the running too! I have to say I haven't ran for a while as I sit at my desk and write this thesis, so I'd better get back to it. I hope to see you at the pub after I have submitted, for a quiz that you and Nikki will know all the answers to, and I will be of zero help unless the questions are about dogs or Taylor Swift.

Savvas, Are you working? The Age-Old Question and Potential Answers, *The Journal of Hollister and Superdry*

Savvas my crazy PhD pal together from Day 1! You are a great friend and I hope to visit you in Cyprus soon, maybe I can be the Royal escort next time. I had so much fun with you, at conferences, at parties with the doctor, playing games, talking about Barbie and Pegasus, and also just every day in the lab. We were a great pranking team. Simona probably still hasn't recovered, if she comes to Cyprus with me and the Queen we can continue where we left off with some new pranks.

Simona, Reasons why pineapple should not be allowed on pizza, *The Journal of Very Loud Ladies*

Doctor S… Where to start! With the science first, you are incredible. You are so dedicated and clever, and you have been an amazing teacher to me. You always encourage me to do more and make me believe I can. I hope many people can experience your teaching because you are very inspiring and empowering. You are also a hilarious, LOUD and amazing person – and an even better friend. You have supported me, more than you probably know, and I've never felt I don't have someone to turn to when you are around. Thank you for always supporting me and for being one of my best friends in the whole world.

Finally, my family and friends. To my mum, the best person in my world, my endless support and love, thank you for everything you have done for and given me to allow me to be where I am today. To my dad, you gave me the confidence to be who I am and I've never known unconditional love like it. Heidi, Suzie and Toby who made my childhood so much sweeter, and Marley, Biscuit and Clover who have taken over the job now. Thank you to Jules, whose love and support got me through this thesis! I promise to make up all the late nights and weekends at my computer to you! And thanks to my best friends, the Boys and Ailidh, Tony and Smallie – who I can rely on always.

Author's Declaration

I, Sophie Claydon hereby declare that all the work in this thesis was performed personally, with the following exceptions mentioned below. No part of this thesis has been submitted for other degree or award at this or another university.

Sophie Claydon

Chapter 4

Dr David Sumpton performed the LC-MS analysis, generation of graphs showing the XIC data of each sample (Chapter 4 - Creating stable ATP-F-actin) (Metabolomics – Institute Central Services) and provided the protocol for this (2.2.4.7).

Chapter 5

Sergio Lilla performed the mass spectrometry and analysis of our affinity column eluate (Proteomics – Institute Central Services) and provided the protocol for this (2.2.5.2 and 2.2.5.3). Kelly Hodge generated the volcano plots in Figure 5-3, Figure 5-6, Figure 5-9 and Figure 5-12.

Chapter 8

Experiments and data analysis in Figure 8-2, Figure 8-3 and Figure 8-4 were performed in our lab by Dr Simona Buracco. I assisted with some experiments from this study.

Publications

Burgess S, Paul N, Richards M, Ault J, Askenatzis L, **Claydon S**, Corbyn R, Machesky L, Bayliss R (2024) A Nanobody inhibitor of Fascin-1 actin-bundling activity and filopodia formation. (accepted Open Biology, in revision)

Buracco S, Singh S**, Claydon S**, Paschke P, Tweedy L, Whitelaw J, McGarry L, Thomason P, Insall R (2022) The Scar/WAVE complex drives normal actin protrusions without the Arp2/3 complex, but proline-rich domains are required. bioRxiv 2022.05.14.491902; doi: https://doi.org/10.1101/2022.05.14.491902

Buracco S, **Claydon S**, Insall R (2019) Control of actin dynamics during cell motility. F1000Res. 2019 Nov 25;8:F1000 Faculty Rev-1977. doi: 10.12688/f1000research.18669.1. PMID: 31824651; PMCID: PMC6880267.

Francis S, Croft D, Schüttelkopf AW, Parry C, Pugliese A, Cameron K, **Claydon S**, Drysdale M, Gardner C, Gohlke A, Goodwin G, Gray CH, Konczal J, McDonald L, Mezna M, Pannifer A, Paul NR, Machesky L, McKinnon H, Bower J (2019) Structure-based design, synthesis and biological evaluation of a novel series of isoquinolone and pyrazolo[4,3-c]pyridine inhibitors of fascin 1 as potential anti-metastatic agents. Bio org Med Chem Lett. 2019 Apr 15;29(8):1023-1029. doi: 10.1016/j.bmcl.2019.01.035.

Abbreviations

°C: Celsius degrees

A ----------

Abi: ABL interactor
ABD: Actin binding domain
ABL1: Tyrosine-protein kinase ABL1
ABL2: Tyrosine-protein kinase ABL2
ADF: Actin depolymerising factor
ARP: Actin related protein
ARHGAP17: Rho GTPase-activating protein 17
ARHGEF1: Rho guanine nucleotide exchange factor 1
ARHGEF7: Rho guanine nucleotide exchange factor 7
ArpC: Actin-related protein complex
AMP: Adenosine monophosphate
ADP: Adenosine diphosphate
ATP: Adenosine triphosphate
ATPγS: Adenosine gamma-triphosphate
AMP-PnP: Adenylyl imidodiphosphate

B ----------

BAIAP2: Brain-specific angiogenesis inhibitor 1-associated protein 2
BAIAP2L1: Brain-specific angiogenesis inhibitor 1-associated protein 2-like protein 1
BSA: Bovine serum albumin

C ----------

$CaCl_2$: Calcium chloride
CAPZA1: F-actin-capping protein subunit alpha-1
CAPZA2: F-actin-capping protein subunit alpha-2
Cdc42: Cell division control protein 42
CIP: Alkaline phosphatase calf intestinal
CK2: Casein kinase 2
CORO1A: Coronin-1A
CORO1B: Coronin-1B
CORO1C: Coronin-1C
CP: Capping protein
CPI: capping protein inhibitor
CRUK: Cancer Research United Kingdom
Cryo-EM: Cryogenic electron microscopy
CSRP1: Cysteine and glycine-rich protein 1

D ----------

Dbl: Diffuse B-cell lymphoma
DH: Dock homology
DHR-2: Dock homology region 2
DRFs: Diaphanous related formins
DMEM: Dulbecco's Modified Eagle's Medium
DMSO: Dimethyl sulfoxide
DNA: Deoxyribonucleic acid
DOCK: Dedicator of cytokinesis
D-loop: DNase 1 binding loop

E ----------

EDTA: Ethylenediaminetetraacetic acid
EGFR: Epidermal growth factor receptor
Ena/VASP: Enabled/vasodilator-stimulated phosphoprotein
Eps8: EGFR pathway substrate 8
Eps8L1: EGFR pathway substrate 8 like 1
Eps8L2: EGFR pathway substrate 8 like 2
Eps8L3: EGFR pathway substrate 8 like 3

F

F-actin: Filamentous actin
FBS: Fetal bovine serum
FDR: False discovery rate
FH2: Formin homology 2
FLNB: Filamin-B
FMNL2: Formin-like protein 2
FSCN: Fascin

G

g: grams
G-actin: Globular actin
G-protein: Guanine nucleotide binding protein
GAP: GTPase-activating protein
GDP: Guanosine diphosphate
GEF: Guanine nucleotide-exchange factors
GFP: Green fluorescent protein
GH: Gelsolin homology
GO: Gene Ontology
GTP: Guanosine triphosphate

H

HEK: human embryonic kidney
Hscp300: Haematopoietic stem/progenitor cell protein 300
Hsp70: Heat-shock protein 70
HRP: Horse radish peroxidase

I

IF: Intermediate filament
IRSp53: Insulin receptor tyrosine kinase substrate 53 kDa

J

JVM3: Chronic B cell leukaemia cell line

K

kDa: Kilodalton
KO: Knockout

L

LC-MS: Liquid chromatography – mass spectrometry
LiCl: Lithium chloride

M

M: Molar
mDia1: Mammalian diaphanous-related formin 1
MEF: Mouse embryonic fibroblast
Mg^{2+}: Magnesium ion
min: Minutes
ml: Millilitre
mRNA: Messenger RNA
MS: Mass spectrometry

N

N-WASP: Neuronal Wiskott-Aldrich syndrome protein
Nap1: Nck-associated protein 1
NPF: Nucleation promoting factor
ns: not significant

P

PBS: Phosphate buffer saline
PCR: Polymerase chain reaction
PDAC: Pancreatic ductal adenocarcinoma
pH: Potential of hydrogen
Pi: Inorganic phosphate
PIP_2: phosphatidylinositol 4,5-bisphosphate
PP: Polyproline
PPI: Protein-protein interaction
PTB: Phosphotyrosine binding

R

Rac1: Ras-related C3 botulinum toxin substrate 1
Ras: Rat sarcoma protein
Rpm: Rotation per minute

S

SD: Standard deviation
SDS: Sodium dodecyl sulfate
SDS-PAGE: Sodium dodecyl sulfate polyacrylamide gel electrophoresis
SEM: Standard error of the mean
SFM: Serum free media
SOC: Super optimal broth with catabolite repression
SH3: Src homology 3
SOS: Son of Sevenless

T ----------

TAE: Tris base, Acidic and EDTA
TBS-T: Tris-buffered saline-Tween
Tβ4: Thymosin β 4
TIRF: Total internal reflection fluorescence
Tpm3.1: Tropomyosin isoform 3.1

U ----------

UV: Ultraviolet
VCA: Verprolin Cofilin Acidic domain

V ----------

VCA: Verprolin homology, central and acidic region

W ----------

WASP: Wiskott-Aldrich syndrome protein
WAVE: WASP-family veprolin homology protein
WH2: WASP homology 2
WRC: WAVE Regulatory complex
WT: Wild type

X ----------

XIC: Extracted ion chromatogram

Y ----------

YAP1: Yes-associated protein 1

β ----------

β: beta
β-actin: beta-actin

μ ----------

M: micro
μg: microgram
μL: microliter
μM: micro molar
μm: micrometer

γ ----------

γ: gamma
γ-actin: gamma actin

1 Introduction

1.1 Cancer

Cancer is a disease of uncontrollable cell growth that leads to nearly one in six of all deaths worldwide (Ferlay et al., 2021). This is the result of accumulation of genetic mutations in the cell that allow them to bypass checkpoints that would normally stop unwanted growth. These genetic mutations are caused by exposure to carcinogens which can be physical, chemical or biological, or are simply accumulated over time by errors in DNA replication during cell division (Basu, 2018). Some physical and chemical carcinogen exposure risk comes from everyday lifestyle circumstances, such as exposure to UV light and consumption of tobacco products or alcohol. Biological carcinogen exposure is a result of infection by some bacteria or viruses, some of which can be vaccinated against such as the Human Papillomavirus (HPV) (Balhara et al., 2024).

The death rates from cancer have declined over the years due to global research and treatment advances. Early detection and treatment can also have a huge impact on the outcome of the patient. Screening for certain cancer types is now routine in populations of people who are at risk by factors such as age and gender, and is an important way to increase the early detection of cancers and ensure the trend of increasing survival rates continues to tick upwards (Crosby et al., 2022).

Though early detection and cancer survival rates are increasing, it is important to acknowledge that this was disrupted by the coronavirus 2019 (COVID-19) pandemic. Due to delayed diagnosis and treatment caused by the pandemic, some incidences were diagnosed later than they potentially could have been, leading to a delay in treatment and potentially more progressed disease (Yabroff et al., 2022).

1.1.1 Cell invasion and migration in metastasis

Cancerous cells have many properties which set them apart from “normal” cells and allow them to grow and spread, progressing the disease (reviewed in Hanahan and Weinberg, 2000; Hanahan and Weinberg, 2011; Hanahan, 2022).

Invasion and migration are processes that allow cancer cells to disseminate from their initial tumour site and spread to secondary locations. This is called metastasis and is the leading cause of most of cancer deaths (Lambert et al., 2017). Screening and early detection aims to diagnose cancers before they have reached the advanced stage of metastasis, to allow for a better treatment outcome.

The stages of metastasis include migration of tumour cells from their initial tumour site, travelling in the circulation and finally extravasation and migration into a secondary site, where secondary tumours are formed (Fares et al., 2020). Therapies that focus on impeding the motility of cancer cells would provide huge benefits to patients compared to current highly cytotoxic therapies and are referred to as migrastatic therapies (Raudenska et al., 2023). The cytoskeleton and its dynamics are required for all forms of cancer cell motility. Hence it is imperative to understand the basic biology behind these mechanisms to allow treatments against metastasis to be developed.

CK2 is a serine/threonine kinase that is involved in many signalling pathways crucial to cancer and metastasis (Borgo et al., 2021), including the regulation of the cytoskeleton and cell motility (D'Amore et al., 2019). For example, CK2 has been shown to be involved in the regulation of both formins (Iskratsch et al., 2010) and Arp2/3 via coronins (Xavier et al., 2012). A small molecule inhibitor of CK2, named CX-4945, was developed and entered clinical trials some years ago (Marschke et al., 2011). In vitro CX-4945 has been shown to inhibit the migration of cancer cells (Lettieri et al., 2019) and it is now considered to be more effective as part of a multi target therapeutic approach as preclinical studies have shown it exhibits a synergistic effect when combined with other anti-cancer therapies (D'Amore et al., 2020).

Drugs that directly target actin have also been developed to either de-stabilise, such as cytochalasins or latrunculin, or stabilise actin filaments, such as Jasplakinolide. Though these compounds have never entered clinical trials due to their cytotoxicity caused by non-specific targeting of "normal" cell actin (Newman and Cragg, 2004), they remain highly important practical tools for the study of actin dynamics and will be important later in this thesis. To overcome the challenges of non-specificity it was suggested that the identification of

tropomyosin isoforms that are upregulated and bind to actin filaments in cancer cells could pave the way to directly target the motility of transformed cells (Stehn et al., 2006). TR100, a drug targeting such isoforms of tropomyosin was developed and showed promising results both in vitro and in vivo. Importantly, it did not have the widespread cytotoxic effects of previous classes of actin inhibiting drugs (Stehn et al., 2013). Tpm3.1 is the major tropomyosin isoform in tumour cells and the promising effect it showed upon targeting the actin cytoskeleton led to further investigation and the discovery of another small molecule, ATM-3507, which exerted the same effect (Currier et al., 2017). The best results achieved with these two drugs, both in vitro and in vivo, have been in combination with another anti-cancer agent that targets microtubule dynamics (Wang et al., 2020).

1.2 Cytoskeleton

Movement and polarity are vital mechanisms in cellular life, allowing important processes ranging from the separation of cells during mitosis to the hunting of foreign particles by macrophages. Importantly, these mechanisms are also what facilitate the migration and invasion needed for cancers to metastasise. None of this would be possible without the cytoskeleton, a dynamic network of proteins that grant the cell organisation, structure and motility. The cytoskeleton is composed of three types of filaments (Figure 1-1), each of which are assembled into polymers from their respective monomer protein. This thesis will focus on the smallest filament in the cytoskeleton, F-actin. Therefore, I will only briefly introduce the other components.

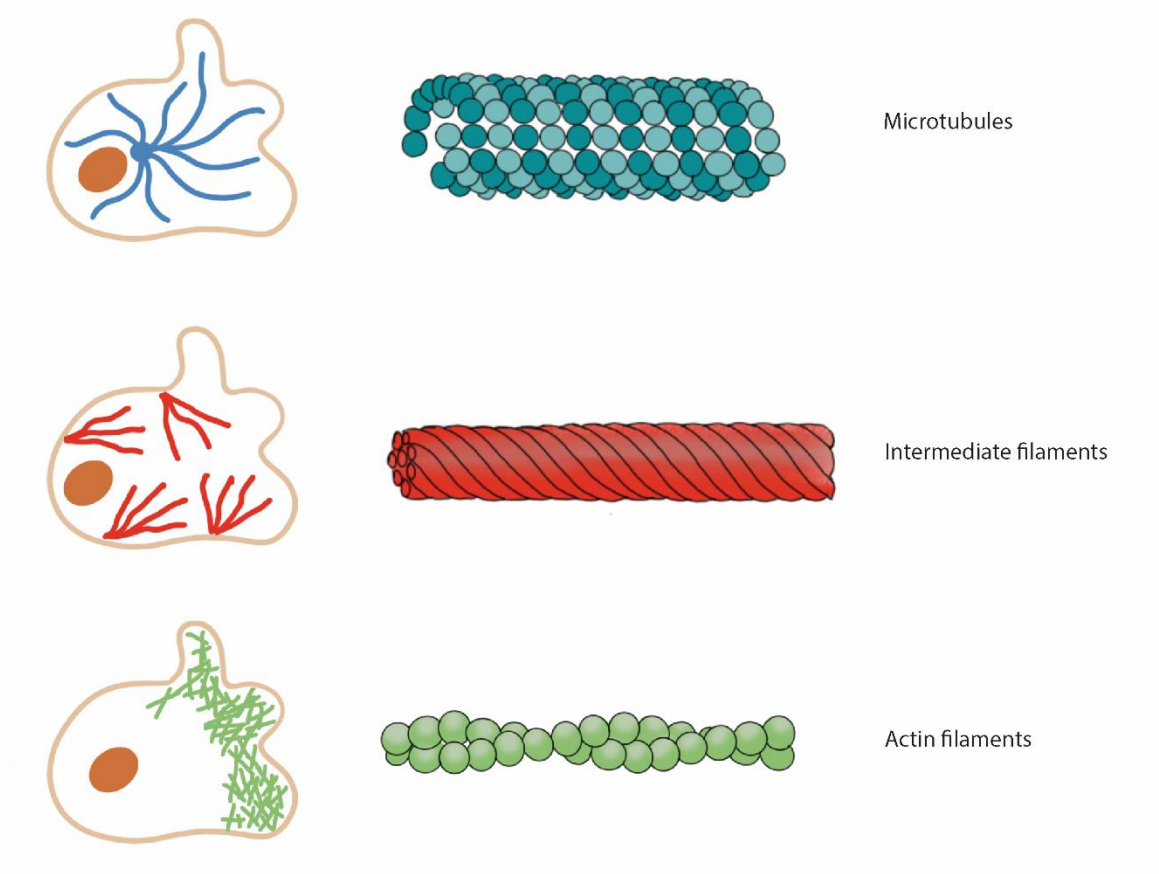

Figure 1-1 Components of the cytoskeleton
Diagram showing microtubules, intermediate filaments and actin filaments and illustration of their polymer structure.

1.2.1 Microtubules

Microtubules are the largest of the three components of the cytoskeleton, with a diameter of around 25nm. They play a crucial role in formation of the mitotic spindle, the structure responsible for separation of chromosomes during mitosis. These hollow, tubular structures also provide structure and organisation to the cell and allow for the travel of motor proteins along their length, transporting materials and organelles such as vesicles. Alpha and Beta tubulin are the monomers that form the microtubule polymer and, like actin, their polymerisation is highly dynamic and dependent on nucleotide hydrolysis. For more information please refer to this review article (Goodson and Jonasson, 2018).

1.2.2 Intermediate filaments

Intermediate filaments (IFs) are so named because of their width of 10nm, being an intermediate size between those of actin filaments and microtubules. Unlike microfilaments and microtubules, intermediate filaments are not made from the polymerisation of globular units, but fibrous protein subunits. Intermediate filaments display self-assembly into polymer form without the need for nucleotides and no nucleotides are known to bind IF proteins. Their main characterised role is to provide structural support to the cell due to their properties of flexibility and stress resistance. A more in-depth explanation of intermediate filaments and their interaction with the rest of the cytoskeleton can be found in these review articles (Herrmann and Aebi, 2016; Pollard and Goldman, 2018).

1.2.3 Actin microfilaments

For cell movement, the most important cytoskeletal polymer is the microfilament, composed of actin monomers. Actin is responsible for a number of different structures within the cell and is crucial for cell migration. The nucleotide dependent polymerisation of actin monomers into filamentous actin (F-actin) leads to the formation of protrusions that drive cell movement. Since this thesis will focus on F-actin and its binding partners, I will go into more detail in the following section.

1.3 Actin

1.3.1 Actin Structure

Actin is an abundant and highly evolutionary conserved protein that resides in a superfamily with Hsp70, sugar kinases and hexokinases (Bork et al., 1992). The crystal structure of G-actin was solved by X-ray analysis in complex with DNAse1, which prevents its polymerisation, and it has been revealed that the protein consists of two domains, between which there are two clefts, one of which is occupied by ADP or ATP and a divalent cation (Kabsch et al., 1990). Since then, an abundance of G-actin structures have been reported, mostly in complex with different actin binding proteins or small molecules (Dominguez & Holmes, 2011). However, it has been more difficult to obtain a high-resolution structure of F-

actin, as the polymerisation of actin hinders crystallisation (Holmes et al., 1990). More recently, X-ray fibre diffraction analysis has been employed to elucidate a high-resolution structure of F-actin and uncover the structural differences that occur during the transition of actin from the globular to filamentous state (Oda et al., 2009). Importantly, the main difference appears to be the angle of distance between the two domains of the monomer, resulting in a flatter structure when they are together in filamentous actin. It was also observed that the other cleft is important for binding actin regulating proteins (Oda et al., 2009). A similar structure has been observed by Fujii et al, using cryogenic electron microscopy (Fujii et al., 2010).

1.3.2 Actin isoforms

The wide range of roles actin can play (e.g. motility, division and organisational structure) in the cell can be partially explained by the fact that it is not only one protein encoded by one gene. In fact, six isoforms of actin exist, four of which are expressed in muscle cells and two which are expressed in non-muscle cells (Perrin and Ervasti, 2010). All the isoforms are highly similar, with only slight variations in the amino acid sequences (Herman, 1993). However, it has been shown that each of these isoforms have a specific role, as *in vivo* experiments in which the isoforms were knocked out individually gave rise to mice with differing phenotypes (Perrin and Ervasti, 2010). There are differing views on how these isoforms carry out their specific functions, either through differential interaction properties or differential localisation in the cell, and these may both play a part in the function. For example, it has been shown that β-actin mRNA is localized to the plasma membrane when a cell is motile and actively protruding, and if this localisation is abolished there is a detrimental effect on cell polarity, speed and effective steering (Shestakova et al., 2001). It has also been shown that β-actin, compared to the other isoforms, can preferentially interact with actin binding proteins, such as the bundling protein L-plastin (Namba et al., 1992). We are most interested in the isoforms of actin that reside in non-muscle cells, as these are most relevant to cell motility. Both β- and γ- actin are found in non-muscle cells, however there is disagreement in the literature over their localization. β-actin has been commonly reported to localize near the lamellipodium and is associated with polymerisation in moving cells (Hoock et

al., 1991). More recent studies have found that β-actin is in fact enriched in cellular structures such as stress fibres, and that the dominant actin isoform found at the lamellipodium is γ- actin (Dugina et al., 2009). Interestingly, evidence suggests that β- and γ- actin can co-polymerise, creating filaments of mixed isoform population, and that this can have an effect on the stability and the dynamics of the filament (Bergeron et al., 2010). For example, in this study it was shown that during treadmilling, filaments composed of β-actin exhibit much faster phosphate release on the addition of new monomers than that of filaments composed of γ- actin (Bergeron et al., 2010). Perhaps the incorporation of different isoforms in polymerisation could be a mechanism to achieve filaments with different properties and capabilities. This is reflective of an analogy written by Perrin and Ervasti, 2010, in which they present actin as a cellular "steel", and in the same way different metals are combined to give steel different properties, different isoforms of actin may be combined intentionally to give the filament different potential (Perrin and Ervasti, 2010).

A recent study sought to determine the differences in structure between the isoforms of actin using cryo-electron microscopy. Four isoforms were studied (two of which were muscular, 2 being cytoplasmic) and the high-resolution structures showed subtle differences in the shape of the N-terminus of the different isoforms, most significantly near the nucleotide binding cleft. This is to be expected: although the actin isoform sequences are highly conserved, the main differences are in the N-terminus range of the sequence (Arora et al., 2023). These differences may explain the separate binding partners different actin isoforms can interact with. This is of the utmost importance to the localisation and therefore function of the different isoforms.

1.4 Actin Dynamics

1.4.1 Polymerisation and treadmilling

For actin to carry out its broad range of cellular functions, it must first transition from its globular monomer (G-actin) into its filamentous polymer (F-actin). This reversible process is named polymerisation and is composed of three stages which are nucleation, elongation and steady state (Wegner and Engel, 1975). The initial step is nucleation, in which two or three actin monomers join into a

structure known as the nucleus. This is known as the lag phase, as spontaneous nucleation is rare. The nucleus acts as a base for the elongation step, in which numerous actin monomers join onto both ends of the forming filament (Mullins et al., 1998). In the steady state, monomers can join at one end and dissociate at the other, with the length of the filament remaining the same (Lodish et al., 2013). The growth of an actin filament is associated with the hydrolysis of the bound nucleotide, ATP, and subsequent release of Pi (Straub & Feuer, 1950). The release of Pi decreases the strength of the bonds between the actin subunits in the filament, and facilitates depolymerisation (Korn et al., 1987).

For polymerisation to occur, the levels of G-actin in the cell must exceed what is known as the critical concentration. Simply put, when the levels of G-actin exceed the critical concentration, the formation of filaments will occur. In reality, it is not this simple, as the critical concentration can depend on the number of filaments already in existence (Pantaloni et al., 1984). Further, the two distinct ends of an actin filament, as will be discussed below, have different critical concentrations for additions of monomers (Wegner, 1976). ATP-actin is preferentially incorporated into the filament (rather than ADP) as it has a lower critical concentration for polymerisation (Pollard, 1986).

Actin filaments exist as helical polymers and exhibit polarity, displaying two distinct ends (Pollard, 2016). One end, the plus or barbed end, is associated with fast growth. The other end, which is named the pointed end, is less dynamic although both ends can facilitate growth of the filament. This polarity of actin filaments can be visualised through binding experiments using myosin S1 heads, which give an image of the myosin subunits “pointing” towards the namely pointed end of the filament (Moore et al., 1970). Further experiments have concluded that these ends have different dynamic growth properties and the barbed end is associated with faster growth (Woodrum et al., 1975).

The hydrolysis of ATP upon monomer addition and polarity of the filament give rise to the phenomenon of actin treadmilling whereby “aged” parts of the filament are subject to depolymerisation, ADP-bound actin monomers are recycled by the exchange of their ADP for ATP, ready for incorporation at the barbed end of the filament (Figure 1-2). This regulates the length and dynamics

of the filament in the steady state of polymerisation (Bugyi and Carlier, 2010). Actin treadmilling was discovered some 40 years ago by Wegner (1976) when he carried out experiments with radio-labelled G-actin and its addition to F-actin. It was observed that the actin filament could simultaneously grow at one end (the barbed end) and shorten at the other (Wegner, 1976).

When ATP-actin is added to the growing actin filament, ATP is hydrolysed at the γ-phosphate – a reaction which is facilitated by the significant increase in the ATPase activity of actin when it is incorporated into a filament (Pollard and Weeds, 1984). When ATP is hydrolysed, the phosphate is not immediately released and therefore monomers within the filament will be ADP-Pi bound, and in fact this has been shown to be the most abundant monomer state in a filament (Carlier & Pantaloni, 1986). Eventually, Pi is released, giving rise to the last monomer state in the filament, ADP-bound. The newly incorporated ATP-bound actin is of most interest to us, as we are keen to know whether any conformational change in actin monomers within a filament, namely whether they are ATP or ADP bound, could change the proteins they interact with and subsequently the effects they have in the cell.

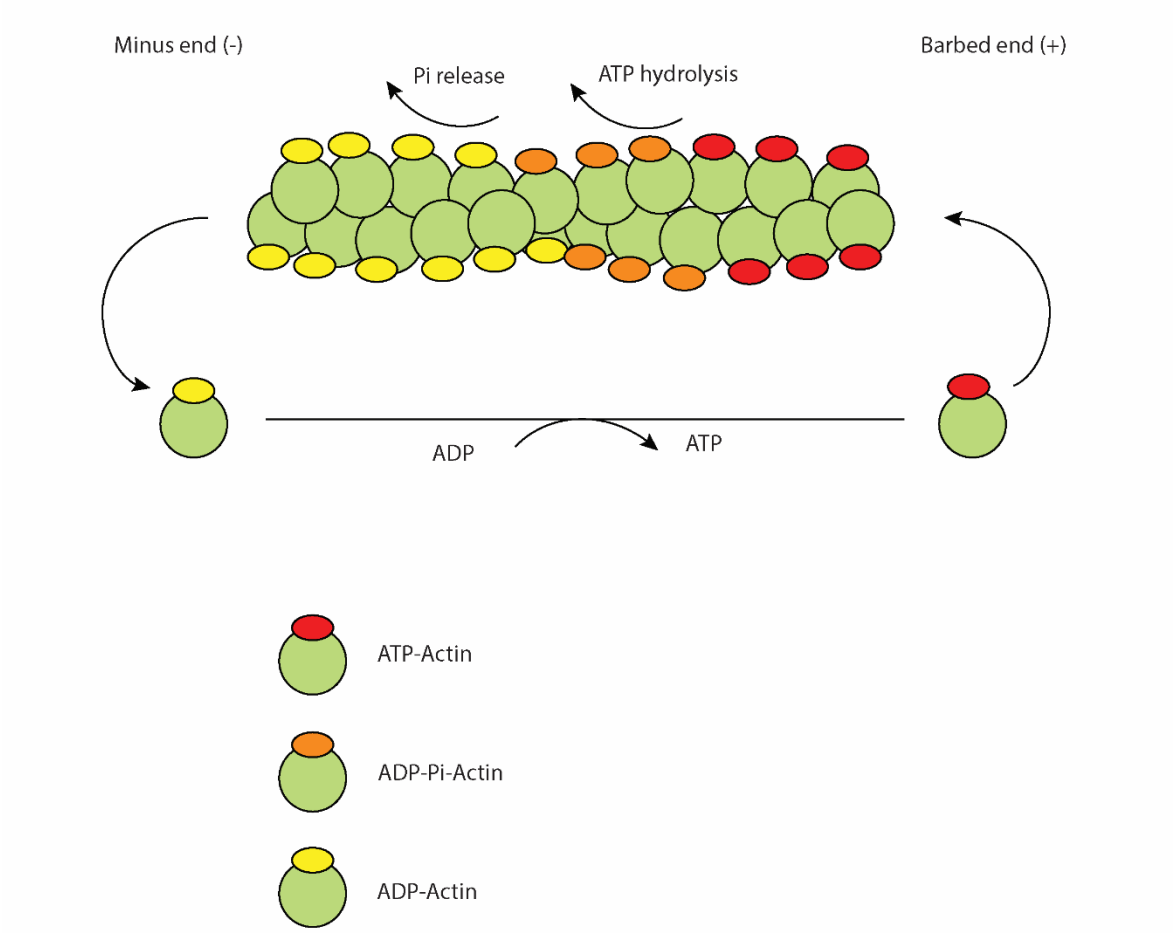

Figure 1-2 Actin treadmilling
Schematic diagram showing a simplified version of a polymerising filament and the stages of nucleotide hydrolysis and release. ADP-actin monomers are then recycled with an exchange of their nucleotide for ATP and become viable for incorporation to the barbed end of actin filaments.

1.4.2 ATP- and ADP-actin

The bound nucleotide is of utmost importance to the fate of the actin monomer and the interactions it will undergo. However, strangely the structure of G-actin appears similar no matter which nucleotide state it has been solved in (Dominguez and Holmes, 2011). It has been shown that the bound nucleotide has significant effects on the rate of interaction with the actin binding protein profilin, which encourages the exchange of ADP for ATP on the actin monomer, and the subsequent incorporation of this ATP- monomer at the barbed end of a filament (Korenbaum et al., 1998). Interestingly, in kinetic experiments designed to examine the binding affinities of profilin for actin monomers and subunits in the filament at the barbed end, a significant difference was found. When AMP-PnP, a non-hydrolysable analogue of ATP, was incorporated into

filaments, profilin displayed a 200-fold lower affinity for binding the barbed end than when it was ADP bound (Courtemanche and Pollard, 2013). This implies there is a difference in the interactions of the barbed filament end depending on the bound nucleotide. Profilin provides an example of how actin binding proteins that are involved in the treadmilling process can recognise a specific nucleotide-bound conformation and influence the dynamics of a filament (Kudryashov & Reisler, 2013). Perhaps other proteins can recognise this difference, and ATP-actin barbed end filaments can interact with different proteins than those that recognise ADP-actin.

While it seems that the bound nucleotide causes a difference to the barbed end of filaments that other proteins can distinguish, the exact details are unknown. There is conflict in the literature regarding the effect on the nucleotide binding cleft when Pi is released. If we consider actin in the context of its superfamily (actin, hexokinase and hsp70) who share a structural ATPase domain, it would be logical to hypothesise that actin would share a similar shape change on ATP hydrolysis and Pi release as the rest of the family. That is, an opening of the cleft (Bork et al., 1992). However, there are many X-ray structures of actin, both in ADP- and ATP-bound states which clearly show the nucleotide binding cleft in a closed position (Rould et al., 2006).

While there seems to be little known about difference in the structure of actin depending on the bound nucleotide, the rigidity of filaments has been studied under different conditions. Data has shown that ADP-actin is more flexible than ADP-Pi-Actin, meaning the “newer” parts of the filament are more rigid (Isambert et al., 1995). Infact, the “older” ADP-actin is more than twice as flexible (De La Cruz et al., 2010).

As mentioned in the “structure of actin” section, actin takes on a flatter structure when incorporated into a filament due to the rotation of the two subdomains (Oda et al., 2009). Work from Chou and Pollard has shown that this flattened state is present regardless of bound nucleotide and is therefore caused by the polymerisation of a filament itself and not by hydrolysis or release of Pi (Chou and Pollard, 2019). Recently, two studies utilising high-resolution electron microscopy and advanced analysis tools have confirmed this at a higher

resolution (Reynolds et al., 2022; Oosterheert et al., 2022) and provided more details of what this flatter conformation means for the structure and function of the filament. They showed that the difference in position of a water molecule promotes ATP hydrolysis, and divalent cations that associate with the nucleotide can change as the filament “ages”, and that this contributes to the change in flexibility of the filament (Oosterheert et al., 2022). This is proposed to be the reason for some actin binding proteins to bind actin filaments differentially based on nucleotide state.

1.5 Binding partners of actin

1.5.1 Actin monomers in the cell

Under normal physiological conditions in the cell, the majority of G-actin exists in a complex with binding or sequestering proteins, which serves to inhibit spontaneous polymerisation due to the concentration levels. One such protein is profilin, a small, abundantly expressed protein in non-muscle cells. Profilin was first isolated from spleen cells in a complex with G-actin (Carlsson et al., 1976) and it was shown shortly after that association of actin with profilin in a 1:1 ratio is enough to keep it in the monomeric (G-actin) state (Carlsson et al., 1977).

Much more is now known about profilin, and in addition to its ability to bind monomeric actin, it can also deliver actin to the barbed end of filaments (Tilney et al., 1983) and assist in the exchange of ADP/ATP on actin monomers (Mockrin and Korn, 1980; Selden et al., 1999).

In addition to the actin binding domain of profilin (Schutt et al., 1993), there is also a polyproline binding domain (Björkegren et al., 1993; Archer et al., 1994) that allows it to bind to other actin binding proteins such as formins.

Thymosin ß 4 (Tß4) is another actin binding protein that sequesters monomeric actin, however it differs from profilin in that it inhibits the exchange of the bound nucleotide (Goldschmidt-Clermont et al., 1992). Both of these proteins exchange rapidly on and off globular actin (Goldschmidt-Clermont et al., 1992). Because of this rapid exchange, profilin can utilise actin monomers previously

bound by Tβ4 to incorporate into the barbed end of actin filaments during polymerisation (Pantaloni and Carlier, 1993). Unlike profilin, which has similar affinity for both ATP-G-actin and ADP-G-actin (Selden et al., 1999) Tβ4 has a far higher affinity for ATP-G-actin than ADP-G-actin. This suggests that its role is to maintain a pool of actin monomers that are ready for polymerisation (ATP-bound) (Carlier et al., 1993).

Therefore, most of the monomeric actin in the cell exists in a complex with these proteins, ready for polymerisation but preventing it happening spontaneously.

1.5.2 Actin nucleators

Since spontaneous interaction is so unfavourable, the cell has mechanisms in place to control actin polymerisation both spatially and temporally. Proteins called actin nucleators can be targeted to areas of the cell, by tightly regulated cellular signalling, where polymerisation should occur. Different actin nucleators can promote the formation of different types of actin-based protrusions and therefore different modes of cell migration.

1.5.2.1 Arp2/3 complex

The Arp2/3 complex is the most well-known actin nucleator and was first discovered in a screen for binding partners of profilin (Machesky et al., 1994), the actin monomer binding protein discussed in the previous section. Arp2 and Arp3 are the aptly named actin related proteins and are both structured to bind ATP and a divalent cation (Kelleher et al., 1995). There are five other subunits and the complex has been shown when purified to contain one of each, at a stoichiometry of 1:1:1:1:1:1:1. When purified, the complex also binds to actin monomers at a stoichiometry of 1:1. This study also showed that the complex binds the side of actin filaments near the leading edge of the cell (Mullins et al., 1997). Later work from the same group showed that the angle the complex bound actin filaments at was consistently 70 degrees, and thus was thought to be responsible for branching networks of actin at the cell edge during motility (Mullins et al., 1998). The contribution of Arp2/3 to the nucleation of daughter filaments from existing mother filaments, and therefore the formation of

lamellipodia, is now widely studied and recognised as hugely important in cellular motility. Arp2/3 is also now known to be involved in a vast array of different cellular functions including DNA repair and autophagy, with its ability to generate networks of branched actin filaments at the core of all functions (Rottner and Schaks, 2019).

However, the Arp2/3 complex is intrinsically inactive and requires activation from molecules named nucleation promoting factors (NPFs) (Machesky et al., 1999; Welch et al., 1998). The Arp 2 and 3 subunits are moved closer together upon activation of the complex by NPFs, allowing them to mimic the actin dimer. This, combined with the binding to an existing actin filament (the mother filament), allows the polymerisation of a new, branched filament from this dimer. Upon activation of the complex, the five other subunits act as scaffolds to achieve this conformation and anchor the complex to the mother filament from which the branching will take place (Robinson et al., 2001). Arp 2 and 3 proteins then act as the first two subunits of the new branched filament (Volkmann et al., 2001). It later became known that the binding of not one, but two NPFs to one Arp2/3 complex is responsible for activation (Padrick et al., 2011) and even more recently it was shown that having two NPFs binding the complex does not only increase the performance of the complex but that both are necessary and perform distinct functions during the activation (Zimmet et al., 2020). These branched actin networks created by Arp2/3 are responsible for structures called lamellipodia, which will be covered in a later section. Arp2/3 is the only actin nucleator which produces branched actin networks, with the other nucleators producing unbranched filaments, the most well understood of which is the formin family.

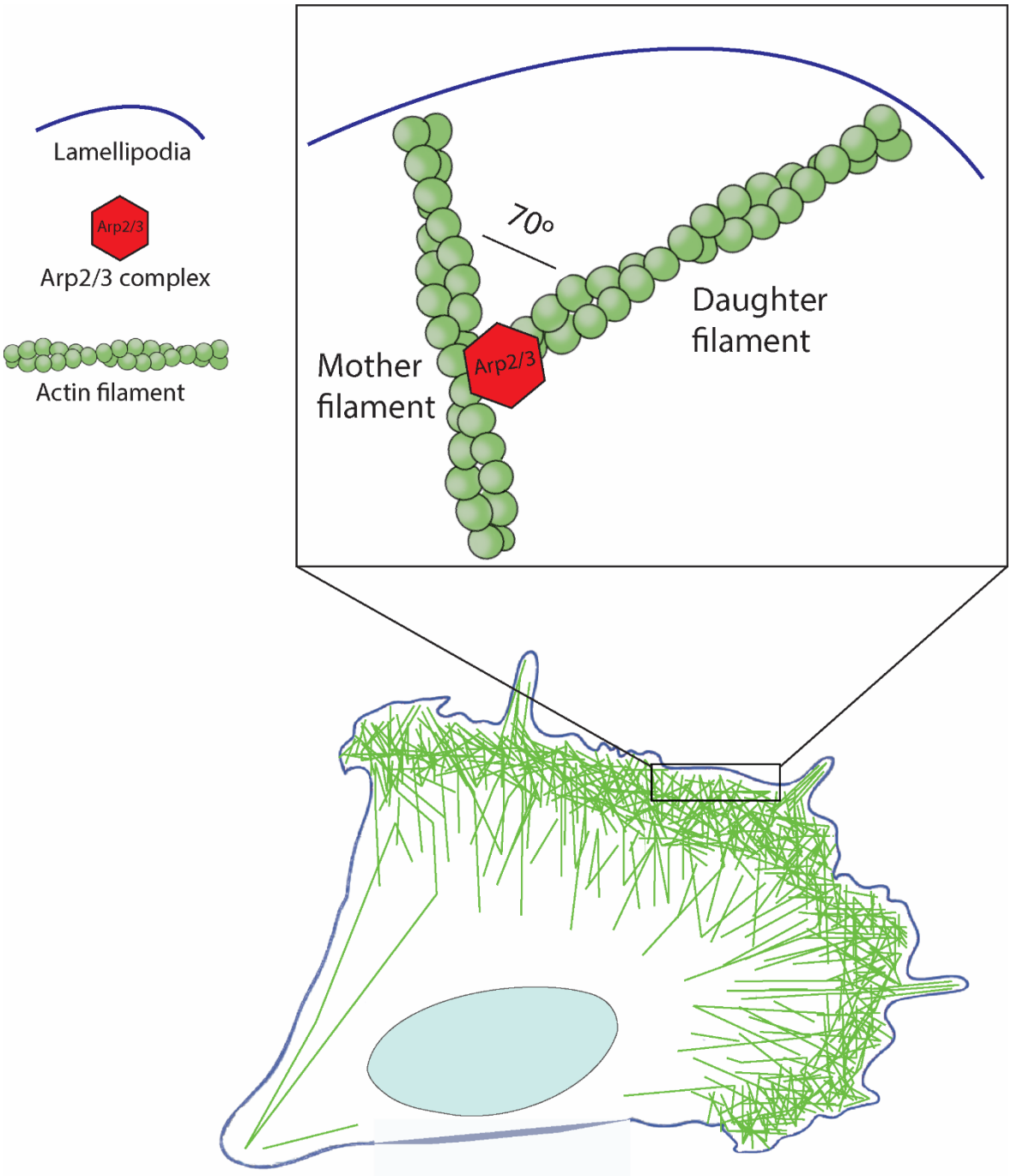

Figure 1-3 Arp2/3 complex nucleates branched actin networks
Schematic diagram showing a simplified example of actin filament branching carried out at the lamellipodia by Arp2/3.

1.5.2.2 Formins

Formins are another family of actin nucleators which were first shown to nucleate actin filaments in studies of budding yeast (Evangelista et al., 2002). Utilising their formin homology 2(FH2) domains, they stabilise actin dimers and trimers, overcoming the barrier to polymerisation. The largest family of formins in vertebrates are DRFs (Diaphanous related formins). Formins of the DRF family contain a conserved Rho GTPase binding domain (Watanabe et al., 1997), Dia-autoregulatory domain (DAD) (Alberts, 2001) and as well as their formin

homology (FH) domains (Castrillon and Wasserman, 1994). The DAD domain interacts with the Rho GTPase binding domain, keeping the formin in an inactive state until it is bound by an active Rho GTPase (Alberts, 2001; Krebs et al., 2001).

Further studies revealed they can remain bound to the barbed ends of actin filaments via their formin homology 2(FH2) domain as the filament grows (Pruyne et al., 2002). This gives rise to the elongation of linear filaments, unlike the branched filaments formed by the Arp2/3 complex. Since formins have been shown to display this capping behaviour but still permit elongation of the filament, they are described as “leaky cappers”. This allows them to compete with capping proteins that would otherwise halt elongation (Zigmond et al., 2003). Formins have been shown to be involved in the formation of a wide range of actin protrusions (Breitsprecher and Goode, 2013; Courtemanche, 2018), with their involvement in the formation of filopodia (Pellegrin and Mellor, 2005; Schirenbeck et al., 2005) and lamellipodia (Yang et al., 2007) being the most relevant to this thesis.

1.5.2.3 Ena/VASP and nucleator cooperation

Ena/VASP are another family of actin nucleators that upon tetramerization can bind to F-actin (Bachmann et al., 1999; Faix and Rottner, 2022). As mentioned previously, the majority of monomeric actin in the cell exists in a complex with a sequestering protein, such as profilin. Ena/VASP proteins, via their polyproline domain, can recruit profilin-actin complexes, and, when profilin is released, the actin monomer is proposed to join the barbed end of F-actin (Ferron et al, 2007). The G-actin binding domain also acts as a WASP homology 2 (WH2) domain and this can bind and incorporate actin monomers to F-actin, independent of profilin (Breitsprecher et al., 2011).

Although the actin nucleator discussed in this and previous sections have distinct mechanisms of promoting polymerisation, there are many examples of involvement of multiple nucleators in the formation of complex actin structures. For example, in the case of Ena/VASP proteins they have been shown to be vital for proper lamellipodial function and dynamics. Studies in B16F1 melanoma cells have shown that with the loss of Ena/VASP lamellipodia shape is changed and

size is decreased (Damiano-Guercio et al., 2020). Similar findings have also been observed for formins. Loss of function FMNL2 and -3 in B16F1 and fibroblast cells decreases both the size and force exerted by the lamellipodia (Kage et al., 2017).

1.5.3 WASP family proteins

As mentioned in the previous section, actin nucleator Arp2/3 requires interaction with NPFs (nucleation promoting factors) to become active. The WASP family proteins have been studied and characterised for many years with the activation of Arp2/3 being their main function (Veltman and Insall, 2010). Wiskott-Aldritch syndrome protein (WASP), identified in studies of an immunodeficiency syndrome (Derry et al., 1994), was the first member of the family to be discovered. The WASP family share homologous domains including the VCA domain (verprolin homology, central and acidic region), which is their main catalytic domain (Miki et al., 1998). The WH2 (wasp homology 2) domain that facilitates the binding of actin is in the “V” of this domain, while the “CA” region is responsible for binding Arp2/3 and together they are responsible for regulating the actin cytoskeleton (Machesky and Insall, 1998) by activating the nucleation of filaments by Arp2/3 (Machesky et al., 1999).

1.5.3.1 WAVE regulatory complex (WRC)

WAVE (WASP family Verprolin homolog) is the WASP family member responsible for the regulation of lamellipodia formation via the induction of branched F-actin networks nucleated by Arp2/3 (Nakagawa et al., 2001). WAVE, along with the other members Nap1/NCKP1, PIR121/CYFIP, Abi and HSPC300, exist as an autoinhibited complex that, after activation by different cellular signals, can in turn promote actin polymerisation by Arp2/3 (Eden et al., 2002). This autoinhibition of the WRC is due to the structure of the complex with the VCA domain sequestered inside it. When activated, for example after binding with active Rac, the VCA domain is released and becomes accessible to Arp2/3 which it can then activate (Chen et al., 2010).

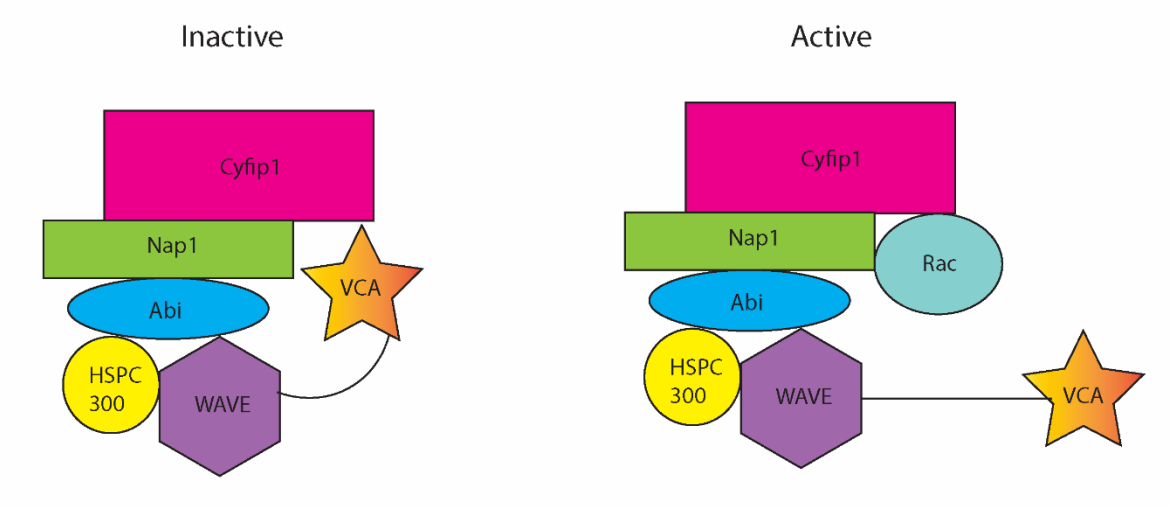

Figure 1-4 Wave regulatory complex activation
Simplified diagram showing the WRC in its inactive state where the VCA domain is inaccessible. Upon binding of activated Rac, the conformation of the complex shifts, exposing the VCA domain and allowing the subsequent activation of Arp2/3.

1.5.4 Capping protein

First discovered in 1980, capping protein (CP) was purified, characterised, and shown to physically stop the addition of new actin monomers to the barbed ends of F-actin filaments by binding them tightly (Isenberg et al., 1980). Regulation of capping protein and its activity has been widely studied as it was shown in vitro that its rate of dissociation from an actin filament on its own was very slow (Schafer et al, 1996). A motif termed CPI (capping protein inhibitor) was discovered (Bruck et al.,2006) and found to be present on a range of proteins that bind and inhibit the activity of CP, and that are otherwise unrelated (Hernandez-Valladares et al., 2010). These negative regulators can act either directly, binding capping protein itself and preventing its interaction with actin, or indirectly, by binding the barbed end of an actin filament so capping protein is physically unable to. Proteins containing this CPI motif have also been shown to be necessary for correct localisation of capping protein in the cell, further confirming their important role in the regulation of CP and therefore actin dynamics (Edwards et al., 2015).

While capping proteins are vital for the halting of addition of monomers to the barbed end and therefore the polymerisation of actin filaments, they also inhibit the dissociation of monomers and therefore the disassembly and recycling of the

filament. This role is carried out by severing proteins, as will be discussed in the next section.

1.5.5 Severing proteins

Given the wide range of functions and dynamics of F-actin, it is paramount for the cell to have "recycling" options available, allowing the depolymerisation of actin where it is no longer needed and rapid polymerisation to occur where it is required. There are two main families of proteins orchestrating this: the ADF/-cofilin and Gelsolin families.

1.5.5.1 ADF/ Cofilin

Actin depolymerising factor (ADF) was the first member of the ADF/-cofilin family to be discovered in 1980 in a bid to find proteins which promote the disassembly of actin (Bamburg et al., 1980). Cofilin was isolated in porcine brain extract in 1984 (Nishida et al., 1984). These two proteins were initially thought to belong to different classes of actin depolymerising proteins but are now understood to be members of the same family and have since been identified as necessary proteins in many cellular functions that require actin polymerisation. Unlike other proteins which inhibit polymerisation, ADF/-cofilin proteins do not cap filaments, but act by causing them to be severed (Maciver et al., 1991).

ADF/-cofilin proteins bind ADP-actin with much higher affinity than ATP- or ADP-Pi-actin (Maciver and Weeds, 1994; Carlier et al., 1997), meaning they preferentially bind to "aged" areas of actin filaments to promote depolymerisation. In addition, when cofilin does bind ADP-Pi-actin, it promotes the release of γ phosphate and therefore the structural aging of the filament (Blanchoin and Pollard, 1999). The effect of ADF/-cofilin binding actin is a twist is the filament, as it binds co-operatively between two actin subunits (McGough et al., 1997). Cofilin binds to actin in a stoichiometric fashion (De La Cruz, 2005), creating areas of the filament that are "decorated" with cofilin. Severing of the filament can occur at either end of these decorated areas, towards the barbed or pointed end of the polarised actin filament (Wioland et al., 2017). There is however a bias towards severing of the boundary at the pointed end of the filament, and recent cryo-EM analysis has shown that the disruption of actin

conformation by binding of cofilin is more significant at the pointed end, explaining the bias (Huehn et al., 2020). This has been further explored, and it is thought that, while the change in conformation of actin, by way of a disrupted DNase 1 binding loop (D-loop), is present at both ends of the decorated area, it is more severe at the pointed end because of less subunits of actin directly in contact with cofilin (Hocky et al., 2021).

Therefore, ADF/-cofilin act to sever actin filaments and create more pointed ends from which depolymerisation may occur. This creates free G-actin and more barbed filament ends, both of which allow profilin to recycle and deliver G-actin to sites where polymerisation is needed.

1.5.5.2 Gelsolin

Gelsolin is another actin binding protein that has severing activity as well as other functions. First discovered in 1979, gelsolin was shown to bind and affect F-actin in a calcium dependent manner (Yin and Stossel, 1979). In addition to being activated by calcium, it was also shown to be inhibited by phosphatidylinositol 4,5-bisphosphate ($PIP_{2)}$ (Janmey and Stossel, 1987). Further investigation revealed that gelsolin contains multiple actin binding sites, as well as calcium binding sites, and the regulation of these controls the function of gelsolin, be it severing, capping or monomer sequestering. The protein contains six repeating gelsolin homology (GH) domains, known as GH1-6, and the crystal structure shows a closed conformation that hides the actin binding sites (Burtnik et al., 1997). Indeed, these domains are arranged in such a way that prevents the binding of actin, until binding of calcium shifts the conformation and allows filament capping and severing to occur (Robinson et al., 1999).

Interestingly, though the sequence is different, the structural fold of the GH domain is similar to that of ADF/-cofilin (Hatanaka et al., 1996). A striking difference between the two is the presence of a calcium binding site which is conserved in the GH domains but is not present in ADF/cofilin (Choe et al., 2002). These conserved calcium binding sites are designated “type 2”. The type 2 calcium binding sites are of utmost importance for the activation of the protein as upon binding helices in G3 and 6 are straightened, causing the globular conformation to become more open and thus exposing actin binding

sites (Wang et al., 2009). “Type 1” calcium binding sites refers to those present on the actin binding sites located on G1 and G4. These are responsible for the binding of two calcium ions between gelsolin and actin, therefore increasing their interaction (McLaughlin et al., 1993). In total gelsolin can bind 8 calcium ions, six type 2 and two type 1 (Choe et al., 2002). Maximum activation of the protein and its severing and capping function is achieved when all 8 calcium binding sites are filled (Nag et al., 2009).

Although the six GH domains are highly conserved, gelsolin is often thought of in two halves, as G1-3 are even more so similar to G4-6. Whilst the N-terminal half of the protein (G1-3) is thought to be responsible for the severing function of gelsolin, and can do so on its own in vitro, it is much more potent when the full-length protein is present, suggesting that co-operation between both halves facilitate the full severing potential (Selden et al., 1998). When gelsolin is activated and bound to actin, it can disrupt the hydrophobic bonds between actin subunits, leading to severing of the filament (McLaughlin et al., 1993). After, gelsolin remains on the barbed end of the severed filament, capping it. For these capped filaments to be available for new polymerisation, they must be uncapped. PIP_2 can transduce extracellular signals to regulate actin binding proteins, including gelsolin. It’s effect on gelsolin is inhibition of capping and increasing polymerisation from the previously capped filaments (Doi et al., 1991a). Gelsolin has three binding sites for PIP_2 and when these are occupied, interaction between gelsolin and actin is diminished resulting in uncapping (Janmey and Stossel, 1987). This may be explained by local concentrations of PIP_2 at the cell membranes transducing extracellular signals for new polymerisation to take place (Hartwig et al., 1995). The binding of PIP_2 to gelsolin may physically interrupt the binding of gelsolin and actin, causing them to separate (Liepina et al., 2003).

1.6 F-actin structures and signalling in cell migration

The dynamics of actin and the interplay of all the previously mentioned actin binding proteins are what initiate and regulate the cells ability to move. The plasma membrane protrusions of actin dictate how and when a cell can move. Depending on the mode of cell migration, different structures are formed with help from actin binding proteins previously discussed, under the control of Rho

GTPase signalling complexes. Most relevant to cell migration, and therefore this thesis, are lamellipodia and filopodia. These structures are formed by actin nucleators that form branched and unbranched F-actin, respectively.

1.6.1 Lamellipodia

The lamellipodia is a thin sheet-like structure found at the leading edge of a migrating cell that was first identified as the leading edge or leading lamella in fibroblast cells (Abercrombie, 1980). Subsequent studies showed that actin is responsible for this membrane protrusion (Heath and Holifield, 1993). Indeed, the lamellipodia is constructed of a branched actin network, nucleated by the Arp2/3 complex (Machesky and Insall, 1998; Svitkina and Borisy, 1999). These branched networks of actin generated by the Arp2/3 complex are in turn under the control of the Wave regulatory complex (WRC) (Machesky and Insall, 1998), which is mainly regulated via Rho GTPase signalling protein Rac (Ridley et al., 1992; Miki et al., 1998).

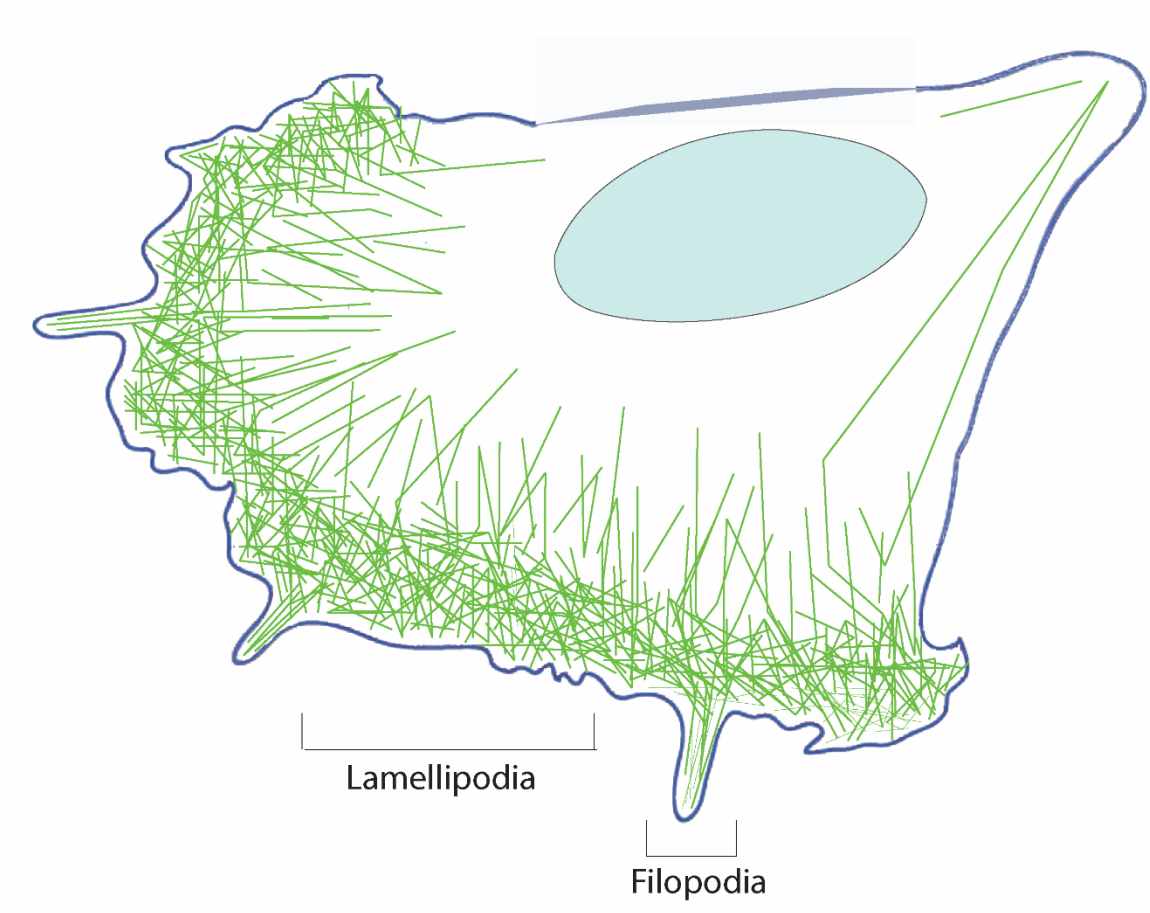

Figure 1-5 Lamellipodia and filopodia at the cell leading edge

Simplified diagram depicting a migrating cell with an actin network at the leading edge. Lamellopodia are highlighted as wide protrusions at the leading edge whilst filopodia are highlighted as narrow and “finger-like” protrusions.

1.6.2 Filopodia

Rho GTPase Cdc42 is responsible for the formation of filopodia (Nobes and Hall, 1995), another kind of dynamic actin protrusion used for cell migration. These protrusions are made up of linear actin filaments, instead of branched networks like in lamellipodia, and are often described as finger like. The nucleators involved in the linear actin networks needed for filopodia formation are the DRFs (Diaphanous related formins) (Krebs et al., 2001).

As discussed in 1.5.2, formins are kept in an autoinhibited state by way of their DAD domain interacting with their Rho GTPase binding domain, until an active Rho GTPase binds and activated the formin. The activated formins are then able to nucleate actin filaments (Evangalista et al., 2002) leading to the formation of linear F-actin to create filopodia protrusions (Pellegrin and Mellor, 2005; Schirenbeck et al., 2005).

1.6.3 Rho GTPase signalling

Although the mode of migration and types of protrusions can differ significantly in different cell types, they have in common the input from Rho GTPase signalling. Rho GTPases are a family of small G-proteins (guanine nucleotide binding proteins) that act as molecular switches, allowing the transmission of important information and instructions to regulate cell migration when they are active.

Rho GTPases are active and can signal to their downstream targets when bound by the nucleotide guanosine triphosphate (GTP) and inactive when GTP has been hydrolysed to guanosine diphosphate (GDP). This nucleotide state is controlled by proteins called guanine nucleotide exchange factors (GEFs) and GTPase activating proteins (GAPs). GEFs promote the exchange of GDP for GTP, activating the Rho GTPase, whereas GAPs activate the GTPase activity of the Rho GTPase, leading to the hydrolysis of GTP and therefore inactivation. There are some Rho GTPases to whom these processes do not apply, but for the scope

of this thesis we will focus on three well studied examples that are involved in protrusion types of interest.

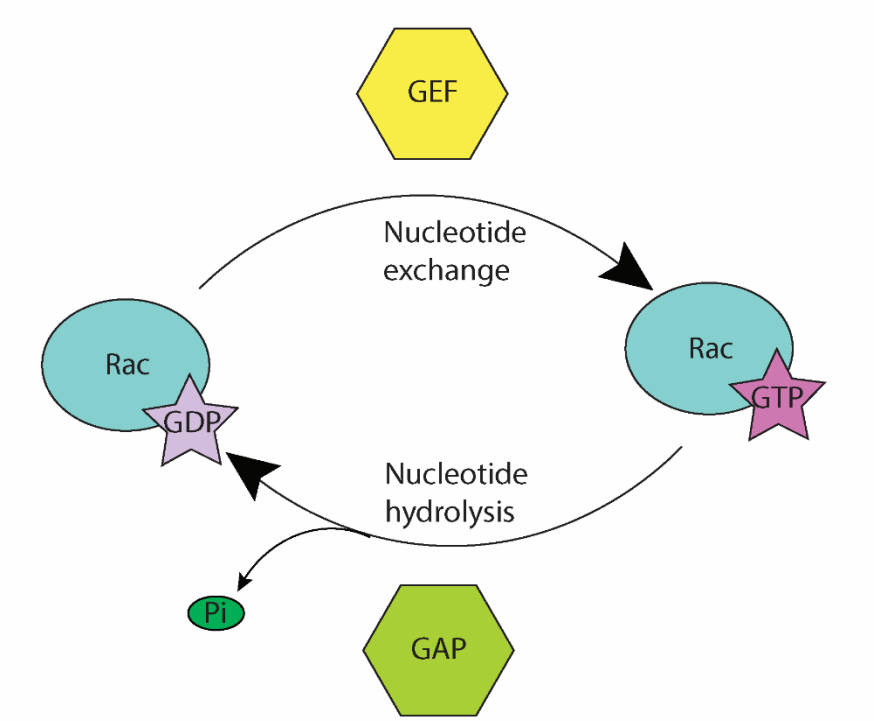

Figure 1-6 GEFs and GAPs regulated Rho GTPases
Simplified diagram showing Rho GTPase Rac and its activation and inactivation cycle as regulated by GEFs and GAPS. GEFs promote the exchange of GDP for GTP to activate Rho GTPases. GAPs promote the hydrolysis of the bound GTP and the release of phosphate, giving a Rho GTPase bound by GDP and therefore inactive.

The three most characterised Rho GTPases are Rho, Rac and Cdc42 and their involvement in cell migration has been studied for almost 30 years (Ridley et al., 1995; Nobes and Hall, 1995). We will introduce Rac and Cdc42, and their activators, being the Rho GTPases most well characterised for their role in lamellipodia and filopodia/invadopodia formation, respectively (Ridley et al., 1995; Nobes and Hall, 1995). These proteins are under stringent spatiotemporal control in migrating cells (Martin et al., 2016) to allow the right type of protrusion to form where and when it is needed. Rac and Cdc42 have both been shown to be activated at the leading edge of the cell (Kraynov et al., 2000; Nalbant et al., 2004) and this precise spatial activation is regulated by GEFs and GAPs. When activated, Rac binds the WRC, allowing the VCA domain to interact with Arp2/3 and promote the assembly of branched F-actin networks (Eden et al., 2002; Chen et al., 2010). Cdc42 is more commonly involved in the formation of filopodia (Nobes and Hall, 1995), via their interaction with formins (Krebs et

al., 2001) which nucleate actin and allow the polymerisation of linear filaments (Evangelista et al., 2002).

Given that GEFs and GAPs are critical players in the control of Rho GTPases and any downstream effects, it is no wonder much work has gone into dissecting these proteins and their pathways. There are more than 80 members of the GEF family, with 20 of them known to act directly on Rac alone (Marei and Malliri, 2017). These 80 family members are also further characterised, based upon differing catalytic domains, into two families: Dbl and DOCK.

The first Dbl family protein was shown to directly activate Cdc42 (Hart et al., 1991) and the rest of the family are characterised by a Dbl-homology (DH) domain that was shown to be responsible for the catalytic nature of the protein (Hart et al., 1994). The DOCK family protein characterisation came about as a result of the investigation of how DOCK180, a protein that acted as a Rac GEF but had no DH domain, exerted its catalytic effect upon Rac. A domain termed the Dock Homology Region-2 (DHR-2) was discovered to be necessary for this catalytic effect and a new family of GEFs with this domain was established (Cote and Vuori, 2002).

GAPs, though less well studied, are just as important in the regulation of Rho GTPases. The role of GAPs is to activate the intrinsic GTPase activity (GTP hydrolysing) activity of the Rho GTPase (Garrett et al., 1989; Lamarche and Hall, 1994), leading to its inactivation and halting of downstream communication. GAPs contain a conserved RhoGAP domain (Zheng et al., 1993) which allows the binding and effect on Rho GTPases (Peck et al., 2002). The control of Rho GTPases by GEFs and GAPs is what allows strict spatiotemporal control of their activity and the creation of cellular protrusions for migration.

1.7 Aims of the thesis

The actin cytoskeleton plays a huge role in everyday cellular function, and therefore in health and disease. During cancer metastasis, cells use this machinery to move around the body and form secondary tumours. Therefore, it is of utmost importance to understand the basic biology and chemistry of the actin cytoskeleton dynamics as thoroughly as possible. Actin has many binding

partners that regulate its dynamics in a spatiotemporal manner and understanding these is crucial to its role in cell migration and beyond.

The aim of this thesis will be to identify proteins that differentially bind to actin filaments dependent on their differential nucleotide bound state. To date, most of the work to identify F-actin binding proteins has been carried out using actin polymerised with ATP as its bound nucleotide, which is rapidly hydrolysed to ADP. This means that we do not have a clear idea of the proteins that could be binding ATP-actin.

To identify possible specific interactors of ATP-actin, several steps of methodology optimisation are required as follows:

- Optimisation of F-actin affinity columns including conditions for coupling F-actin to affinity media and subsequent constructions of columns

- Optimisation of chromatography on F-actin (ADP-bound) affinity columns and subsequent mass spectrometry to ensure binding of known actin binding proteins and confirm functionality

- Optimisation of methodology to create stable “ATP-F-actin” by loading G-actin with non-hydrolysable analogues of ATP and inducing polymerisation

- Ensuring these filaments contain only the non-hydrolysable analogue of ATP as their bound nucleotide by liquid chromatography – mass spectrometry (LC-MS)

- Optimisation of lysate preparation of two highly motile cell lines for the loading input of affinity columns

Once all the previous steps are optimised we can then perform ADP- and ATP-F-actin affinity chromatography for analysis by mass spectrometry to identify proteins which preferentially bind the latter. With this data we can investigate our hypothesis and explore key questions such as:

- What is the method of ATP-F-actin binding?

- Are the proteins identified as preferentially binding ATP-F-actin doing so in a direct or indirect way?

- What is the biological relevance and function of proteins binding preferentially to ATP-F-actin?

Since our hypothesis is that proteins that preferentially bind ATP-F-actin may be involved in positive regulation of polymerisation, we are particularly interested in any hits involved in Rho GTPase signalling pathways, given their role in regulation of cellular protrusions and movement.

2 Materials and methods

2.1 Materials and reagents

2.1.1 Cell lines

Table 2-1 Cell lines used

Mammalian cell lines		
Name	Description	Source
HEK293T	Human embryonic kidney cell line	Prof L M Machesky
PDAC-B	Pancreatic ductal adenocarcinoma cell line	Prof L M Machesky
JVM3	Chronic B cell leukaemia cell line	Dr Luke Tweedy
COS-7	Monkey kidney fibroblast-like cell line	ATCC 1651
MEF	Mouse embryonic fibroblast cell line	ATCC 1040
B16-F1	Mouse melanoma cell line	Prof L M Machesky
Bacterial strains		
Name	Description	Source
E.coli DH5 alpha	Chemically competent cells (Im, 2011)	Homemade

2.1.2 Reagents

Table 2-2 Reagents used

Mammalian cell culture		
Name	Description	Source
DMEM (Dulbecco's Modified Eagle's Medium)	N/A	Gibco 21969-035
L-Glutamine	N/A	Gibco 25030081
FBS (Fetal Bovine Serum)	N/A	Gibco 16000044
DMEM fully complemented	DMEM + L-glutamine + FBS	Homemade
DMEM SFM (serum free media)	DMEM +L-glutamine	Homemade
RPMI (Roswell Park Memorial Institute) 1640	N/A	Gibco 11875-093
RPM1 1640 fully complemented	RPMI 1640 + FBS	Homemade
FBS (Fetal bovine serum)	N/A	Gibco 10270-106
Trypsin (2.5%, no phenol red)	Mixture of proteases derived from porcine pancreas	Gibco 15090046

PBS (Phosphate buffer saline)	3.3mM KCl, 137mM NaCl, 8mM Na_2PO_4, 1.5mM KH_2PO_4, pH 7.3	Institute central services
PE	0.037% EDTA in PBS	Institute central services
DMSO (Dimethyl sulfoxide)	N/A	Fisher chemical; D/4121/PB08
Cryopreservation media	90% FBS, 10% DMSO	Homemade
Fibronectin bovine plasma	N/A	Sigma-Aldrich F1141
Laminin	N/A	Roche 11243217001
Cell treatments		
Name	Description	Source
Jasplakinolide	Macrocyclic peptide isolated from marine sea sponge *Jaspis johnstoni*, capable of inducing polymerisation and stabilising actin.	Biotechne 2792
Cytochalasin-D	Mycotoxin capable of disrupting actin polymerisation by binding the barbed end of F-actin.	Sigma C2618
Latrunculin-A	Isolated from the marine sea sponge *Latruculia magnifica* and shown to disrupt actin	Calbiochem 428021

	filaments *in vitro*, and sequester actin monomers.	
Affinity chromatography, mass spectrometry and metabolomics		
Name	Description	Source
Actin protein from human platelet	Non-muscle actin purified from human platelets. Isotype composition is 85% ß-actin and 15% γ-actin.	Cytoskeleton APHL99-E
Affi-Gel 10	N/A	Biorad 1536099
Sepharose CL-6B	N/A	Sigma CL6B200
Phalloidin	N/A	Sigma P2141
Zeba spin desalting columns 7K MWCO 2ml	N/A	Thermo 10341164
G-buffer	10mM HEPES-KOH pH8, 0.2mM $CaCl_2$, 0.2mM ATP, 0.5mM DTT	Homemade
G-buffer (No ATP or $CaCl_2$)	10mM HEPES-KOH pH8, 0.5mM DTT	Homemade
F-buffer 10x stock (No ATP)	500mM HEPES-KOH pH8, 20mM $MgCl_2$, 500mM KCl, 5mM DTT	Homemade
F-buffer	50mM HEPES-KOH pH8, 2mM $MgCl_2$, 50mM KCl, 0.5mM DTT, 1mM ATP	Homemade

F-buffer (No ATP)	50mM HEPES-KOH pH8, 2mM $MgCl_2$, 50mM KCl, 0.5mM DTT	Homemade
Post coupling blocking buffer	1M Ethanolamine-HCl pH8	Homemade
Acid elution buffer	100mM Glycine-HCl pH 2.7	Homemade
Salt elution buffer	50mM HEPES-KOH pH8, 0.1M KCl, 2mM DTT	Homemade
Disposable columns 2ml	N/A	Thermo
Sterile H_2O	N/A	Institute central services
Neutralisation buffer for mass spectrometry	100mM AmBic	Homemade
Apyrase	N/A	NEB M0398L
CIP (Alkaline phosphatase calf intestinal)	N/A	New England Biolabs M0525S
EDTA (Ethylenediaminetetra acetic acid)	N/A	Thermo 17892
ADP (Adenosine diphosphate)	N/A	Sigma 1905
AMP-PnP (Adenylyl imidodiphosphate)	N/A	Sigma 10102547001

AMP (Adenosine monophosphate)	N/A	Sigma 1930
ATPγS (Adenosine gamma-triphosphate)	N/A	Jena Bioscience NU-406050
ATP (Adenosine triphosphate)	N/A	Sigma A3377
Protein lysate preparation, SDS-PAGE and Western blotting		
Name	Description	Source
Digitonin	N/A	Sigma D141
Hexylene glycol 99%	N/A	Sigma 112100
Protease Inhibitor cocktail	N/A	Roche 11697498001
Digitonin lysis buffer	50mM HEPES-KOH pH8, 150mM NaCl, 0.5g/ml hexylene glycol, 0.024mg/ml Digitonin	Homemade
SDS-buffer (10x)	Institute central services	1% SDS, 250mM TRIS, 1.9M Glycine
MOPS-SDS running buffer (20x)	N/A	NOVEX NP0001
SDS-PAGE running buffer	MOPS-SDS running buffer (20x) and distilled water	Homemade
4-12% NuPage Bis-Tris gels	10,12 and 15 well	Invitrogen

Sample buffer (4x)	N/A	NOVEX NP0007
Reducing agent (10x)	500mM DTT (Dithiothreitol)	NOVEX NP0004
PageRuler protein ladder	N/A	Thermo 26616
Nitrocellulose blotting membrane 0.45µm	N/A	GE Healthcare 10600002
TBST (Tris-buffered saline-Tween)	150mM NaCl, 10mM TRIS-HCl pH 7.4, 2.7mM KCl, 0.1% Tween20	Institute central services
Transfer buffer	20% methanol, 10x SDS buffer, distilled water	Homemade
Ponceau S	N/A	Sigma P710
BSA (Bovine serum albumin)	N/A	Sigma 10735108001
Blocking buffer	5% BSA, TBST	Homemade
PageBlue Protein Staining Solution	N/A	Thermo 24620
GFP-trap		
Name	Description	Source
GFP-Trap A beads	N/A	Chromotek gta-20
Lysis buffer	25mM Tris HCl pH 7.5, 100mM NaCl, 5mM $MgCl_2$, 0.5% NP-40,	Homemade

	protease inhibitor cocktail, phosphate inhibitor cocktail	
Wash buffer	10mM Tris-HCl pH 7.5, 100mM NaCl, 5mM $MgCl_2$	Homemade
Antibodies and dyes for western blotting and live cell imaging		
Name	Description	Source
Rabbit anti-Arhgef1	Used 1:1000 as primary antibody for western blotting	Abcam 223759
Mouse anti-gelsolin	Used 1:1000 as primary antibody for western blotting	Abcam 11081
Mouse anti-α-tubulin	Used 1:1000 as primary antibody for western blotting	CST 86298S
Rabbit anti-Eps8	Used 1:1000 as primary antibody for western blotting	CST 43114S
Mouse anti-Eps8	Used 1:1000 as primary antibody for western blotting	BD Biosciences 610143
Mouse anti-β-actin	Used 1:1000 as primary antibody for western blotting	CST 3700S
Rabbit anti-β-actin	Used 1:1000 as primary antibody for western blotting	CST 4967S
Rabbit anti-C-Abl	Used 1:1000 as primary antibody for western blotting	CST 2862S

Mouse anti-GFP	Used 1:1000 as primary antibody for western blotting	CST 2955S
Goat anti-mouse DyLight 800	Used 1:10,000 as secondary antibody for western blotting	Thermo 35521
Goat anti-rabbit Alexa Fluor 680	Used 1:10,000 as secondary antibody for western blotting	Invitrogen 21076
Donkey anti-mouse Alexa Fluor 680	Used 1:10,000 as secondary antibody for western blotting	Invitrogen 10038
Donkey anti-rabbit DyLight 800	Used 1:10,000 as secondary antibody for western blotting	Invitrogen 1004
Molecular Biology		
Name	Description	Source
L-broth	N/A	Institute central services
LB-agar 10cm dish	N/A	Institute central services
SOC (Super optimal broth with catabolite repression) media	10mM NaCl, 2mM KCl, 10mM $MgCl_2$, 2% tryptone, 0.5% yeast extract	Formedium SOC0201
TAE (Tris base, Acidic and EDTA) buffer	50x – 2M Tris, 50mM EDTA, 1M Glacial acetic acid pH8.3	Institute central services
Molecular biology grade agarose	N/A	Melford MB12000

DNA gel loading dye (6x)	N/A	Thermo R0611
GeneRuler 1kb DNA ladder	N/A	Thermo SM0311
Gibson assembly master mix	N/A	NEB E2611
Cutsmart buffer	N/A	NEB B7204
Kanamycin monosulphate	N/A	Formedium KAN0025
Ampicillin sodium	N/A	Formedium AMP25
DNA constructs		
Name	Description	Source
pEGFP-N1	Empty backbone for cloning	Prof L M Machesky
pEGFP-C1	Empty backbone for cloning	Prof L M Machesky
LifeAct-TagRFP	LifeAct-mTagRFP-T backbone	Addgene 54586
pEGFP-C1-Eps8-WT	pEGFP-C1 backbone	Addgene 74950
pEGFP-C1-Eps8-Δcap	pEGFP-C1 backbone	Addgene 74786
pEGFP-C1-Eps8-Δbund	pEGFP-C1 backbone	Addgene 74889
pEGFP-C1-Eps8-Δcapbund	pEGFP-C1 backbone	Addgene 74891
pEGFP-C1-Fam107b	pEGFP-C1 backbone	Homemade

pEGFP-C1-Eps8-WT-ABD	pEGFP-C1 backbone	Homemade
pEGFP-C1-Eps8-Δcap-ABD	pEGFP-C1 backbone	Homemade
pEGFP-C1-Eps8-Δbund-ABD	pEGFP-C1 backbone	Homemade
pEGFP-C1-Eps8-Δcapbund-ABD	pEGFP-C1 backbone	Homemade
pEGFP-C1-Eps8-WT-minusABD	pEGFP-C1 backbone	Homemade
pEGFP-C1-Eps8-WT-SH3only	pEGFP-C1 backbone	Homemade
pEGFP-C1-Eps8-WT-PTB	pEGFP-C1 backbone	Homemade
pEGFP-C1-Eps8-WT-PTB-PP	pEGFP-C1 backbone	Homemade
pEGFP-C1-Eps8-WT-ABD-P	pEGFP-C1 backbone	Homemade
pEGFP-C1-Eps8-WT-ABD-P-SH3	pEGFP-C1 backbone	Homemade
pEGFP-C1-Eps8-WT-SH3-PP	pEGFP-C1 backbone	Homemade
Primers		

Name	Sequence	Source
Eps8seq1	ATGTCTAACCGCTCCAGTG	Thermo (Designed on SnapGene)
Eps8seq2	GATGAGGTTAAGGCAAAC	Thermo (Designed on SnapGene)
Eps8seq3	AAGTTGAAGTCCCATATC	Thermo (Designed on SnapGene)
Eps8seq4	TCAACTCCTAATCACCAA	Thermo (Designed on SnapGene)
Eps8seq5	AGATACAAACAACTCCCA	Thermo (Designed on SnapGene)
Eps8seq6	ATCAAAAGACTCCACTCC	Thermo (Designed on SnapGene)
Eps8seq7	GGCAGAAGGAGTGTCAGC	Thermo (Designed on SnapGene)
Eps8seq8	GGACACATTGGAATGCTC	Thermo (Designed on SnapGene)
Eps8seq9	TTTTTGGAGTTTGGTGAT	Thermo (Designed on SnapGene)
Eps8seq10	ATGCGAGATTGTGTTTAG	Thermo (Designed on SnapGene)
Eps8_minusABD_fwd	actcagatctcgagctcaGAATGGTC ATATGTCTAACCGC	Thermo (Designed on NEBuilder for Gibson assembly)

Eps8_minusABD_rev	gttatctagatccggtgTCAGGGCAC AGAAACGGG	Thermo (Designed on NEBuilder for Gibson assembly)
Esp8_ABD+P fwd	actcagatctcgagctcaTCCTTCTG CCCCATCACC	Thermo (Designed on NEBuilder for Gibson assembly)
Eps8_ABD+P rev	agttatctagatccggtgTCAGTGGC TGCTCCCTTC	Thermo (Designed on NEBuilder for Gibson assembly)
Eps8_ABD+P+S fwd	actcagatctcgagctcaACAACCCA AGAAATACGCC	Thermo (Designed on NEBuilder for Gibson assembly)
Eps8_PTB_cds3-591 FWD	actcagatctcgagctcaGAATGGTC ATATGTCTAACCGCTC	Thermo (Designed on NEBuilder for Gibson assembly)
Eps8_PTB_cds3-591 REV	agttatctagatccggtgCTACTCCG GCCGCCTCTTC	Thermo (Designed on NEBuilder for Gibson assembly)
EPS8_PTB_PP_CDS3-660 REV	agttatctagatccggtgCTATGGCA CAGGGGCAGG	Thermo (Designed on NEBuilder for Gibson assembly)
Eps8_sh3only_fwd	tcagatctcgagctcaACAACCCAAG AAATACGCC	Thermo (Designed on NEBuilder for Gibson assembly)
Eps8_sh3only_rev	gttatctagatccggtgCTATGGCAC AAACCCAGAG	Thermo (Designed on NEBuilder for Gibson assembly)

Eps8_511-647 fwd	actcagatctcgagctcaGCCTTTCAAGTCAACTCCTAATC	Thermo (Designed on NEBuilder for Gibson assembly)
Eps8_511-600 fwd	actcagatctcgagctcaGCCTTTCAAGTCAACTCCTAATCACC	Thermo (Designed on NEBuilder for Gibson assembly)
Eps8_511-600 rev	agttatctagatccggtgTCATGGGGGGTCAGCGCG	Thermo (Designed on NEBuilder for Gibson assembly)
Eps8_222-821_fwd	actcagatctcgagctcaGGGGACTGTCACACAGGTG	Thermo (Designed on NEBuilder for Gibson assembly)
Eps8_222-821_rev	agttatctagatccggtgTCAGTGGCTGCTCCCTTC	Thermo (Designed on NEBuilder for Gibson assembly)
Eps8_222-647_rev	agttatctagatccggtgTCAGGGCACAGAAACGGG	Thermo (Designed on NEBuilder for Gibson assembly)

Table 2-3 Kits, glass/plasticware and software used

Commercially available kits		
Name	Description	Source
Precision red advanced protein assay kit	Kit protocol available on manufacturers website	Cytoskeleton ADV02

Pierce BCA protein assay kit	Kit protocol available on manufacturers website	Thermo 23225
Pierce silver stain kit	Kit protocol available on manufacturers website	Thermo 24612
Super signal west femto maximum sensitivity substrate kit	Kit protocol available on manufacturers website	Thermo 34095
Lipofectamine 2000	Kit protocol available on manufacturers website	Invitrogen 116680019
Gel DNA Recovery kit Zymoclean	Kit protocol available on manufacturers website	Zymo Research D4007
Cell Line Nucleofector Kit T	Kit protocol available on manufacturers website	Lonza VCA-1002
Glass and Plastic materials		
Name	Description	Source
35mm glass bottom dish	Live cell imaging	MATTEK P35G
10cm cell culture dish	Cell culture	Corning 430167

6-well cell culture plate	Cell culture and transfection	Falcon 353046
15cm cell culture dish	Cell culture and harvesting	Corning 430599
Pierce Disposable 2ml columns	Used for main chromatography experiments	Thermo 29920
3.2ml thickwall polycarbonate tube	For high-speed centrifugation	Beckman 362305
Nunc non-treated T175 EasYFLask with filter cap	Cell culture of suspension cells	Thermo 159927
Software and websites		
Name	Description	Version or link
NEBuilder	New England Biolabs	Version 2.8.2
ImageStudioLite	LICOR	Version 5.2
Prism	GraphPad	Version 9.2.0
Fiji	ImageJ	Version 1.8.0_322
Nucleotide BLAST	National Center for Biotechnology Information	https://blast.ncbi.nlm.nih.gov/
Zotero	Digital Scholar	Version 6.0.30

Adobe Illustrator	Adobe	Version 28.1
Zen microscopy	Zeiss	Version 3.9
SnapGene	Dotmatics	Version 7.1
Gene Ontology	Global Core Biodata Resource	https://geneontology.org/
STRING Protein-Protein Interaction Networks	Global Core Biodata Resource	https://version-12-0.string-db.org/

2.2 Methods

2.2.1 Cell culture

2.2.1.1 Culture conditions

HEK293T, PDAC-B, COS-7, MEF and B16-F1 cells (all adherent cell lines used) were cultured in 10cm dishes in Dulbecco's Modified Eagle Medium (DMEM) supplemented with 10% FBS and 2mM L-Glutamine. JVM-3 cells were cultured in Nunc Non-treated T175 EasYFlasks with filter caps, due to their non-adherent nature, and in Roswell Park Memorial institute (RPMI) 1640 media supplemented with 10% FBS (RPMI 1640 already contains L-Glutamine). All cells were kept in incubators maintaining an environment of 37ºC and 5% CO_2.

2.2.1.2 Cell collection, subculture and counting

Upon reaching the desired confluency, adherent cells were collected by washing with phosphate buffered saline (PBS) and detached by using 0.25% trypsin in PE buffer and incubating at 37ºC. Cells were checked under a light microscope to ensure proper detachment and then resuspended in the appropriate

complemented media to abolish the activity of trypsin. A small amount of this suspension was used with the cell counter and the amount was calculated automatically; this was performed in triplicate for accuracy. This was performed for each cell line being used for an experiment and allowed the correct number of cells to be used. Cells were then passaged at either 1 in 10 or 1 in 20 ratios depending on the speed of their growth. Passage number was recorded on each dish and the cells were disposed of around passage 20.

2.2.1.3 Cryopreservation and recovery

Cells were collected as above in a 15ml falcon tube and centrifuged at 1000 rpm for 5 minutes. The pellets were then suspended in PBS and pelleted again as a wash step. The pellets were then suspended in freezing media (90% FBS/ 10% DMSO) and aliquoted into 2ml cryogenic tubes. There were then placed in "Mr Frosty" freezing containers that ensure 1ºC/minute cooling rate before being placed in a -80ºC freezer. They were moved to liquid nitrogen cell stores the following day. To recover the cells, the vials were collected from liquid nitrogen stores and immediately incubated at 37ºC in a water bath. Upon defrosting, the contents of the vial were diluted in 10ml fully complemented media appropriate for that cell line in a 15ml falcon tube. This was centrifuged at 1000 rpm for 5 minutes and the pellet suspended in fresh media to remove DMSO content. The cells were then plated in 10cm dishes, and the media was changed the following day to remove any dead unattached cells. Once the cells were confluent they were maintained as described above.

2.2.2 Cell transfection

2.2.2.1 Lipid-based transfection

Cells were collected and counted as above, then plated into a 6-well dish at $1x10^6$ cells/well. These were incubated and allowed to adhere throughout the day. 250µl lipofectamine transfection "mastermix" was prepared per well. To do this, 2.5µg of each plasmid was added to 125µl SFM and 5µl lipofectamine was added to 125µl SFM and these were then mixed and incubated at room temperature for 10 minutes before adding to the appropriate wells of the 6-well plate prepared earlier in the day. The following morning the cells were checked under a light microscope to ensure they remained healthy, then checked under a

fluorescence microscope to check if transfection was successful. If successful, the cells were then collected, counted, and plated on a 35mm glass bottom dish for imaging. This method was used for B16-F1 and COS-7 cells.

2.2.2.2 Electroporation-based transfection

MEF cells were transfected using AMAXA-T kit. Cells were collected and counted as before and $1x10^6$ cells were added to a falcon tube and centrifuged at 1000 rpm for 5 minutes to pellet the cells. They were then washed with PBS, centrifuged again and the PBS supernatant aspirated carefully leaving only the cell pellet. The AMAXA-T buffer was then prepared by adding 83 µl buffer "T" to 17µl of "supplement 1". 5µg of plasmid DNA was added and the entire mixture was used to resuspend the cell pellet which was then transferred into an electroporation cuvette. The mixture was then electroporated using program "T-20" and then removed from the electroporator. Media was added to the cuvette and the mix was transferred into a 6-well dish with fully complemented media. The following morning the cells were checked under a light microscope to ensure they remained healthy, then checked under a fluorescence microscope to check if transfection was successful. If successful, the cells were then collected, counted, and plated on a 35mm glass bottom dish for imaging.

2.2.3 Live cell imaging

35mm glass bottom dishes were coated with laminin to allow cells to adhere and migrate on the surface. 250µl 1:100 laminin in PBS was added to each dish and they were incubated either for an hour at room temperature or overnight at 4ºC with gentle agitation on a rocker to ensure even coverage. Before use the dishes were washed 3x with PBS. The following morning cells were collected, counted, and transferred onto the glass bottom dishes and left to adhere in the incubator maintaining an environment of 37ºC and 5% CO_2. Cells were then checked under a light microscope to check adherence; media was changed, and they were transferred to the incubator in the microscopy facility. The Zeiss 880 LSM Airyscan microscope was prepared for live cell imaging at 37ºC and 5% CO_2. The glass bottom dish or plate was then transferred into the microscope and left to settle for 10 minutes before imaging commenced using a 63x objective. Still images or videos were taken depending on the cell type or experiment. Airyscan

processing of the images or videos was done in ZEN software and the analysis was carried out in Fiji.

2.2.4 Affinity Chromatography

2.2.4.1 Reconstituting purified actin

Lyophilised purified non-muscle actin was stored at 4ºC until it was reconstituted by adding 100µl sterile H_2O and incubated at room temperature and on ice, for 30 minutes each for a total of three cycles. This process gives 10mg/ml actin in 5mM Tris-HCl pH8, 0.2mM $CaCl_2$, 0.2mM ATP.

2.2.4.2 Buffer exchange

Since the activated affinity media we used for construction of the columns is amine reactive, the purified actin was transferred into a suitable buffer. This was done using 0.5ml Zeba spin desalting columns with 7k molecular weight cut off. The spin columns were centrifuged to remove their storage buffer then equilibrated with HEPES based G-buffer. The exact composition of the G-buffer was dependant on the desired nucleotide state of the eventual actin filaments. Briefly, the G-buffer had different $CaCl_2$ and actin concentrations depending on the experiment. The columns were equilibrated with the appropriate G-buffer by going through three cycles of adding 300µl G-buffer, centrifuging at 1500g for one minute and discarding the flow through buffer. The actin was then passed through the exchange columns and collected in a tube containing an appropriate amount of G-buffer as needed for the next steps. Protein concentration was checked before and after the exchange to ensure no loss of protein.

2.2.4.3 Nucleotide loading of G-actin

To prepare ADP-F-actin, the buffer change in the previous section was carried out but there was no need for nucleotide loading. This is because the ATP will naturally be hydrolysed to ADP upon polymerisation. For the ATP-F-actin columns, three methods were optimised to facilitate the exchange of ATP to a non-hydrolysable analogue, ATPγS. To begin, all actin samples were diluted in the same G-buffer composition they were exchanged into to a final

concentration of 2mg/ml actin. All methods consisted of three cycles of treatments and buffer exchanges.

For the method using EDTA, the G-buffer was made without $CaCl_2$ and for all three methods, without any ATP. Upon dilution the first round of treatments were added to the purified actin. EDTA was added to a final volume of 5mM, 50 units of CIP added, and 10 units of apyrase added each to the appropriate sample. For all three methods 5mM ATPγS was added at the same time. The $CaCl_2$ concentration of the samples with CIP or apyrase were adjusted to 5mM. These samples were then left to incubate with gentle agitation at 4ºC for six hours. The buffer exchange was carried out using 2ml Zeba spin desalting columns, due to the higher volume of the samples after dilution. These were equilibrated with the appropriate composition of G-buffer and the samples were passed through the column, and the same additions of "treatment" and excess nucleotide as before were added. This process was repeated three times to ensure maximal nucleotide exchange. As in the previous section, the protein concentration of each sample was checked after each exchange.

2.2.4.4 Polymerising actin

10x F-buffer was added to each sample to induce polymerisation. F-buffer with ATP was only used for samples with no nucleotide loaded, to be used as ADP-F-actin columns. Samples were left to incubate for one hour at room temperature and phalloidin was added to a final concentration of 75µg/ml, giving a 2x molar excess of phalloidin to actin. Phalloidin treatment was necessary to stabilise the polymerised actin and allow the preparation of the affinity columns.

2.2.4.5 Affinity resin preparation and coupling

250µl Affi gel 10 resin was prepared per column by three cycles of washing with F-buffer (no ATP) and centrifugation at 2000g for 1 minute. Polymerised actin was added to the resin slurry, making a final volume of 1ml and $CaCl_2$ concentration was adjusted to 80mM for the coupling reaction only. Resin and actin mixtures were then left to couple overnight at 4ºC with gentle agitation.

2.2.4.6 Blocking, packing and analysing coupling

To block any remaining active esters of the affinity media 25µl of 1M Ethanolamine-HCl was added to each mixture of 1ml, and the samples were incubated for 1 hour at 4ºC with gentle agitation. 250µl Sepharose CL-6B beads were prepared for each resin mixture by washing (same method as Affi gel) and added to each sample. They were then incubated for a further 30 minutes at 4ºC with gentle agitation to ensure they were thoroughly mixed.

2ml disposable columns were then prepared by adding the stopper and washing with F-buffer (no ATP), always leaving some in the column and capping them. The samples were then transferred into the appropriately labelled columns and left to settle for 30 minutes at 4ºC. The columns were then uncapped, and the coupling supernatant collected before the columns were washed 5 times with F-buffer (no ATP) to remove any uncoupled protein. The washes were also collected for analysis by SDS-PAGE to determine whether coupling was successful. A sample of each column was then taken for analysis by metabolomics and SDS-PAGE.

2.2.4.7 Liquid chromatography – mass spectrometry

The LC-MS to analyse the nucleotide composition of samples was carried out by Dr David Sumpton who provided the following methodology: Metabolites from the biological extracts were injected (5 µl) and separated using a ZIC-pHILIC column (SeQuant; 150 mm × 2.1 mm, 5 µm; Merck) coupled with a ZIC-pHILIC guard column (SeQuant; 20 mm × 2.1 mm) using an Ultimate 3000 HPLC system (Thermo Fisher Scientific). Chromatographic separation was performed using a 15-min linear gradient starting with 20% ammonium carbonate (20 mM, pH 9.2) and 80% acetonitrile, terminating at 20% acetonitrile at a constant flow rate of 200 µl min^{-1}. The column temperature was held at 45 °C. A Q Exactive Orbitrap mass spectrometer (Thermo Fisher Scientific) equipped with electrospray ionization was coupled to the HPLC system for both metabolite profiling and metabolite identification. For profiling, the polarity switching mode was used with a resolution of 35,000 or 70,000 at 200 m/z to enable both positive and negative ions to be detected across a mass range of 75 to 1,000 m/z (automatic gain control (AGC) target of 1 × 106 and maximal injection time (IT) of 250 ms).

2.2.4.8 Preparation of lysate

Cells were plated two days prior to chromatography experiments to allow them to reach desired confluency. HEK293T and PDAC-B cells were grown in 60 15cm dishes and JVM-3 cells were grown in 30 T175 flasks with filter caps because they grow in suspension. To harvest the cells JVM3 the cell suspension from each flask was transferred into falcon tubes to be centrifuged at 500g for 10 minutes. The cell pellets were then washed in ice cold PBS and aliquoted into smaller falcon tubes before centrifuging again and removing the supernatant. HEK293T and PDAC-B cell lines were collected by washing with PBS and detached by using 0.25% trypsin in PE buffer and incubating at 37ºC. Cells were checked under a light microscope to ensure proper detachment and then resuspended in the appropriate complemented media to abolish the activity of trypsin. The cell suspensions were then centrifuged at 500g for 10 minutes and the cell pellet was washed with PBS, and aliquoted in the same way as the suspension cells. Digitonin lysis buffer was then used to resuspend the cell pellet at a ratio of 10:1 to the size of the pellet e.g. a 100µl pellet was resuspended in 1ml digitonin lysis buffer. Lysates were then incubated for one hour at 4ºC on an end-over-end rotator before being centrifuged at 2000g for 10 minutes at 4ºC. The supernatant was collected and centrifuged again at 100,000g for one hour to ensure only cytosolic lysate was present and any polymerised actin in the lysate was removed. The lysate protein concentration was quantified and diluted to 2mg/ml with a total volume of 2ml lysate for each column.

2.2.4.9 Chromatography

Columns were equilibrated by washing with 1ml lysis buffer each before the lysate was loaded on the uncapped columns and allowed to flow through. The columns were then washed 5 times with lysis buffer before the elution step using 1ml 100mM glycine-HCl pH 2.7. The eluate was collected in tubes containing 500µl 100mM ammonium bicarbonate to neutralise.

2.2.5 Mass spectrometry analysis of eluate

The mass spectrometry and analysis were carried out by Sergio Lilla who provided the following methodology.

2.2.5.1 Sample preparation for mass spectrometry

Glycine buffer column eluates were neutralised using 100mM ammonium bicarbonate to a final pH of 8.0. Proteins were reduced with 10mM DTT and subsequently alkylated in the dark with 55 mM Iodoacetamide, both reactions were carried out at room temperature. Alkylated proteins were then cleaved using a two-step digestion: first with Endoproteinase Lys-C (ratio 1:33 enzyme: lysate, Promega) for 1 hour at 37 °C then with Trypsin (ratio 1:33 enzyme: lysate, Promega) overnight at 35 °C. Samples were desalted after digestion using StageTip (Rappsilber et al., 2007) prior to MS analysis.

2.2.5.2 Mass spectrometry

Peptides resulting from all digestions were separated by nanoscale C18 reverse-phase liquid chromatography using an EASY-nLC II 1200 (Thermo Scientific) coupled to an Orbitrap Q-Exactive HF (Thermo Scientific). All acquisitions were carried out in data-dependent acquisition mode (DDA) using Xcalibur software (Thermo Scientific). A nanoelectrospray ion source (Sonation) was used for ionisation in positive mode. Chromatography was carried out at a flow rate of 300 nl/min using 20 cm fused silica emitters (New Objective) packed in house with reverse phase Reprosil Pur Basic 1.9 µm (Dr. Maisch GmbH). An Active Background Ion Reduction Device (ABIRD) was used to decrease air contaminants signal level. Peptides were eluted with a two-step gradient method, over a total run time of 125 mins. A full scan was acquired at a resolution of 60000 at 200 m/z, over mass range of 375-1400 m/z. HCD fragmentation was triggered for the top 15 most intense ions detected in the full scan. Ions were isolated for fragmentation with a target of 1E5 ions, for a maximum of 75 ms, at a resolution of 15,000 at 200 m/z. Ions that have already been selected for MS2 were dynamically excluded for 30 sec.

2.2.5.3 Mass spectrometry data analysis

All acquired MS raw data were processed using MaxQuant (Cox and Mann, 2008) version 1.5.5.1 or 1.6.3.3 and searched with Andromeda search engine (Cox et al., 2011) against the Uniprot *Homo sapiens* database. First and main searches were carried out with a precursor mass tolerance of 20 ppm for the first search, 4.5 ppm for the main search and for the MS/MS the mass tolerance was set to 20

ppm. Minimum peptide length was 7 amino acids and trypsin cleavage was selected allowing up to 2 missed cleavage sites. Methionine oxidation and N-terminal acetylation were selected as variable modifications and Carbamidomethylation as a fixed modification.

All MaxQuant outputs were processed with Perseus (Tyanova et al., 2016) version 1.5.5.3. The Reverse, Contaminant and "Only identified by site" hits were removed, and only protein groups identified with at least one unique peptide were allowed in all lists of identified protein groups. The protein abundance was measured using label-free quantification algorithm available in MaxQuant (Cox et al., 2014) and reported in the ProteinGroups.txt file. Only proteins robustly quantified in all three replicates in at least one group, were allowed in the list of quantified proteins. Missing values were imputed separately for each column, and significantly enriched proteins were selected using a permutation-based Student's t-test with FDR set at 5%.

2.2.6 SDS-PAGE, Coomassie staining, silver staining, western blotting and chemiluminescence

2.2.6.1 Preparation of samples

Protein lysate samples were prepared as in previous section and were quantified using Precision red advanced protein assay and diluted to a concentration of 1mg/ml or normalised to the lowest concentration of lysate per experiment. NuPAGE reducing agent and sample buffer was then added to samples before incubation at 100ºC for 10 minutes.

2.2.6.2 SDS-PAGE

4-12% NuPage Bis-Tris pre-cast acrylamide gels were used with either 10, 12 or 15 wells depending on experiment, number of samples or the subsequent staining steps. Gels were prepared by washing the wells with MOPS running buffer and placed into an electrophoresis tank containing the same buffer. The recommended volume of sample was added to each well according to the manufacturer's instructions for each size and 5µl pre-stained PageRuler protein ladder was added to gels for Coomassie staining and western blotting, and 1µl pre-stained PageRuler protein ladder was added to gels for silver staining and

chemiluminescence. The gels were then run at 130V for 90 minutes with checks throughout to ensure no error or interruptions.

2.2.6.3 Coomassie staining

For visualisation of protein bands directly on the acrylamide gels from the previous section, Coomassie staining was carried out using PageBlue Protein Staining Solution. Gels were transferred from the tank into a plastic dish and washed three times with distilled H_2O for 10 minutes each and then incubated in 50ml PageBlue Protein Staining Solution for 1 hour at room temperature with gentle agitation. Gels were then washed with distilled H_2O every 30 minutes for a total of 3 hours, and then imaged using a LICOR Odeyssey CLx scanner and analysed using Image Studio Lite.

2.2.6.4 Silver staining

For more sensitive visualisation of protein bands directly on the acrylamide gels from the previous section, Pierce Silver Stain kit was used. The gel was washed in distilled H_2O twice for 5 minutes each, fixed in a solution of 10% acetic acid and 30% ethanol, washed in 10% ethanol twice for 5 minutes each and then washed again in distilled H_2O twice for 5 minutes each. Sensitiser working solution was then prepared from the kit and the gel was incubated in this for 1 minute, and then washed in distilled H_2O twice for 1 minutes each. Stain working solution was then prepared from the kit using the enhancer and stain solutions, and the gel was stained with this solution for 30 minutes with gentle agitation. Developer working solution was then prepared using the enhancer and developer kit solutions. After 30 minutes of staining the gel was washed twice for 20 seconds each in distilled H_2O before the developer solution was added and the gel developed for 1-2 minutes, with the reaction being closely watched and stopped when optimal staining was achieved. This differed per experiment due to the difference in concentration of samples per experiment. The reaction was stopped by incubating the gel in a solution of 5% acetic acid for 10 minutes. The gels were then washed in distilled H_2O for 10 minutes before imaging using a back-lit portable gel doc system and analysing in Image Studio Lite.

2.2.6.5 Western blotting

Separated proteins from polyacrylamide gels and SDS-PAGE were transferred onto 0.45µm nitrocellulose blotting membranes in a BioRad electrotransfer tank. The gels were prepared in cassettes for the BioRad tank using sponges and paper as well as the membranes. The cassettes were then placed in the tank which had an ice pack added and then filled with transfer buffer before running at 100V for 90 minutes. To ensure the transfer was successful, the membranes were placed in plastic dishes containing ponceau S solution to allow instant visualisation of transferred proteins. The membranes were then washed three times for 10 minutes each in TBST wash buffer before being blocked at room temperature for one hour with gentle agitation using a TBST buffer with 5% BSA added. Primary antibody solutions were prepared in the same buffer and incubated at 4ºC overnight with gentle agitation. The following morning the membranes were washes three times with TBST wash buffer for 10 minutes each before incubating for 1 hour at room temperature with different Alexa-Fluor conjugated secondary antibodies at a dilution of 1:10,000, depending on the species of primary antibodies that were used per experiment. After incubation, the membranes were washed three times in TBST wash buffer for 10 minutes each before imaging on the LICOR Odyssey CLx scanner. Analysis was carried out in Image Studio Lite.

2.2.6.6 Chemiluminescence

For extremely sensitive detection of protein on membranes prepared by western blotting, Thermo SuperSignal West Femto Maximum Sensitivity kit was used. Membranes were prepared in the same way as the previous section until the stage of secondary antibody addition. Instead, a secondary antibody HRP (horse radish peroxidase) conjugate was used at a dilution of 1:100,000 and incubated at room temperature for one hour with gentle agitation. The membranes were then thoroughly washed with distilled H_2O six times for 5 minutes each. Whilst washing, the substrate working solution was prepared by mixing equal parts of the substrate and stable peroxide solutions from the kit to a total volume of 10ml per membrane. The membranes were then incubated with the substrate working solution for 5 minutes before being places in between two clear plastic wrap protectors and any excess liquid or bubbles removed by pressing carefully.

The membranes were then imaged using a ChemiDoc Bio-Rad system and analysed using Image studio Lite.

2.2.7 GFP-trap

GFP-trap is an affinity resin designed to facilitate immunoprecipitation of GFP-tagged proteins. The agarose beads are coupled with a GFP nanobody which allows target proteins to be collected from cell lysate.

B16-F1 cells were cultured and transfected in 15cm dishes with no construct, GFP-only and GFP- construct of interest using lipofectamine as in 2.2.2.1 sections. The following morning the cells were washed twice with PBS before 400µL GFP-trap lysis buffer was added and cells detached using a cell scraper and collected in a 1ml Eppendorf tube which was kept on ice for one hour. Lysate was then centrifuged at 13krpm for 15 minutes and the supernatant was collected in a new tube. The amount of protein in the lysate was then quantified using precision red advanced protein assay. GFP-trap beads were washed three times in 500µl GFP-trap wash buffer by suspension and centrifugation at 2000g for 1 minute each time. The cell lysate was then added to the beads and the mixture was incubated for 2 hours at 4ºC with gentle agitation. After incubation the mixture was centrifuged at 2000g for 2 minutes, resuspended and washed in GFP-trap wash buffer and incubated for 5 minutes at 4ºC. This process was repeated three times to ensure beads were washed thoroughly. The washed beads were then suspended in the appropriate amount of prepared 2x sample buffer and SDS-PAGE and western blotting was carried out as in previous sections.

2.2.8 Molecular biology and cloning

2.2.8.1 Primer design

Primers were designed using either SnapGene or NEBuilder website (for Gibson assembly reactions). Forward and reverse primers were designed based on the required DNA fragments and chosen restriction sites. The primers designed using NEBuilder were set to have an overlap of 18 nucleotides between fragments and Phusion HF polymerase was chosen. TE buffer was added to primers to give 100µM stock solutions.

2.2.8.2 PCR (Polymerase chain reaction)

25µl reactions were prepared for each PCR consisting of 1x Primestar Max enzyme/nucleotide/buffer mix, 0.5µM primers and 1-10ng DNA template and made up to target volume with H_2O. Each reaction was performed twice at the following program:

1. Initial Denaturation at 98ºC for 5 minutes
2. Denaturation for all repeat cycles at 98ºC for 10 seconds
3. Annealing at 60ºC for 10 seconds
4. DNA synthesis at 72ºC for 90 seconds
5. Steps 2-4 repeated 14 times for a total of 15 cycles
6. Final extension at 72ºC for 10 minutes
7. Reaction finished at 4ºC

2.2.8.3 Restriction digest

Digestion mixtures were made up to a total volume of 20µl containing 0.5µl of each enzyme, 2µl enzyme buffer (all enzymes and buffers from NEB- CutSmart buffer used), 1µl of plasmid DNA (~3-4µg), 0.5µl BSA and H_2O. The reaction was incubated at 37ºC for 2 hours before agarose gel electrophoresis and purification.

2.2.8.4 Agarose gel electrophoresis and purification of DNA

0.8% agarose gel prepared using molecular biology grade agarose dissolved in 1xTAE with heating (microwave) and periodic agitation. Suspension left to cool before adding Midori Green Advance DNA stain (Geneflow) (2µl per 100ml gel) and casting into a tray: gel was allowed to set for 1 hour. Samples prepared in 1x DNA loading buffer were loaded into the gel alongside GeneRuler DNA ladder and electrophoresis was performed at 70V for 1 hour. DNA bands were then

visualised with a long-wave UV lamp (365nm), cut out from the gel and purified using ZymoClean DNA recovery kit following manufacturer's instructions.

2.2.8.5 Gibson assembly

100ng of vector and a 2-fold molar excess of insert (prepared with primers designed for Gibson assembly on NEBuilder) was mixed with 10µl Gibson assembly master mix and made up to a final volume of 20µl with H_2O before incubation at 50ºC for 1 hour.

2.2.8.6 Transformation of competent cells

E.coli Dh5α competent cells were mixed with 4µl of DNA mixture and left on ice for 30 minutes. The cells were then subjected to 90 seconds heatshock at 42ºC and placed back on ice for 2 minutes before 500µl SOC media was added and incubated at 37ºC for an hour with gentle agitation. LB-agar plates containing either ampicillin (50μg/ml) or kanamycin (50μg/ml) were warmed at 37ºC and cells were then spread on the plates before leaving at 37ºC overnight.

2.2.8.7 Miniprep and maxiprep

For minipreps, colonies were picked from the LB-agar plates using a sterile pipette tip and transferred into a sterile tube with 3ml LB medium and antibiotic (ampicillin or kanamycin, (50μg/ml)) and incubated at 37ºC overnight with agitation. Institute central services performed purification of the plasmids using QIAprep miniprep kit. Miniprep products were analysed by restriction digestion to check if insertion was successful, with successful samples being sent for sequencing, again performed by the Institute central services. Aliquots of cultures of successful clones were re-grown in 250ml LB media and appropriate antibiotic overnight with agitation at 37ºC overnight. Maxipreps were performed by Institute central services and provided in nuclease free water at a DNA concentration of roughly 5mg/ml.

2.2.9 Statistical analysis

Statistical analysis was carried out in GraphPad Prism version 9.2.0. The statistical tests used in any given dataset is named in the figure legend.

Statistical significance was recognised if $p<0.05$ and was denoted with asterisks as follows: $p<0.05$ *, $p<0.01$ **, $p<0.001$ *** and $p<0.0001$ ****.

3 Optimising F-actin affinity columns for chromatography

3.1 Introduction

To identify proteins which bind differentially to ADP- and ATP-F-actin using chromatography, we had to first optimise a methodology for preparing affinity columns with immobilised actin. The actin had to be in the filamentous form, and stable enough to remain bound to the column throughout washing and all subsequent chromatography steps. Another consideration was the optimum concentration and properties of the lysate to be used on the column. The method of elution of "target" proteins also had to be optimised and prepared in a way that was suitable for the subsequent steps of mass spectrometry of the samples. The first columns made were those containing ADP-F-actin only, to optimise the method and validate that the columns could bind known actin binding proteins, and that these could be identified in the next step of mass spectrometry.

3.2 Results

3.2.1 Preparation of F-actin and affinity resin

Lyophillized non-muscle actin was reconstituted to a concentration of 10mg/ml and transferred into a buffer suitable for chromatography using equilibrated Zeba spin desalting columns with collection in a HEPES-based G-buffer. The prepared protein solution was then diluted with G-buffer to give an actin concentration of 2mg/ml. The concentration of salts and ATP were then adjusted to transform the buffer into F-buffer which promotes polymerisation of the G-actin into F-actin. Phalloidin was then added to the sample, to a final concentration of 75µg/ml to achieve a 2x molar excess of phalloidin:actin which stabilises the actin in its filamentous form. Activated affinity chromatography media was prepared in F-buffer and incubated with the F-actin in solution overnight. To ensure no active esters remained after the coupling that would disrupt the chromatography the samples were incubated with a blocking solution of ethanolamine-HCl. To improve the flow properties of the samples for chromatography, a suspension of agarose cross-linked beads (Sepharose CL6B)

was added before the prepared actin-resin was packed into columns and washed. Finally, a small sample of the resin was taken to be analysed by SDS-PAGE to check the coupling of actin to the resin had been successful. The supernatant from coupling and the various washes were also collected for analysis by SDS-PAGE to allow for trouble shooting in the case of failed coupling or to identify steps on which it could be further optimised.

3.2.2 High concentrations of calcium are required for preparation of F-actin affinity columns

Since we required a buffer with specific properties and concentrations of salt to stabilise actin in its filamentous form, it was important to investigate the effect of these properties on the coupling reaction. SDS-PAGE analysis of the samples from a coupling reaction in the unmodified F-buffer showed high amounts of actin in the coupling supernatant and not in the resin, meaning the coupling was unsuccessful (Figure 3-1a). The addition of salts is recommended by the manufacturer to increase coupling efficiency of acidic proteins to the affinity media in use. For this reason, $CaCl_2$ concentration was adjusted to the recommended 80mM, and stable and efficient coupling was achieved (Figure 3-1b). The SDS-PAGE analysis of these samples showed small amounts of actin in the coupling supernatant and large amounts in the resin sample, comparable to the control (Figure 3-1c-f).

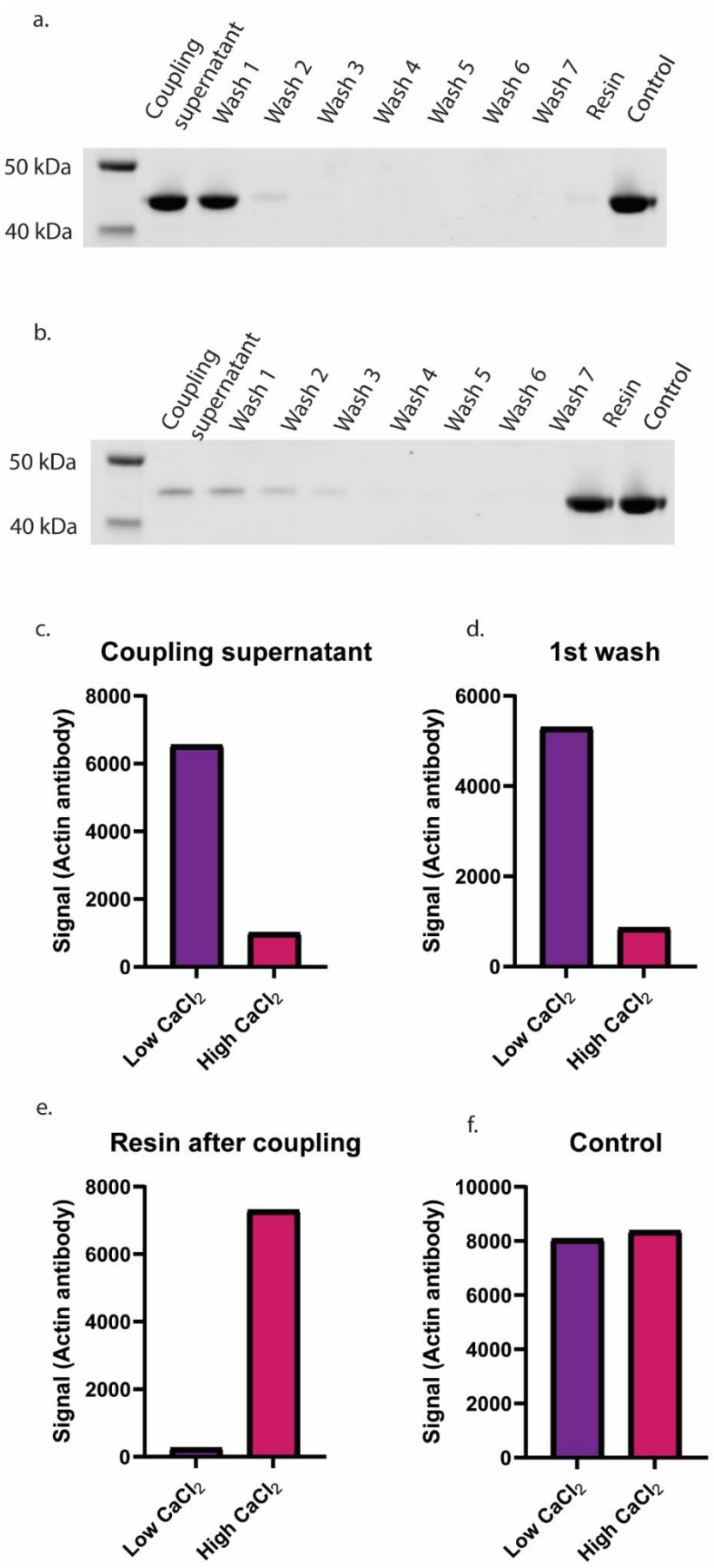

Figure 3-1 Increased calcium concentration allows F-actin to couple to resin

a. SDS-PAGE of supernatant, wash, resin. Final well has 1.6µg actin as a control. Resin column shows a low amount of actin, indicating unsuccessful coupling. The molecular weight markers are shown on the left of the imaged gel.

b. SDS-PAGE of supernatant, wash, resin. Final well has 1.6µg actin as a control. Resin column shows a high amount of actin, indicating successful coupling. The molecular weight markers are shown on the left of the imaged gel.

c. Quantification of the protein concentration (actin) from the coomassie stainings in A and B comparing for each indicated stage of the coupling the conditions of low and high calcium. The data show high actin concentration in low calcium samples during the process of coupling, and low for the high calcium samples (c-d). The post coupling sample of the resin shows high actin concentration indicative of successful coupling (e). Control samples of known amount of actin from both conditions show similar signals (f).

3.2.3 Preparation of cellular lysate for affinity chromatography

For the first chromatography experiments using only columns prepared with ADP-F-actin and for the sake of optimisation of the process, human embryonic kidney cells (HEK) were selected for ease of culture and high protein concentration. Several different methods of lysis and lysis buffers were tested to ensure efficiency for large amounts of protein and the stability of the protein in the lysate. The preferred method was collection of cells by trypsinisation, centrifugation and resuspension followed by agitation of the pelleted cells in a gentle lysis buffer containing digitonin for the solubilisation of the cytosolic fraction only, as it cannot disrupt organelle or nucleus membranes due to different concentrations of cholesterol (Baghirova et al., 2015).

To ensure optimum binding of proteins to the F-actin immobilised on the column, cells were treated with phalloidin upon lysis and before centrifugation to remove cellular F-actin from the lysate (Figure 3-2).

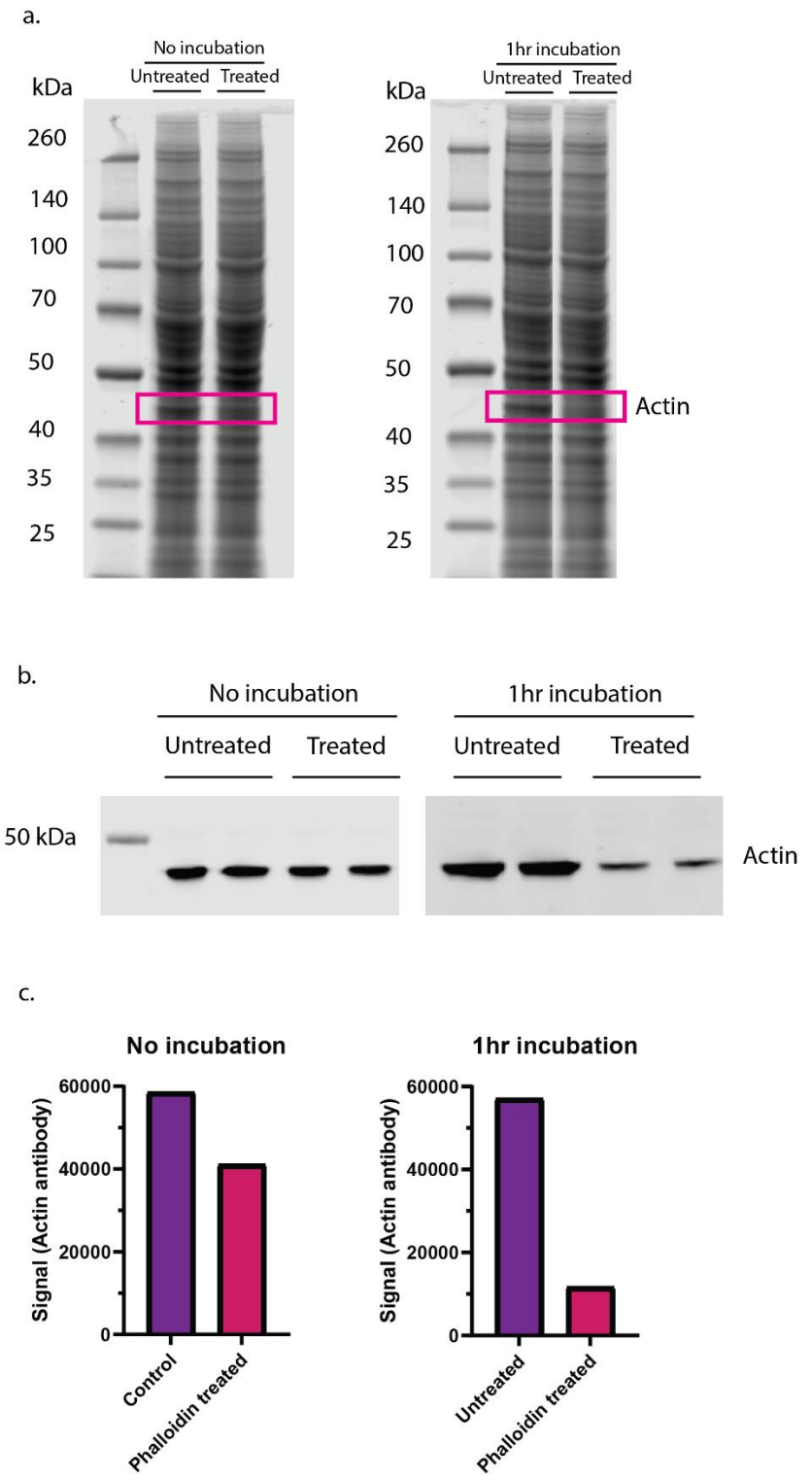

Figure 3-2 Phalloidin treatment can remove majority of F-actin from cytosolic lysate with centrifugation

a. SDS-PAGE analysis of HEK cell ultracentrifuged cytosolic lysate obtained by lysing cells immediately after adding phalloidin (no incubation) and by lysing cells with one hour incubation with phalloidin. Pink box highlights protein bands of interest (actin) which were confirmed by western blotting (b). The molecular weight markers are shown on the left of the imaged gel. Lysis buffer is 50mM HEPES-KOH pH8, 150mM NaCl, 0.5g/ml hexylene glycol, 0.024mg/ml Digitonin.

b. Western-blot images comparing the presence of actin between ultracentrifuged samples immediately lysed with phalloidin and those incubated for one hour. Actin levels are strongly reduced after one hour phalloidin treatement. The molecular weight markers are

shown on the left of the imaged gel. Lysis buffer is 50mM HEPES-KOH pH8, 150mM NaCl, 0.5g/ml hexylene glycol, 0.024mg/ml Digitonin. Duplicates of each condition are shown.

c. Quantification of reduction of actin as seen by Western-blot analysis in b. Immediate lysis with phalloidin samples show ~30% reduction and one hour incubated samples show ~80% reduction. Lysis buffer is 50mM HEPES-KOH pH8, 150mM NaCl, 0.5g/ml hexylene glycol, 0.024mg/ml Digitonin.

3.2.4 Optimisation of elution

After we had optimised the preparation of the affinity columns and the lysate to be run on them, we performed some preliminary experiments to test the functionality of the columns and other practical issues such as flow rate. The optimum concentration of cytosolic lysate to allow an efficient flow rate on the column was determined to be 2mg/ml so they were prepared to this concentration for all chromatography experiments.

Firstly, elution buffers that would not denature the captured proteins were tested. Stepwise salt elution buffers initially removed some of the captured protein (Figure 3-3 sample 9) but analysis of the resin post elution showed a lot of bound protein remained (Figure 3-3 sample 12).

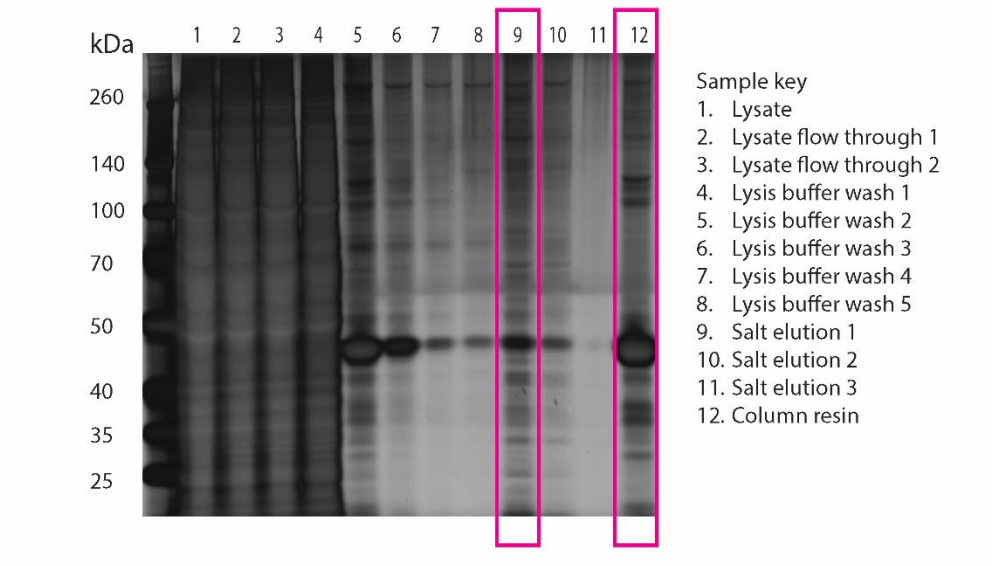

Figure 3-3 Stepwise salt elution buffers are not enough to remove captured proteins
Image of silver stained SDS-PAGE analysis of samples from chromatography of an ADP-F-actin column. Pink boxes show lanes of interest, a partial elution by salt buffer in lane 9 and protein remaining on the column in lane 12. The lanes of the imaged gels are numbered with a sample key on the right. The molecular weight markers are shown on the left of the imaged gel.

Several other elution buffers were tested which would change the conditions of the resin by lowering the pH (Glycine-HCl), increasing the ionic strength (LiCl) and denaturing the bound protein (SDS). The Glycine-HCl acid buffer that lowered the pH of the column was the most efficient elution (Figure 3-4) and was used for the rest of the chromatography experiments.

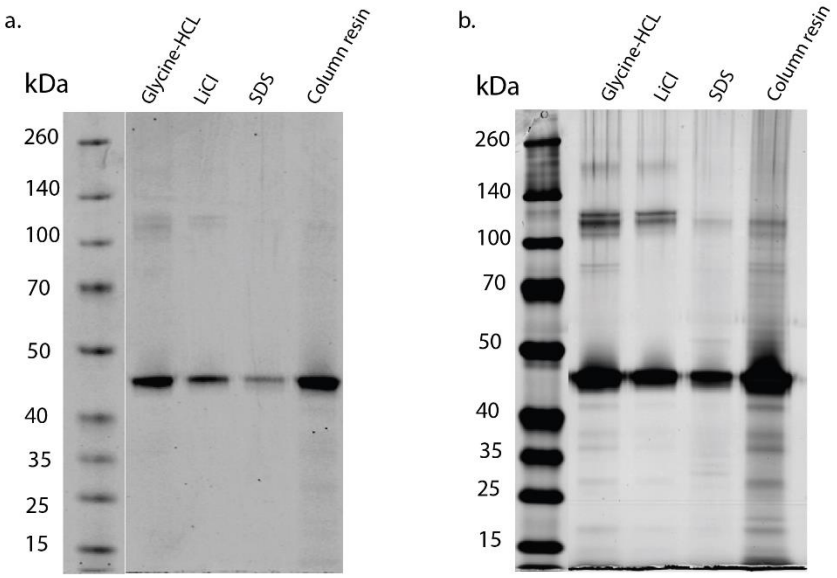

Figure 3-4 Acid elution buffer (Glycine-HCl) is the most effective
Coomassie (a.) and silver stained (b.) SDS-PAGE analysis of the performance of denaturing elution buffers. The molecular weight markers are shown on the left of the imaged gel.

3.2.5 ADP-F-actin affinity column chromatography

Once the methodology of the previous steps was optimised the experiment was performed using ADP-F-actin to ensure the captured proteins were indeed actin binding proteins. ADP-F-actin was prepared using the methods optimised in the previous sections, and successful coupling was confirmed by SDS-PAGE analysis and Coomassie staining (Figure 3-5). The data show a large amount of ADP-F-actin in the sample taken from the washed and packed resin column, and a small amount of actin lost in the coupling and washing processes.

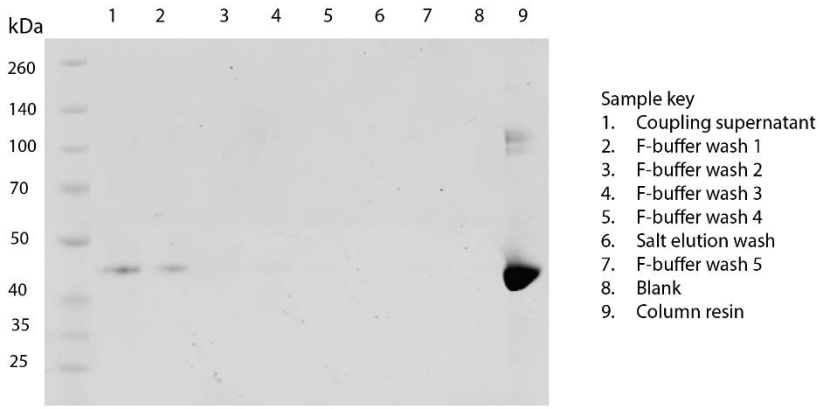

Figure 3-5 ADP-F-actin successfully coupled to column
SDS-PAGE analysis of supernatant, washes and column resin showing successful coupling of actin to the resin and minimal loss of actin during the coupling process and subsequent washes. The molecular weight markers are shown on the left of the imaged gel.

Cytosolic lysate was then prepared by collecting HEK cells from 60 confluent 15cm dishes by trypsination and lysing with digitonin buffer. After treatment with trypsin cells were pelleted by centrifugation and washed with PBS, before being pelleted again and resuspended in lysis buffer. Lysate was treated with phalloidin for 1 hour before centrifugation at 100,000g to remove all polymerised actin and non-cytosolic proteins from the sample. The prepared column was then equilibrated with lysis buffer before the lysate was loaded and thorough washing was completed before the final elution step using Glycine-HCl buffer. All washes and elutions were analysed by SDS-PAGE and stained using both Coomassie and silver staining techniques for extra sensitivity. The data show that the washes removed all non-bound material from the columns and the elution worked well to remove the captured proteins of interest (Figure 3-6).

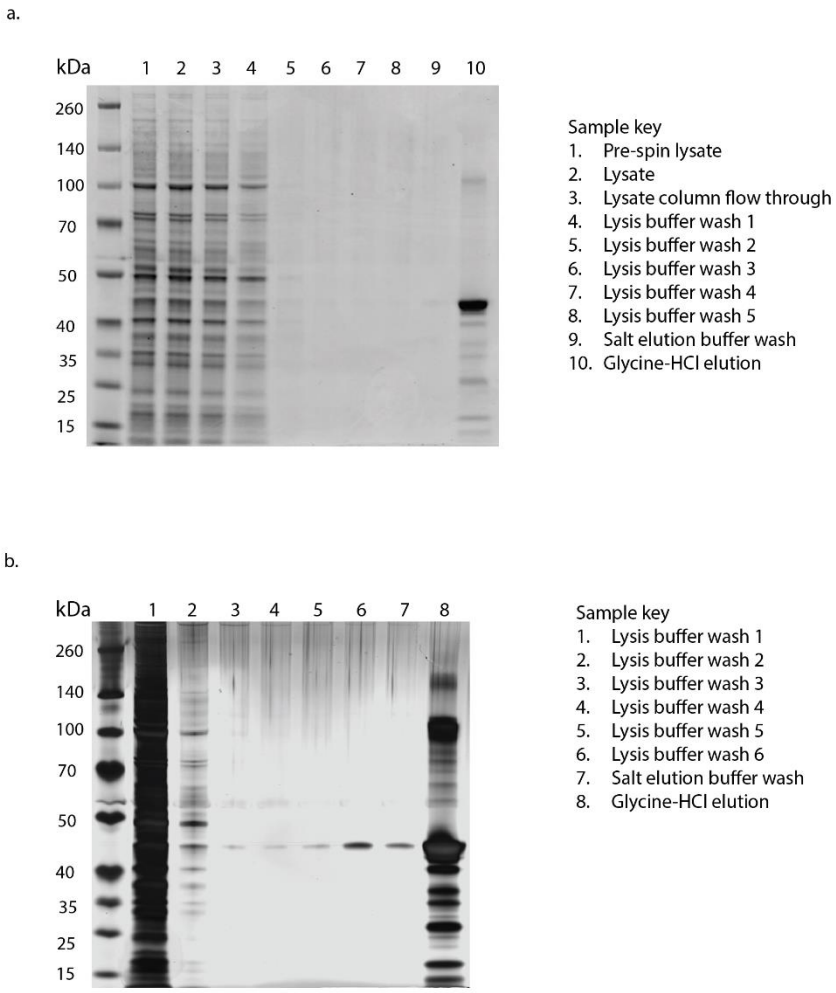

Figure 3-6 Unbound material removed from column and proteins of interest collected
SDS-PAGE analysis of all collected samples from the chromatography of an ADP-F-actin column. Staining was done with both Coomassie (a.) and silver staining (b.) for a more sensitive approach. The lanes of the imaged gels are numbered with a sample key on the right. The molecular weight markers are shown on the left of the imaged gel.

To ensure that the proteins captured by the ADP-F-actin column were indeed actin binding proteins, western blot analysis was carried out to detect some proteins of interest that were hypothesised to either bind the column, or not, as indicated by current knowledge of actin binding proteins from the literature. Firstly, α-tubulin was selected as a widely expressed cytosolic protein due to its role as a building block in microtubules. We would expect α-tubulin to be present in the lysate but not enriched in the elution of captured proteins, and this was indeed confirmed by western blot (Figure 3-7a). Secondly, we performed western blot analysis of the lysate and eluate for Gelsolin, since as a known actin binding protein we would expect Gelsolin to be enriched in the eluate and indeed this was shown (Figure 3-7b).

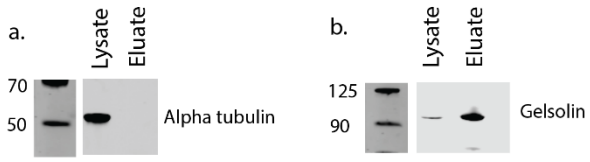

Figure 3-7 Known actin binding proteins present in eluate
Western blot analysis of the lysate and eluate probed with anti-α-tubulin and anti-gelsolin. The molecular weight markers are shown on the left of the imaged blots.

3.2.6 ADP-F-actin mass spectrometry

Three biological repeats of ADP-F-actin affinity chromatography were performed with all previously optimised methodology. The most abundant proteins detected are shown in Table 3-1 with actin itself highlighted in red and known actin binding proteins highlighted in yellow. Since this is an optimisation experiment only a small number of the most abundant proteins are shown and discussed. These results were highly encouraging confirmation that all steps in F-actin affinity chromatography had been optimised sufficiently and were working as expected. This allowed us to move on to the next step of creating stable ATP-F-actin that could be used to construct affinity columns in the same way, as will be discussed in the next chapter.

All mass spectrometry data analysis for this and subsequent experiments is included in appendices.

Table 3-1 ADP-F-actin binding proteins
Mass spectrometry data from ADP-F-actin affinity chromatography. Proteins detected with an intensity of $3x10^8$ or above are listed. Actin is highlighted in red and known actin binding proteins are highlighted in yellow. Data is the result of three repeats of chromatography and subsequent mass spectrometry analysis.

Protein names	Gene names	Unique peptides	Intensity (LFQ)
Actin, cytoplasmic 1	ACTB	2	2.87E+09
Alpha-actinin-4	ACTN4	22	1.56E+09
Filamin-A	FLNA	50	1.45E+09
Angiomotin	AMOT	17	7.88E+08
Protein phosphatase 1 regulatory subunit 12A	PPP1R12A	21	6.77E+08
Plastin-3	PLS3	15	6.43E+08

MARCKS-related protein	MARCKSL 1	12	5.53E+08
EF-hand domain-containing protein D2	EFHD2	11	3.76E+08
Alpha-actinin-1	ACTN1	15	3.72E+08
Drebrin	DBN1	13	3.56E+08
Myristoylated alanine-rich C-kinase substrate	MARCKS	7	3.51E+08
F-actin-capping protein subunit beta	CAPZB	12	3.06E+08

3.3 Discussion

In this chapter we have shown that we have successfully optimised the methodology for polymerising, stabilising and coupling F-actin to affinity activated media. The conditions in which these reactions perform best have been thoroughly tested to ensure stable columns which will allow us to produce robust and dependable samples for subsequent mass spectrometry analysis.

The methodology used was adapted and optimised from many studies of F-actin chromatography utilising different species and isoforms, including yeast (Drubin et al., 1988), *Drosophila* (Miller et al., 1989), rabbit muscle (Luna et al., 1982; Miller and Alberts, 1989), *Dictyostelium* (Wuestehube et al., 1991), *Plasmodium falciparum* (Forero and Wasserman, 2000) and zucchini (*Cucurbita pepo L.*) (Hu et al., 2000). However, these available studies of F-actin affinity chromatography have been carried out using actin purified from skeletal muscle.

In mammals, six isoforms of actin exist and are produced in different cell types and have different localisations and functions. Four of these isoforms are expressed in muscle cells with the remaining two found in non-muscle cells only (Perrin and Ervasti, 2010). This was of utmost importance to this project, as the F-actin we wished to study was produced in non-muscle cells and responsible for the highly dynamic population of actin filaments found in migrating cells. All isoforms of actin, whether they originate from muscle or non-muscle cells, are hugely similar with only small variations in sequence (Herman, 1993). However, they have been shown to have different roles and different binding partners

(Namba et al., 1992). Therefore, the actin sourced for this project was purified from non-muscle human platelet cells.

The differences between the isoforms of actin are most prominent at the N-terminus where a variation in amino acid sequence is most consistent (Mounier and Sparrow, 1997). These differences, though subtle, affect the isoelectric point of the isoform (Vandekerckhove and Weber, 1978) and this is of particularly import for the assembly of affinity chromatography columns, as the coupling chemistry between the affinity media and actin is highly affected by these characteristics of the protein. The isoelectric point of actin protein even differs between the two non-muscle isoforms (Bergeron et al., 2010). We kept this difference in consideration as our purified non muscle actin consisted of 15% γ-actin and 85% ß-actin. The conditions of our coupling reactions were therefore optimised with this is mind.

Another key consideration in the optimisation of F-actin affinity column preparation was that our immobilised ligand is a filamentous structure and not a monomeric protein. This results in a more densely packed column and therefore may alter flow rates and properties of the column. It could also result in more non-specific binding, due to washes not being as effective at removing unbound protein which could have a negative effect on the quality of the final proteomics data sets. For this reason, the flow of the columns and the effectiveness of the wash steps was paid close attention during the optimisation stages of the project. The concentration and final volume of the cell lysate was optimised and consistently passed over the column at a concentration of 2mg/ml and volume of 2ml, which allowed the columns to flow completely using only gravity. An extra step of high-speed centrifugation was also performed to improve the flow properties of the lysate by ensuring cytosolic lysate only was used. To ensure the washes were effective and that the filamentous nature of the affinity protein was not causing any discrepancies, each wash step was collected and analysed by SDS-PAGE and further sensitive methods of protein detection such as silver staining.

One of the most important steps in the chromatography process is the collection of the eluate, the target results. Interestingly, recreating the elution processes used for many of the available studies of F-actin chromatography mentioned

previously was not sufficient for our purposes. We found stepwise salt elution buffers to be ineffective. After testing different methods, we found that an acid elution buffer was the best for our purposes, as long as the collected sample was then neutralised before the digestion by trypsin for mass spectrometry analysis.

For the last step of optimisation, the eluate was analysed by western blotting with gelsolin being chosen as a positive validation target for enrichment. This is because of the ability of gelsolin to bind F-actin in different ways, and at different structural parts of the filament (Sun et al, 1999).

As everything seemed to be working correctly, the ADP-F-actin chromatography was repeated to give three biological replicates for mass spectrometry analysis. The majority of the abundant proteins detected were known actin binding proteins (Table 3-1), indicating that each optimised step of the chromatography was working correctly.

In conclusion, in this chapter we showed the optimisation of a methodology for creating functional non-muscle F-actin affinity chromatography columns. Each stage of the process was thoroughly tested and optimised to give clean and consistent results despite the challenges of using a filamentous protein as a ligand and a differing isoform of the protein compared to the one used in available studies in the literature.

4 Creating stable ATP-F-actin

4.1 Introduction

Since we have an optimised and validated methodology for creating F-Actin columns, preparing the input lysate and eluting and analysing the target proteins, the next step was to optimise the method of creating stable ATP-F-actin. As discussed in the introduction, when new monomers are incorporated to an actin filament during polymerisation, the ATP bound to each monomer is rapidly hydrolysed to ADP, which changes the shape and properties of the filament. Most of the data from the literature focuses on this change of the filament to the ADP-bound form, and its function in "ageing" the filament and promoting depolymerisation of the filament and recycling of the components. Since so many proteins are known to preferentially bind ADP-F-actin it raises the question whether some proteins can preferentially bind ATP-F-actin. This is a harder question to answer, since the lifetime of ATP-F-actin at the barbed end of a filament is highly transient. There are some proteins known to bind the barbed end of the filament, and therefore ATP-F-actin, for example capping protein which "caps" the end of filaments to stop further polymerisation. These proteins will be important controls for this thesis, as we try to identify novel binders of ATP-F-actin and investigate the biological consequence of this.

The first method we have optimised for creating stable ATP-F-actin was to polymerise F-actin using actin monomers loaded with non-hydrolysable analogues of ATP. Theoretically, this would allow the generation of a stable form of F-actin that does not change its shape and properties upon polymerisation.

4.2 Results

4.2.1 Loading actin with non-hydrolysable analogues of ATP

The first step in loading actin with non-hydrolysable analogues of ATP is to remove the bound ATP from G-actin, as this would be quickly hydrolysed upon polymerisation to create ADP-F-actin. We optimised three different methods for doing this.

To ensure we would be able to identify the loaded nucleotide on the actin immobilised on the column, we tested a methodology using liquid chromatography-mass spectrometry to detect which nucleotide, or non-hydrolysable analogue, was loaded on F-actin. We prepared standards of all the compounds that we wanted to detect to see if we could indeed detect them and separate them from one another via their differing retention times. The retention time refers to the time it takes each nucleotide to pass through the column, and as shown in Figure 4-1, each nucleotide could be seperated by time on their ion chromatogram.

a.

Compound	Formula	Neutral mass	M-H	M+H	RT
ADP	C10H15N5O10P2	427.02942	426.0216	428.03722	8.79
ATP	C10H16N5O13P3	506.99575	505.988	508.00355	9.74
AMP-PNP	C10H17N6O12P3	506.011738	505.0039	507.019538	9.5
ATP-γ-S	C10H16N5O12P3S	522.972911	521.9651	523.980711	10.62
AMP	C10H14N5O7P	347.063088	346.0553	348.070888	

b.

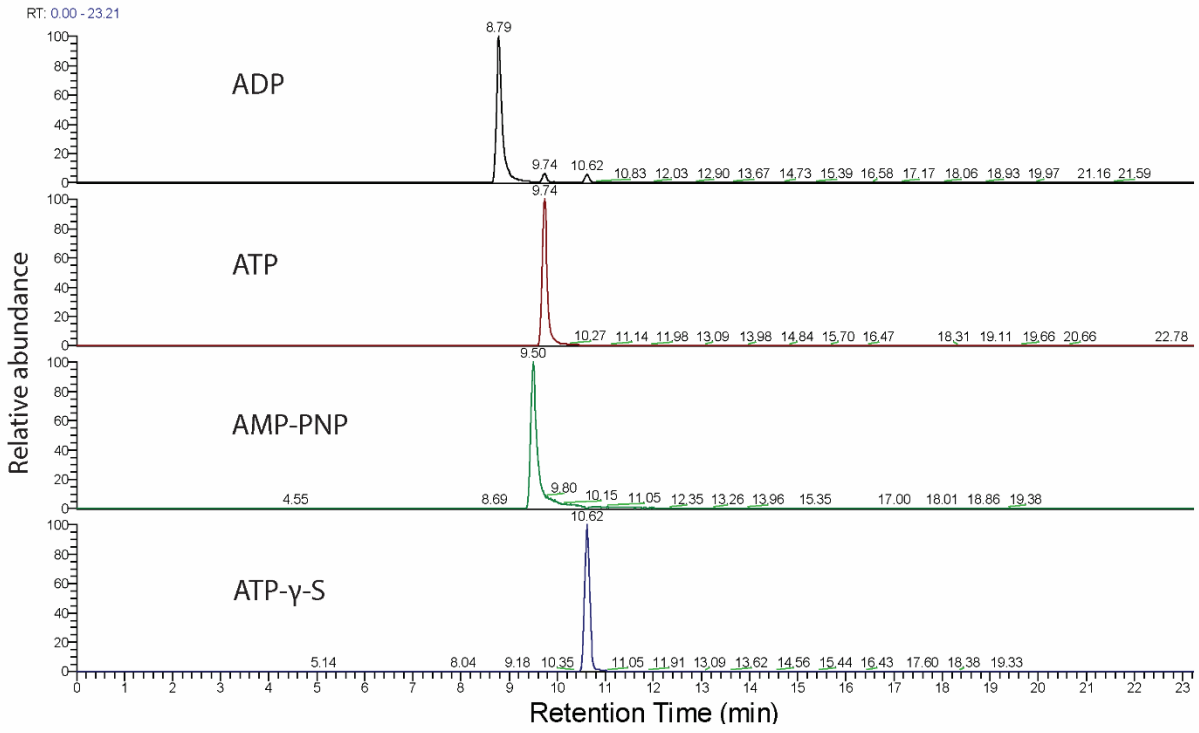

Figure 4-1 All nucleotides of interest can be detected by LC-MS

a. Table showing data of the nucleotides of interest, most importantly the retention times to show they can be separated on the column.
b. Graphs showing the extracted ion chromatogram (XIC) of each nucleotide.

The three different methods optimised for loading non-hydrolysable analogues of ATP all consisted of a series of buffer exchanges, a "treatment" to reduce the amount of ATP present and an excess of ATPγS added to each sample.

Firstly, a method utilising apyrase was optimised. Apyrase is an ATP-diphosphohyrdolase that catalysis the hydrolysis of ATP to ADP and then AMP sequentially, and in a calcium dependent manner (Pilla et al., 1996). Desalting columns were equilibrated with G-buffer containing no ATP and G-actin was passed through this column and immediately treated with an excess of ATPγS, the apyrase enzyme and 5mM calcium to ensure activation. This process was repeated 3 times with incubation periods and gentle agitation at 4°C. Protein concentrations of the samples were checked after each buffer exchange and treatment with no reduction. Next, the treated G-actin sample was adjusted to polymerising conditions and coupled to resin to form the F-actin affinity columns. A sample of the washed and packed columns was then taken to be prepared for Liquid chromatography – mass spectrometry (LC-MS) so that the nucleotides present in the sample could be identified.

As a second method, we applied the same process but replaced apyrase with another enzyme, Alkaline phosphatase calf intestinal (CIP), which has also phosphohydrolase activity. All the steps of the method using CIP are identical to those used with Apyrase, except the use of CIP as the enzyme ("treatment").

Thirdly, a method for nucleotide loading with no enzyme involvement was optimised using ethylenediaminetetraacetic acid (EDTA) to promote nucleotide exchange. Indeed, EDTA treatment has been shown to enhance the rate of nucleotide exchange in GTPases (Korlach et al., 2004). The main difference in this methodology to the previous two is the lack of calcium treatment, due to the fact that EDTA is a chelating agent. Since the nucleotide bound to monomeric actin is accompanied by a metal ion, EDTA was used to bind it and, by doing so, increase the off-rate of the bound nucleotide and facilitate exchange for the non-hydrolysable analogue. A large excess of ATPγS was included in this methodology, since we are simply increasing the rate of nucleotide exchange, and not removing the ATP from the sample. The samples for LC-MS were prepared and analysed in the same way for all three methods.

The optimised nucleotide loading methods were all successful. However, we observed some small differences in their efficiency. Both samples generated using the apyrase (Figure 4-2) and EDTA (Figure 4-3) methods had ATPγS loaded successfully, but still retained some ADP and AMP bound. The treatment with CIP was the most successful, with ATPγS being loaded and no fully formed peaks for either ADP or AMP in the LC-MS analysis (Figure 4-3). Therefore, the method using CIP was selected to be used for the nucleotide loading experiments that would make the samples for the ATP-F-actin columns.

a.

Compound	Formula	Neutral mass	M-H	M+H	RT
ADP	C10H15N5O10P2	427.02942	426.0216	428.03722	8.79
ATP	C10H16N5O13P3	506.99575	505.988	508.00355	9.74
AMP-PNP	C10H17N6O12P3	506.011738	505.0039	507.019538	9.5
ATP-γ-S	C10H16N5O12P3S	522.972911	521.9651	523.980711	10.62
AMP	C10H14N5O7P	347.063088	346.0553	348.070888	

b. Apyrase

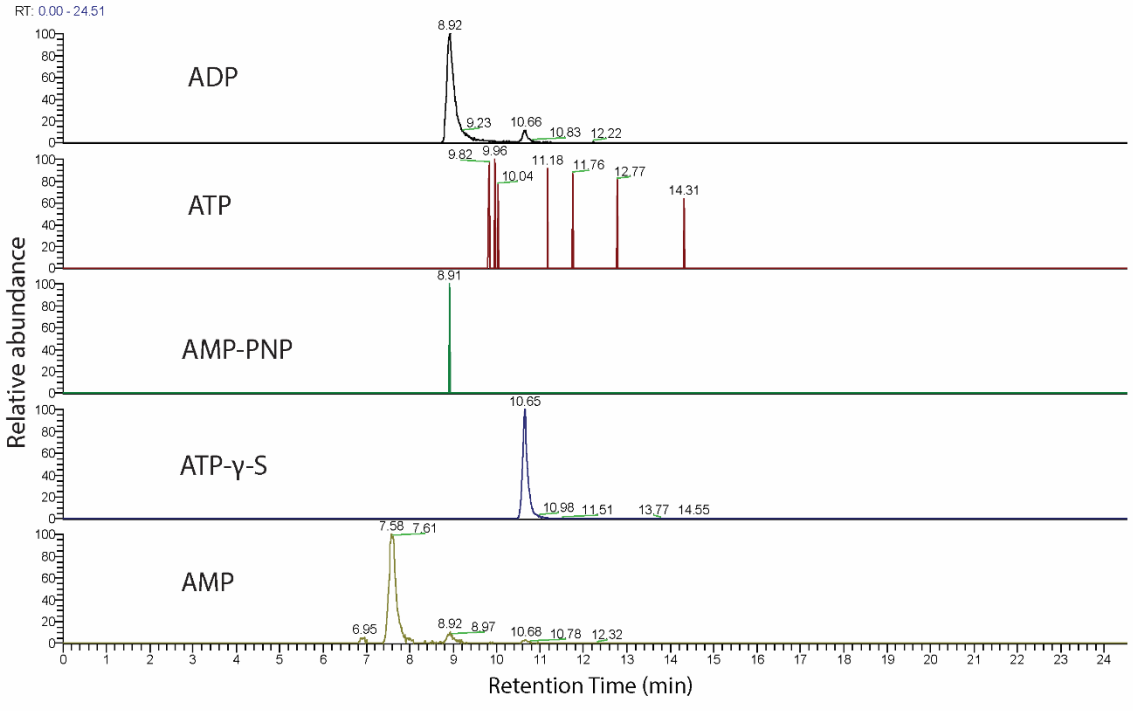

Figure 4-2 Analysis of nucleotides on samples loaded with Apyrase method.

a. Table showing data of the nucleotides of interest, most importantly the retention times to show they can be separated on the column.
b. Graph showing the XICs of nucleotides of interest from samples loaded with apyrase method.

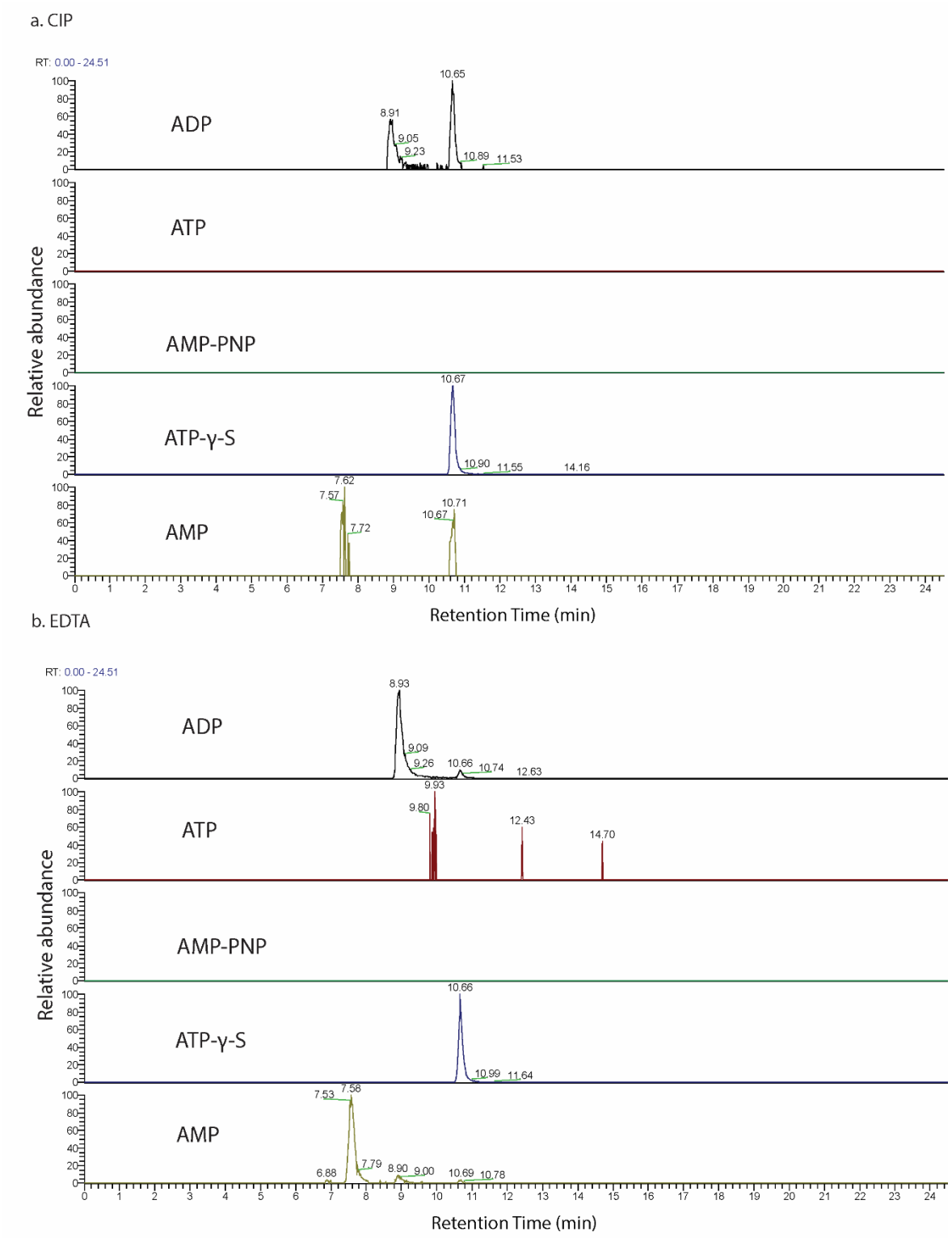

Figure 4-3 Analysis of nucleotides on samples loaded with CIP and EDTA method.
a. Graph showing the XICs of nucleotides from samples loaded with CIP method.
b. Graph showing the XICs of nucleotides from samples loaded with EDTA method.

Using the optimised methods from this and the previous chapter, ADP-F-actin and ATP-F-actin affinity columns were prepared for chromatography and subsequent mass spectrometry analysis. As in the optimisation experiments, a sample of each column resin was taken post washing and packing, to analyse the

bound nucleotide(s) in each column. As expected, the ATP-F-actin column contained only ATPγS and the ADP-F-actin column contained ADP, ATP and AMP (Figure 4-4). These columns were used with HEK cell lysate, in order to optimise the experiment from start to finish with large cells with high protein content.

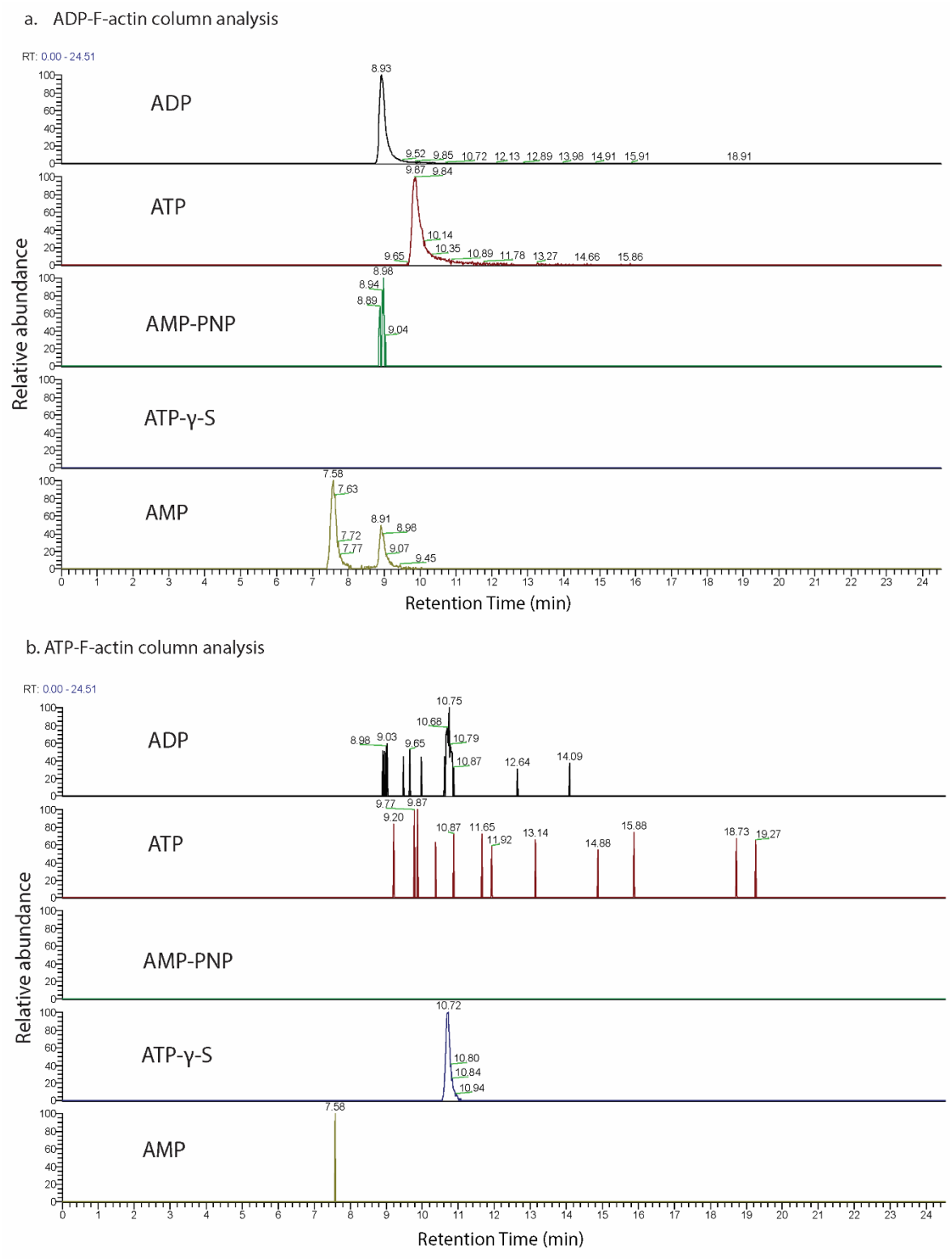

Figure 4-4 Analysis of F-actin affinity columns loaded nucleotide(s)

a. Graph showing the XICs of nucleotides in the ADP-F-actin column.
b. Graph showing the XICs of nucleotides in the ATP-F-actin column.

Once the methodology for identifying proteins that differentially bind ATP- and ADP-F-actin was optimised (including making the F-actin affinity columns, loading non-hydrolysable analogues of ATP and the subsequent mass spectrometry analysis), the whole process was applied to two other cell lines of interest for their high motility. We selected JVM3, a chronic B cell leukemia cell line, and PDAC, a pancreatic ductal adenocarcinoma cell line. F-actin affinity columns were produced following the previous methodology and ATPγS was successfully loaded in the ATP-F-actin columns for both experiments with PDAC (Figure 4-5) and JVM3 cells (Figure 4-6).

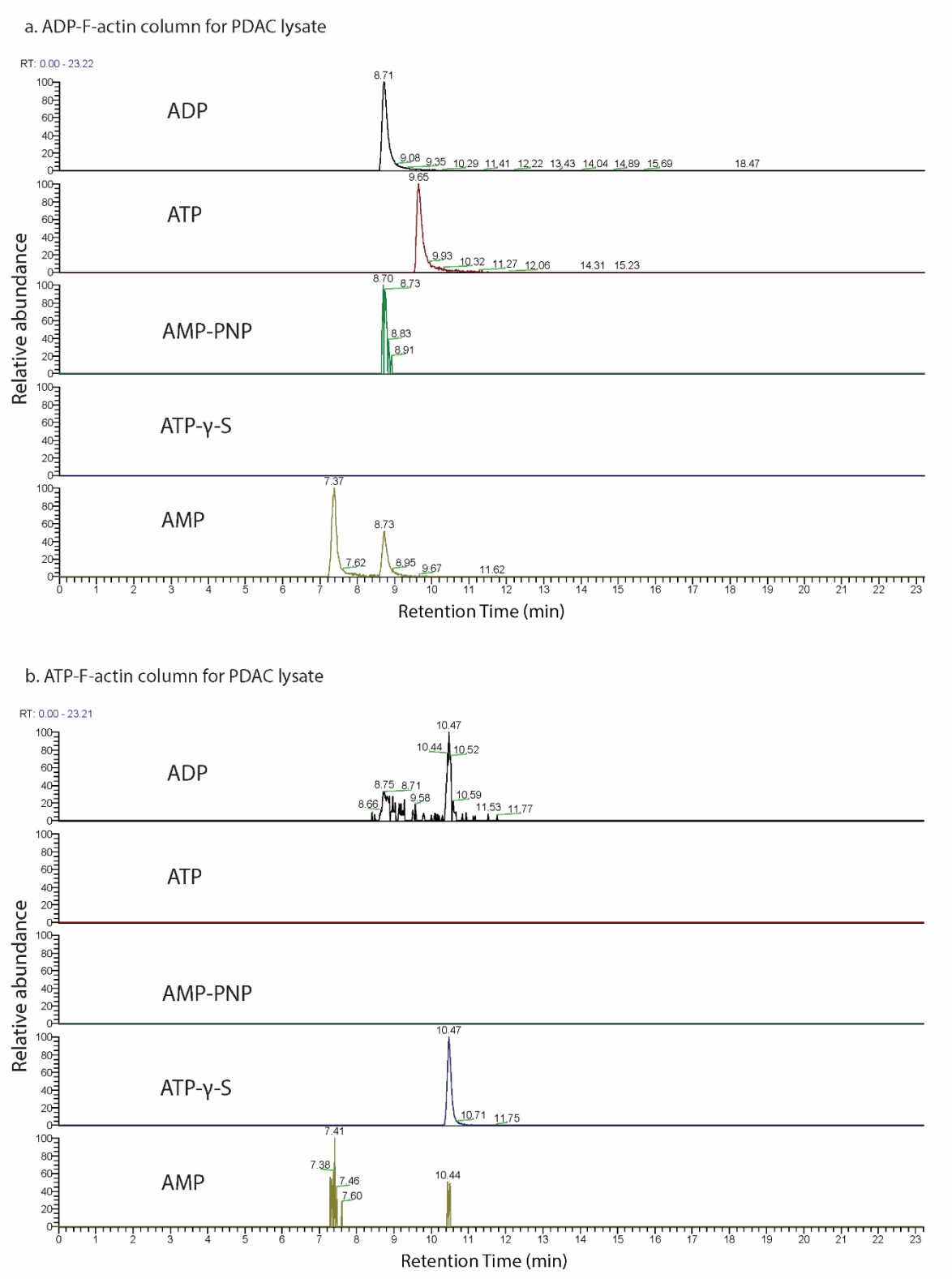

Figure 4-5 Analysis of F-actin affinity columns loaded nucleotide(s) for PDAC columns

a. Graph showing the XICs of nucleotides in the ADP-F-actin column.
b. Graph showing the XICs of nucleotides in the ATP-F-actin column.

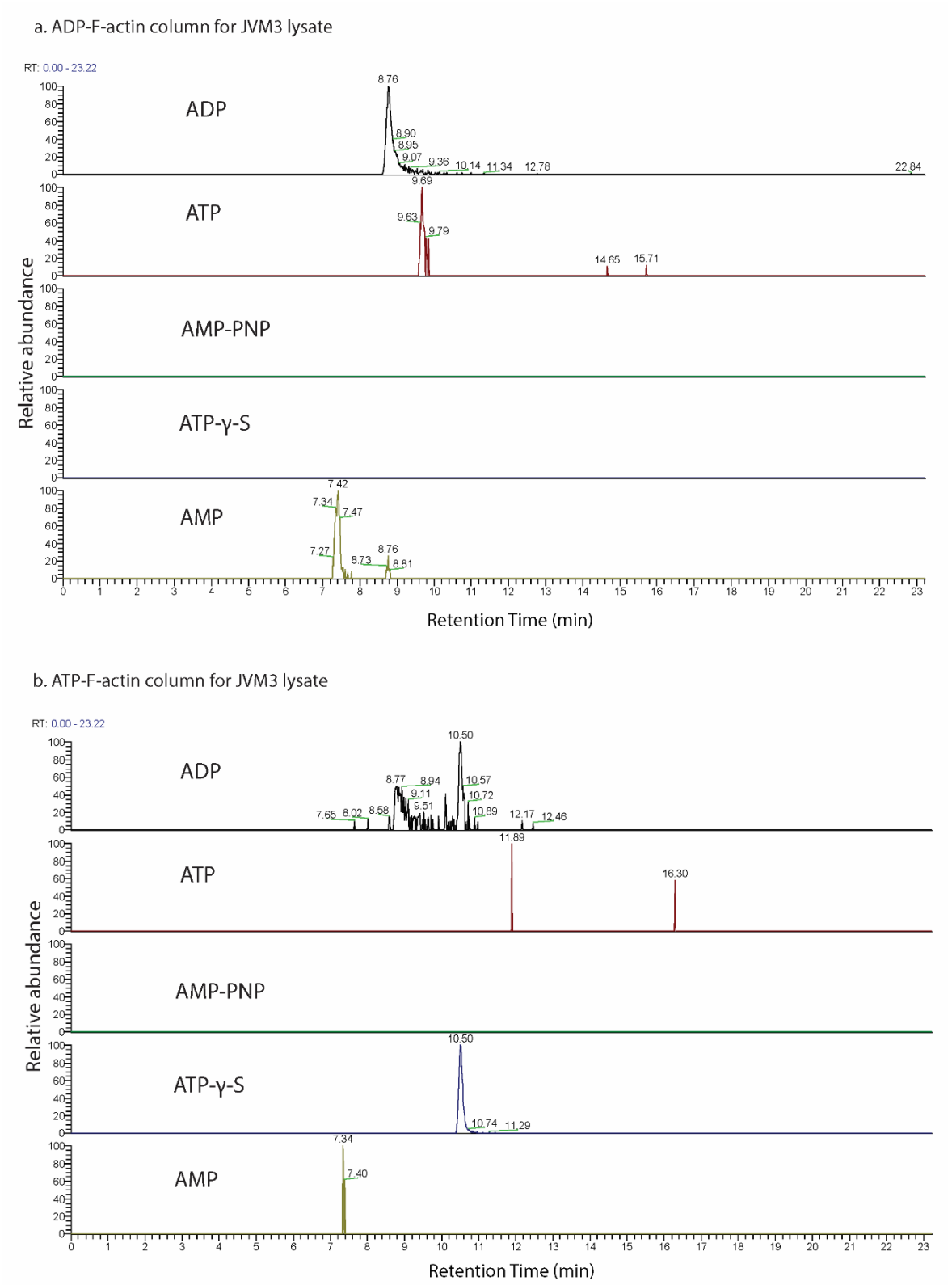

Figure 4-6 Analysis of F-actin affinity columns loaded nucleotide(s) for JVM3 columns

a. Graph showing the XICs of nucleotides in the ADP-F-actin column.
b. Graph showing the XICs of nucleotides in the ATP-F-actin column.

Despite being widely studied and utilised in the literature, we chose not to use AMP-PnP as our non-hydrolysable analogue as in our hands it was not as stable as

ATPγS. AMP-PnP was detectable and easily separated from the other nucleotides using LC-MS analysis in our control samples (Figure 4-7). However, when tested in the same way as ATPγS, it was either not present in the LC-MS analysis or appeared to be broken down (Figure 4-8). Therefore, the mass spectrometry analysis of which proteins can differentially bind ATP-F-actin and ADP-F-actin were made using ATPγS loaded filaments as our "ATP" that was stable and would not be hydrolysed.

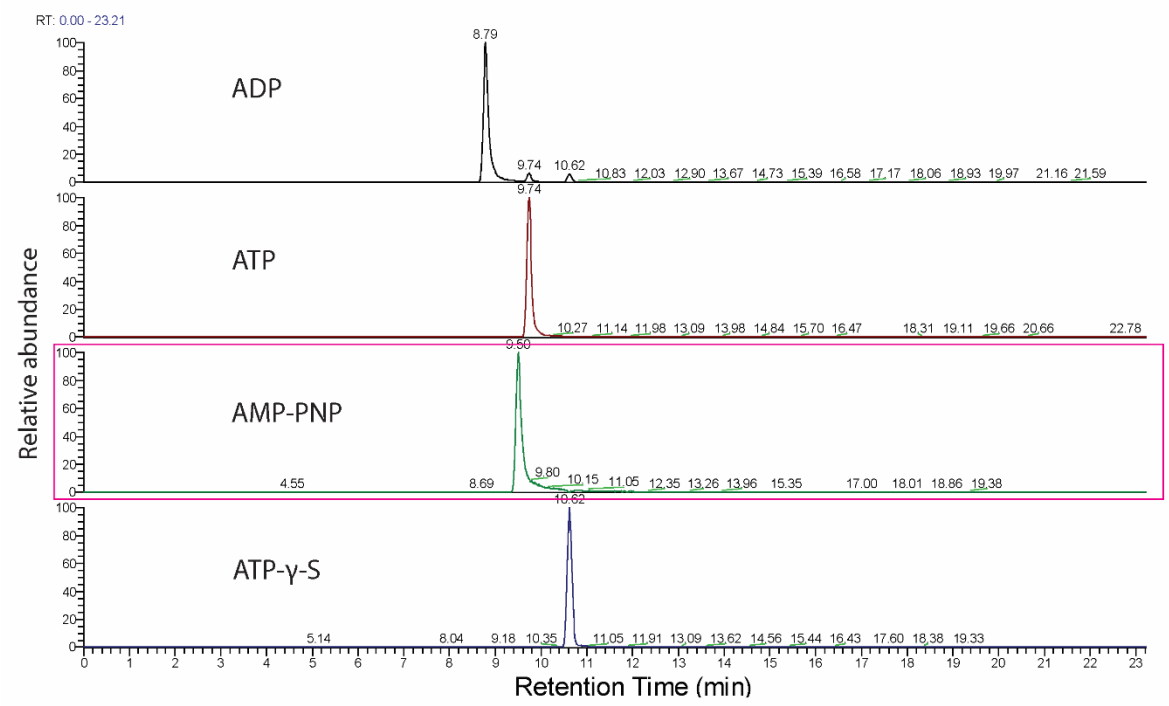

Figure 4-7 AMP-PnP is detectable by LC-MS
Graphs showing the XICs of each nucleotide, with a pink box highlighting that of AMP-PnP.

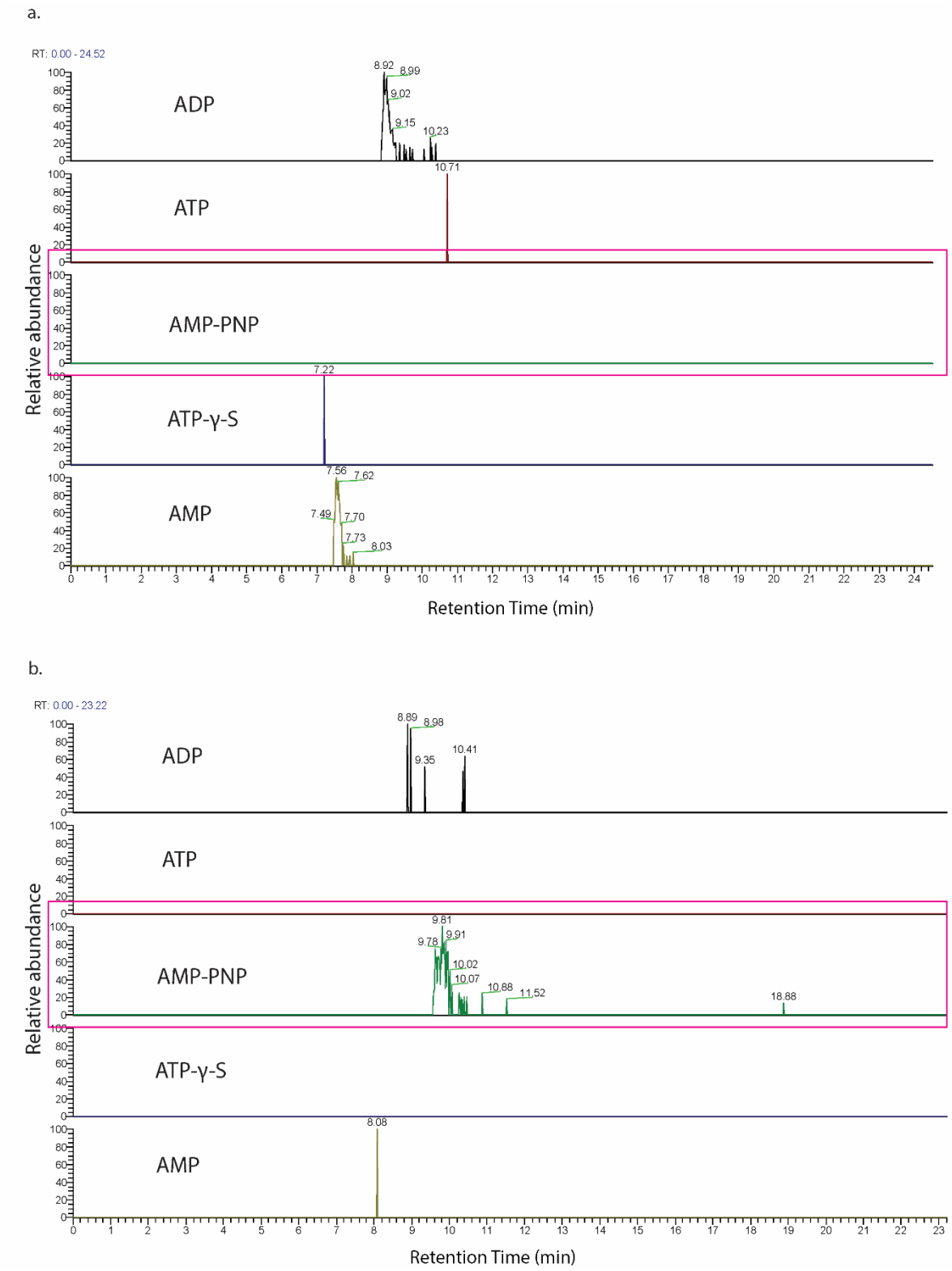

Figure 4-8 AMP-PnP is broken down or lost during column preparation.
Graphs showing the XICs of nucleotide from samples loaded with AMP-PnP with no detection (a.) or detection of breakdown (b.).

4.3 Discussion

In this chapter, we have shown that we optimised a methodology to successfully load non-hydrolysable analogues of ATP into G-actin, in exchange for its bound ATP. This G-actin is capable of polymerising without issue and allows us to study F-actin filaments in their pre-hydrolytic state, mimicking the highly dynamic ATP-F-actin state present at the barbed end of filaments in a stable manner.

As discussed in Chapter 1, the hydrolysis of ATP is triggered upon polymerisation due to the increase in intrinsic ATPase activity of actin (Pollard and Weeds, 1984). This is a highly dynamic process, with the rate of ATP hydrolysis in F-actin being $0.3s^{-1}$ with magnesium present as the divalent cation (Mg-F-actin) (Blanchoin and Pollard, 2002). Without incorporation of a non-hydrolysable analogue of ATP, this project would not have been possible.

Non- or slowly hydrolysable analogues of nucleotides have been important tools in biochemistry for many years. These compounds are developed by the modification of phosphate groups, as opposed to the sugar or base (Eckstein, 1970). ATPγS was developed to have increased resistance to alkaline phosphatase whilst being indistinguishable from ATP by electrophoresis (Goody and Eckstein, 1971). This non hydrolysable analogue of ATP is altered at the γ phosphate, where an oxygen molecule is replaced with sulfur (Bagshaw et al., 1972) and has been shown to be hydrolysed 1000-fold slower than ATP (Bagshaw et al.,1974). There are now several commercially available non- or slowly hydrolysable analogues of ATP, and these may be suitable for different applications. We tested two of the most studied analogues and found ATPγS was the most suitable for our needs.

It is worth discussing the transitional state between ATP-F-actin and ADP-F-actin that is ADP-Pi-F-actin. This has been shown to be the most abundant state in a polymerising filament due to the difference in the rate of hydrolysis and subsequent release of the hydrolysed phosphate (Carlier and Pantaloni, 1986). This state of actin filament may be easier to study naturally than ATP-actin since the rate of dissociation of the phosphate is in the order of minutes ($0.0002s^{-1}$; Pollard et al., 2000), unlike its hydrolysation. However, ADP-Pi-F-actin has been shown to be structurally similar to ATP-F-actin (Belmont et al., 1999) so the

conformational change we believe to be responsible for the differential binding of proteins to ADP- or ATP-F-actin should be the same in ADP-Pi-actin as it is in ATP-actin. It has also been shown that the stability of the filament is similar between ATP-F-actin and ADP-Pi-F-actin (Levitsky et al., 2008) so we assume that the loss in stability of ADP-F-actin is associated with the conformational change.

Interestingly, a study concerning actin binding protein Coronin 1B made use of the slow rate of phosphate dissociation from ADP-Pi-F-actin to investigate the nucleotide preference (state of F-actin) of this particular protein. They polymerised actin using monomers of actin with either ADP or ATP. Because of the longevity of ADP-Pi-actin, they performed co-sedimentation with their protein of interest immediately after polymerisation and found that it bound to ATP/ADP-Pi-F-actin (the actin polymerised with ATP) with almost 50-fold higher affinity than ADP-F-actin (Cai et al., 2007). This method is of great interest. However, Coronin 1B was already known to bind actin. Using our methodology of stabilised ATP-F-actin for chromatography allows the potential for novel actin binding proteins to be discovered, as well as those that may only bind ATP-F-actin and not ADP-F-actin and might therefore not have been identified in previous studies.

In conclusion, in this chapter we have shown optimised methodology for loading G-actin with non-hydrolysable analogues of ATP that are incorporated into F-actin during polymerisation. This method allows stable and reproducible creating of ATP-F-actin filaments suitable for immobilisation on affinity chromatography columns.

5 ATP-F-actin mass spectrometry results

5.1 Introduction

In this chapter we will present and discuss the mass spectrometry data from F-actin affinity columns prepared with ADP- and ATP-F-actin. The first experiments of affinity chromatography and mass spectrometry were achieved by loading actin with a non-hydrolysable analogue of ATP, as optimised in the previous chapter. By comparing the mass spectrometry on the eluate from the chromatography performed with ADP- or ATP-F-actin we will were able to investigate the differences in the pool of proteins that binds these two variants of actin.

The data from these experiments is highly encouraging as expected proteins were enriched in ATP-F-actin samples, as will be discussed. We also optimised and performed these experiments using Jasplakinolide treatment in the place of loading a non-hydrolysable analogue of ATP. Jasplakinolide is known to be capable of inducing polymerisation of actin and stabilising the filaments but, most importantly, it can change the conformation of F-actin to mimic that of ATP-F-actin (Pospich et al., 2020). This conformational change involves the DNase 1 binding loop (D-loop) of each actin monomer within a filament. Studies have shown that this difference in D-loop conformation is indicative of the nucleotide state of a filament, namely whether it has hydrolysed the bound ATP or not, with the D-loop in a “closed” or “open” conformation indicating ADP- or ATP-F-actin, respectively.

As mentioned previously in the column input optimisation, for experiments using non-hydrolysable analogues of ATP and Jasplakinolide treatment we used PDAC and JVM3 cells due to their highly migratory nature.

5.2 Results

ATP-F-actin was prepared by multiple rounds of buffer exchange and enzyme treatment to replace ATP with a non-hydrolysable analogue, ATPγS, on G-actin before inducing polymerisation. ADP-F-actin was prepared by simply polymerising G-actin, as the ATP would be quickly hydrolysed upon

polymerisation. The prepared F-actin was then coupled to activated affinity media, as optimised previously, and affinity columns were constructed. The nucleotide state of the F-actin in each column was analysed and confirmed to be correct using LC-MS as described and shown in the previous chapter, for each of the three biological repeats per condition.

For experiments using Jasplakinolide treatment, samples for both conditions were prepared by buffer exchange, polymerisation of G-actin and then treatment with phalloidin (ADP-F-actin) or Jasplakinolide (to mimic ATP-F-actin, as previously described). As described in the previous chapters, phalloidin is used to stabilise the actin filaments and allow them to be immobilised on the affinity media. However, Jasplakinolide also stabilises actin and the two molecules have overlapping binding sites on the actin filaments (Merino et al., 2018). For this reason, phalloidin was not used in Jasplakinolide treated samples. Since treatment with Jasplakinolide does not alter the nucleotide state of actin, but instead alters the conformation regardless of the bound nucleotide we could not use LC-MS to confirm the filaments were truly ATP-F-actin. For this reason, we compared the results of these experiments with those using non-hydrolysable analogues and also investigated the effects of Jasplakinolide treatment on live cells in later chapters.

Once, when possible, the experimental columns nucleotide state was confirmed, large quantities of cellular lysate were collected and prepared for both PDAC and JVM3 cell types, giving three repeats per cell line and per nucleotide state of column. Eluate from the chromatography were each analysed by SDS-PAGE with Coomassie and silver staining and prepared for digestion and subsequent mass spectrometry.

The data were analysed to investigate the differences between the proteins captured by the ADP- and ATP-F-actin columns, and most importantly those enriched in the latter. Mass spectrometry data collection and analysis was performed using MaxQuant and Perseus, and significantly enriched proteins were selected using a permutation-based Student’s t-test with FDR set at 5%.

The data for each experiment will be presented separately below, depending on cell line used and method of creating F-actin. They will, however, be considered

and discussed together. The data are organised, with hyperlinks to each figure or table, in Table 5-1 as follows:

Table 5-1 Organisation of mass spectrometry data

	PPI map with proteins involved in actin cytoskeletal organisation	Statistical data of enrichment of proteins involved in actin cytoskeletal organisation	PPI map with proteins involved in actin cytoskeletal organisation and signalling by Rho GTPases	Statistical data of enrichment of proteins involved in actin cytoskeletal organisation and signalling by Rho GTPases	Volcano plot highlighting interesting hits and their statistical data
Mass spectrometry data showing proteins enriched in ATP-F-actin samples prepared using non-hydrolysable analogue of ATP, ATPγS					
JVM3	Figure 5-1	Table 5-2	Figure 5-2	Table 5-3	Figure 5-3
PDAC	Figure 5-4	Table 5-4	Figure 5-5	Table 5-5	Figure 5-6
Mass spectrometry data showing proteins enriched in ATP-F-actin samples prepared using Jasplakinolide treatment					
JVM3	Figure 5-7	Table 5-6	Figure 5-8	Table 5-7	Figure 5-9
PDAC	Figure 5-10	Table 5-8	Figure 5-11	Table 5-9	Figure 5-12

5.2.1 ATP-F-actin binding proteins (ATPγS)

Significantly enriched proteins in ATP-F-actin chromatography elutions using JVM3 cells and ATPγS are presented in a Protein-Protein Interaction (PPI) map (Figure 5-1) and those identified as being involved in actin cytoskeletal organisation by Gene Ontology analysis shown as red nodes, and their data shown in Table 5-2 Mass spectrometry data of proteins enriched in ATP-F-actin (JVM3-ATPγS).

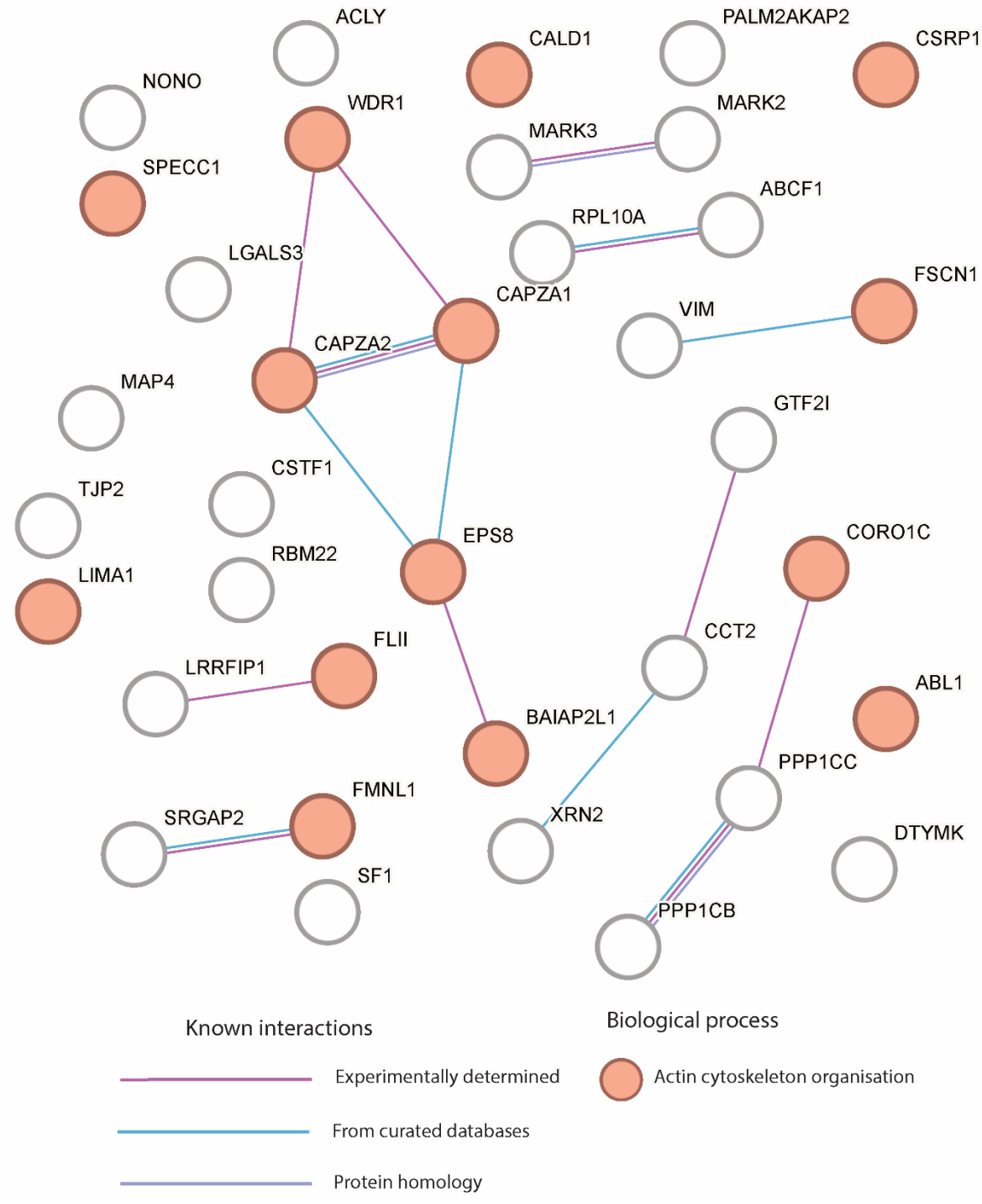

Figure 5-1 Protein-protein interaction map of ATP-F-actin binding proteins (JVM3-ATPγS)

PPI map from STRING v12.0 showing proteins significantly enriched in ATP-F-actin samples from mass spectrometry data using JVM3 cells and ATPγS as a non-hydrolysable analogue of ATP. Network nodes represent proteins (gene names shown) and red nodes represent proteins involved in actin cytoskeletal organisation (data from Gene Ontology). Interactions or homology are shown with different coloured lines connecting protein nodes (data from STRING v12.0).

Table 5-2 Mass spectrometry data of proteins enriched in ATP-F-actin (JVM3-ATPγS)
Table listing proteins enriched in ATP-F-actin samples from mass spectrometry data using JVM3 cell lysates and ATPγS as a non-hydrolysable analogue of ATP, and involved in the biological process of actin cytoskeletal organisation (data from Gene Ontology). For each protein their name, gene name, and statistical data are shown. Students T-test fold difference value indicates preference for ATP-F-actin, and "+" in the subsequent column indicates if this difference is significant. In the last column "+" indicates whether the data was significant by p-value only.

Actin Cytoskeletal Organisation (Biological Process – Gene Ontology)				
Protein names	**Gene names**	**Student's T-test fold Difference JVM3 (ADP-ATPgS)**	**Student's T-test Significant JVM3 (ADP-ATPgS)**	**Student's T-test Significant JVM3 (ADP-ATPgS) p-value only**
Cytospin-B	SPECC1	-3.18		+
WD repeat-containing protein 1	WDR1	-2.12		+
Caldesmon	CALD1	-4.89	+	+
Cysteine and glycine-rich protein 1	CSRP1	-5.10	+	+
F-actin-capping protein subunit alpha-2	CAPZA2	-5.78	+	+
F-actin-capping protein subunit alpha-1	CAPZA1	-3.50		+
Fascin	FSCN1	-3.86		+
LIM domain and actin-binding protein 1	LIMA1	-0.68		+
Epidermal growth factor receptor kinase substrate 8	EPS8	-3.68		+
Protein flightless-1 homolog	FLII	-2.54		+
Coronin-1C	CORO1C	-6.10	+	+
Brain-specific angiogenesis inhibitor 1-associated protein 2-like protein 1	BAIAP2L1	-5.09	+	+
Tyrosine-protein kinase ABL1	ABL1	-4.90	+	+
Formin-like protein 1	FMNL1	-0.71		+

As mentioned in the Introduction (Chapter 1), we are particularly interested in ATP-F-actin binding proteins that may be involved in positive feedback and promotion of polymerisation. Since Rho GTPases are key players in the promotion of cell migration, we decided to investigate our results with them in mind for each mass spectrometry dataset. In Figure 5-2 and Table 5-3, data from Gene Ontology was used in the PPI map and table, highlighting ATP-F-actin binding proteins that are involved in Signalling by Rho GTPases in yellow (Reactome Pathway, Gene Ontology). Proteins identified as being involved in actin cytoskeletal organisation, as discussed previously are presented in purple. Those proteins which are identified as belonging to both of these groups are split purple/yellow in the PPI map and marked as yellow with thick bordered rows in the table.

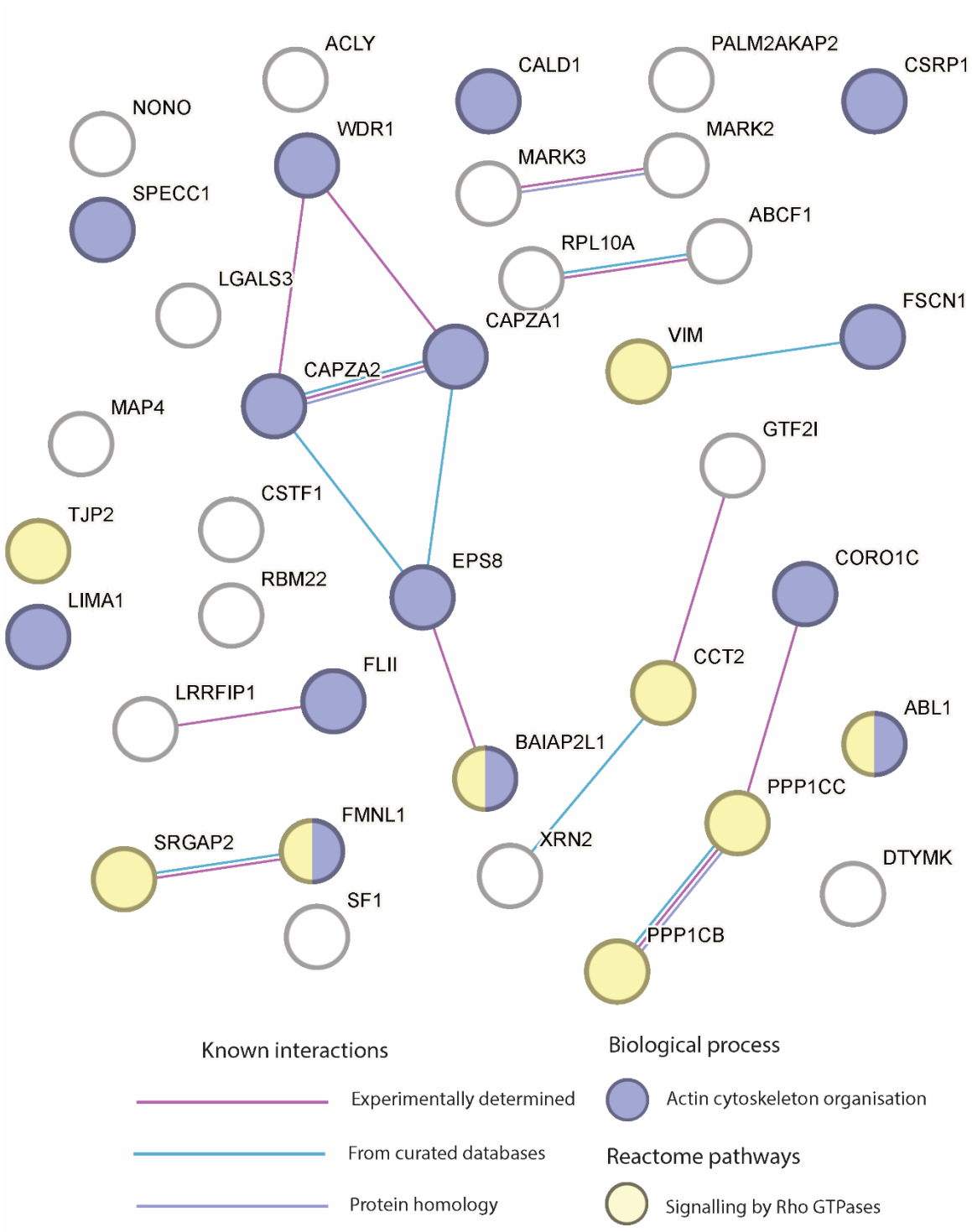

Figure 5-2 Protein-protein interaction map of ATP-F-actin binding proteins (JVM3-ATPγS) with Rho GTPase signalling data from Gene Ontology
PPI map from STRING v12.0 showing proteins significantly enriched in ATP-F-actin samples from mass spectrometry data using JVM3 cells and ATPγS as a non-hydrolysable analogue of ATP. Network nodes represent proteins (gene names shown), purple nodes represent proteins involved in actin cytoskeletal organisation and yellow nodes represent proteins involved in signalling by Rho GTPases (data from Gene Ontology). Interactions or homology are shown with different coloured lines connecting protein nodes (data from STRING v12.0).

Table 5-3 Mass spectrometry data of proteins enriched in ATP-F-actin (JVM3-ATPγS) and involved in Rho GTPase signalling as derived from Gene Ontology
Table listing proteins enriched in ATP-F-actin samples from mass spectrometry data using JVM3 cells and ATPγS as a non-hydrolysable analogue of ATP, and involved in the biological process of actin cytoskeletal organisation and in the Rho GTPase signalling (data from Gene Ontology). For each protein their name, gene name, and statistical data are shown. Students T-test difference value indicates preference for ATP-F-actin. Also shown is whether this difference was significant ("+"), and whether the data was significant by p-value only ("+"). Data from Gene Ontology shows proteins involved in actin cytoskeletal organisation in purple and signalling by Rho GTPases in yellow. Those involved in both are shown in yellow with bold text and bold borders

Actin cytoskeletal organisation (Biological process – Gene ontology)				
Signalling by Rho GTPases (Reactome pathway)				
Protein names	Gene names	Student's T-test Difference JVM3 (ADP-ATPgS)	Student's T-test Significant JVM3 (ADP-ATPgS)	Student's T-test Significant JVM3 (ADP-ATPgS) p-value only
Cytospin-B	SPECC1	-3.18		+
WD repeat-containing protein 1	WDR1	-2.12		+
Caldesmon	CALD1	-4.89	+	+
Cysteine and glycine-rich protein 1	CSRP1	-5.10	+	+
F-actin-capping protein subunit alpha-2	CAPZA2	-5.78	+	+
F-actin-capping protein subunit alpha-1	CAPZA1	-3.50		+
Fascin	FSCN1	-3.86		+
LIM domain and actin-binding protein 1	LIMA1	-0.68		+
Epidermal growth factor receptor kinase substrate 8	EPS8	-3.68		+
Protein flightless-1 homolog	FLII	-2.54		+
Coronin-1C	CORO1C	-6.10	+	+
Brain-specific angiogenesis inhibitor 1-associated protein 2-like protein 1	**BAIAP2L1**	**-5.09**	**+**	**+**
Tyrosine-protein kinase ABL1	**ABL1**	**-4.90**	**+**	**+**
Formin-like protein 1	**FMNL1**	**-0.71**		**+**
Tight junction protein ZO-2	TJP2	-1.03		+
Vimentin	VIM	-2.10		+

T-complex protein 1 subunit beta	CCT2	-0.71		+
SLIT-ROBO Rho GTPase-activating protein 2	SRGAP2	-3.60		+
Serine/threonine-protein phosphatase PP1-beta catalytic subunit	PPP1CB	-1.43		+
Serine/threonine-protein phosphatase PP1-gamma catalytic subunit	PPP1CC	-2.79		+

Finally, a volcano plot in Figure 5-3 shows the full data set plotted with the Students T-test difference against the -Log of the t-test p-value only. Non-significant or non-highlighted hits are denoted by grey boxes, while highlighted hits significant in difference by p-value only (dark blue) or both (light blue) are shown with blue boxes. While only hits that were deemed interesting are shown here, all significant hits were shown in the previous PPI maps and tables. Filamin B (FLNB) was found to be significantly enriched in ADP-F-actin samples, as expected since it is a filament cross-linking protein. Encouragingly, both CAPZA1 and CAPZA2 were significant hits, being enriched in ATP-F-actin eluate, which we would expect since they are capping proteins and are thus expected to specifically bind the barbed ends of actin filaments.

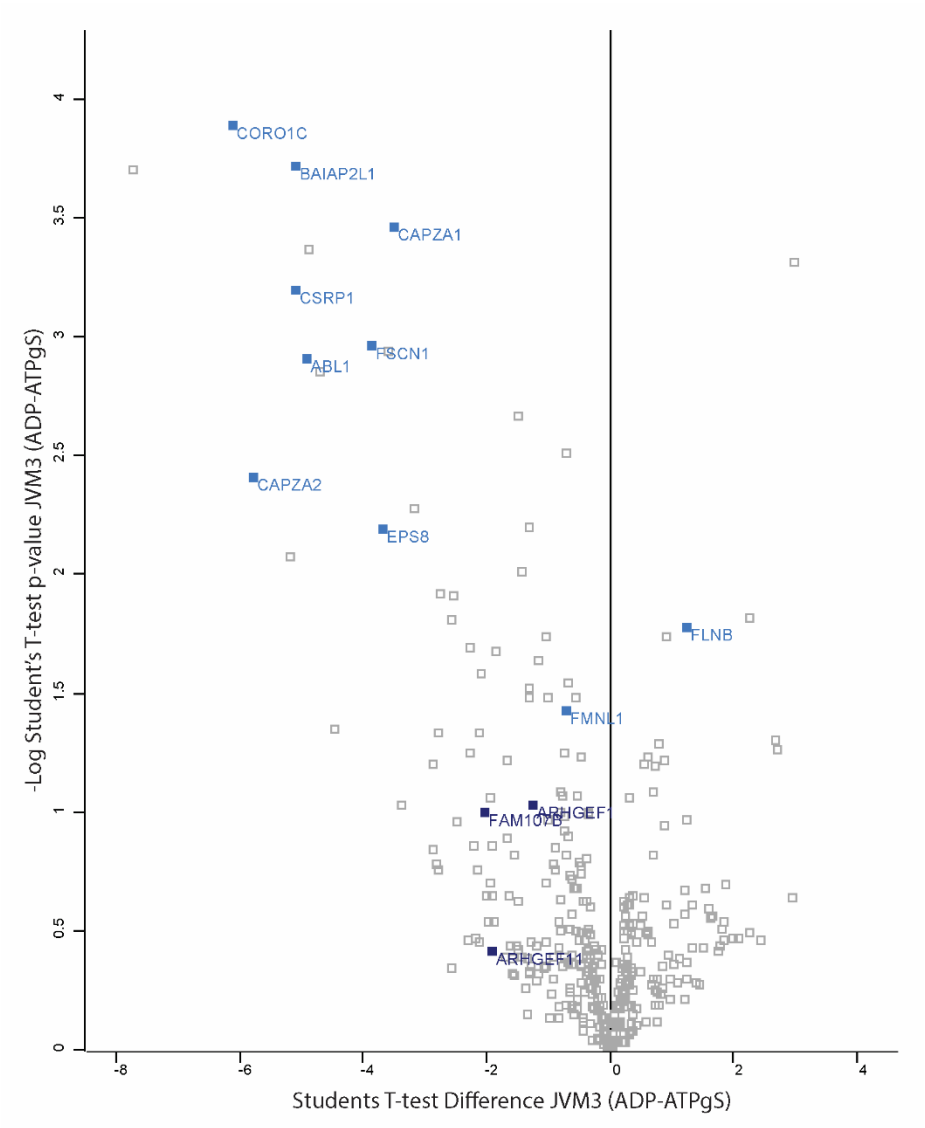

Figure 5-3 Volcano plot of ATP-F-actin binding proteins (JVM3-ATPγS)
Volcano plot showing Students T-test difference of identified proteins between ADP- and ATP-F-actin and p-value only of all proteins identified. Proteins of interest are highlighted, with light blue squares representing those in which the Students T-test difference between conditions was significant, and dark blue squares representing those proteins with significant p-value only. P<0.05 and FDR 5%.

Significantly enriched proteins in ATP-F-actin chromatography elutions using PDAC cells and ATPγS are presented in a Protein-Protein Interaction (PPI) map (Figure 5-4) and those identified as being involved in actin cytoskeletal organisation by Gene Ontology analysis shown as red nodes, and their data shown in Table 5-4.

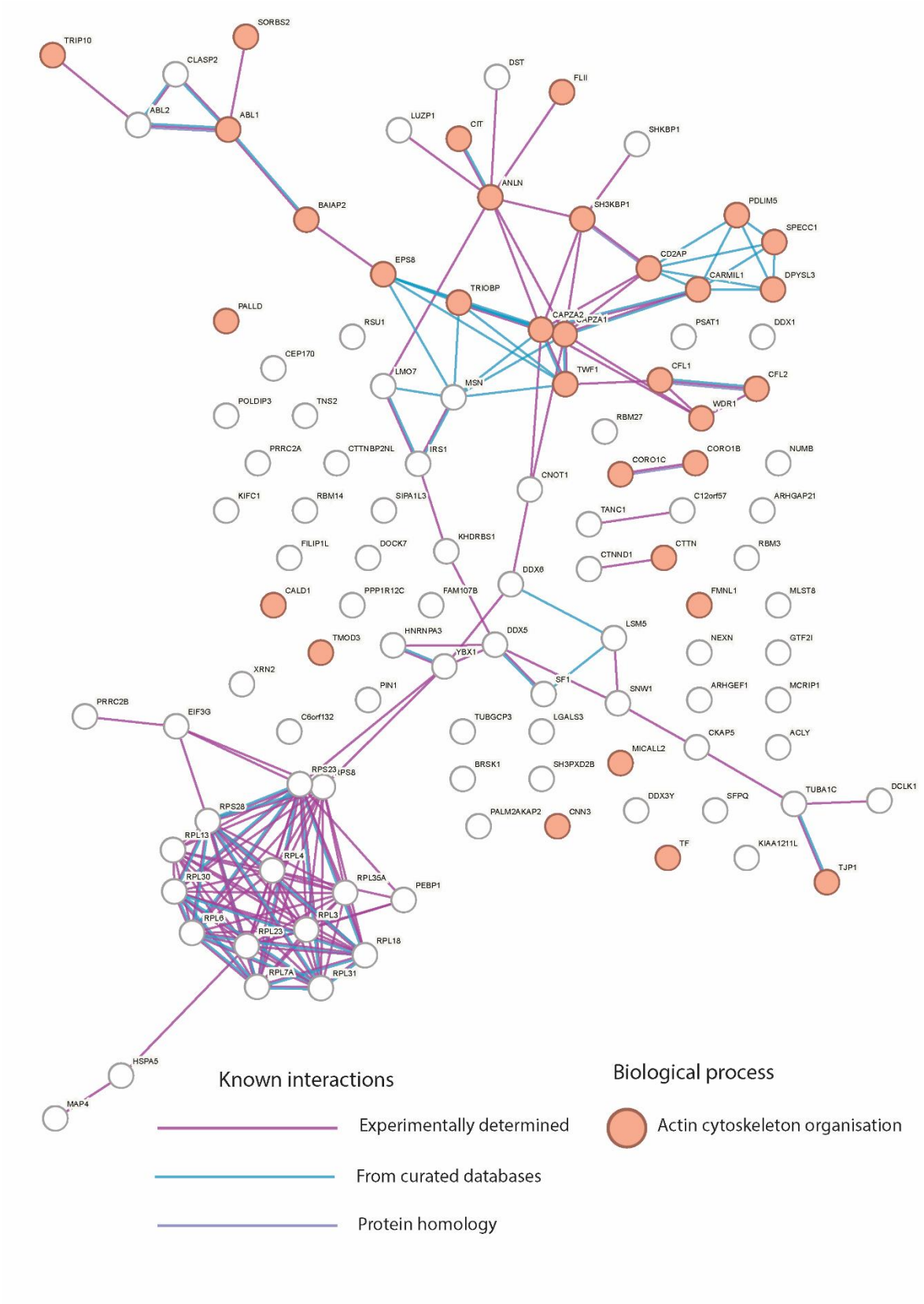

Figure 5-4 Protein-protein interaction map of ATP-F-actin binding proteins (PDAC-ATPγS) PPI map from STRING v12.0 showing proteins significantly enriched in ATP-F-actin samples from mass spectrometry data using PDAC cells lysates and ATPγS as a non-hydrolysable analogue of ATP. Network nodes represent proteins (gene names shown) and red nodes represent proteins involved in actin cytoskeletal organisation (data from Gene Ontology). Interactions or homology are shown with different coloured lines connecting protein nodes (data from STRING v12.0).

Table 5-4 Mass spectrometry data of proteins enriched in ATP-F-actin (PDAC-ATPγS)
Table listing proteins enriched in ATP-F-actin samples from mass spectrometry data using PDAC cell lysates and ATPγS as a non-hydrolysable analogue of ATP, and involved in the biological process of actin cytoskeletal organisation (data from Gene Ontology). For each protein their name, gene name, and statistical data are shown. Students T-test difference value indicates preference for ATP-F-actin. Also shown is whether this difference was significant ("+"), and whether the data was significant by p-value only ("+").

Actin cytoskeletal organisation (Biological process – Gene ontology)				
Protein names	**Gene names**	**Student's T-test Difference PDAC2 (ADP-ATPgS)**	**Student's T-test Significant PDAC2 (ADP-ATPgS)**	**Student's T-test Significant PDAC2 (ADP-ATPgS) p-value only**
Coronin-1B	CORO1B	-1.58	+	+
Coronin-1C	CORO1C	-0.99		+
Sorbin and SH3 domain-containing protein 2	SORBS2	-0.83		+
F-actin-capping protein subunit alpha-2	CAPZA2	-1.82	+	+
Protein flightless-1 homolog	FLII	-1.81		+
SH3 domain-containing kinase-binding protein 1	SH3KBP1	-4.04	+	+
Epidermal growth factor receptor kinase substrate 8	EPS8	-0.86		+
TRIO and F-actin-binding protein	TRIOBP	-0.72		+
Palladin	PALLD	-2.28		+
F-actin-capping protein subunit alpha-1	CAPZA1	-1.41	+	+
CD2-associated protein	CD2AP	-5.43	+	+
PDZ and LIM domain protein 5	PDLIM5	-1.04	+	+
Leucine-rich repeat-containing protein 16A	LRRC16A	-7.52	+	+
Cytospin-B	SPECC1	-3.74		+

Dihydropyrimidinase-related protein 3	DPYSL3	-4.51	+	+
Cofilin-2	CFL2	-3.38		+
WD repeat-containing protein 1	WDR1	-2.07	+	+
Caldesmon	CALD1	-2.25	+	+
MICAL-like protein 2	MICALL2	-4.80	+	+
Calponin-3	CNN3	-4.23		+
Serotransferrin	TF	-2.94	+	+
Tight junction protein ZO-1 (Fragment)	TJP1	-0.70		+
Cdc42-interacting protein 4	TRIP10	-1.68	+	+
Abelson tyrosine-protein kinase 2	ABL2	-1.71	+	+
Tyrosine-protein kinase ABL1	ABL1	-1.00		+
Citron Rho-interacting kinase	CIT	-3.34	+	+
Brain-specific angiogenesis inhibitor 1-associated protein 2	BAIAP2	-1.74	+	+
Actin-binding protein anillin	ANLN	-1.51	+	+
Twinfilin-1	TWF1	-2.08	+	+
Cofilin-1	CFL1	-1.54		+
Src substrate cortactin	CTTN	-2.37	+	+
Tropomodulin-3	TMOD3	-3.68		+
Formin-like protein 1	FMNL1	-5.11	+	+

As was displayed for data from JVM3 cells, identified ATP-F-actin binding proteins involved in Signalling by Rho GTPases (Reactome Pathway, Gene Ontology) are highlighted in yellow for PDAC cells on a PPI map (Figure 5-5) and table with their mass spectrometry data (Table 5-5).

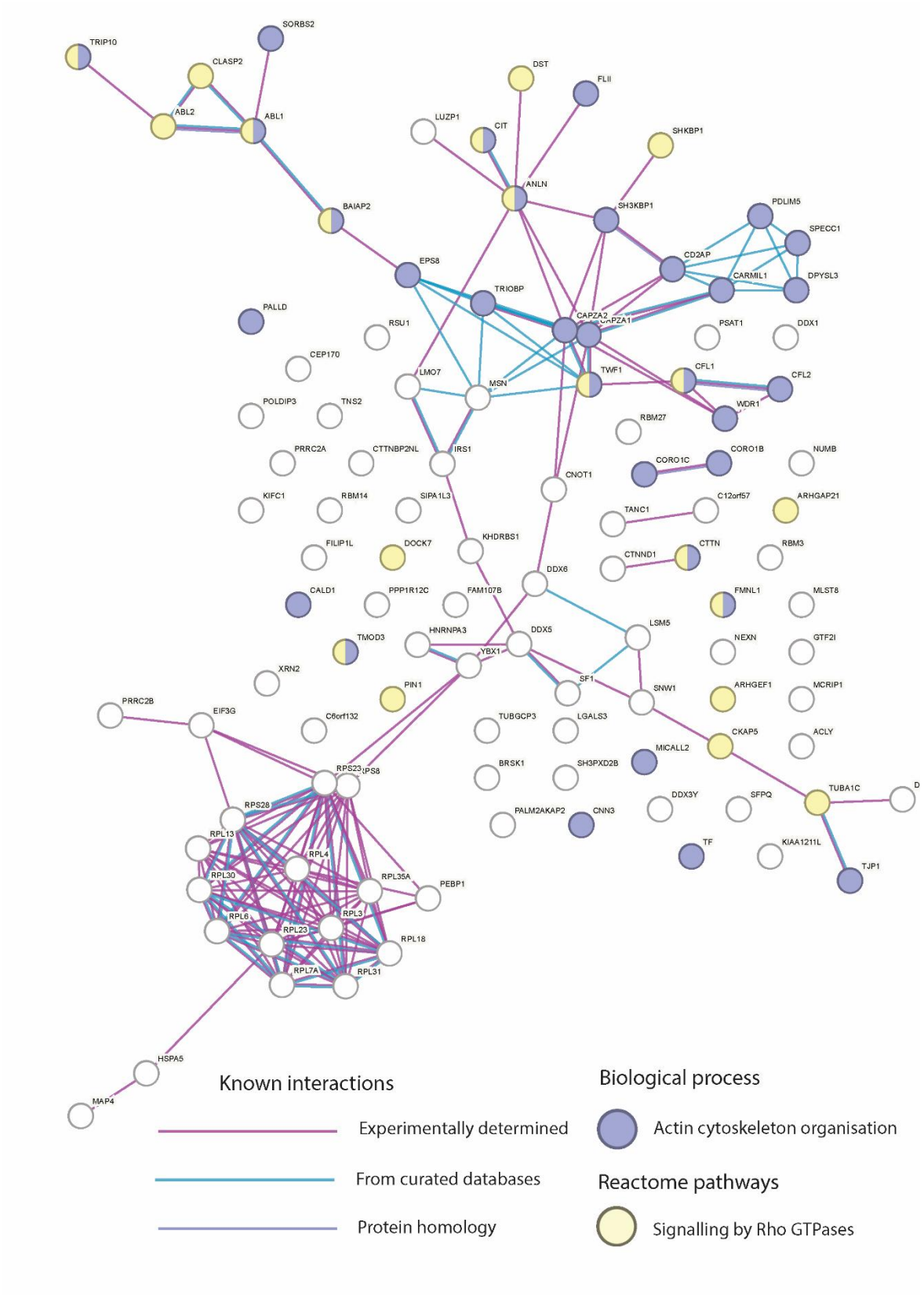

Figure 5-5 Protein-protein interaction map of ATP-F-actin binding proteins (PDAC-ATPγS) with Rho GTPase signalling data from Gene Ontology

PPI map from STRING v12.0 showing proteins significantly enriched in ATP-F-actin samples from mass spectrometry data using PDAC cell lysates and ATPγS as a non-hydrolysable analogue of ATP. Network nodes represent proteins (gene names shown), purple nodes represent proteins involved in actin cytoskeletal organisation and yellow nodes represent proteins involved in signalling by Rho GTPases (data from Gene Ontology). Interactions or homology are shown with different coloured lines connecting protein nodes (data from STRING v12.0).

Table 5-5 Mass spectrometry data of proteins enriched in ATP-F-actin columns (PDAC-ATPγS) and involved in Rho GTPase signalling as derived from Gene Ontology
Table listing proteins enriched in ATP-F-actin samples from mass spectrometry data using PDAC cells lysates and ATPγS as a non-hydrolysable analogue of ATP, and involved in the biological process of actin cytoskeletal organisation (data from Gene Ontology). For each protein their name, gene name, and statistical data are shown. Students T-test difference value indicates preference for ATP-F-actin. Also shown is whether this difference was significant ("+"), and whether the data was significant by p-value only ("+"). Data from Gene Ontology shows proteins involved in actin cytoskeletal organisation in purple and signalling by Rho GTPases in yellow. Those involved in both are shown in yellow with bold text and bold borders

Actin cytoskeletal organisation (Biological process – Gene ontology)				
Signalling by Rho GTPases (Reactome pathway)				
Protein names	**Gene names**	**Student's T-test Difference PDAC2 (ADP-ATPgS)**	**Student's T-test Significant PDAC2 (ADP-ATPgS)**	**Student's T-test Significant PDAC2 (ADP-ATPgS) p-value only**
Coronin-1B	CORO1B	-1.58	+	+
Coronin-1C	CORO1C	-0.99		+
Sorbin and SH3 domain-containing protein 2	SORBS2	-0.83		+
F-actin-capping protein subunit alpha-2	CAPZA2	-1.82	+	+
Protein flightless-1 homolog	FLII	-1.81		+
SH3 domain-containing kinase-binding protein 1	SH3KBP1	-4.04	+	+
Epidermal growth factor receptor kinase substrate 8	EPS8	-0.86		+
TRIO and F-actin-binding protein	TRIOBP	-0.72		+
Palladin	PALLD	-2.28		+
F-actin-capping protein subunit alpha-1	CAPZA1	-1.41	+	+
CD2-associated protein	CD2AP	-5.43	+	+
PDZ and LIM domain protein 5	PDLIM5	-1.04	+	+
Leucine-rich repeat-containing protein 16A	LRRC16A	-7.52	+	+

Cytospin-B	SPECC1	-3.74		+
Dihydropyrimidinase -related protein 3	DPYSL3	-4.51	+	+
Cofilin-2	CFL2	-3.38		+
WD repeat-containing protein 1	WDR1	-2.07	+	+
Caldesmon	CALD1	-2.25	+	+
MICAL-like protein 2	MICALL2	-4.80	+	+
Calponin-3	CNN3	-4.23		+
Serotransferrin	TF	-2.94	+	+
Tight junction protein ZO-1 (Fragment)	TJP1	-0.70		+
Cdc42-interacting protein 4	**TRIP10**	**-1.68**	**+**	**+**
Abelson tyrosine-protein kinase 2	**ABL2**	**-1.71**	**+**	**+**
Tyrosine-protein kinase ABL1	**ABL1**	**-1.00**		**+**
Citron Rho-interacting kinase	**CIT**	**-3.34**	**+**	**+**
Brain-specific angiogenesis inhibitor 1-associated protein 2	**BAIAP2**	**-1.74**	**+**	**+**
Actin-binding protein anillin	**ANLN**	**-1.51**	**+**	**+**
Twinfilin-1	**TWF1**	**-2.08**	**+**	**+**
Cofilin-1	**CFL1**	**-1.54**		**+**
Src substrate cortactin	**CTTN**	**-2.37**	**+**	**+**
Tropomodulin-3	**TMOD3**	**-3.68**		**+**
Formin-like protein 1	**FMNL1**	**-5.11**	**+**	**+**
CLIP-associating protein 2	CLASP2	-2.29	+	+
Dystonin	DST	-1.64	+	+
SH3KBP1-binding protein 1	SHKBP1	-1.91	+	+
Rho guanine nucleotide exchange factor 7;Rho guanine nucleotide exchange factor 6	ARHGEF7;ARHGEF6	-3.20		+
Rho guanine nucleotide exchange factor 1	ARHGEF1	-2.13		+

Rho GTPase-activating protein 21	ARHGAP21	-0.50		+
Dedicator of cytokinesis protein 7	DOCK7	-0.57		+
Peptidyl-prolyl cis-trans isomerase NIMA-interacting 1	PIN1	-7.79	+	+
Cytoskeleton-associated protein 5	CKAP5	-3.03	+	+
Tubulin alpha-1C chain	TUBA1C	-4.91	+	+

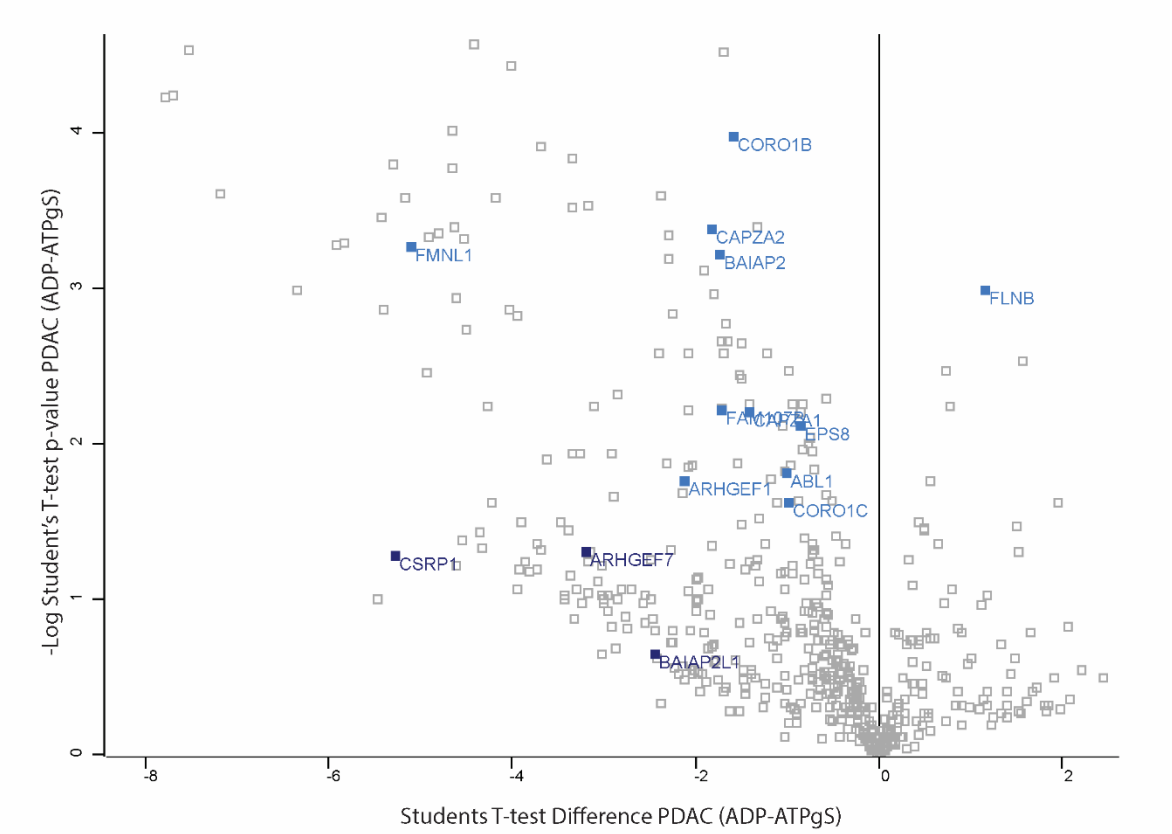

Figure 5-6 Volcano plot of ATP-F-actin binding proteins (PDAC-ATPγS)
Volcano plot showing Students T-test difference of identified interactors of ADP- and/or ATP-F-actin and p-value only of all proteins identified. Proteins of interest are highlighted, with light blue squares representing those in which the Students T-test difference between conditions was significant, and dark blue squares representing those proteins with significant p-value only. P<0.05 and FDR 5%.

As in the data from JVM3 cells, various expected protein hits gave us confidence in the results. Again, CAPZA1 and CAPZA2 are enriched in ATP-F-actin samples, with Filamin B showing preference for ADP-F-actin as expected. Moreover, various proteins involved in Signalling by Rho GTPases (Reactome Pathway, Gene Ontology) give interesting results for discussion and future work.

5.2.2 ATP-F-actin binding proteins (Jasplakinolide)

Significantly enriched proteins in ATP-F-actin chromatography elutions using JVM3 cells and Jasplakinolide are presented in a Protein-Protein Interaction (PPI) map (Figure 5-7). Hits identified as being involved in actin cytoskeletal organisation by Gene Ontology analysis are shown as red nodes, and their data are also presented in Table 5-6. Those involved in Rho GTPases signalling are presented as in section 5.2.1, with the PPI map (Figure 5-8) and table (Table 5-7) highlighting ATP-F-actin binding proteins involved in Actin Cytoskeletal Organisation (Gene Ontology) and Signalling by Rho GTPases (Reactome Pathway, Gene Ontology) in purple and yellow, respectively.

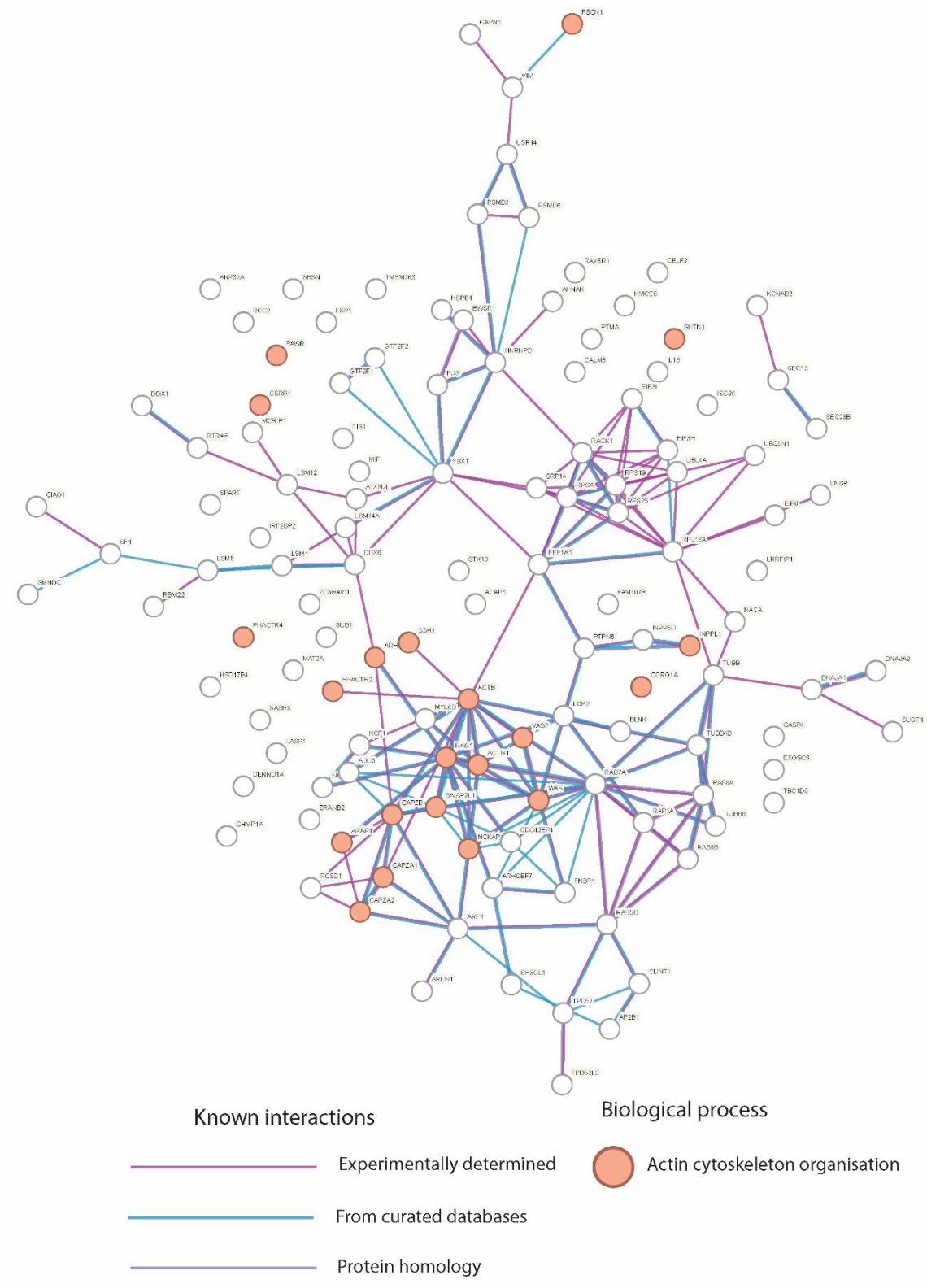

Figure 5-7 Protein-protein interaction map of ATP-F-actin binding proteins (JVM3-Jasplakinolide)
PPI map from STRING v12.0 showing proteins significantly enriched in ATP-F-actin samples from mass spectrometry data using JVM3 cells and Jasplakinolide treated F-actin. Network nodes represent proteins (gene names shown) and red nodes represent proteins involved in actin cytoskeletal organisation (data from Gene Ontology). Interactions or homology are shown with different coloured lines connecting protein nodes (data from STRING v12.0).

Table 5-6 Mass spectrometry data of proteins enriched in ATP-F-actin (JVM3-Jasplakinolide)
Table listing proteins enriched in ATP-F-actin samples from mass spectrometry data using JVM3 cells and Jasplakinolide treated F-actin, and involved in the biological process of actin cytoskeletal organisation (data from Gene Ontology). For each protein their name, gene name, and statistical data are shown. Students T-test difference value indicates preference for ATP-F-actin. Also shown is whether this difference was significant ("+"), and whether the data was significant by p-value only ("+").

Actin cytoskeletal organisation (Biological process – Gene ontology)				
Protein names	**Gene names**	**Student's T-test Difference JVM3-ADP_JVM3-Jas**	**Student's T-test Significant JVM3-ADP_JVM3-Jas**	**Student's T-test Significant JVM3-ADP_JVM3-Jas p-value only**
PRKC apoptosis WT1 regulator protein	PAWR	-0.96	+	+
Shootin-1	SHTN1	-1.52	+	+
Cysteine and glycine-rich protein 1	CSRP1	-2.44	+	+
Phosphatase and actin regulator 4	PHACTR4	-0.63		+
Protein phosphatase Slingshot homolog 1	SSH1	-1.10	+	+
Phosphatidylinositol 3,4,5-trisphosphate 5-phosphatase 2	INPPL1	-1.59	+	+
Rho GTPase-activating protein 17	ARHGAP17	-1.16	+	+
Phosphatase and actin regulator 2	PHACTR2	-1.21	+	+
Coronin-1A	CORO1A	-0.87	+	+
Actin, cytoplasmic 1	ACTB	-1.79	+	+
Vasodilator-stimulated phosphoprotein	VASP	-1.08	+	+
Ras-related C3 botulinum toxin substrate 1	RAC1	-0.59	+	+
Actin, cytoplasmic 2	ACTG1	-1.92	+	+
Wiskott-Aldrich syndrome protein	WAS	-1.07	+	+
Brain-specific angiogenesis inhibitor 1-associated protein 2-like protein 1	BAIAP2L1	-1.82	+	+
F-actin-capping protein subunit beta	CAPZB	-1.25	+	+
Arf-GAP with Rho-GAP domain, ANK repeat and PH domain-containing protein 1	ARAP1	-1.02	+	+

Nck-associated protein 1-like	NCKAP1L	-0.81	+	+
F-actin-capping protein subunit alpha-1	CAPZA1	-1.31	+	+
F-actin-capping protein subunit alpha-2	CAPZA2	-1.07	+	+

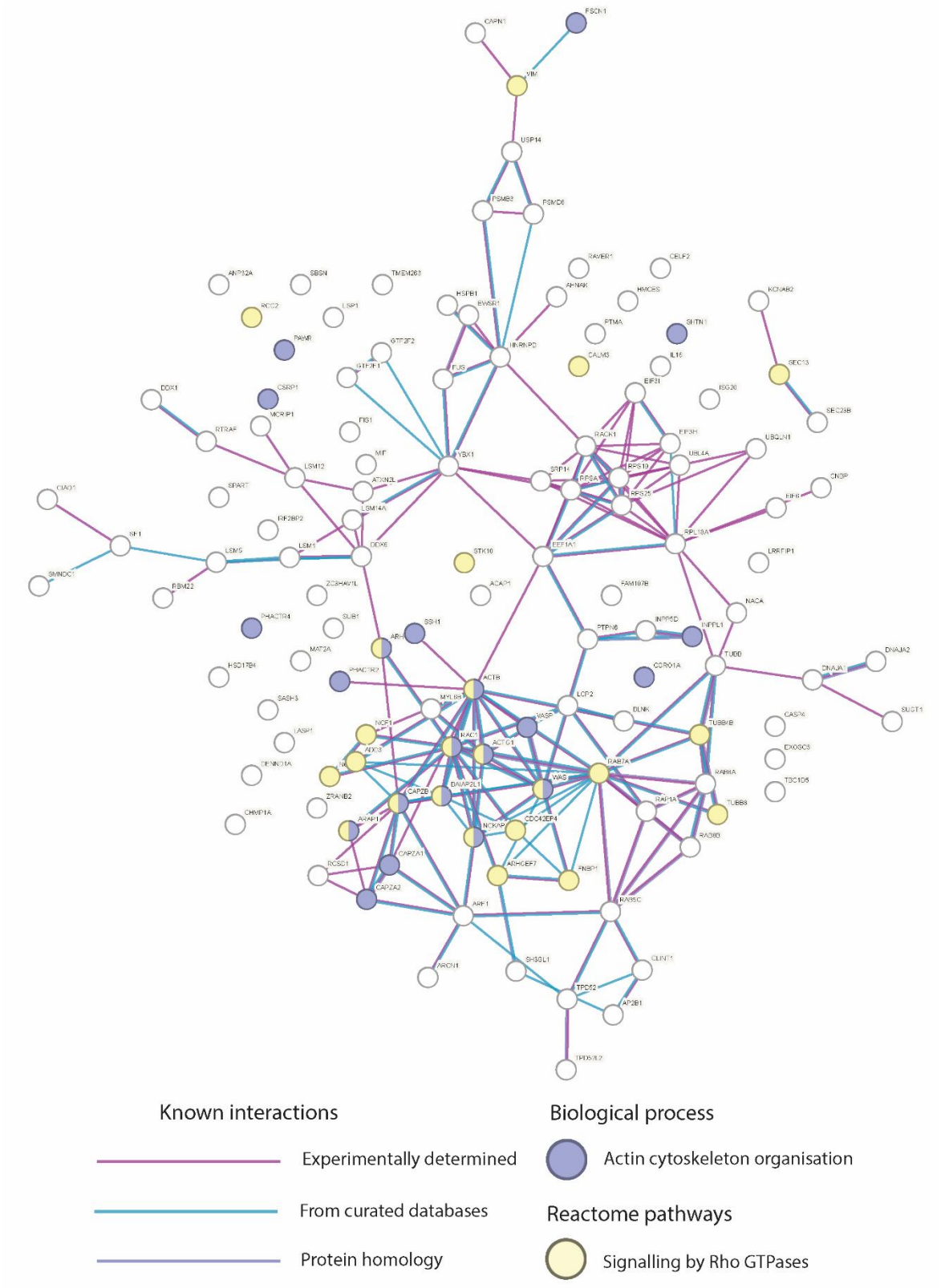

Figure 5-8 Protein-protein interaction map of ATP-F-actin binding proteins (JVM3-Jasplakinolide) with Rho GTPase signalling data from Gene Ontology
PPI map from STRING v12.0 showing proteins significantly enriched in ATP-F-actin samples from mass spectrometry data using JVM3 cell lysates and Jasplakinolide treated F-actin. Network nodes represent proteins (gene names shown), purple nodes represent proteins involved in actin cytoskeletal organisation and yellow nodes represent proteins involved in signalling by Rho GTPases (data from Gene Ontology). Interactions or homology are shown with different coloured lines connecting protein nodes (data from STRING v12.0).

Table 5-7 Mass spectrometry data of proteins enriched in ATP-F-actin columns (JVM3-Jasplakinolide) with Rho GTPase signalling data from Gene Ontology
Table listing proteins enriched in ATP-F-actin samples from mass spectrometry data using JVM3 cell lysates and Jasplakinolide treated F-actin, and involved in the biological process of actin cytoskeletal organisation and signalling by Rho GTPases (data from Gene Ontology). For each protein their name, gene name, and statistical data are shown. Students T-test difference value indicates preference for ATP-F-actin. Also shown is whether this difference was significant ("+"), and whether the data was significant by p-value only ("+"). Data from Gene Ontology shows proteins involved in actin cytoskeletal organisation in purple and signalling by Rho GTPases in yellow. Those involved in both are shown in yellow with bold text and bold borders.

Actin cytoskeletal organisation (Biological process – Gene ontology)				
Signalling by Rho GTPases (Reactome pathway)				
Protein names	**Gene names**	**Student's T-test Difference JVM3-ADP_JVM3-Jas**	**Student's T-test Significant JVM3-ADP_JVM3-Jas**	**Student's T-test Significant JVM3-ADP_JVM3-Jas p-value only**
PRKC apoptosis WT1 regulator protein	PAWR	-0.96	+	+
Shootin-1	SHTN1	-1.52	+	+
Cysteine and glycine-rich protein 1	CSRP1	-2.44	+	+
Phosphatase and actin regulator 4	PHACTR4	-0.63		+
Protein phosphatase Slingshot homolog 1	SSH1	-1.10	+	+
Phosphatidylinositol 3,4,5-trisphosphate 5-phosphatase 2	INPPL1	-1.59	+	+
Rho GTPase-activating protein 17	**ARHGAP17**	**-1.16**	**+**	**+**
Phosphatase and actin regulator 2	PHACTR2	-1.21	+	+
Coronin-1A	CORO1A	-0.87	+	+
Actin, cytoplasmic 1	ACTB	-1.79	+	+
Vasodilator-stimulated phosphoprotein	VASP	-1.08	+	+
Ras-related C3 botulinum toxin substrate 1	**RAC1**	**-0.59**	**+**	**+**
Actin, cytoplasmic 2	ACTG1	-1.92	+	+

Wiskott-Aldrich syndrome protein	**WAS**	**-1.07**	**+**	**+**
Brain-specific angiogenesis inhibitor 1-associated protein 2-like protein 1	**BAIAP2L1**	**-1.82**	**+**	**+**
F-actin-capping protein subunit beta	**CAPZB**	**-1.25**	**+**	**+**
Arf-GAP with Rho-GAP domain, ANK repeat and PH domain-containing protein 1	**ARAP1**	**-1.02**	**+**	**+**
Nck-associated protein 1-like	**NCKAP1L**	**-0.81**	**+**	**+**
F-actin-capping protein subunit alpha-1	CAPZA1	-1.31	+	+
F-actin-capping protein subunit alpha-2	CAPZA2	-1.07	+	+
Rho guanine nucleotide exchange factor 7	ARHGEF7	-2.31	+	+
Formin-binding protein 1	FNBP1	-1.66	+	+
Protein RCC2	RCC2	-1.66	+	+
Calmodulin-3	CALM3	-0.78	+	+
Protein SEC13 homolog	SEC13	-1.22	+	+
Serine/threonine-protein kinase 10	STK10	-1.37	+	+
Neutrophil cytosol factor 1;Putative neutrophil cytosol factor 1B;Putative neutrophil cytosol factor 1C	NCF1;NCF1B;NCF1C	-1.10	+	+
Neutrophil cytosol factor 2	NCF2	-2.64	+	+
Gamma-adducin	ADD3	-3.12	+	+
Ras-related protein Rab-7a	RAB7A	-1.49	+	+
Tubulin beta-4B chain;Tubulin beta-4A chain	TUBB4B;TUBB4A	-1.13	+	+
Cdc42 effector protein 4	CDC42EP4	-2.07	+	+
Vimentin	VIM	-1.96	+	+

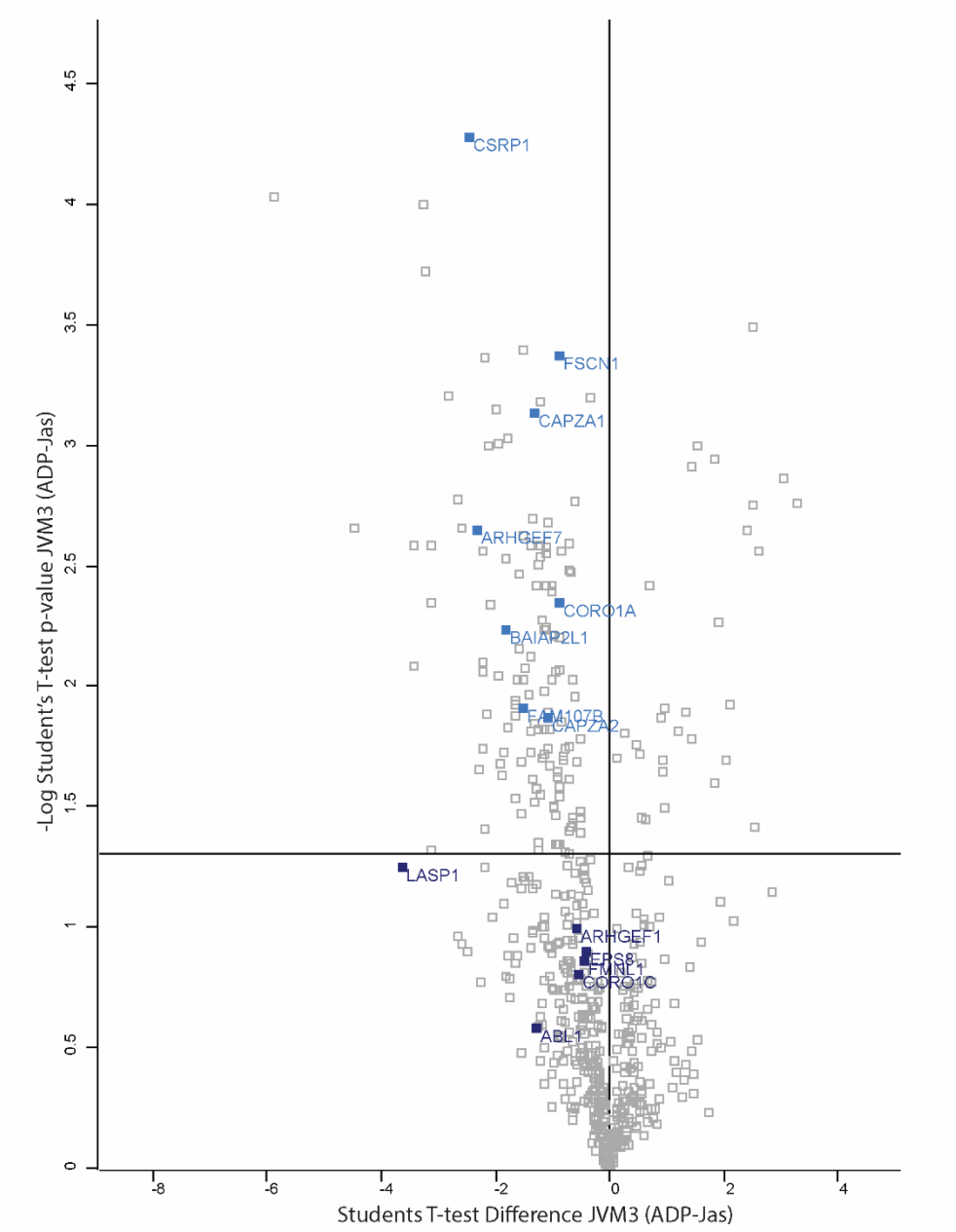

Figure 5-9 Volcano plot of ATP-F-actin binding proteins (JVM3-Jasplakinolide)
Volcano plot showing Students T-test difference of identified proteins between ADP- and ATP-F-actin and p-value only of all proteins identified. Proteins of interest are highlighted, with light blue squares representing those in which the Students T-test difference between conditions was significant, and dark blue squares representing those proteins with significant p-value only. P<0.05 and FDR 5%.

Significantly enriched proteins in ATP-F-actin chromatography elutions using PDAC cells and Jasplakinolide are presented in a Protein-Protein Interaction (PPI) map (Figure 5-10) and those identified as being involved in actin cytoskeletal organisation by Gene Ontology analysis are shown as red nodes, and their data are listed in Table 5-8.

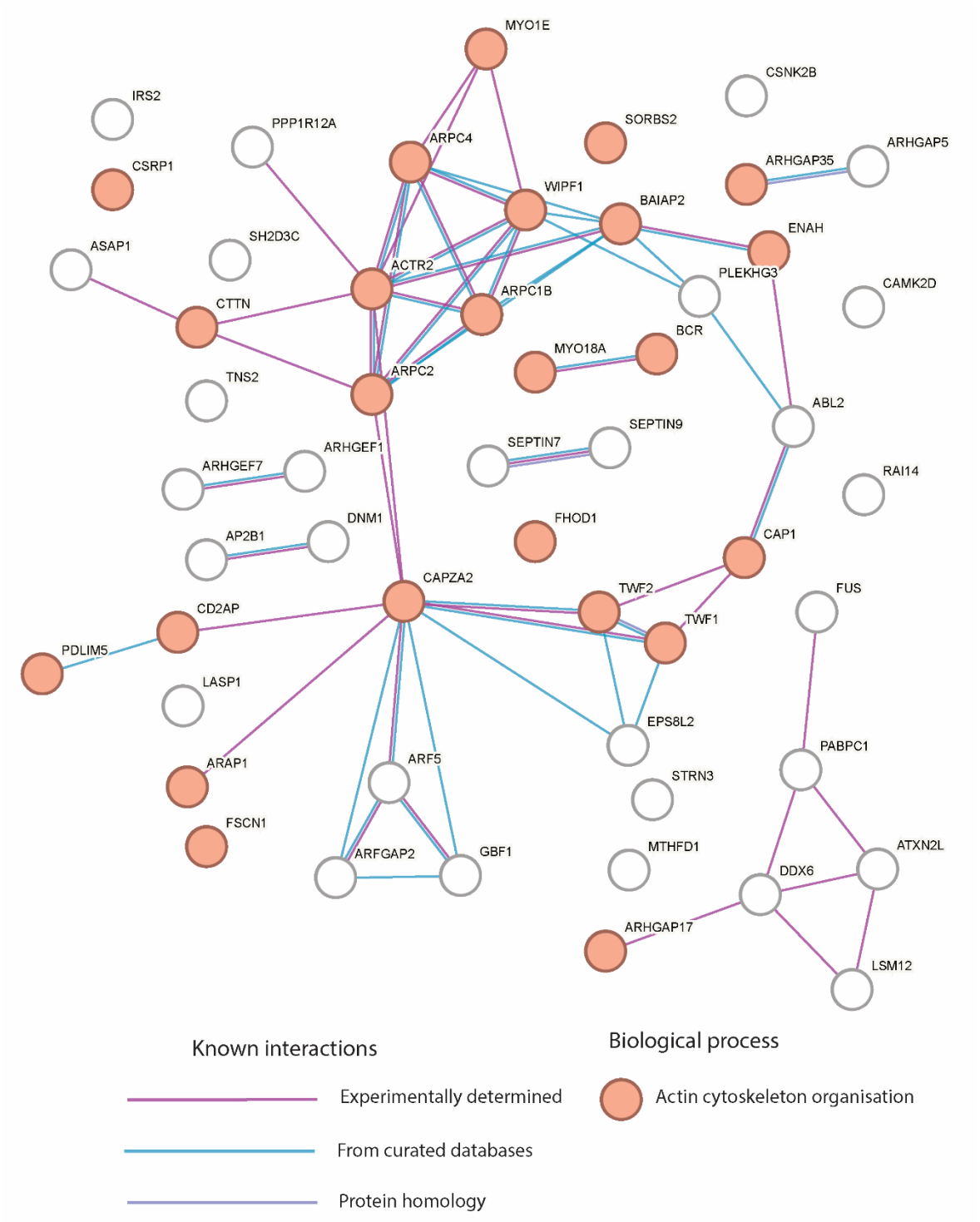

Figure 5-10 Protein-protein interaction map of ATP-F-actin binding proteins (PDAC-Jasplakinolide)
PPI map from STRING v12.0 showing proteins significantly enriched in ATP-F-actin samples from mass spectrometry data using PDAC cell lysates and Jasplakinolide treated F-actin. Network nodes represent proteins (gene names shown) and red nodes represent proteins involved in actin cytoskeletal organisation (data from Gene Ontology). Interactions or homology are shown with different coloured lines connecting protein nodes (data from STRING v12.0).

Table 5-8 Mass spectrometry data of proteins enriched in ATP-F-actin columns (PDAC-Jasplakinolide)
Table listing proteins enriched in ATP-F-actin samples from mass spectrometry data using PDAC cells lysates and Jasplakinolide treated F-actin, and involved in the biological process of actin cytoskeletal organisation (data from Gene Ontology). For each protein their name, gene name, and statistical data are shown. Students T-test difference value indicates preference for ATP-F-actin. Also shown is whether this difference was significant ("+"), and whether the data was significant by p-value only ("+").

Actin cytoskeletal organisation (Biological process – Gene ontology)				
Protein names	**Gene names**	**Student's T-test Difference PDAC-ADP_PDAC-Jas**	**Student's T-test Significant PDAC-ADP_PDAC-Jas**	**Student's T-test Significant PDAC-ADP_PDAC-Jas p-value only**
Unconventional myosin-Ie	MYO1E	-2.80	+	+
Cysteine and glycine-rich protein 1	CSRP1	-1.86	+	+
Actin-related protein 2/3 complex subunit 4	ARPC4	-0.66		+
WAS/WASL-interacting protein family member 1	WIPF1	-2.48	+	+
Sorbin and SH3 domain-containing protein 2	SORBS2	-1.74		+
Brain-specific angiogenesis inhibitor 1-associated protein 2	BAIAP2	-0.92		+
Rho GTPase-activating protein 35	ARHGAP35	-1.33		+
Protein enabled homolog	ENAH	-0.80		+
Actin-related protein 2	ACTR2	-0.85		+
Actin-related protein 2/3 complex subunit 1B	ARPC1B	-0.74		+
Src substrate cortactin	CTTN	-2.07		+
Actin-related protein 2/3 complex subunit 2	ARPC2	-1.04		+
Unconventional myosin-XVIIIa	MYO18A	-1.10		+
Breakpoint cluster region protein	BCR	-2.54		+
Adenylyl cyclase-associated protein 1	CAP1	-1.39		+
FH1/FH2 domain-containing protein 1	FHOD1	-0.74		+
Twinfilin-2	TWF2	-2.26		+
Twinfilin-1	TWF1	-2.28	+	+

F-actin-capping protein subunit alpha-2	CAPZA2	-1.04		+
CD2-associated protein	CD2AP	-0.91		+
PDZ and LIM domain protein 5	PDLIM5	-1.12	+	+
Arf-GAP with Rho-GAP domain, ANK repeat and PH domain-containing protein 1	ARAP1	-1.33		+
Fascin	FSCN1	-1.03	+	+
Rho GTPase-activating protein 17	ARHGAP17	-2.50		+

ATP-F-actin binding proteins identified as being involved in Rho GTPase signalling are again shown highlighted in yellow in a PPI map (Figure 5-11) and table (Table 5-9).

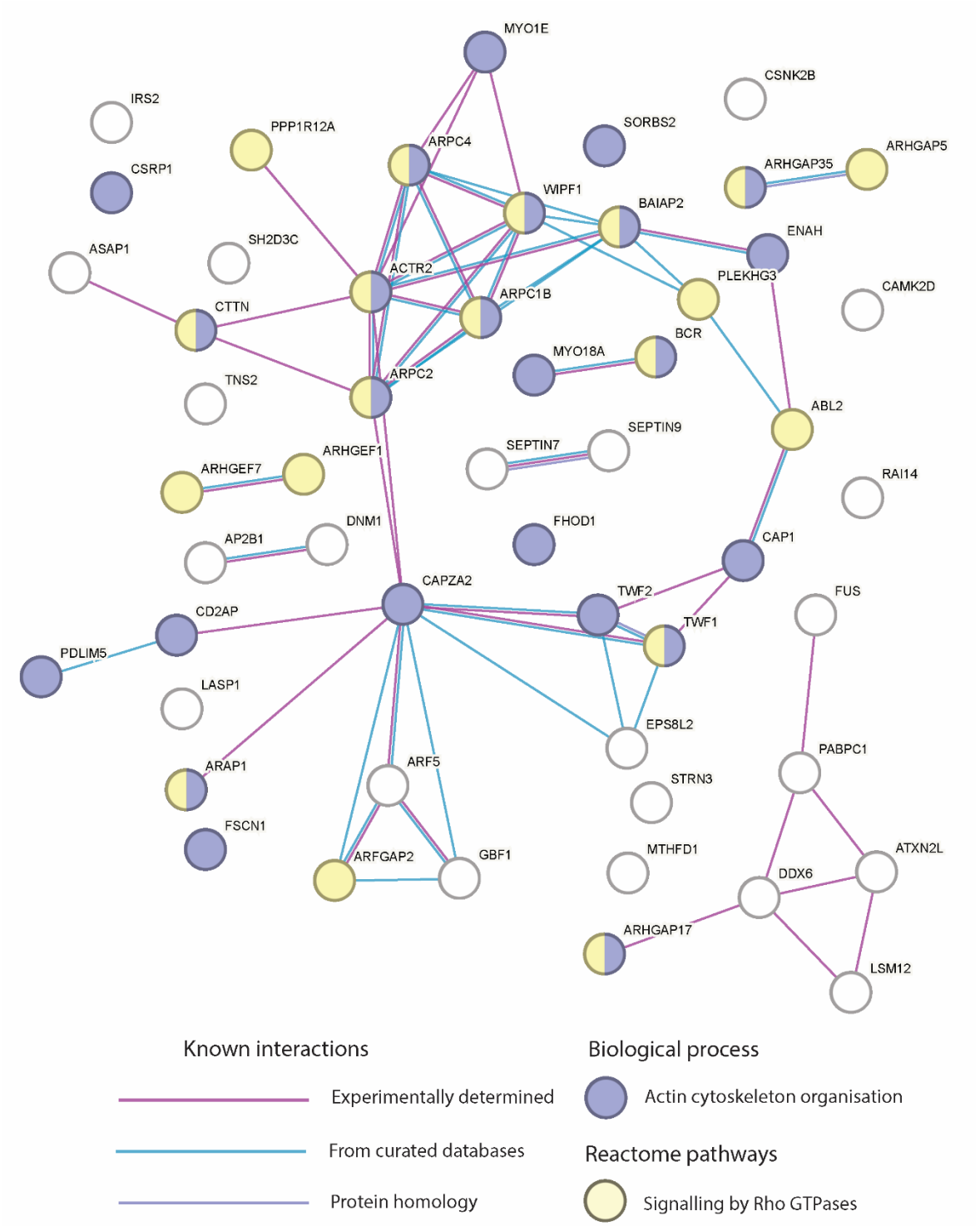

Figure 5-11 Protein-protein interaction map of ATP-F-actin binding proteins (PDAC-Jasplakinolide) with Rho GTPase signalling data from Gene Ontology
PPI map from STRING v12.0 showing proteins significantly enriched in ATP-F-actin samples from mass spectrometry data using PDAC cells lysates and Jasplakinolide treated F-actin. Network nodes represent proteins (gene names shown), purple nodes represent proteins involved in actin cytoskeletal organisation and yellow nodes represent proteins involved in signalling by Rho GTPases (data from Gene Ontology). Interactions or homology are shown with different coloured lines connecting protein nodes (data from STRING v12.0).

Table 5-9 Mass spectrometry data of proteins enriched in ATP-F-actin columns (PDAC-Jasplakinolide) with Rho GTPase signalling data from Gene Ontology
Table listing proteins enriched in ATP-F-actin samples from mass spectrometry data using PDAC cells lysates and Jasplakinolide treated F-actin, and involved in the biological process of actin cytoskeletal organisation and signalling by Rho GTPases (data from Gene Ontology). For each protein their name, gene name, and statistical data are shown. Students T-test difference value indicates preference for ATP-F-actin. Also shown is whether this difference was significant ("+"), and whether the data was significant by p-value only ("+"). Data from Gene Ontology shows proteins involved in actin cytoskeletal organisation in purple and signalling by Rho GTPases in yellow. Those involved in both are shown in yellow with bold text and bold borders.

Actin cytoskeletal organisation (Biological process – Gene ontology)				
Signalling by Rho GTPases (Reactome pathway)				
Protein names	**Gene names**	**Student's T-test Difference PDAC-ADP_PDAC-Jas**	**Student's T-test Significant PDAC-ADP_PDAC-Jas**	**Student's T-test Significant PDAC-ADP_PDAC-Jas p-value only**
Unconventional myosin-Ie	MYO1E	-2.80	+	+
Cysteine and glycine-rich protein 1	CSRP1	-1.86	+	+
Actin-related protein 2/3 complex subunit 4	**ARPC4**	**-0.66**		**+**
WAS/WASL-interacting protein family member 1	**WIPF1**	**-2.48**	**+**	**+**
Sorbin and SH3 domain-containing protein 2	SORBS2	-1.74		+
Brain-specific angiogenesis inhibitor 1-associated protein 2	**BAIAP2**	**-0.92**		**+**
Rho GTPase-activating protein 35	**ARHGAP35**	**-1.33**		**+**
Protein enabled homolog	ENAH	-0.80		+
Actin-related protein 2	**ACTR2**	**-0.85**		**+**
Actin-related protein 2/3 complex subunit 1B	**ARPC1B**	**-0.74**		**+**
Src substrate cortactin	**CTTN**	**-2.07**		**+**
Actin-related protein 2/3 complex subunit 2	**ARPC2**	**-1.04**		**+**
Unconventional myosin-XVIIIa	MYO18A	-1.10		+

Breakpoint cluster region protein	**BCR**	**-2.54**		**+**
Adenylyl cyclase-associated protein 1	CAP1	-1.39		+
FH1/FH2 domain-containing protein 1	FHOD1	-0.74		+
Twinfilin-2	TWF2	-2.26		+
Twinfilin-1	**TWF1**	**-2.28**	**+**	**+**
F-actin-capping protein subunit alpha-2	CAPZA2	-1.04		+
CD2-associated protein	CD2AP	-0.91		+
PDZ and LIM domain protein 5	PDLIM5	-1.12	+	+
Arf-GAP with Rho-GAP domain, ANK repeat and PH domain-containing protein 1	**ARAP1**	**-1.33**		**+**
Fascin	FSCN1	-1.03	+	+
Rho GTPase-activating protein 17	**ARHGAP17**	**-2.50**		**+**
Abelson tyrosine-protein kinase 2	ABL2	-2.75	+	+
Protein phosphatase 1 regulatory subunit 12A	PPP1R12A	-1.87	+	+
Rho GTPase-activating protein 5	ARHGAP5	-1.93	+	+
Pleckstrin homology domain-containing family G member 3	PLEKHG3	-1.70	+	+
Rho guanine nucleotide exchange factor 7	ARHGEF7	-1.52		+
Rho guanine nucleotide exchange factor 1	ARHGEF1	-1.88	+	+
ADP-ribosylation factor GTPase-activating protein 2	ARFGAP2	-2.65		+

Interesting hits are presented in a volcano plot in Figure 5-12 as before and include CAPZA1 and CAPZA2 as well as various proteins involved in Rho GTPase signalling and actin dynamics.

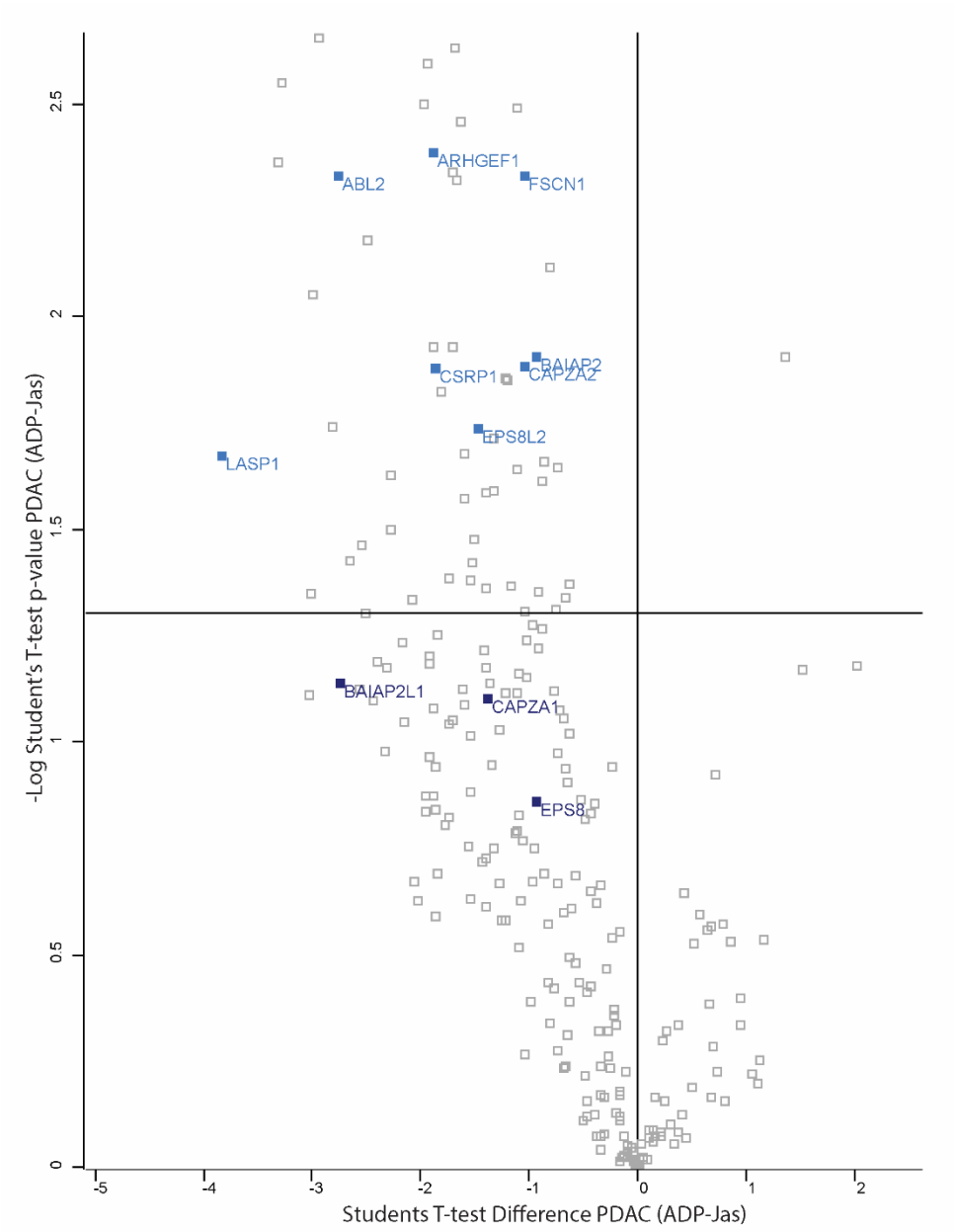

Figure 5-12 Volcano plot of ATP-F-actin binding proteins (PDAC-Jasplakinolide)
Volcano plot showing Students T-test difference of identified interactors of ADP- and ATP-F-actin and p-value only of all proteins identified. Proteins of interest are highlighted, with light blue squares representing those in which the Students T-test difference between conditions was significant, and dark blue squares representing those proteins with significant p-value only. P<0.05 and FDR 5%.

5.3 Discussion

In this chapter we have presented data showing proteins enriched in ATP-F-actin samples created by using both non-hydrolysable analogues of ATP (ATPγS) and Jasplakinolide treatment. The experiments for each of those methods were performed with two different cell lines, JVM3 and PDAC, both selected for their highly migratory nature. This was to ensure the cellular lysate we used would have high expression of actin binding and regulating proteins.

When hypothesising which proteins would preferentially bind ATP-F-actin we were particularly interested in those involved in positive regulation of actin polymerisation, whether that be directly or indirectly. Proteins involved in Rho GTPase signalling are crucial for regulating actin dynamics and the formation of cellular protrusions that allow the cell to migrate (Lawson and Ridley, 2018). Therefore, these proteins are of special interest. Also of interest are proteins that are known to bind actin, but that are not necessarily dependent on its nucleotide state. Proteins involved indirectly in Rho GTPase signalling, for example those involved in complex formation or localisation, are also great candidates for investigation.

It is also worth mentioning that these proteins identified as ATP-F-actin binding are not all assumed to be binding ATP-F-actin directly, but they may be part of complexes. However, it is encouraging that proteins that we know directly bind actin are enriched in the ATP-F-actin samples, such as capping proteins.

Importantly, it is worth discussing hits which were present in at least two of the data sets. These have been split into two lists for consideration. One list of proteins contains those where the two hits are from two different cell lines and includes Eps8, CSRP1, ABL1, FMNL1, FSCN, ARHGAP17 and ARHGEF7. The other list consists of proteins whose two hits were present in two datasets of the same cell line and includes BAIAP2, BAIAP2L1, ABL2 and ARHGEF1 (Table 5-10).

Table 5-10 ATP-F-actin enriched proteins in multiple datasets

Hits present in at least two mass spectrometry datasets	
Present in at least one dataset from each cell line, PDAC and JVM3	Present in two datasets of the same cell line
Eps8, CSRP1, ABL1, FMNL1, FSCN, ARHGAP17 and ARHGEF7	BAIAP2, BAIAP2L1, ABL2 and ARHGEF1

All of these hits are interesting and warrant investigation. However, for the sake of progress, we will discuss only those that act as positive controls, those that

were immediately investigated, and those that are a priority for future directions.

5.3.1 Positive controls

Capping proteins (CAPZA1 and CAPZA2) have been considered positive controls, since by their nature they bind the barbed end of actin filaments, where the nucleotide conformation is known to be ATP-F-actin. The enrichment of both of these capping proteins in ATP-F-actin samples was significant by Students T-test for the difference between ATP- and ADP-F-actin samples in all four mass spec datasets, except CAPZA1 in PDAC-Jasplakinolide which was significant by p-value only (Figure 5-12). The enrichment of capping proteins in our ATP-F-actin samples confirm our affinity columns are working as they should.

5.3.2 Coronin family proteins

Other encouraging hits enriched in our ATP-F-actin datasets are the members of the coronin family. Coronins were discovered as actin binding proteins in studies with *Dictylostelium*, where they were found to localise to the leading edge of migrating cells (de Hostos et al., 1991). Their activity was first described in yeast (yeast coronin – Crn1) as polymerisation promoters and cross-linkers, but not stabilisers (Goode et al., 1999). It was later shown that coronins are involved in negative regulation of polymerisation, and more specifically regulation of the Arp2/3 complex (Humphries et al., 2002).

Seven coronin family proteins have been found in mammals so far and are named coronin 1-7 (Liu et al., 2016). Coronin 1B has been shown to directly regulate Arp2/3 (Cai et al., 2007a) by promoting the dissociation of Arp2/3 from branched filaments (Cai et al., 2008). This occurs through the direct interaction of coronin 1B with the complex and is dependent on the dephosphorylation of coronin 1B by slingshot phosphatase (SSH1L), which decreases their interaction. Interestingly, coronin 1B also regulates cofilin indirectly via SSL1L, with reduced levels of coronin 1B resulting in an increase in cofilin phosphorylation which in turn alters the rate of filament turnover (Cai et al., 2007a).

Coronin 1B is of special interest to this project as it is one of the only actin binding proteins (besides capping proteins) known to preferentially bind ATP-F-actin. This was shown in co-sedimentation experiments with F-actin in the form of ADP or ATP actin, using a different approach as the one described in this thesis. The ADP-F-actin filaments were prepared by polymerising G-actin with ADP as its bound nucleotide. The ATP-F-actin was prepared from G-actin with ATP and the co-sedimentation was performed taking into account the rate of hydrolysis and release of phosphate from actin filaments. Importantly, they found that coronin 1B bound ATP-F-actin with over 40-fold higher affinity than ADP-F-actin, and that F-actin binding was crucial for coronin 1B to exert an effect on actin dynamics and cell migration (Cai et al., 2007b).

In our mass spectrometry data we identified three coronin isoforms as ATP-F-actin binders, including coronin 1B (Table 5-4) in "PDAC – ATPγS". Coronin 1C was also identified as an ATP-F-actin binder in the same dataset, but was significant by p-value only (Table 5-4). Coronin 1C and coronin 1A were also found to preferentially bind ATP-F-actin in "JVM3 – ATPγS" (Table 5-2) and "JVM3 – Jasplakinolide" (Table 5-6), respectively. These results provide encouragement for the validity and relevance of the rest of the proteins identified as ATP-F-actin binders.

Interestingly, the slingshot phosphatase SSH1 was identified as preferentially binding ATP-F-actin in our data from "JVM3 – Jasplakinolide" (Table 5-6). SSH1 is the shorter isoform of SSH1L, which we discussed previously as an important regulator of the activity of coronin 1B (the L that differentiates them means longer isoform) (Ohta et al, 2003). This invites the question of the method of ATP-F-actin binding to coronin and SSH1: is it binding to one of them directly and hence the other indirectly? Or is it binding them independently and causing co-localisation of the complex to allow its function? These questions are important for any ATP-F-actin protein identified, and an exciting insight to future work.

5.3.3 Eps8

Eps8 is an actin binding protein known to localise at lamellipodia (Provenzano et al., 1998), where it binds and activates Rac GEF Sos1 (Scita et al., 2001) as part

of a complex with Abi1 (Scita et al., 1999). As well as its role in Rac activation and therefore Rho GTPase signalling, Eps8 was also identified to directly bind F-actin, with capping and bundling capabilities *in vitro* (Disanza et al., 2004). A role in the regulation of actin dynamics independent of Rac1 was also identified for Eps8, in which it acts in a complex with IRSp53 under the control of Cdc42 to regulate the formation of filopodia (Disanza et al., 2006).

Interestingly, IRSp53 (also known as BAIAP2), was significantly enriched in ATP-F-actin samples in "PDAC-ATPγS" and significant by p-value only in "PDAC-Jasplakinolide". Further, BAIAP2L1, another member of the IRSp53 family (Chao et al., 2015) which shares the same SH3 domain as BAIAP2 (Scita et al., 2008), was also found to be significantly enriched in ATP-F-actin samples in both "JVM3- ATPγS" and "JVM3-Jasplakinolide". Like Eps8, IRSp53 can bind actin (Yamagishi et al., 2004), displays a similar localisation (Nakagawa et al., 2003) and also has an interesting role in the formation of complexes involved in Rac signalling, having Rac binding function in its N-terminal and the ability to bind a number of proteins involved in regulating actin dynamics via its SH3 domain, including WAVE2 (Miki et al., 2000) and Eps8 (Disanza et al., 2006). IRSp53 would indeed be another interesting candidate for investigation into the mechanism of ATP-F-actin binding, and certainly may be acting in a similar way to Eps8 considering their overlapping pathways and shared binding partners.

Finally, an Eps8 related protein family, consisting of Eps8L1, Eps8L2 and Eps8L3, was also identified as enriched in our ATP-F-actin datasets. All members of this family are able to interact with Abi/Sos1; however not all are able to activate Sos1 or localise to ruffles and lamellipodia (Offenhauser et al., 2004). Encouragingly, Eps8L2, which was identified in our data as preferentially binding ATP-F-actin, is able to activate Sos1 GEF activity and localise to sites of dynamic actin processes in the same manner as Eps8 (Offenhauser et al., 2004).

The previously described capping capabilities of Eps8, and their involvement in Rho GTPase signalling pathways, make it a logical candidate for ATP-F-actin binding. Given the wealth of knowledge on Eps8 and its involvement in actin-based processes it is an excellent target for the exploration of how it and other proteins bind ATP-F-actin. This will be investigated and discussed in the next chapter.

5.3.4 ATP-F-actin binders involved in Rho GTPase signalling

As introduced in the first chapter, Rho GTPase signalling controls the formation of cellular protrusions that allow cells to migrate. This makes proteins involved in Rho GTPase signalling excellent candidates for ATP-F-actin binding proteins that may lead to positive feedback in polymerisation. GEFs that act on Rac1 or Cdc42 are of particular interest, due to their positive regulation of the formation of lamellipodia and filopodia/invadopodia, respectively. An attractive hypothesis is that ATP-F-actin binding causes the localisation of these proteins (and their complexes if applicable).

ARHGAP17, found significantly enriched in ATP-F-actin in "JVM3-Jasplakinolide" (Table 5-7) and significant by p-value in "PDAC-Jasplakinolide" (Table 5-9), is a RHO GTPase activating protein (GAP) which was identified in a study investigating the binding partners of the SH3 domain of a Cdc42 interacting protein (Richnau and Aspenstrom, 2001). *In vitro* assays have demonstrated that ARHGAP17 catalysed the hydrolysis of GTP on both Rac1 and Cdc42 (Richnau and Aspenstrom, 2001). Importantly, the Cdc42 interaction protein that was used to identify ARHGAP17 by binding its SH3 domain, TRIP10 (or CIP4 – Cdc42 interacting protein 4), was also found to be significantly enriched in ATP-F-actin samples in "PDAC-ATPγS".

Recently, ARHGAP17 has been identified as an important negative regulator of invadopodia via its GAP activity on Cdc42 under strict spatiotemporal control (Kreider-Letterman et al., 2023). Interestingly, the shift in spatial control that allows ARHGAP17 to inactivate Cdc42 and promote invadopodia disassembly is a result of interaction with TRIP10 which we also identified as preferentially binding ATP-F-actin. These two proteins that work together to regulate Cdc42, and the cellular protrusions it initiates, are very interesting candidates for future investigation on the relevance of ATP-F-actin binding on such a complex.

ARHGEF7, found significantly enriched in ATP-F-actin in "JVM3-Jasplakinolide" (Table 5-7) and significant by p-value in "PDAC-Jasplakinolide" (Table 5-9), was originally discovered in a study for new interactors of PAK (Bagrodia et al., 1998) and shown to be involved in the activation of Cdc42 and Rac (Manser et al., 1998). Interestingly, like Eps8, ARHGEF7 has been shown to bind Abi1 *in vitro*,

and co-localise at sites of dynamic actin protrusions such as membrane ruffles (Campa et al., 2006). Indeed, it had previously been shown to be involved in the regulation of membrane ruffles (Lee et al., 2001).

Of great interest to this project, ARHGEF7 has been shown to form a complex with coronin 1A (also identified as preferentially binding ATP-F-actin, in our dataset "JVM3 – Jasplakinolide" (Table 5-6)) that contributes to a positive feedback loop that promotes the translocation of Rac from the cytosol to the membrane, and increases the amount of active Rac at the latter (Castro-Castro et al., 2011). Crucially, this process is dependent on direct binding of coronin 1A to F-actin, and could be disrupted when the binding to F-actin is interrupted via a point mutation (R-D missense mutation at pos29) (Castro-Castro et al., 2011). This mutation is the same as the R30D mutation in coronin 1B which was shown to abolish its F-actin binding that allowed it to exert its effect on actin dynamics (Cai et al., 2007b). Most importantly, as previously discussed in 5.3.2, coronin 1B was shown the preferentially bind ATP-F-actin with over 40-fold increase in affinity (Cai et al., 2007b). This is greatly encouraging and warrants future investigation, as it provides the most evidence for the role of ATP-F-actin in a positive feedback loop via translocation and activation of Rac.

In conclusion, our data show that there are indeed a pool of proteins that preferentially bind ATP-F-actin, whether it be directly or indirectly. The presence of capping proteins, as well as coronin family members gives us great confidence in the results and from the rest of the data, many exciting avenues for exploration. We hypothesise that these proteins enriched in ATP-F-actin samples are involved in positive feedback of actin polymerisation and investigation of the method and relevance of this is of utmost importance.

6 ATP-F-actin in live cells

6.1 Introduction

Though we can use biochemical tools such as non-hydrolysable analogues of ATP to replicate ATP-F-actin with purified actin protein, this is not possible in live cells. To study the dynamics of actin polymerisation, and therefore the presence of ATP-F-actin, we rely on several cell permeable compounds that affect cellular actin by inducing stabilisation, polymerisation or depolymerisation/prevention of polymerisation. As mentioned in the introduction, drugs targeting actin microfilaments have never made it to clinical trials for cancer patients due to high toxicity. However, they are highly useful tools for the study of actin both biochemically and biologically.

One of the most interesting proteins we identified as preferentially binding ATP-F-actin was Eps8 and in this chapter we will utilise a GFP-tagged construct of this protein to investigate the effect of disruption or increase of ATP-F-actin on the localisation of Eps8 using several actin targeting drugs.

The Cytochalasin and Latrunculin families of compounds are characterised by their ability to destabilise actin, causing depolymerisation or preventing polymerisation. Jasplakinolide will be used to induce polymerisation, increase stability and cause a conformational shift in actin in the cell to mimic that of ATP-F-actin.

6.2 Results

6.2.1 Effect of Jasplakinolide on the localization of the ATP-F-actin binding protein Eps8

Jasplakinolide is a macrocyclic peptide isolated from marine sea sponge *Jaspis johnstoni,* capable of inducing polymerisation and stabilising actin. As well as this, it can induce a change in the conformational state, mimicking that of an ATP-actin filament, in a filament that has already hydrolysed its ATP (Pospich et al., 2020). This effect, plus the fact that Jasplakinolide is cell permeable, make it an excellent tool for studying actin dynamics in live cells.

In normal and untreated cells, Eps8 is localised at the leading edge of the cells (Figure 6-1). This tight localisation is where we would expect actin polymerisation, and therefore the generation of ATP-F-actin is indeed where we would expect to see ATP-F-actin proteins localised.

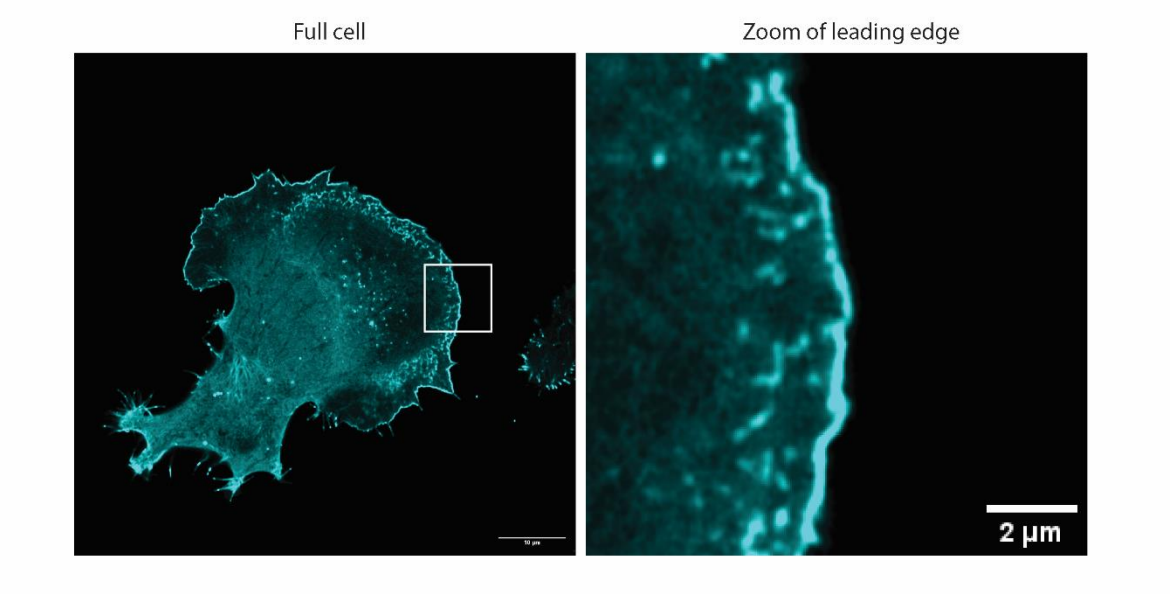

Figure 6-1 Eps8 localises at the leading edge of cells
B16-F1 cells transfected with GFP-Eps8 and imaged live with still images shown. GFP-Eps8 shown in cyan. Scale bars are 10µm and 2µM for representative image of full cell and zoom of leading edge, respectively.

Since Jasplakinolide alters the conformational state of F-actin into the ATP-F-actin state we would expect it to also alter the localisation of ATP-F-actin binding proteins in the cell. Our hypothesis was that treatment with Jasplakinolide would lead to a more diffuse localisation of GFP-Eps8, though still enriched in the actin rich lamellipodia (Figure 6-2). For this experiment we chose to use B16-F1 mouse melanoma cells because of their highly migratory nature and large lamellipodia.

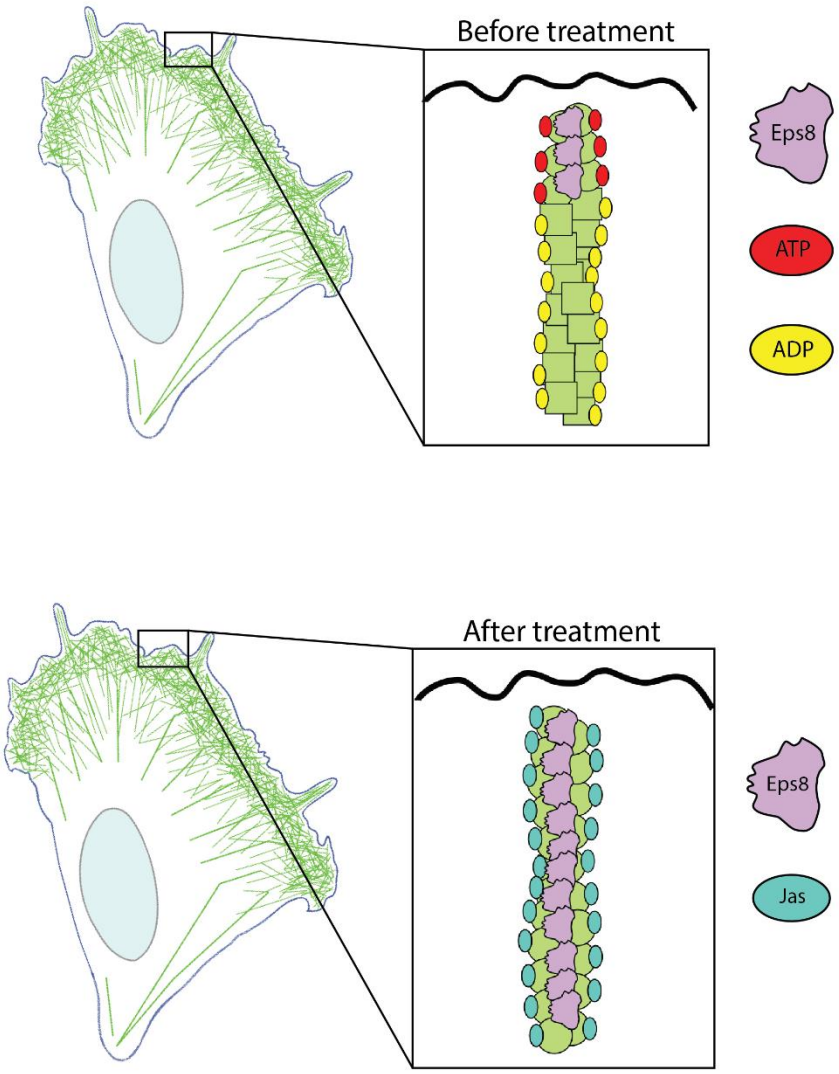

Figure 6-2 Expected change to Eps8 binding to F-actin after Jasplakinolide treatment. Before treatment illustration shows Eps8 bound to the barbed end of F-actin at the leading edge of the cell. Simplified illustration of ADP- and ATP-bound portions of the filament highlight the change in conformation of the filament depending on the bound nucleotide, causing Eps8 to bind only the latter. After treatment illustration shows our hypothesised more diffuse localisation of Eps8 on the F-actin in the actin rich lamellipodia. Simplified illustration of Jasplakinolide binding actin indicates it locking the filament into the ATP-F-actin conformation, regardless of the bound nucleotide, causing Eps8 to bind the length of the filament.

To test this hypothesis, B16-F1 transfected with GFP-Eps8 were treated with 1μM Jasplakinolide and imaged every 10 seconds over a period of 34 cycles. For all cells, “before treatment” data was taken from cycle 9 (10 seconds before treatment), Jasplakinolide was added at cycle 10 and “after treatment” data was taken from cycle 16 (50 seconds post treatment). Before treatment the cells showed a sharp localisation of GFP-Eps8 at the leading edge, and upon treatment this localisation became more diffuse, but was still enriched at the leading edge (Figure 6-3a). Still images of the transfected and treated cells were analysed by plotting the fluorescence intensity along a line extending from the

leading edge of the lamellipodia towards the centre of the cell before and after treatment and the data corresponding to the leading edge of the cell were statistically different (Figure 6-3b).

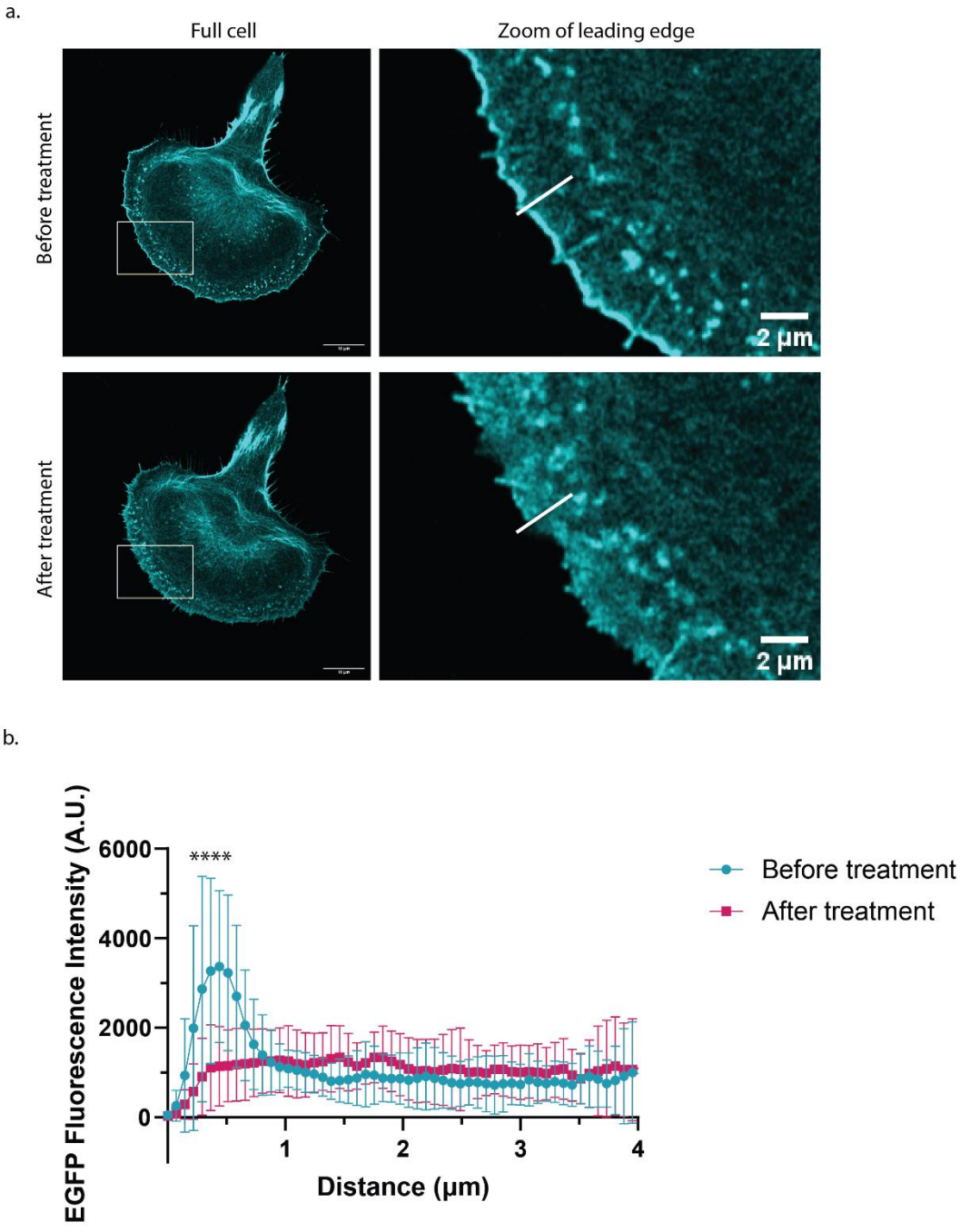

Figure 6-3 Jasplakinolide treatment causes diffuse localisation of Eps8 at the leading edge

a. Representative still images from live cell imaging of B16-F1 cells transfected with GFP-Eps8 and treated with 1µM Jasplakinolide. Images of the full cell (left) and zoom of the leading edge (right) are shown for both before (cycle 9; 10 seconds pre treatment) and after treatment (cycle 16; 50 seconds post treatment). White line on zoom of leading-edge panels is indicative of where the plot was drawn and the data collected.

b. Quantification of fluorescence intensity of GFP-Eps8 at the leading edge of live B16F1 cells along the white line with 0 corresponding to the leading edge of the lamellipodia. along the white line with 0 corresponding to the leading edge of the lamellipodia. 23 cells were analysed using unpaired t tests for the mean of each distance data point. Distances

0.36608, 0.43929 and 0.51251µm were statistically significant with a p-value of >0.0001, as denoted by asterisks in the figure.

This effect of Jasplakinolide on the localisation of GFP-Eps8 increased over time, becoming more diffuse as shown in the images and data of Figure 6-3. We also examined the change in localization of GFP-Eps8 in shorter time frames and this was also analysed by line plots in still images from videos of the treated cells as in the previous experiments (Figure 6-4).

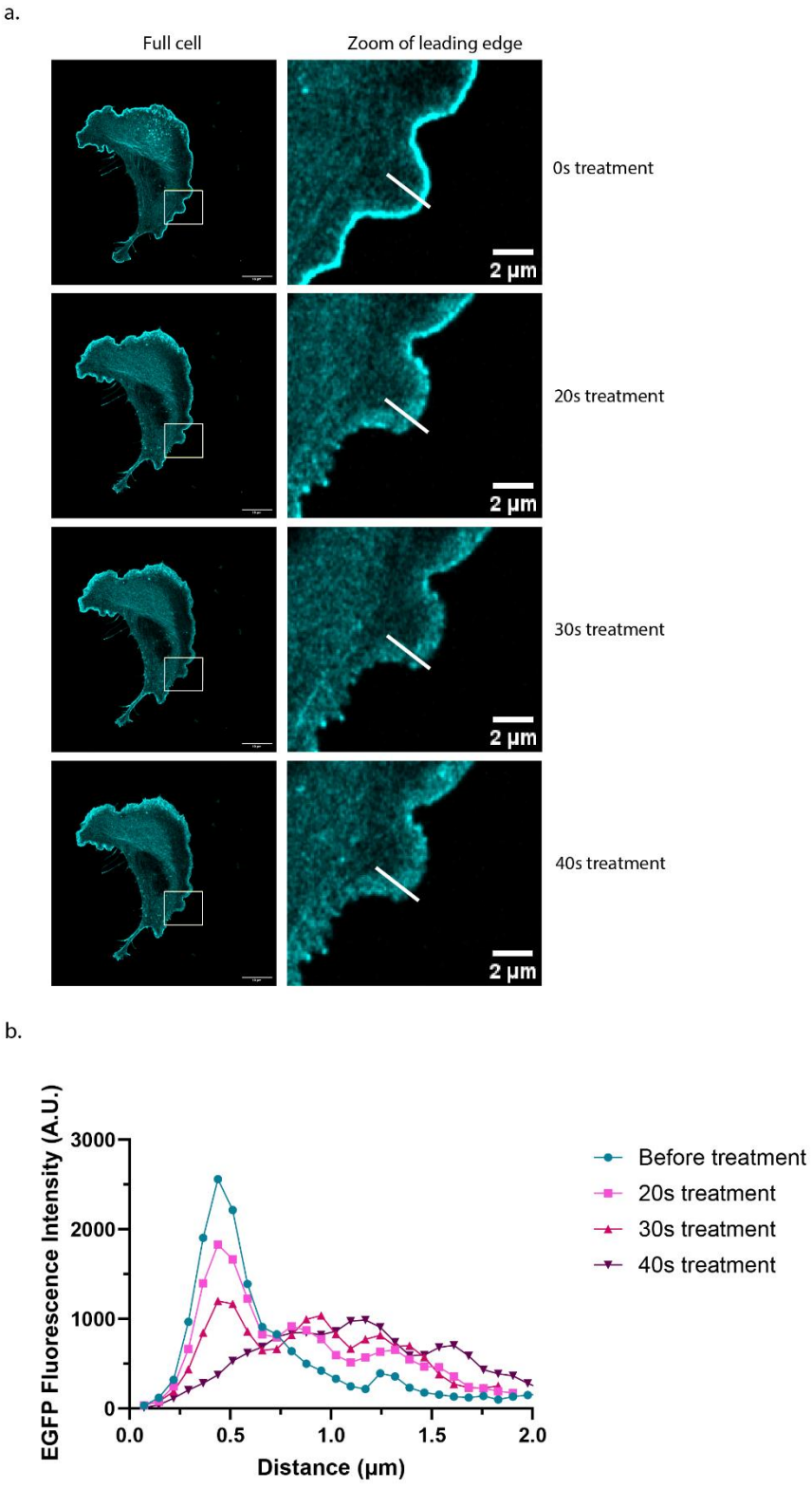

Figure 6-4 Diffuse localisation of Eps8 increases with treatment time.

a. Still images from live cell imaging of one representative B16-F1 cell transfected with GFP-Eps8 and treated with 1µM Jasplakinolide. Images of the full cell (left) and zoom of the leading edge (right) are shown for all timepoints. White line on zoom of leading-edge panels is indicative of where the plot was drawn and the data collected.

b. Quantification of fluorescence intensity of GFP-Eps8 at the leading edge of the B16-F1 cell over four timepoints.

6.2.2 Effect of Latrunculin-A on the localization of the ATP-F-actin binding protein Eps8

Latrunculins were isolated from the marine sea sponge *Latruculia magnifica* and shown to disrupt actin filaments *in vitro* (Spector et al., 1983). This disruption comes from the ability of Latrunculin to bind G-actin in a 1:1 molar ratio, thus rendering them unavailable for polymerisation (Coue et al., 1987). This interruption of polymerisation is valuable for us in live cells to study the effects on proteins which we have identified as preferentially binding ATP-F-actin since the halt in polymerisation should cause a decrease in the amount of ATP-F-actin available. Therefore, we hypothesised that when monomeric actin was sequestered upon Latrunculin treatment, the localisation of GFP-Eps8 at the leading edge would decrease due to the interruption to polymerisation (Figure 6-5). For this experiment, mouse embryonic fibroblasts (MEFs) were used since we struggled to find a concentration of the drug that did not immediately kill the B16-F1 cells, or that gave us confidence the change in the cells was because of the drugs effect on the actin cytoskeleton and not because the cells were dying.

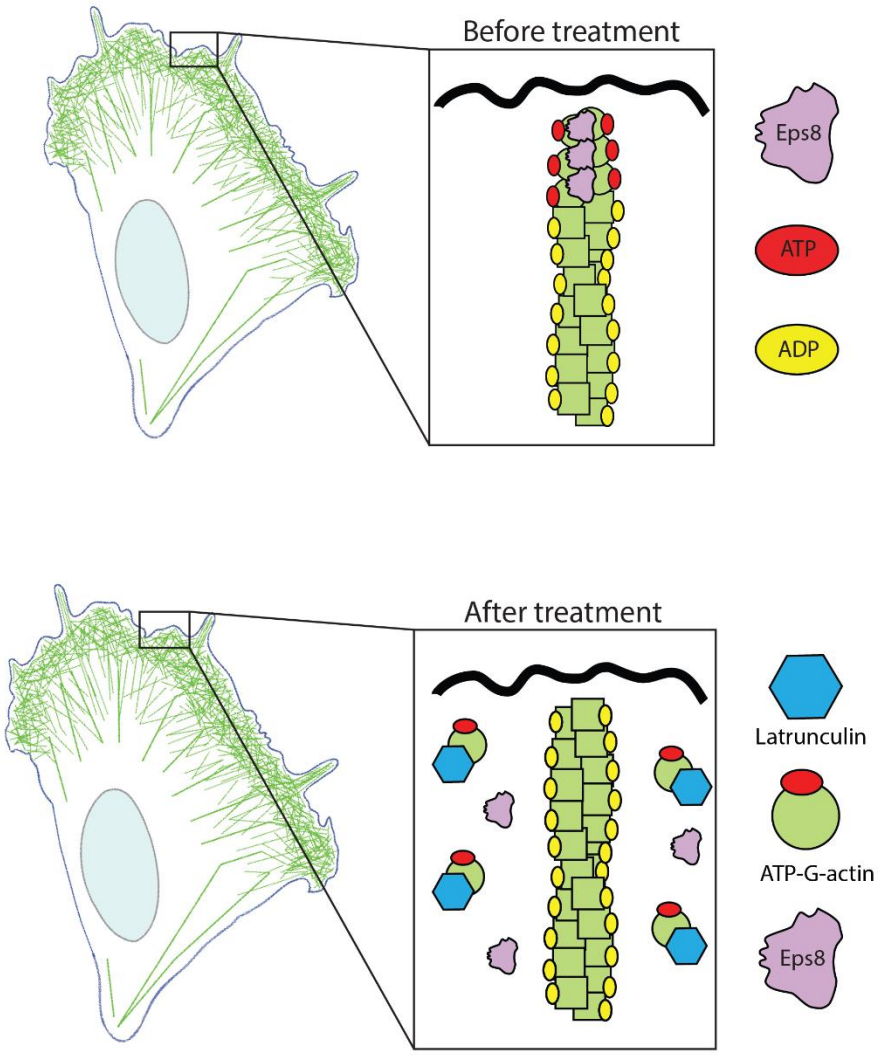

Figure 6-5 Expected change to Eps8 localistion upon Latrunculin treatment.
Before treatment illustration shows Eps8 bound to the barbed end of F-actin at the leading edge of the cell. After treatment illustration shows our hypothesis that Latruculin treatment will cause sequestering of G-actin monomers, leaving them unavailable for polymerisation and causing a loss of Eps8 localisation at the cell edge due to the decrease in polymerisation.

Mouse embryonic fibroblast (MEF) cells were transfected with GFP-Eps8 and LifeAct-TagRed (to visualise actin) and imaged every 10 seconds for a total of 60 cycles. “Before treatment” data was taken from cycle 1, cells were treated with Latrunculin on cycle 4 and “after treatment” data was taken from cycles 35 and 60. Cycle 35 (310 seconds post treatment) data is shown as “5 mins treatment” and cycle 60 (620 seconds post treatment) data is shown as “10 mins treatment”. The reason data was collected from two timepoints post treatment is that the cells were initially affected by Latrunculin, but then recovered with time. After treatment of Latrunculin for 5 minutes, the actin at the leading edge

of the cell appeared to have stopped polymerising causing lamellipodia retreat, and this was accompanied by a loss of GFP-Eps8 localisation at the leading edge (Figure 6-6a). After a further 5 minutes, the cell recovered, with the actin seemingly polymerising and the cell migrating again, and this was accompanied by a return of the localisation of the protein at the leading edge of the cell (Figure 6-6a). This is quantified in Figure 6-6b, where you can see there is a peak of GFP-Eps8 at the leading edge of the cell before treatment, which is drastically reduced after 5 minutes treatment, and has begun to recover after 10 minutes treatment.

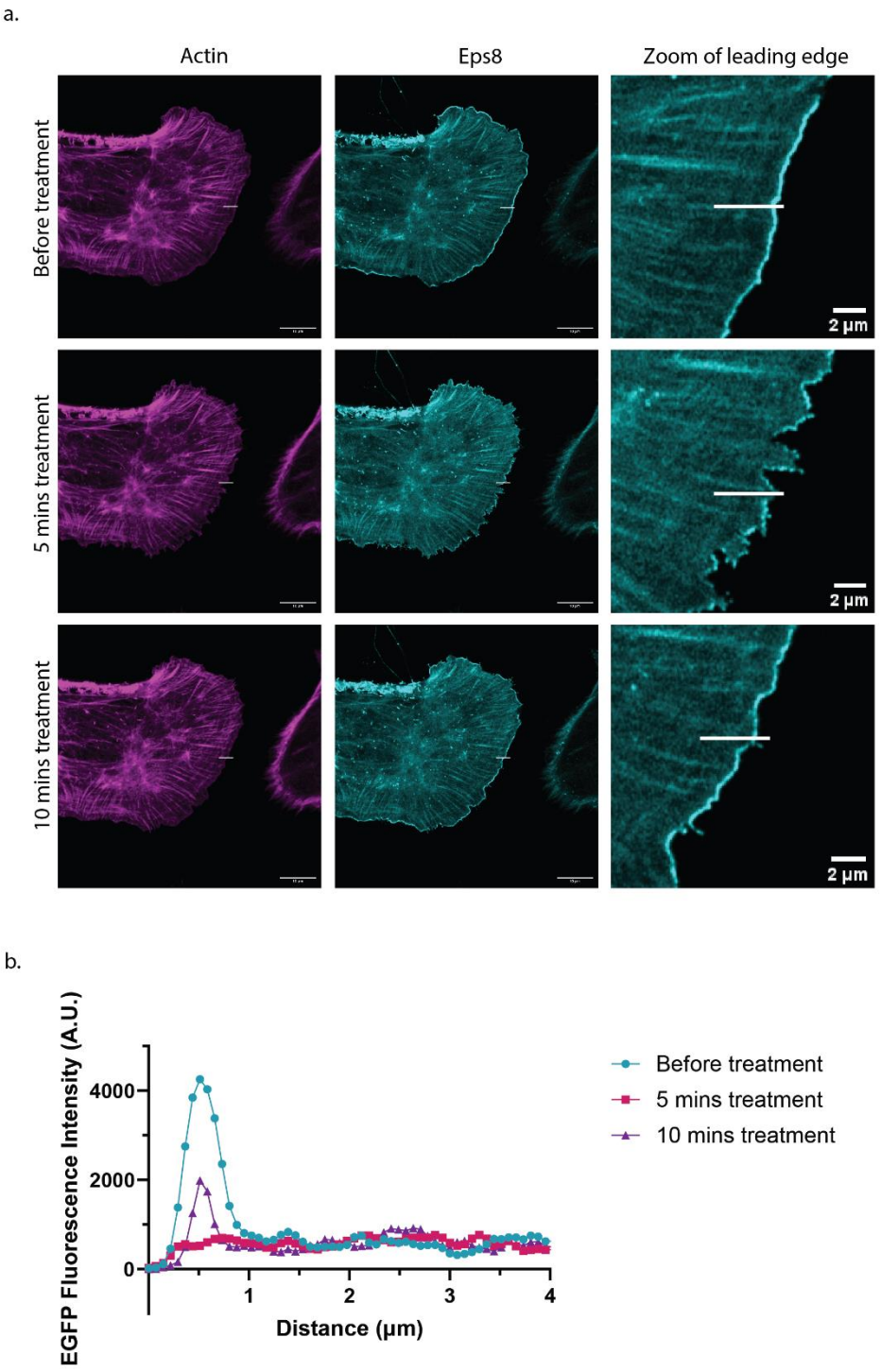

Figure 6-6 Latrunculin treatment causes loss of localisation of Eps8 at leading edge.

a. Still images from live cell imaging of one representative MEF cell transfected with GFP-Eps8 and LifeAct and treated with 5µM Latrunculin-A. Images of the full cell with actin (magenta; left), GFP-Eps8 (cyan; middle) and zoom of GFP-Eps8 at the leading edge (cyan; right) are shown for all timepoints. White line on "zoom of leading edge" panels is indicative of where the plot was drawn and the data collected.

b. Quantification of fluorescence intensity of GFP-Eps8 at the leading edge of the MEF cell over three timepoints.

6.2.3 Effect of Cytochalasin-D on the localization of the ATP-F-actin binding protein Eps8

Cytochalasins are mycotoxins isolated from various fungi (Katagiri and Matsuura, 1971). These toxins disrupt actin polymerisation by binding the barbed end of F-actin and, thus, preventing further polymerisation (Brown and Spudich, 1981). In addition, Cytochalasins can increase the intrinsic ATPase activity of actin (Low and Dancker, 1976) which in turn ages the filament leading to depolymerisation. Therefore, we would expect treatment with Cytochalasin-D to prevent further polymerisation and hence the production of ATP-F-actin which should result in a loss of Eps8 localisation at the leading edge (Figure 6-7).

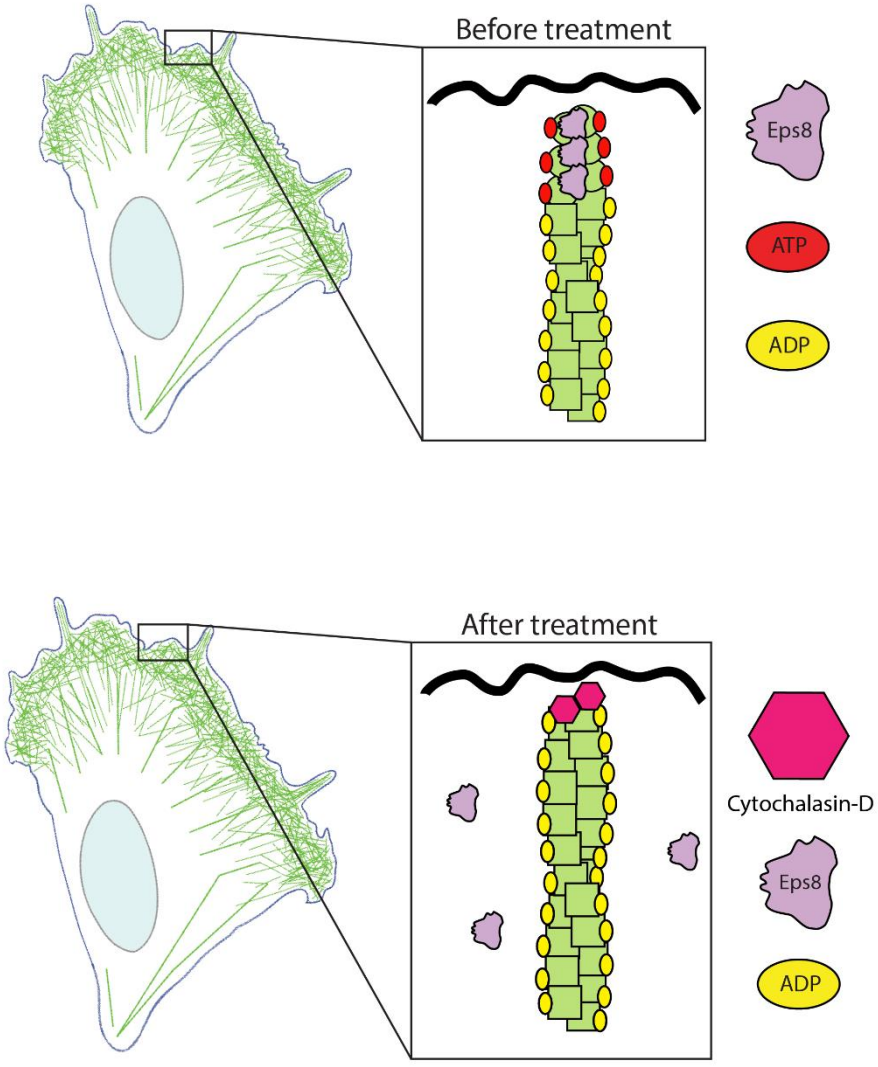

Figure 6-7 Expected change to Eps8 localisation upon Cytochalasin treatment.
Before treatment illustration shows Eps8 bound to the barbed end of F-actin at the leading edge of the cell. After treatment illustration shows our hypothesised loss of localisation of Eps8 at the cell edge when Cytochalasin-D caps the filaments and promotes depolymerisation.

B16-F1 melanoma cells transfected with GFP-Eps8 and LifeAct-TagRed were imaged every 10 seconds for a total of 60 cycles. “Before treatment” data was collected from a still image on cycle 11, Cytochalasin treatment was added on cycle 12 and “4 mins” treatment data was collected from cycle 36 (240 seconds post treatment).

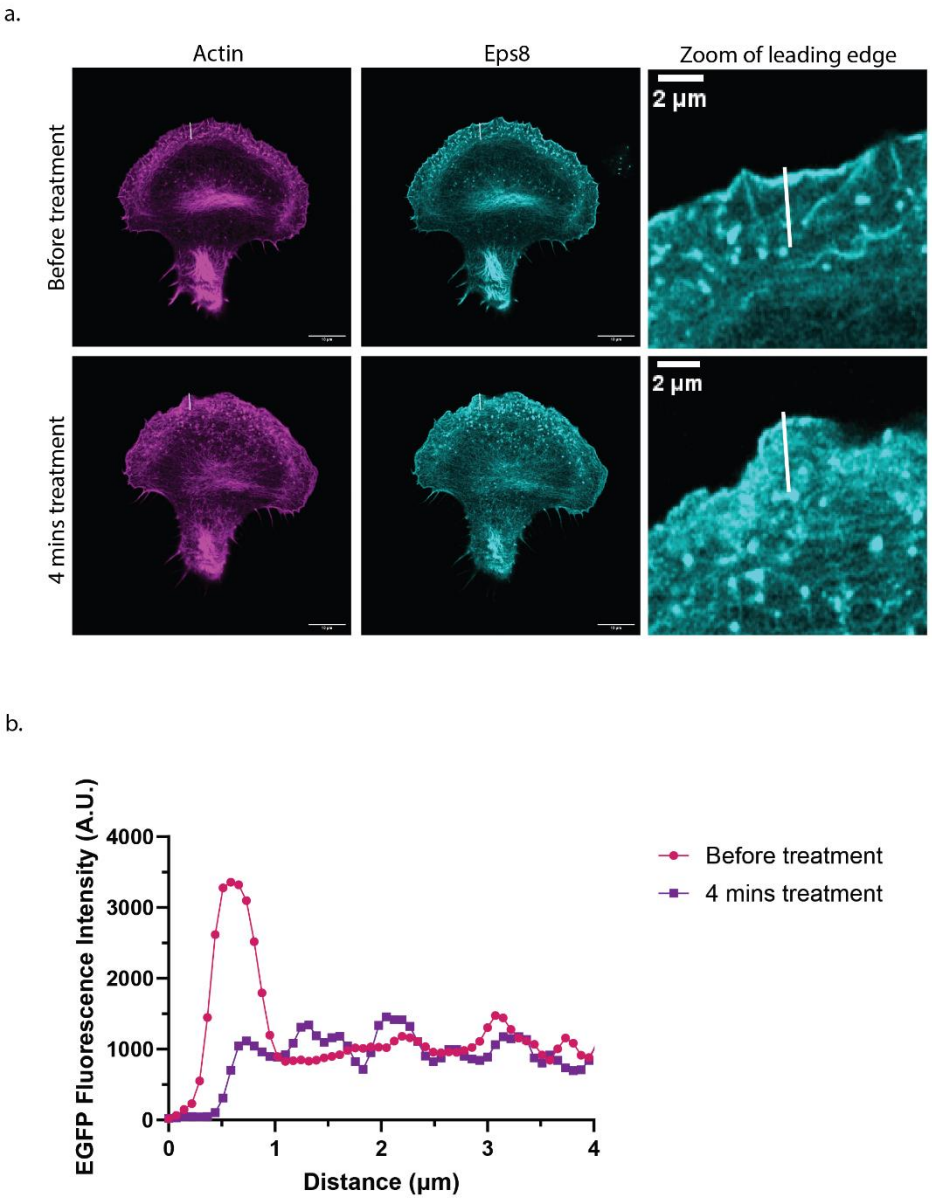

Figure 6-8 Cytochalasin treatment causes loss of localisation of Eps8 at the leading edge.

a. Still images from live cell imaging of one representative B16-F1 cell transfected with GFP-Eps8 and LifeAct and treated with 0.05ug/ml Cytochalasin-D. Images of the full cell with actin (magenta; left), GFP-Eps8 (cyan; middle) and zoom of GFP-Eps8 at the leading edge (cyan; right) are shown for all timepoints. White line on “zoom of leading edge” panels is indicative of where the plot was drawn and the data collected.

b. Quantification of fluorescence intensity of GFP-Eps8 at the leading edge of the B16-F1 cell over three timepoints.

As expected, the cell before treatment showed tight leading-edge localisation of GFP-Esp8, as indicative of binding ATP-F-actin (Figure 6-8a). After 4 minutes of treatment with Cytochalasin-D the leading-edge localisation was replaced by a more diffuse localisation (Figure 6-8a). This can be visualised in Figure 6-8b, where the before treatment data shows a peak of intensity correlating with the sharp localisation of the leading-edge, which is lost after treatment with Cytochalasin-D.

6.3 Discussion

In this chapter, we have shown that treatments to either stabilise or destabilise actin have an effect on the localization of the ATP-F-actin binding protein Eps8 in actin protrusions and, thus, along the F-actin filaments. We hypothesised that actin stabilising drug Jasplakinolide would have a positive effect on the binding to ATP-F-actin, whilst destabilising treatments would have a negative effect due to their ability to interrupt dynamic polymerisation in a migrating cell.

Phalloidin, though not useable in live cells, must be mentioned when discussing drugs targeting actin. Phalloidin is isolated from the toxic mushroom *Amanita phalloides* and has been shown to bind and stabilise actin (Low and Weiland, 1974). Usually used conjugated to fluorophores, phalloidin is a powerful tool for imaging the actin cytoskeleton in cells. Without phalloidin this project would not have been possible, as it is the compound that we use to stabilise our actin filaments, without disturbing the conformational “age” of the F-actin we have prepared (Pospich et al., 2020), and allow us to construct affinity chromatography columns.

As well as inducing polymerisation, Jasplakinolide was also shown to inhibit the binding of phalloidin to actin, suggesting similar binding sites (Bubb et al., 1994). This has been confirmed in recent data that showed by high resolution cryo-EM analysis how Phalloidin and Jasplakinolide have overlapping binding sites on actin (Merino et al., 2018). This study also revealed crucial insights into the increase of intrinsic ATPase activity of actin when incorporated into a filament. The data showed that after incorporation of the filament the catalytic base His161 of the actin monomer changes position resulting in the γ-phosphate being accessible. The DNAse-1-binding loop (D-loop) was shown to exist in two

conformations (termed open and closed) in both ATP-F-actin and ADP-Pi-Actin, while ADP-actin D-loop was only identified in the closed conformation. The closed or open D-loop conformation is seen in the C-terminus, which is extended in the latter (Merino et al., 2018). This difference in the D-loop conformation is understood to be responsible for the differential binding of proteins to ATP- or ADP-F-actin.

Importantly, the structural effect of Jasplakinolide binding to F-actin is very different. While we use phalloidin to stabilise the current conformational state of a filament (dependant on the bound nucleotide), we use Jasplakinolide to induce a change in the conformational state, mimicking that of an ATP-actin filament (Pospich et al., 2020). This is in agreement with the effect we see in B16-F1 cells after treatment with Jasplakinolide: treated cells have a more diffuse localisation of ATP-actin binding protein Eps8, which we would expect if the F-actin at the leading edge had changed conformation to mimic ATP-F-actin.

Our preliminary experiments using actin targeting drugs Cytochalasin D and Latrunculin also fit our hypothesis that under normal conditions ATP-F-actin binding proteins will only be found at the leading edge of cells. Indeed, as shown by our data, these proteins are usually localized as a sharp line at the leading edge of actin protrusions. However, this characteristic localization is disrupted after treatment with F-actin destabilising drugs. This result can easily be explained: these treatments interrupt the ability of the cell to continue dynamic polymerisation and therefore produce new ATP-F-actin. By doing so, both Cytochalasin D and Latrunculin are expected to interfere with the localisation of ATP-F-actin binding proteins.

Interestingly, recent studies with Latrunculin have increased our understanding of the interaction of the drug with F-actin and shown it to destabilise the filament beyond its role in sequestering G-actin (Coue et al., 1987). In particular, Latrunculin A has now been shown to increase the rate of F-actin depolymerisation and even cause severing at high concentrations (Fujiwara et al., 2018). This may explain why we struggled to find a concentration of Latrunculin A that did not immediately kill cells, since the drug targets both G- and F-actin.

In conclusion, our data with Jasplakinolide treatments and preliminary experiments with Latrunculin A and Cytochalasin D showed expected outcomes on the dynamics of F-actin in live cells and therefore the localisation of the ATP-F-actin binding protein Eps8. Our goal with these treatments was to determine if the results from chromatography and mass spectrometry were relevant also in the cell, using Eps8 as a marker and known ATP-F-actin binding protein. As we cannot modify the nucleotide state of the actin filaments in a migrating cell as we did with purified actin, we utilised treatments that interfere with the polymerisation of actin within the cell thereby indirectly affecting their nucleotide state and monitored the effect on localisation of Eps8. The results showed that interference with polymerisation of actin indeed disrupts the localisation of Eps8 strengthening our chromatography results.

7 ATP-F-actin binding investigation with Eps8

7.1 Introduction

In this chapter we will present and discuss the validation of Eps8 binding ATP-F-actin in other assays, and investigation into the mechanism of ATP-F-actin binding. GFP-trap experiments were conducted to validate the binding of Eps8 to ATP-F-actin which were successful and encouraged confidence in our affinity chromatography results.

GFP-constructs of Eps8 in its wild-type form or with point mutations were utilised to investigate the described capping and bundling functionality of Eps8 on ATP-F-actin binding. Finally, different domains of the protein were cloned and investigated with super resolution microscopy to determine localisation and domain responsible for ATP-F-actin binding.

Since Eps8 is known to bind actin directly and is implicated in several Rho GTPase pathways, it was an interesting candidate for us to explore further the question of method of ATP-F-actin binding. Though it was touched upon briefly in the previous chapters, Eps8 will be more thoroughly introduced below.

7.1.1 Eps8

Eps8 is a known actin binding protein that was originally identified as a downstream target of activity of the epidermal growth factor receptor (EGFR) (Fazioli et al., 1993). It was noted that Eps8 appeared to localise to active polymerising actin at structures including lamellipodia and membrane ruffles in fibroblast cells (Provenzano et al., 1998). Importantly, Eps8 contains an effector region at its C-terminus that facilitates interaction with and activation of Rac GEF Sos1 (Scita et al., 2001). This effector region (Figure 7-1) is also responsible for F-actin binding and is thought to ensure the localisation of Eps8 at sites of

active actin polymerisation (Scita et al., 2001). This interaction is part of a complex with Abi1, which Eps8 binds through its SH3 domain (Scita et al., 1999).

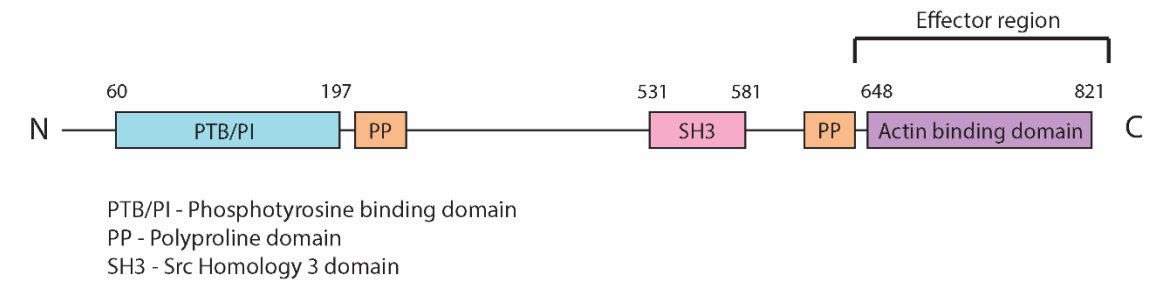

Figure 7-1 Eps8 domains and effector region
Schematic diagram showing the domains and effector regions of Eps8.

As well as F-actin binding, the effector region of Eps8, but not the full-length protein, was also shown to have capping capabilities *in vitro*. The full-length protein was shown to be autoinhibited *in vitro*, and this inhibition was removed upon binding with Abi1 (Disanza et al., 2004). Fibroblast cells not expressing Eps8 were shown to have reduced formation of induced actin-comet tails, leading to the conclusion that Eps8 is required *in vivo* for optimal dynamics in actin processes (Disanza et al., 2004). Furthermore, studies in *Xenopus* showed the recruitment of N-WASP to actin structures induced by Eps8/Abi1 (Roffers-Agarwal et al., 2005). This observation, as well as those of Eps8 capping ability and its role in actin-comet tail formation, led to the idea that Eps8 is also involved in the control of actin dynamics independently of Rac (Disanza et al., 2004; Roffers-Agarwal et al., 2005).

Insulin receptor tyrosine kinase substrate (IRSp53) is an actin crosslinker involved in filopodia and lamellipodia formation that has also been shown to bind Eps8 via its SH3 domain and increase the stability of the Eps8/Abi1/Sos1 complex implicated in the activation of Rac (Funato et al., 2004). Interestingly, Eps8 and IRSp53 have also been shown to form their own complex, which is under the control of Cdc42 and not Rac and synergistically participates in the crosslinking of actin in protrusions such as filopodia (Disanza et al., 2006).

Eps8 is known to have bundling and capping functions on F-actin, so it should be able to bind both ADP- and ATP-F-actin. Since this is known, and structural

information is readily available, it gives a good basis to start the investigation of the method of ATP-F-actin binding in proteins.

7.2 Results

B16F1 cells were transfected with GFP-only, GFP-Eps8 or not-transfected. These cells were then harvested, treated with Jasplakinolide and incubated with GFP-trap beads. The input and output fractions of each condition was analysed by Western blotting. As expected, cells treated with Jasplakinolide and transfected with GFP-Eps8 were able to pull down actin validating our results that Eps8 can either directly or indirectly preferentially bind to ATP-F-actin (Figure 7-2).

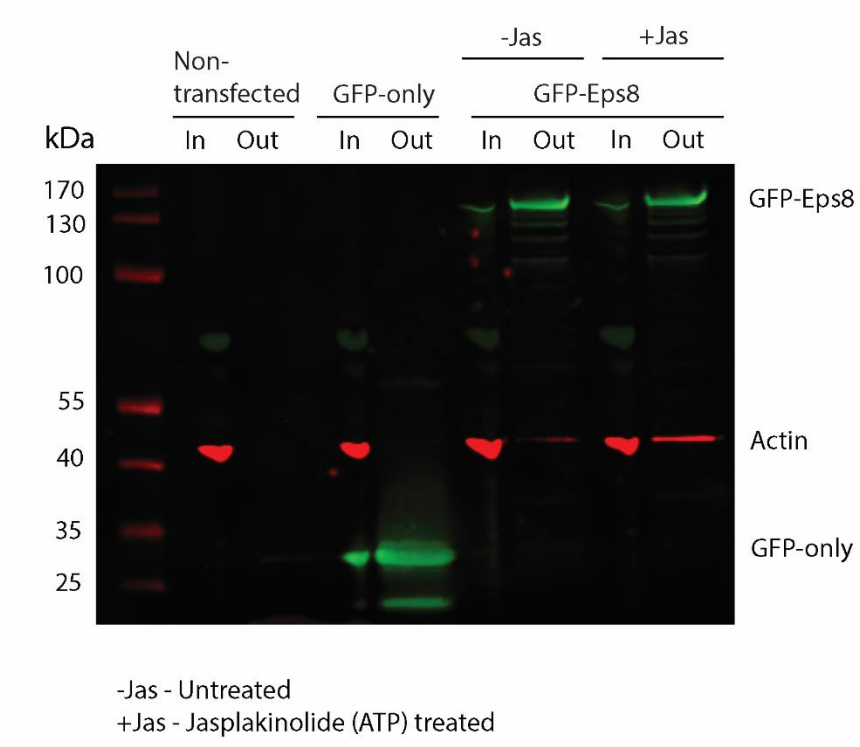

Figure 7-2 Eps8 binds actin in Jasplakinolide treated cells
Western blot of GFP-trap of GFP-only empty vector or GFP-Eps8. Input and output of each condition analysed using anti-actin and anti-GFP antibodies. Molecular weight ladder shown on left.

Since Jasplakinolide is known to promote the stabilisation of actin, further experiments were carried out to ensure that the increase in pull down of actin was because of the increase of ATP-F-actin in the cell and not simply an increase in F-actin. To confirm this, a GFP-trap experiment utilising the same transfection constructs was performed with an additional treatment condition of phalloidin. Phalloidin is also known to promote polymerisation and stabilisation

of actin filaments, but, unlike Jasplakinolide, does not alter the nucleotide state of the filament (Pospich et al., 2020). Therefore, we would expect phalloidin treatment to increase the amount of actin pulled down during centrifugation, regardless of which construct the cells were transfected with or whether they were transfected at all. This was indeed the case: treatment with phalloidin pulled down actin across all conditions of transfections (Figure 7-3). Encouragingly, samples treated with Jasplakinolide only pulled down actin in samples transfected with GFP-Eps8 meaning the increase in actin pull down is a result of binding with Eps8 (Figure 7-3).

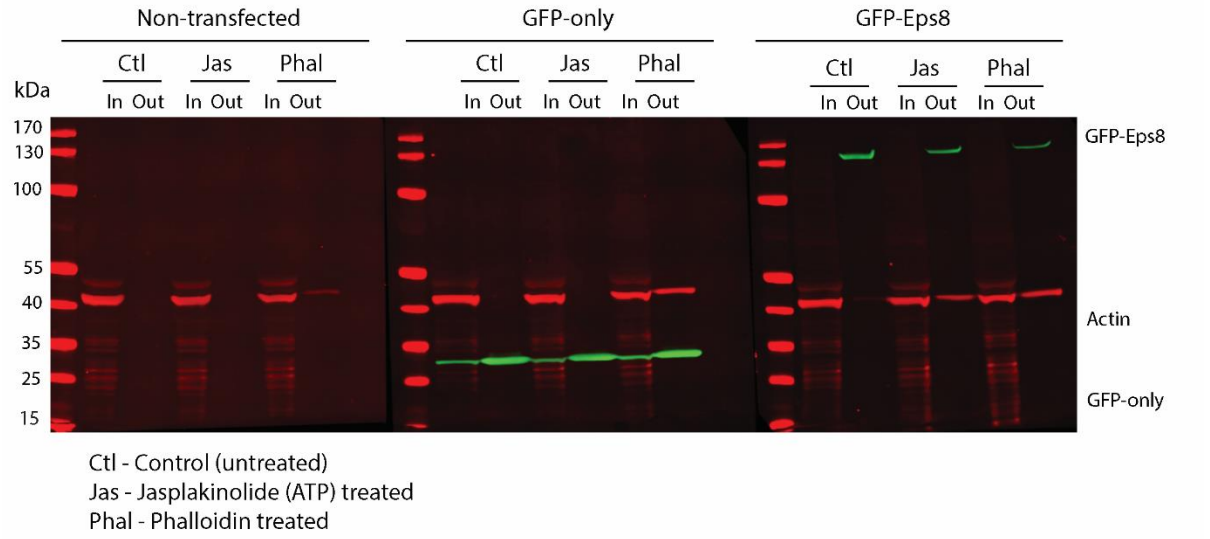

Figure 7-3 Increased actin pull down with Jasplakinolide treatment is a result of Eps8 binding
Western blot of GFP-trap of GFP-only empty vector or GFP-Eps8. Input and output of each condition analysed using anti-actin and anti-GFP antibodies. Molecular weight ladder shown on left.

As mentioned previously, Eps8 is able to cap and bundle F-actin *in vitro* (Disanza et al., 2004). The domains and residues responsible for this have been identified and constructs with point mutations rendering the protein unable to either cap, bundle or both were generated (Hertzog et al., 2010). We hypothesised that the capping mutant would not pull down more actin in the presence of Jasplakinolide. However, the results proved our hypothesis to be wrong, with the wild type and all point mutation constructs still able to pull down actin (Figure 7-4).

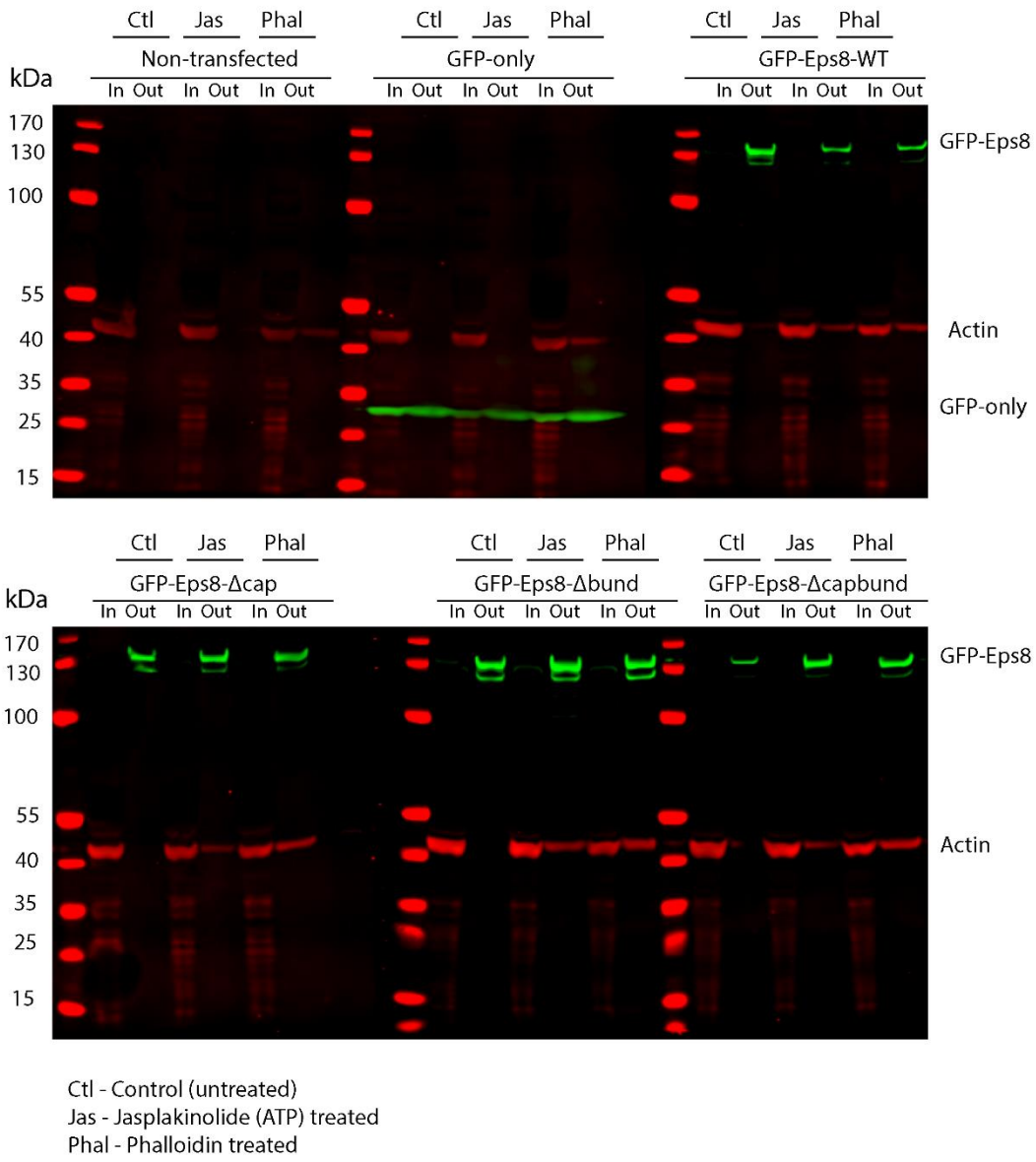

Figure 7-4 Capping mutants pulls down actin with Jasplakinolide treatment
Western blot of GFP-trap of GFP-only empty vector or GFP-Eps8. Input and output of each condition analysed using anti-actin and anti-GFP antibodies. Molecular weight ladder shown on left.

This suggests that the preferential ATP-F-actin binding is not a result of the proteins ability to cap actin filaments. To investigate the mechanism of ATP-F-actin binding of Eps8, several truncated versions of the protein tagged with GFP were generated (Figure 7-5).

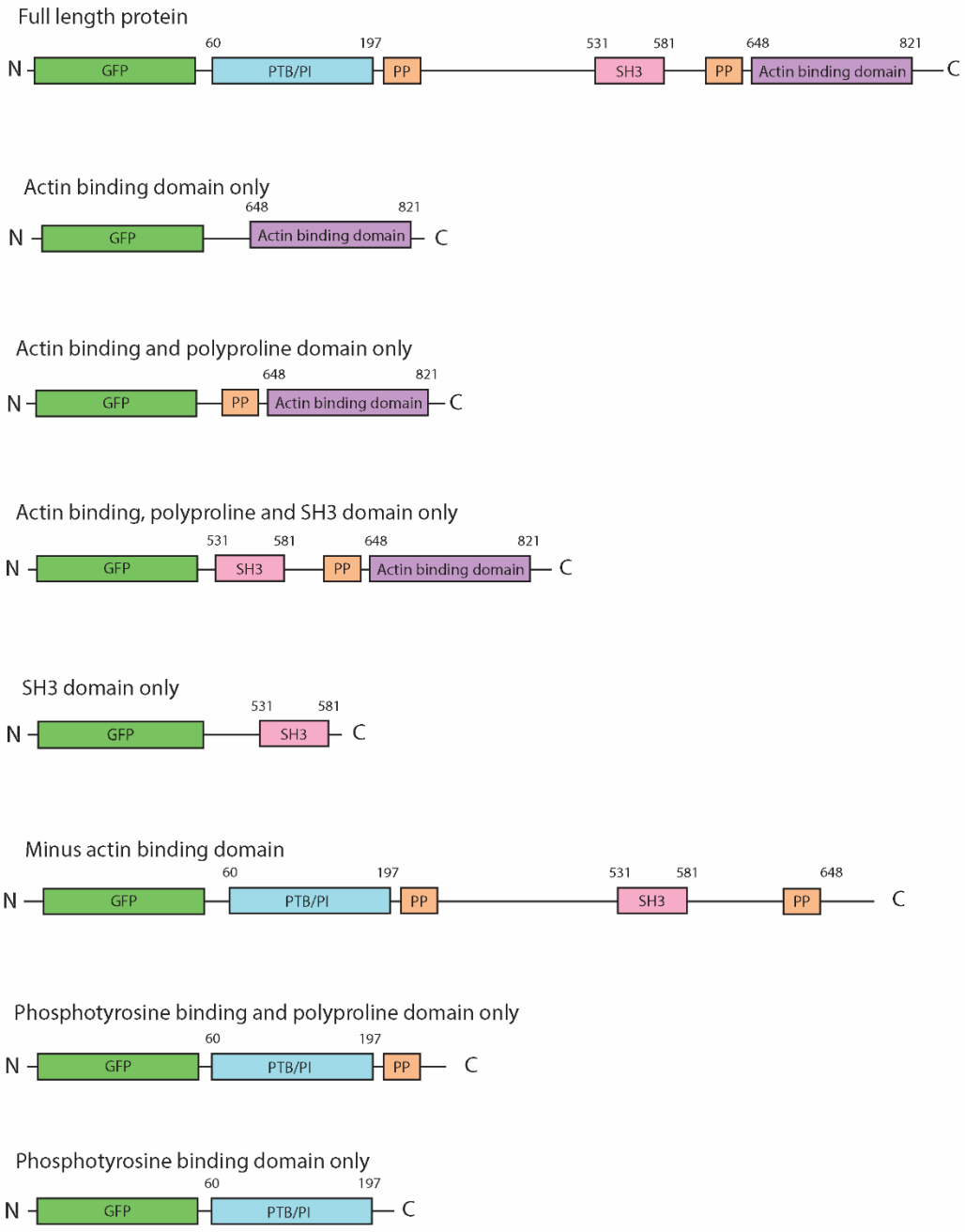

Figure 7-5 Truncated GFP-Eps8 constructs
Schematic diagram showing the truncated versions of Eps8 generated and tagged with GFP for imaging.

Expression of the full length protein confirmed its specific localization at the leading edge (Figure 7-6a). Interestingly, the GFP-Eps8-Actin Binding Domain construct did not display the same tight localisation at the leading edge that we associate with ATP-F-actin binding, but was still enriched across the lamellipodia (Figure 7-6b). This is quantified in Figure 7-6c, where the characteristic peak of fluorescence indicative of tight leading edge localisation is shown for the full

length protein only, with the truncated actin binding domain displaying more diffuse localisation whilst still being enriched at the lamellipodia.

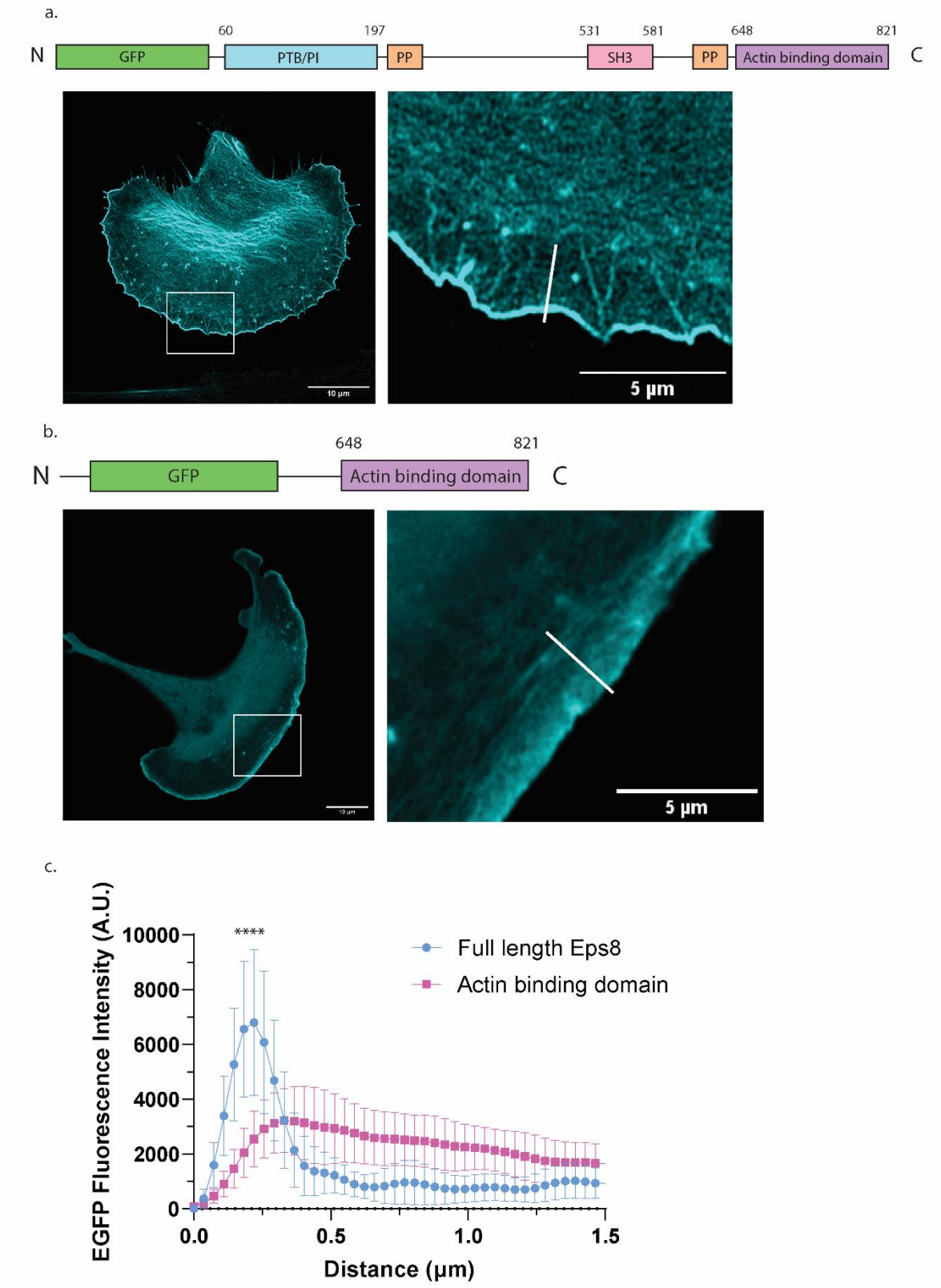

Figure 7-6 Actin binding domain does not show tight leading-edge localisation

a. Representative still images from imaging of B16-F1 cells transfected with GFP-Eps8-Full Length. Images of the full cell (left) and zoom of the leading-edge (right) are shown. White line on zoom of leading-edge panels is indicative of where the plot was drawn and the data

collected. Scale bars are 10µm for full cell images (left) and 5µm for the zooms of the leading edge (right).

b. Representative still images from imaging of B16-F1 cells transfected with GFP-Eps8-Actin Binding Domain. Images of the full cell (left) and zoom of the leading edge (right) are shown. White line on zoom of leading-edge panels is indicative of where the plot was drawn and the data collected. Scale bars are 10µm for full cell images (left) and 5µm for zooms of the leading edge (right).

c. Quantification of fluorescence intensity of GFP-Eps8-Full Length and GFP-Eps8-Actin Binding Domain at the leading edge of live B16F1 cells along the white line with 0 corresponding to the leading-edge of the lamellipodia. 10 cells were analysed for each construct for the plotted mean and standard deviation and statistical difference was evaluated using unpaired t-tests for the mean of each distance data point. Distances 0.1082, 0.14643, 0.18304µm were statistically significant with a p-value of >0.0001, as denoted by asterisks in the figure. Distances 0.07322 and 0.21965µm were statistically significant with a p-value of >0.001 (not denoted by asterisks). Distance 0.25625µm was statistically significant with a p-value of >0.01 (not denoted by asterisks).

Next, a truncated GFP- construct was imaged consisting of the actin binding and polyproline domains. This construct displayed the same diffuse enrichment at the lamellipodia (Figure 7-7a) as the actin binding domain alone (Figure 7-7b).

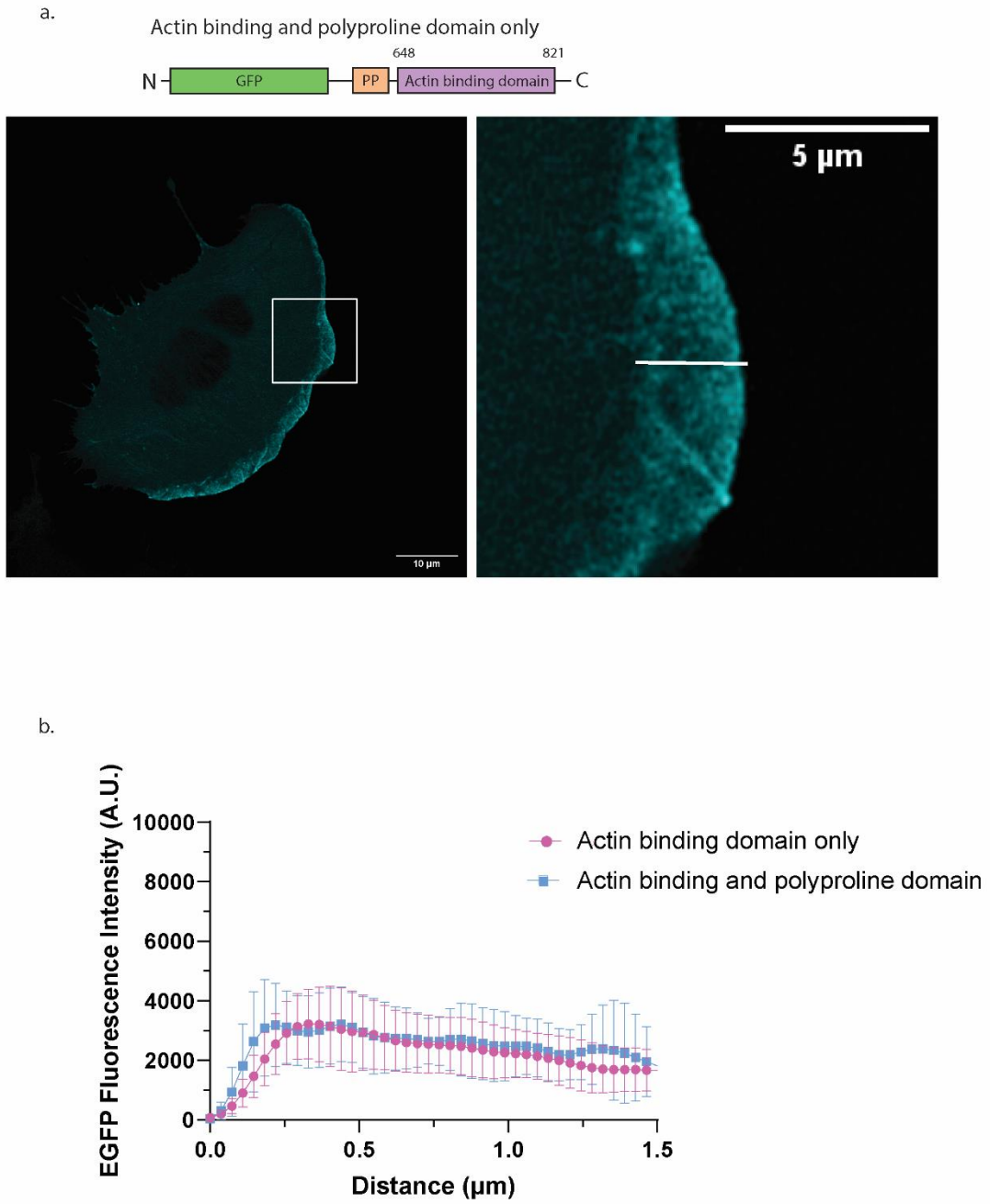

Figure 7-7 Actin binding and polyproline domain does not show tight leading-edge localisation

a. Representative still images from imaging of B16-F1 cells transfected with GFP-Eps8-Actin Binding and Polyproline Domain. Images of the full cell (left) and zoom of the leading edge (right) are shown. White line on zoom of leading-edge panels is indicative of where the plot was drawn and the data collected. Scale bars are 10µm on full cell image (left) and 5µm on zoom of leading-edge image (right).

b. Quantification of fluorescence intensity of GFP-Eps8-Actin Binding Domain and GFP-Eps8-Actin Binding and Polyproline Domain at the leading edge of live B16-F1 cells along the white line with 0 corresponding to the leading-edge of the lamellipodia. 10 cells were analysed for each construct for the plotted mean and standard deviation and statistical differences were evaluated using unpaired t-tests for the mean of each distance data point. No distances were statistically significant.

Expression of GFP-Eps8-Actin binding, polyproline and SH3 domain was able to rescue the tight leading-edge localisation (Figure 7-8a). This data suggests that the SH3 domain is important in the binding of Eps8 to ATP-F-actin, whether it be a direct or indirect interaction. Whilst this construct did return the tight leading-edge localisation, it did not appear as enriched as the full-length protein (Figure 7-8b).

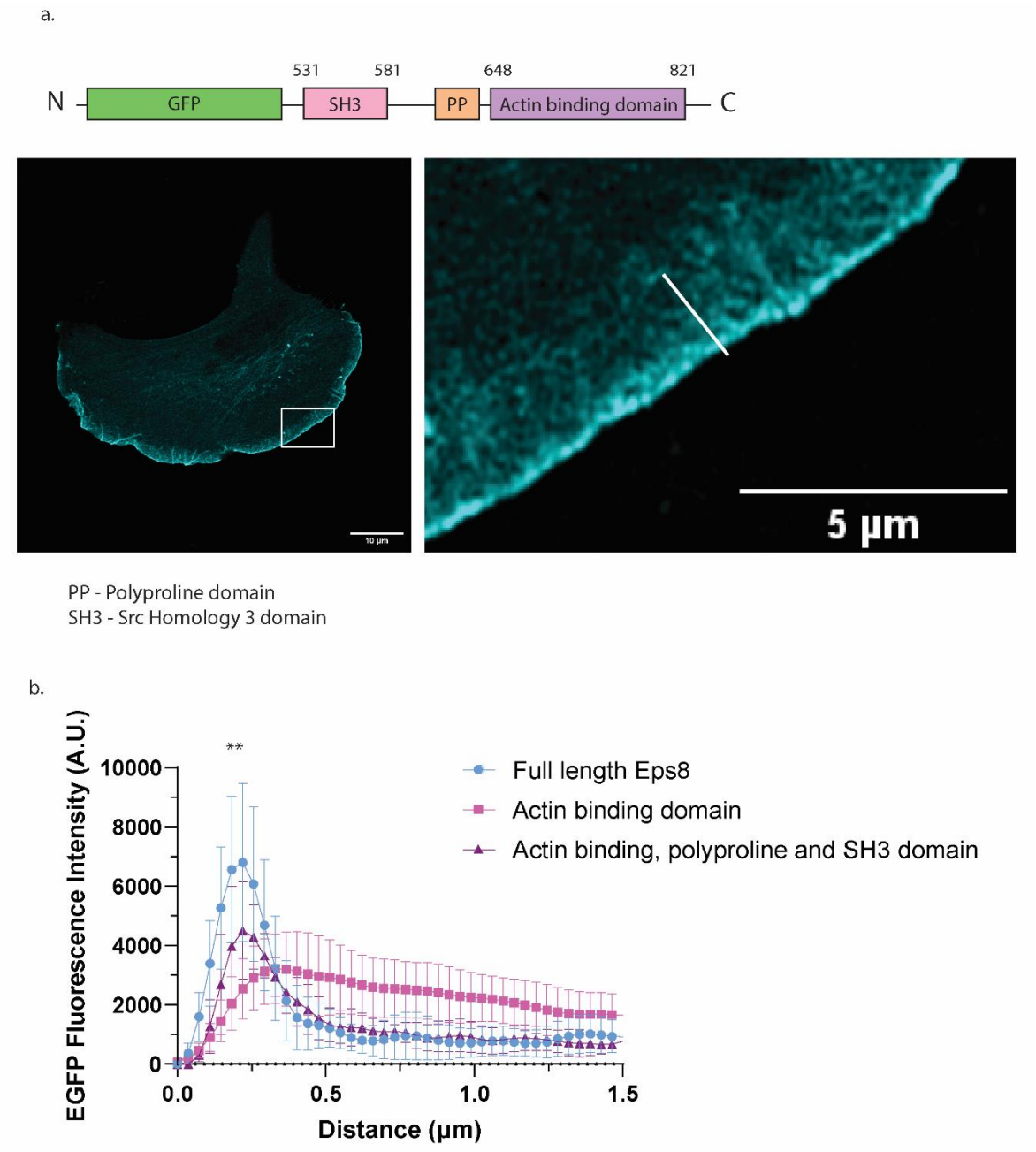

Figure 7-8 Actin Binding, polyproline and SH3 domain construct shows tight leading-edge localisation

a. Representative still images from imaging of B16-F1 cells transfected with GFP-Eps8-Actin Binding, Polyproline and SH3 Domain. Images of the full cell (left) and zoom of the leading-edge (right) are shown. White line on zoom of leading-edge panels is indicative of where the plot was drawn, and the data collected. Scale bars are 10µm on full cell image (left) and 5µm on zoom of leading-edge image (right).

b. Quantification of fluorescence intensity of GFP-Eps8-Full Lenth, GFP-Eps8-Actin Binding Domain and GFP-Eps8-Actin Binding, Polyproline and SH3 Domain at the leading-edge of live B16-F1 cells along the white line with 0 corresponding to the leading edge of the lamellipodia. 10 cells were analysed for each construct for the plotted mean and standard deviation and statistical difference was evaluated using unpaired t-tests for the mean of each distance data point. Distance 0.21965µm was statistically significant with a p-value of >0.01, as denoted by asterisks in the figure. Distances 0.18304 and 0.25625µm were statistically significant with a p-value of >0.05 (not denoted by asterisks).

Interestingly, truncated Eps8 without the actin binding domain displayed some tight localisation at the leading-edge (Figure 7-9a). However, the peak of fluorescence of GFP-Minus ABD was much lower than that of the full-length protein (Figure 7-9b). For comparison, GFP-Minus ABD and GFP-SH3 domain only (to compare to a construct that did not localise) are shown together in Figure 7-9c. There was statistical significance in the difference of these constructs at every data point ($p<0.01$). Moreover, at the 4 distances corresponding to the peak there was a significance of $p<0.001$. These and the previous data indicate that the actin binding domain is responsible for the enrichment of Eps8 across the width of the lamellipodia. However the tight leading-edge localisation that we associate with ATP-F-actin binding appears to be orchestrated by the SH3 domain, and most likely indicates an indirect interaction with ATP-F-actin. The phosphotyrosine, polyproline and SH3 domains alone did not localise to either the width of the lamellipodia or the leading edge (Figure 7-10).

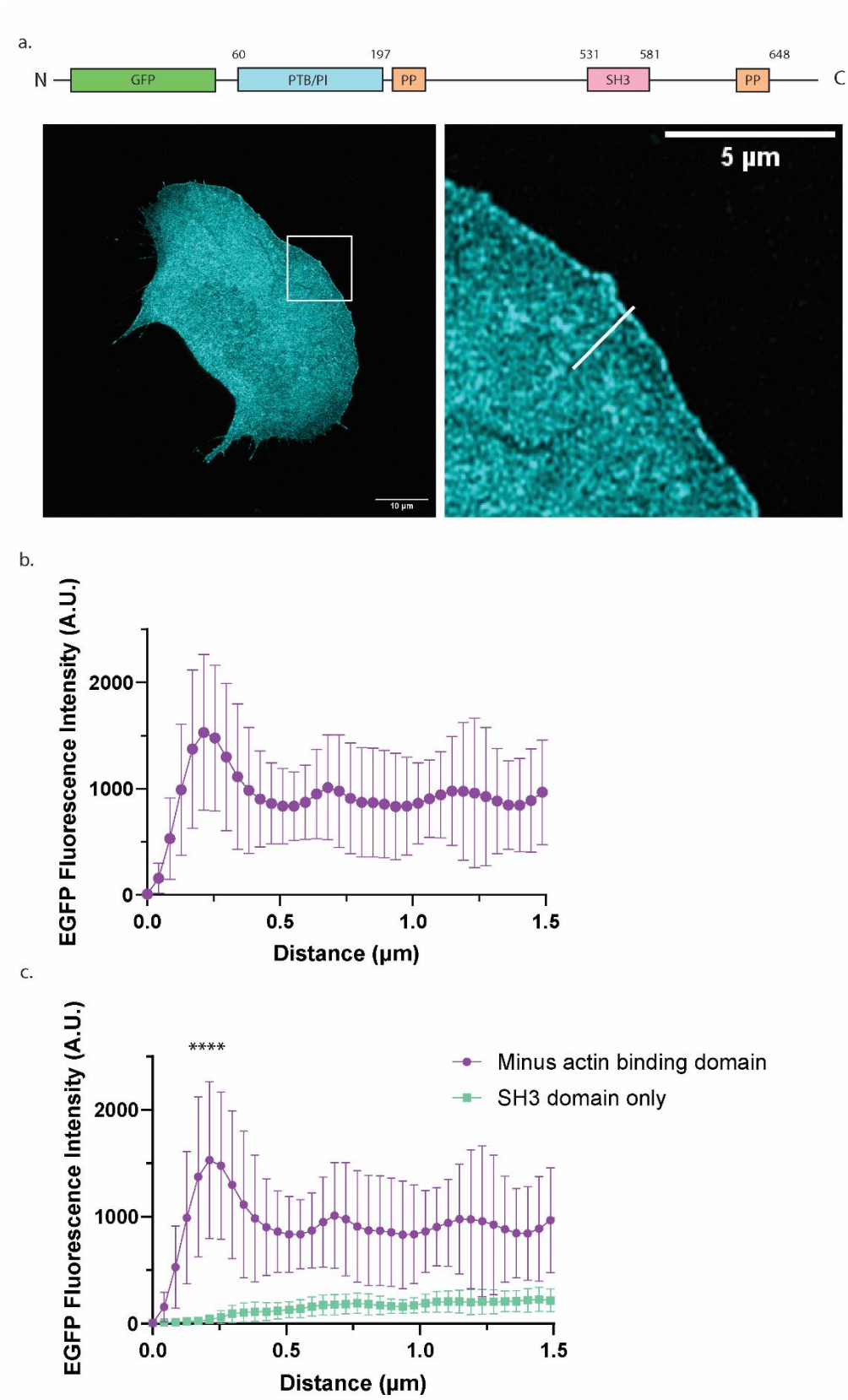

Figure 7-9 Minus Actin Binding domain construct shows slight localisation at leading-edge

a. Representative still images from imaging of B16-F1 cells transfected with GFP-Eps8-Minus Actin Binding Domain. Images of the full cell (left) and zoom of the leading edge (right) are shown. White line on zoom of leading-edge panels is indicative of where the plot was drawn and the data collected. Scale bars are 10µm on full cell image (left) and 5µm on zoom of leading-edge image (right).

b. Quantification of fluorescence intensity of GFP-Eps8-Minus Actin Binding Domain at the leading edge of live B16-F1 cells along the white line with 0 corresponding to the leading-

edge of the lamellipodia. 10 cells were analysed for the construct for the plotted mean and standard deviation.

c. Quantification of fluorescence intensity of GFP-Eps8-Minus Actin Binding Domain and GFP-SH3 only domain at the leading-edge of live B16-F1 cells along the white line with 0 corresponding to the leading-edge of the lamellipodia. 10 cells were analysed for the construct for the plotted mean and standard deviation and statistical differences were evaluated using unpaired t-tests for the mean of each distance data point. Distances 0.14643, 0.18304, 0.21965 and 0.25625µm were statistically significant with a p-value of >0.0001, as denoted by asterisks in the figure. Distances 0.10982 and 0.29286µm were statistically significant with a p-value of >0.001 (not denoted by asterisks). These distances correspond to the peak of fluorescence at the leading edge. The rest of the distances, besides distance 0µm were statistically significant with a p-value of >0.01 due to the difference in baseline fluorescence caused by partial or no localisation.

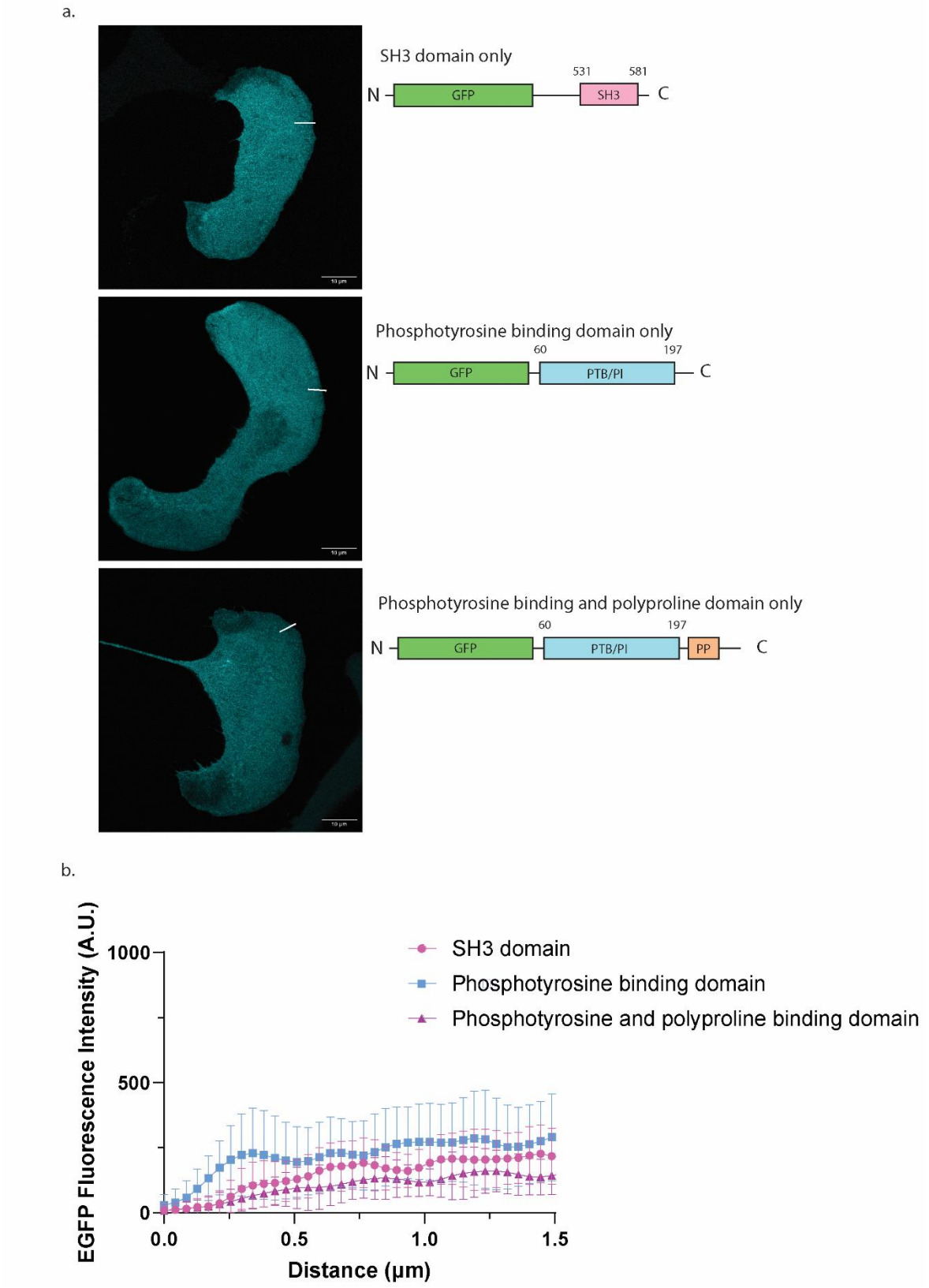

Figure 7-10 Phosphotyrosine, polyproline and SH3 domains did not localise

a. Representative still images from imaging of B16-F1 cells transfected with GFP-Eps8-Actin Binding, Polyproline and SH3 Domain. Images of the full cell are shown. White line is indicative of where the plot was drawn, and the data collected. Scale bars are 10µm.

b. Quantification of fluorescence intensity of GFP-Eps8-SH3 domain, GFP-Eps8-Phosphotyrosine Binding Domain and GFP-Eps8-Phosphotyrosine and Polyproline Domain at the leading-edge of live B16F1 cells along the white line with 0 corresponding to the leading-edge of the lamellipodia. 10 cells were analysed for each construct for the

plotted mean and standard deviation and statistic differences were evaluated using unpaired t-tests for the mean of each distance data point. No distances were statistically significant.

This data can be further clarified and summarised when considering the ratios of the amount of protein at the leading-edge to that in the cytosol. Shown in Figure 1-11, the ratio of leading edge/cytosol of full length Eps8 protein is much higher than the other truncated versions, as is the actin binding domain with SH3. The ratios for these were both statistically significant from all other constructs. The ratio of leading-edge/cytosol of GFP-Minus ABD was higher than that of the constructs with no localisation, and statistically significant in comparison to GFP-SH3 only.

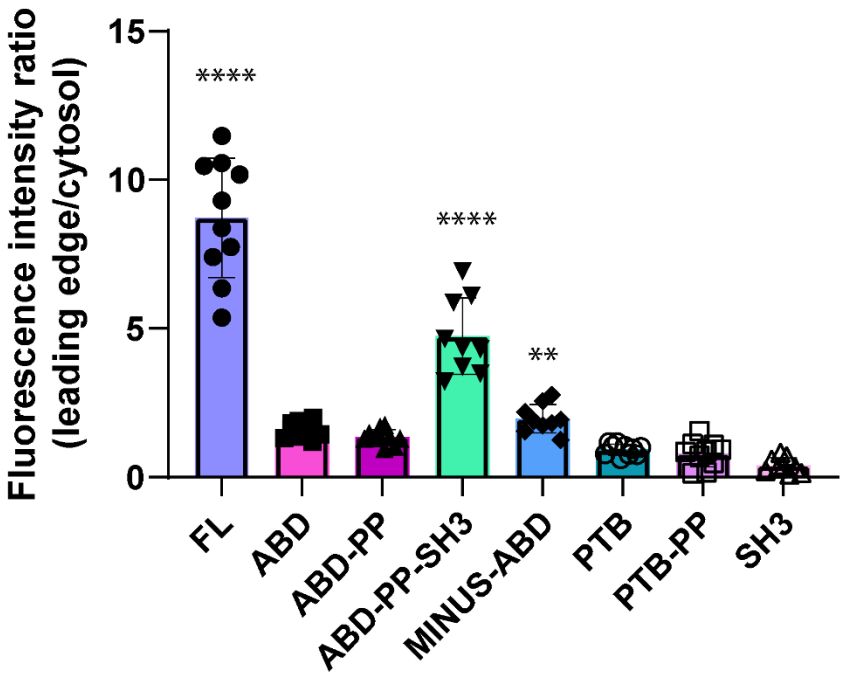

Figure 7-11 Full length, Actin binding domain plus SH3 and Minus actin binding domain constructs have higher recruitment levels to the leading edge
Quantification of Eps8 full length and truncated GFP-tagged constructs recruitment to the leading-edge as ratio between the leading-edge and cytosol. 10 cells were analysed for each construct and the ratio was calculated from the maximum value of the leading edge against the mean of the cytosol. Ordinary one-way ANOVA with multiple comparisons was performed with FL and ABD-PP-SH3 being statistically significant with a p value <0.0001 compared to all other constructs and to each other. Minus-ABD was statistically significant with a p value <0.01 compared to SH3. Denoted by asterisk (**** and **, respectively).

7.3 Discussion

In this chapter we have presented data validating the binding of Eps8 to ATP-F-actin in a different assay, corroborating our affinity chromatography and mass spectrometry data in chapter 5. We then used this same assay, GFP-trap, to investigate the role of the capping and bundling capabilities of Eps8 that were shown *in vitro* (Disanza et al., 2004) and their contribution or otherwise to ATP-F-actin binding. Upon the finding that constructs of this protein with point mutations abrogating these functions (Hertzog et al., 2010) still appeared to preferentially bind ATP-F-actin, we sought to identify the domain or domains of the protein that are responsible for this preference, whether it be direct or indirect (etc. in a complex). Several GFP-tagged and truncated Eps8 constructs were produced for this investigation using live cell imaging of B16-F1 cells. The data from these constructs provided some interesting results and elucidation to the method of ATP-F-actin preferential binding by Eps8.

Utilising Eps8 as the target protein, instead of actin as in our affinity chromatography, GFP-trap experiments showed an increase in pull down of actin from cells that had been treated with Jasplakinolide to increase the amount of ATP-F-actin in the cell. Jasplakinolide causes structural changes to the actin filament, leading to an ATP-bound conformation, whereas phalloidin, though it binds actin in a similar manner, does not change the conformation but instead stabilises the filament in its current nucleotide state (Pospich et al., 2020). Because of the ability of both of these drugs to stabilise F-actin but have differing effects on the nucleotide dependent conformation, we performed the GFP-trap experiments with an extra control condition of phalloidin treatment per construct. Encouragingly, and as we expected, Jasplakinolide treated cells only pulled down more actin when they were expressing GFP-Eps8. Phalloidin treatment, however, caused an increase in pull down of actin in all the cells, regardless of whether they were expressing no GFP-construct, GFP-alone or GFP-Eps8. This is due to phalloidin treatment not altering the nucleotide dependent conformation of F-actin, but promoting the induction of polymerisation and increase in F-actin in the cells (Wehland et al., 1997). This increase in polymerised actin would cause a noticeable increase in the amount of actin present in the centrifuged fraction of the samples, regardless of whether a GFP-tagged construct was present.

With this in mind, and utilising existing knowledge in the literature, we decided to test by GFP-trap constructs of Eps8 that had been produced to abrogate their actin binding roles *in vitro* (Hertzog et al., 2010). These constructs include Δcap, Δbund and Δcapbund. The details of the point mutations are listed in Table 7-1.

Table 7-1 Details of capping and bundling mutant Eps8 constructs

Name (Hertzog et al., 2010)	Biochemical consequence (Hertzog et al., 2010)	Point mutation details (Hertzog et al., 2010)
Δcap	>100 fold decrease in capping capability (affinity for barbed ends)	V689D, L693D
Δbund	Unable to bundle actin filaments	L757A, K759A
Δcapbund	Loss of capping and bundling function on F-actin	V689D, L693D, L757A, K759A

These mutations were carried out in the effector region of Eps8, that is responsible for binding to actin (Scita et al., 2001), and responsible for the capping and bundling functions of Eps8 (Disanza et al., 2004). The effector region contains five helices denoted H1-H5 and investigation revealed that the amphipathic helix H1 is necessary for the capping function, while H2-5 are necessary for the bundling function, providing distinct molecular areas of functionality (Hertzog et al., 2010). The point mutations to abolish capping and bundling capabilities are therefore in H1 and H2-5, respectively. The capping deficient construct was of most interest to us as we hypothesised that the ability to bind the barbed ends of actin filaments and preferentially bind ATP-F-actin are one and the same. Unexpectedly, GFP-trap experiments with Δcap, Δbund and Δcapbund were all able to pull down increased amounts of actin with

Jasplakinolide treatment compared to the control (Figure 7-4). This led us to believe the method of binding ATP-F-actin was probably indirect (via another protein) and not facilitated by the effector (actin binding) domain.

To further our investigation of ATP-F-actin mechanism of binding, we produced several truncated versions of Eps8 tagged with GFP for analysis by live cell imaging. Strikingly, the effector (actin binding) region alone displayed a very different localisation compared to the full length protein, and did not show the characteristic tight leading-edge localisation we have come to associate with ATP-F-actin binding (Figure 7-6). To investigate the protein domains needed to regain the tight leading-edge localisation, GFP-tagged constructs of the effector (actin binding) domain with its adjacent polyproline domain or adjacent polyproline and SH3 domains included were produced and analysed by live cell imaging. Whilst the effector domain and adjacent polyproline construct showed no difference to the effector domain alone (Figure 7-7), the re-introduction of the SH3 domain allowed us to regain the tight leading-edge localisation (Figure 7-8) indicating that the SH3 domain is necessary for this characteristic localisation. Finally, a construct containing the full length Eps8 protein minus the effector (actin binding) domain only showed some, be it far less intense, of this tight leading-edge localisation (Figure 7-9).

From this data we concluded that while the effector domain is indeed responsible for actin binding and localisation at the width of the lamellipodia, the SH3 domain is necessary for the characteristic tight leading-edge localisation. Therefore, the preferential binding of Eps8 for ATP-F-actin witnessed in our affinity chromatography and mass spectrometry results is most likely a result of an indirect interaction with another protein via its SH3 domain.

Indeed, Eps8 has been shown to be involved in multiple distinct complexes that regulate actin dynamics via Rho GTPases, such as Rac (Funato et al., 2004) and Cdc42 (Disanza et al., 2006).

Originally recognised as a sequence of similarity between non-receptor tyrosine kinases (Mayer et al., 1988), SH3 domains are expressed in all eukaryotes and are composed of around 60 amino acids (Kurochkina and Guha, 2013). They specifically recognise and bind to proline rich sequences, in particular PxxP

motifs (where x is any residue) (Ren et al., 1993). Two main classes of SH3 domains have been characterised, however there are some SH3 domains that bind non-typical sequences, and the SH3 domain of Eps8 is one of these, as its target motif is PxxDY (Mongiovi et al., 1999).

The SH3 domain of Eps8 is known to bind a number of target proteins, either alone or in the formation of a complex. SHB (Src homology 2 containing protein B) is an adaptor protein that binds to the SH3 domain of Eps8 and plays a role in signal transduction between Eps8 and tyrosine kinases (Karlsson et al., 1995). SHC (Src homology 2 containing protein C) also binds the SH3 domain of Eps8 (Matoskova et al., 1995) upstream of Rac activation (Khanday et al., 2006). Abi1 (originally called e3b1; Eps8 SH3 binding protein 1) was first discovered in a study to determine binding partners for Eps8s' SH3 domain (Biesova et al., 1997) and is part of the complex with Rac GEF Sos1 (Scita et al., 1999) which acts to localise Rac and its downstream actin polymerisation machinery to sites it is needed (Scita et al., 2001). Importantly, Abi is also a member of the WAVE regulatory complex (WRC), a major regulator of cellular protrusions (Chen et al., 2010). Another binding partner IRSp53, an actin crosslinking protein, acts to stabilise this Rac activating complex (Funato et al., 2004) and it can also form a complex with Eps8 alone to participate in Cdc42 signalling (Disanza et al., 2006).

It is worth discussing that the tight leading-edge localisation of Eps8 when its SH3 domain is intact is almost identical to that of the SCAR/WAVE complex. It was recently shown that without the VCA domain that binds and activates the Arp2/3 complex, SCAR/WAVE was still capable of localising and inducing the formation of lamellipodia. However, this was dependent on the presence of the polyproline domains of Abi1 and WAVE (Buracco et al., 2022)

This is of particular interest since many of our proteins identified as preferentially binding ATP-F-actin have SH3 domains, that recognise and bind proline rich regions, and indeed a lot of them are known to bind and interact with Abi1. This leads us to hypothesise that those proteins enriched in ATP-F-actin samples may be there as a result of the interaction between their SH3 domain and the polyproline domains of WAVE or Abi1.

In conclusion, in this chapter we have validated the preferential binding of Eps8 to ATP-F-actin via different assays, though these do not provide information about whether this interaction is indirect or direct. Utilising GFP-tagged truncated or mutated versions of Eps8 we explored the role of different domains in ATP-F-actin binding and localisation and led us to the hypothesis that the SH3 domain is of utmost importance for ATP-F-actin binding. This suggests that the method of binding is indirect, and attractive candidates for this interaction include WAVE and Abi1 especially due to the newly shown importance of their polyproline domains in the formation of lamellipodia and therefore polymerisation of actin.

8 Conclusions and future directions

The aim of this thesis was to identify proteins which preferentially bind ATP-F-actin over ADP-F-actin, in other words proteins that bind the highly dynamic and transient barbed ends of F-actin that are forming the cellular protrusions that allow the cells to migrate. We know from the literature that many proteins can bind ADP-F-actin preferentially, as their role is to promote the depolymerisation of "aged" filaments and therefore regulate polymerisation in a negative manner. Such proteins include ADF/-cofilin proteins which bind ADP-actin with much higher affinity than ATP- or ADP-Pi-actin (Carlier et al., 1997).

Our hypothesis was that there may be proteins that bind ATP-F-actin preferentially, potentially having a role in positive regulation of polymerisation. Indeed, it has been shown that Coronin 1B binds ATP-F-actin with a higher affinity than that of ADP-F-actin (Cai et al., 2007a). However, the methodology utilised in this study was high-speed actin co-sedimentation, which is not suitable for our purpose to identify proteins that preferentially bind ATP-F-actin from whole cell lysate. This was, however, of great encouragement to our hypothesis since Coronin 1B was identified as preferentially binding ATP-F-actin in our dataset.

Crucially, the effect of Coronin 1B binding to ATP-F-actin was indeed involved in positive regulation of polymerisation, by blocking severing by cofilin in ATP-F-actin portions of a filament, while promoting severing by cofilin in ADP-F-actin (Gandhi et al, 2009). This provides a very interesting question as to whether our identified pool of proteins that preferentially bind ATP-F-actin could also have dual roles in both positive and negative regulation of polymerisation, dependent on nucleotide state.

8.1 Conclusions

The main conclusion we have drawn from this thesis is that there are indeed proteins that preferentially bind ATP-F-actin. Given the pool of proteins we identified, and what is already known of their function in the control of actin dynamics, we do hypothesise involvement in positive feedback of

polymerisation. The milestones allowing us to reach this conclusion and hypothesis are as follows:

1. Optimised affinity columns for polymerised non-muscle actin

2. Optimised the loading of G-actin with non-hydrolysable analogues of ATP and the subsequent polymerisation

3. Ensuring the polymerised actin for “ATP-F-actin” columns are successfully loaded with non-hydrolysable ATP analogues

4. Performed affinity chromatography for ADP-F-actin vs ATP-F-actin using two highly motile cell lines lysate as input and subsequent mass spectrometry analysis

5. Investigated the ATP-F-actin binding method of one of the hits, Eps8, and identified the SH3 domain as important in this interaction, whether it be indirect or direct

Of course, to understand the effect of ATP-F-actin binding we must understand which proteins are binding directly or indirectly. For example, some may be part of a complex with another protein that binds ATP-F-actin directly and this is how they were bound and identified during affinity chromatography. Indeed, this information would also give great insight into the biological relevance of ATP-F-actin binding, if the role of potential complexes was known or investigated.

8.2 Future directions

The mechanism of ATP-F-actin binding and its relevance is crucial for the future progression of this project. To determine whether an identified protein is indirectly or directly binding ATP-F-actin, an attractive study would be to examine this utilising the purified protein in question combined with purified ADP-F-actin and ATP-F-actin and analyse it using Total Internal Reflection Fluorescence (TIRF) microscopy. This has proved a valuable method, as shown by Merino et al., 2018 where the authors compared F-actin with different nucleotide conformations and its effect on the binding of Coronin 1B to the

length of the filaments. A panel is shown from their experiment in Figure 8-1, where Coronin 1B is visualised as strongly binding the length of the filaments in ATP-F-actin samples (prepared by treatment with Jasplakinolide) and with greatly diminished binding to ADP-F-actin.

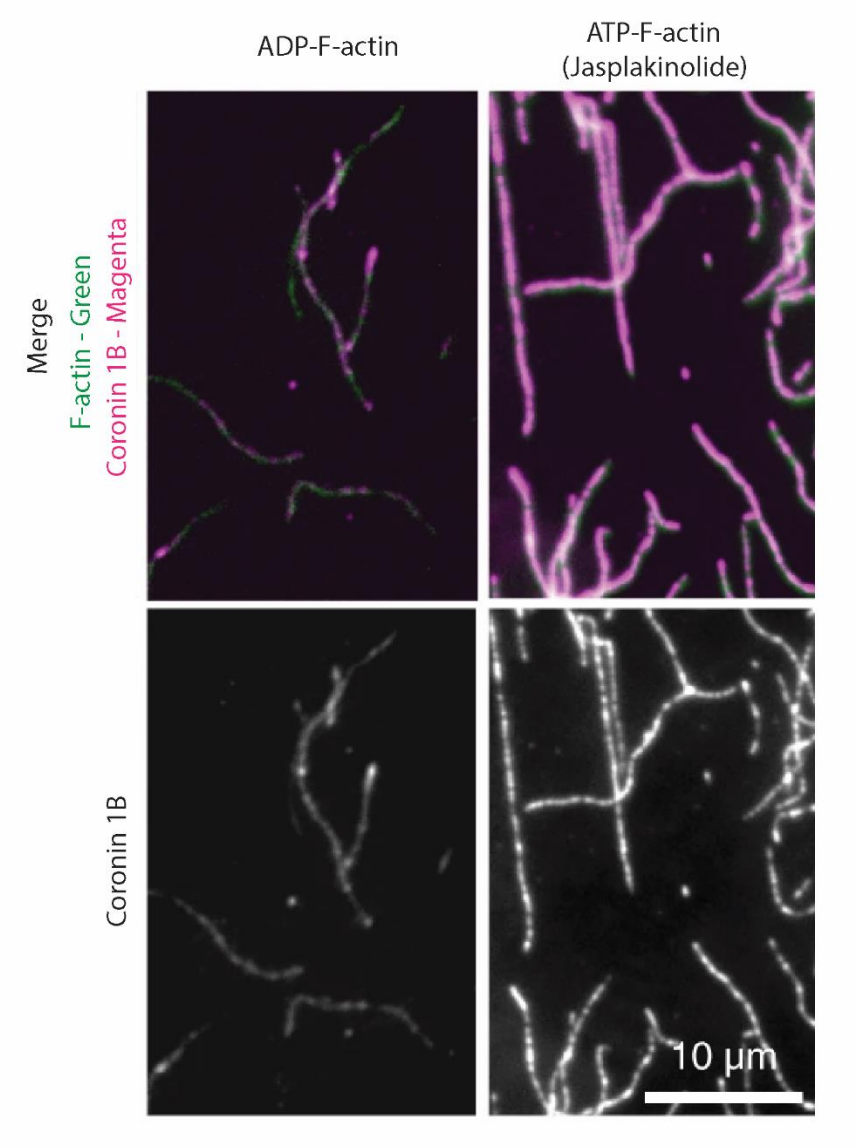

Figure 8-1 Coronin 1B binding to ADP- or ATP-F-actin
Panel of a figure adapted from Merino et al., 2018 showing the binding of Coronin 1B to either ADP-F-actin or ATP-F-actin (via Jasplakinolide treatment) visualised using TIRF microscopy. The two left hand figures depict ADP-F-actin with F-actin in green and Coronin 1B in magenta (top) and Coronin 1B alone in greyscale (bottom). The two right hand figures show ATP-F-actin with F-actin in green and Coronin 1B in magenta (top) and Coronin 1B alone in greyscale (bottom). Scale bar shown is 10µm. Taken from Figure 6a of Merino et al., 2018.

This kind of experiment would be invaluable in determining a direct binding of ATP-F-actin for our proteins of interest, or confirm that they do not directly bind ATP-F-actin, but may be part of a complex with a protein that does. Indeed, it

may be the case that some of our isolated proteins do bind ATP-F-actin directly, and some do not. The latter may be binding through another protein binding ATP-F-actin directly which may or may not be present in our datasets. With this in mind and given the important role we determined of the SH3 domain of Eps8, we highlighted that several of our proteins identified as binding ATP-F-actin have SH3 domains. Therefore, we hypothesise that SH3 domains may be responsible for facilitating indirect binding to ATP-F-actin. Importantly, SH3 domains are known to recognise and bind proline rich sequences, such as polyproline domains.

Recent work on the study of the WAVE regulatory complex (WRC) from our lab has highlighted the importance of the polyproline domains in two members of the complex, which previously have not been thought of as important for the formation of protrusions. The VCA domain of WAVE is thought to be the critical part of the complex, as it binds and activates the Arp2/3 complex leading to the formation of branched actin networks that form the lamellipodia (Machesky and Insall, 1998). However, upon VCA deletion (Figure 8-2a), the association with and localisation of Arp2/3 is greatly diminished, but the polymerisation of actin continues to occur, and the complex remains localised at the leading edge of the cell. This is shown and quantified in Figure 8-2b, where you can visually see the complex at the leading edge, and the peak for fluorescence remains the same with or without an intact VCA domain. The ratio of fluorescence intensity at the leading edge compared to the cytosol also remains the same (Figure 8-2c).

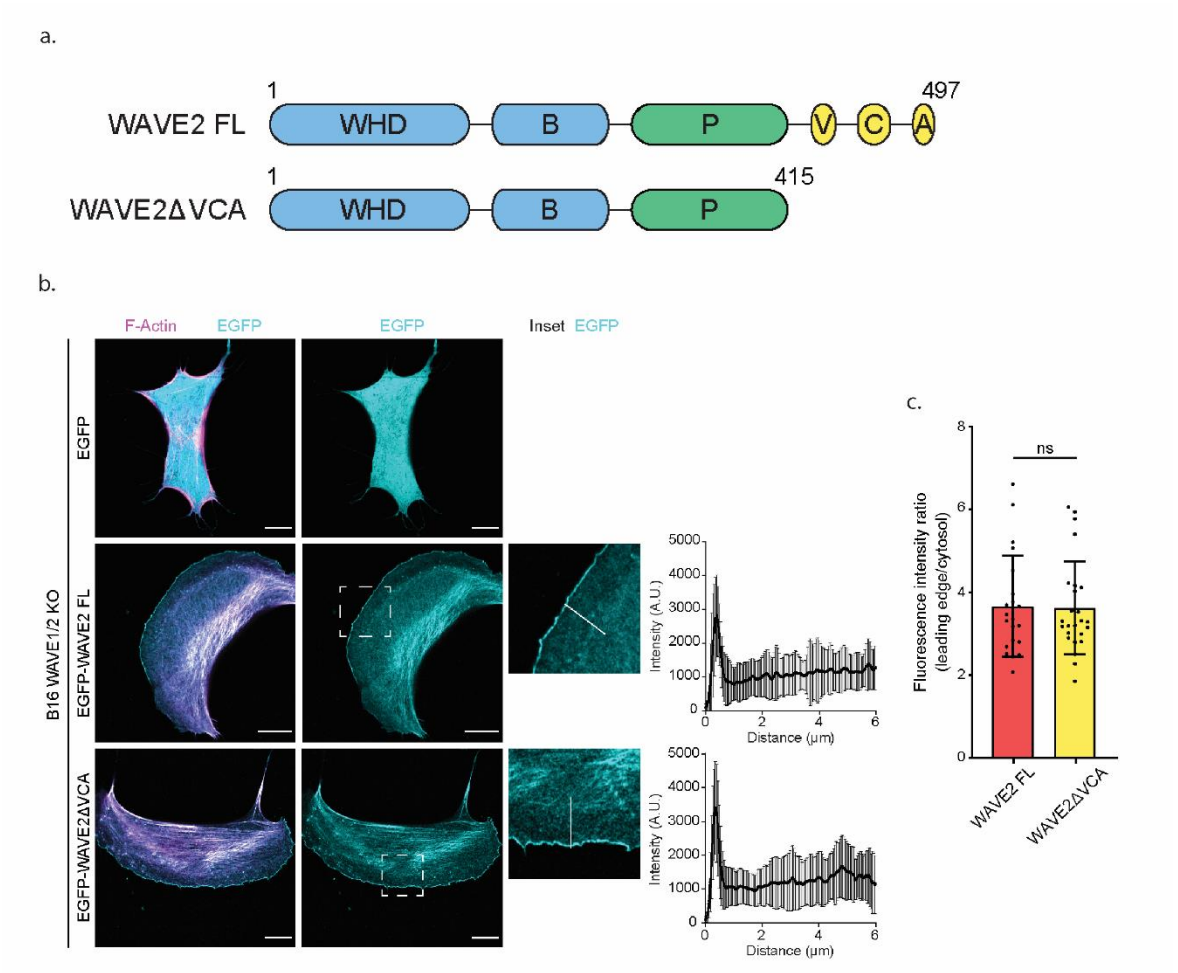

Figure 8-2 VCA domain is not needed for the formation of lamellipodia

a. Schematic diagram showing WAVE 2 FL (full length) and WAVE2ΔVCA (with VCA deleted). Abbreviations depicting domains are as follows: WHD – WASP homology domain, B – Basic domain, P – Polyproline domain, V – Verprolin homology domain, C – Central region and A – acidic region.

b. WAVE1/2 KO B16F1 cells were transfected with LifeAct-TagRed (magenta) and EGFP-tagged WAVE2 (cyan) and representative cells with WRC localisation are shown. EGFP inset depicts an area used for the quantification of WAVE2 intensity. Graphs show the quantification of fluorescence intensity along the white line with 0 corresponding to the leading edge. Scale bar shown in lower right corner of full cell images are 10 μm. 21 cells were analysed for each construct for the plotted mean and standard deviation.

c. Quantification of WAVE 2 FL and WAVE2 ΔVCA GFP-tagged constructs recruitment to the leading edge as ratio between the leading edge and cytosol. 21 cells were analysed for each construct and the ratio was calculated from the maximum value of the leading edge against the mean of the cytosol. Statistical significance assessed by one-way ANOVA gave a p-value of 0.9908 (not significant).

Further, we have shown that actin dynamics are only disrupted when the polyproline domain of both Abi and WAVE are deleted along with the VCA domain; the deletion of either of these alone did not affect lamellipodia formation (Figure 8-3a-b). Therefore, without the VCA domain the polyproline domains are of utmost importance to the activity of the complex. The data show

that the WRC contributes to actin polymerisation beyond its role in activating the Arp2/3 complex, and that the polyproline domains of both WAVE and Abi are essential for this. This was particularly interesting since many of the proteins we have identified as preferentially binding ATP-F-actin have SH3 domains. The majority of SH3 domains preferentially bind xPxxP motifs. However, Eps8 SH3 domain is considered unusual and preferentially binds PxxDY over xPxxP and this is the polyproline motif present in Abi (Mongiovi et al., 1999).

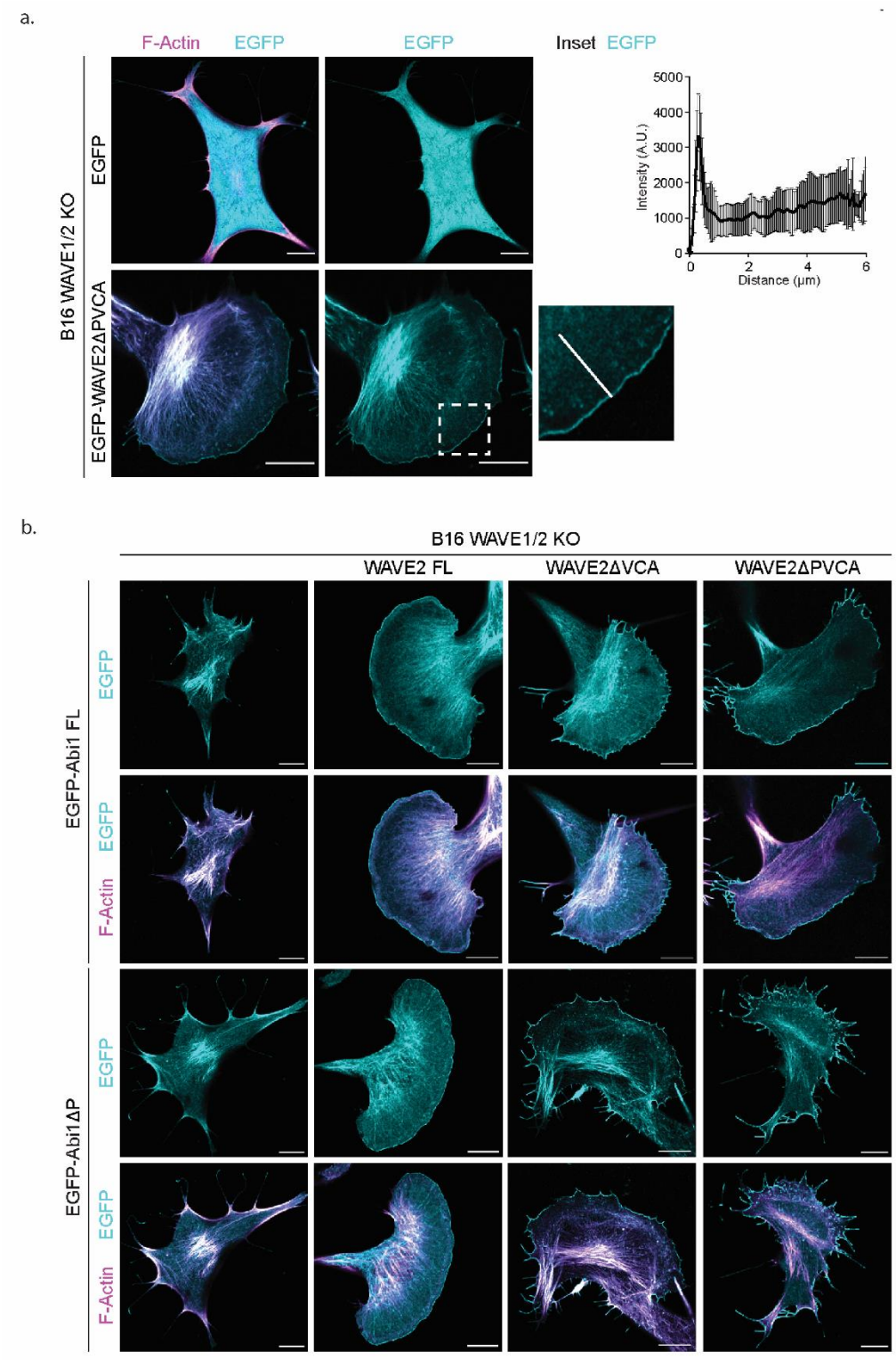

Figure 8-3 WAVE and Abi polyproline domain deletion disrupted lamellipodia formation

a. WAVE1/2 KO B16F1 cells were transfected with LifeAct-TagRed (magenta) and EGFP-tagged WAVE2ΔPVCA (cyan) and representative cells with WRC localisation are shown. Graph shows the quantification of fluorescence intensity along the white line with 0 corresponding to the leading edge. Scale bar shown in lower right corner of images are 10 μm. 21 cells were analysed for each construct for the plotted mean and standard deviation.

b. WAVE1/2 KO B16F1 cells were transfected with LifeAct-TagRed (magenta) and EGFP-tagged Abi1 FL or Abi1ΔP (cyan) and WAVE 2 FL, WAVE2 ΔVCA or WAVE2ΔPVCA as indicated above the images. Scale bar shown in lower right corner of images are 10 μm.

To identify proteins that could potentially be involved in this by binding the polyproline domains, pulldowns were performed with full-length and truncated versions of WAVE2. As expected, mass spectrometry analysis of the full-length protein pulldown identified all members of the Arp2/3 complex and a range of actin binding proteins. These proteins were lost in the pulldown of WAVEΔVCA, confirming WAVE2 requires its intact VCA domain to bind the Arp2/3 complex. Importantly, the pull down with WAVEΔPVCA (missing also the polyproline domain) caused the loss of several more interactors, indicating the polyproline domain is needed for their binding to WAVE. These are listed in the green box above "P" (polyproline domain) in Figure 8-4.

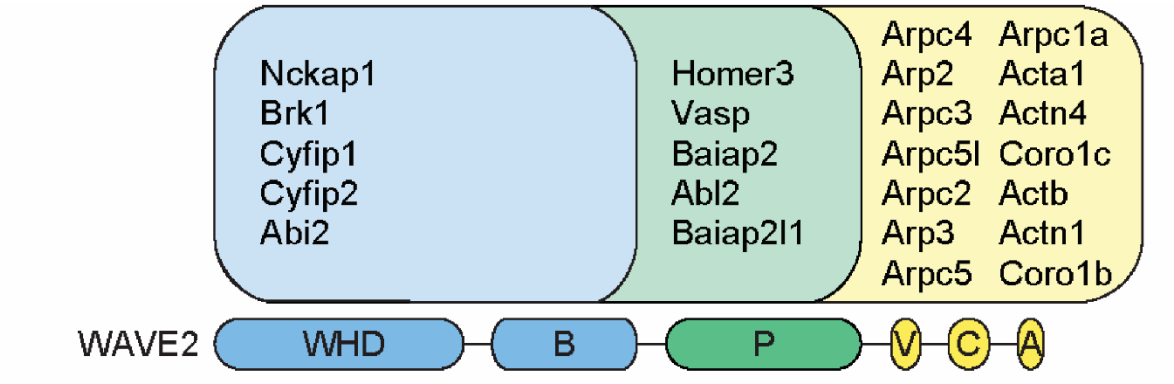

Figure 8-4 Specific domain interactors identified from pulldowns of WAVE2 truncations
Schematic diagram of the domains of WAVE2 with their corresponding binding partners identified by pulldown listed above. Abbreviations depicting domains are as follows: WHD – WASP homology domain, B – Basic domain, P – Polyproline domain, V – Verprolin homology domain, C – Central region and A – acidic region.

Crucially, every protein identified as binding the WAVE polyproline domain (besides one: Homer3) was also identified as preferentially binding ATP-F-actin in at least one of our datasets (Table 8-1).

Table 8-1 ATP-F-actin enriched proteins that bind WAVE polyproline domain

WAVE polyproline domain enriched proteins
ATP-F-actin enriched in "JVM3-ATPγS"

Protein names	Gene names	Student's T-test Difference JVM3 (ADP-ATPgS)	Student's T-test Significant JVM3 (ADP-ATPgS)	Student's T-test Significant JVM3 (ADP-ATPgS) p-value only
Brain-specific angiogenesis inhibitor 1-associated protein 2-like protein 1	BAIAP2L1	-5.09	+	+
ATP-F-actin enriched in "PDAC-ATPγS"				
Protein names	**Gene names**	**Student's T-test Difference PDAC2 (ADP-ATPgS)**	**Student's T-test Significant PDAC2 (ADP-ATPgS)**	**Student's T-test Significant PDAC2 (ADP-ATPgS) p-value only**
Brain-specific angiogenesis inhibitor 1-associated protein 2	BAIAP2	-1.74	+	+
Abelson tyrosine-protein kinase 2	ABL2	-1.71	+	+
ATP-F-actin enriched in "JVM3-Jasplakinolide"				
Protein names	**Gene names**	**Student's T-test Difference JVM3-ADP_JVM3-Jas**	**Student's T-test Significant JVM3-ADP_JVM3-Jas**	**Student's T-test Significant JVM3-ADP_JVM3-Jas p-value only**
Vasodilator-stimulated phosphoprotein	VASP	-1.08	+	+
Brain-specific angiogenesis inhibitor 1-associated protein 2-like protein 1	BAIAP2L1	-1.82	+	+

ATP-F-actin enriched in "PDAC-Jasplakinolide"				
Protein names	**Gene names**	**Student's T-test Difference PDAC-ADP_PDAC-Jas**	**Student's T-test Significant PDAC-ADP_PDAC-Jas**	**Student's T-test Significant PDAC-ADP_PDAC-Jas p-value only**
Brain-specific angiogenesis inhibitor 1-associated protein 2	BAIAP2	-0.92		+
Abelson tyrosine-protein kinase 2	ABL2	-2.75	+	+

This leads us to hypothesise that those proteins enriched in ATP-F-actin samples may be there as a result of the interaction between their SH3 domain and the polyproline domains of WAVE or Abi1 and that these SH3/polyproline interactions could be providing a hub for the recruitment of different proteins involved in actin polymerisation to the site of ATP-F-actin, generating a positive feedback loop of polymerisation.

The investigation of this is therefore the most anticipated future work of this thesis and experiments utilising purified protein to discover the mechanism of and the protein responsible for the direct binding of ATP-F-actin are a significant priority. Non-hydrolysable analogues of ATP and Jasplakinolide will remain crucial tools for this project, as we explore these proteins and their potential interactions with WRC proteins in various methods such as those we used for the investigation of Eps8 to begin with.

The mechanism of ATP-F-actin binding is crucial to understanding the biological relevance of these interactions. For this reason, considerable effort must be spent to investigate it, in particular *in vitro* utilising binding assays of purified proteins and truncated versions of the domains of interest (SH3/polyproline). For the success of this approach, TIRF microscopy would be an excellent tool thanks

to its ability to visualise the direct binding to ATP-F-actin, as it was for coronin 1B (Figure 8-1; Merino et al.,2018).

Another interesting question arising from the data presented in this thesis is the intriguing role of the interaction between the SH3 domains of ATP-F-actin enriched proteins and the polyproline domains of WAVE and Abi in the generation of a positive feedback of actin polymerisation. This important question could be investigated in depth by introducing mutations in key binding residues and analyzing their effects on the interaction (by *in vitro* assays as well as live cell imaging for co-localisation.), on the polymerisation of actin, on the formation of lamellipodia and, lastly but of utmost importance, on cell migration.

In summary, the investigation of which proteins can bind ATP-F-actin directly, and the analysis of their ability to bind the polyproline domains of WAVE and Abi, will give us a clearer understanding of the positive feedback in actin polymerisation and the role the highly transient ATP-F-actin plays in this important phenomenon.

9 References

Abercrombie, M., 1980. The Croonian Lecture, 1978 - The crawling movement of metazoan cells. Proceedings of the Royal Society of London. Series B. Biological Sciences 207, 129–147. https://doi.org/10.1098/rspb.1980.0017

Alberts, A.S., 2001. Identification of a carboxyl-terminal diaphanous-related formin homology protein autoregulatory domain. J Biol Chem 276, 2824–2830. https://doi.org/10.1074/jbc.M006205200

Archer, S.J., Vinson, V.K., Pollard, T.D., Torchia, D.A., 1994. Elucidation of the poly-L-proline binding site in Acanthamoeba profilin I by NMR spectroscopy. FEBS Lett 337, 145–151. https://doi.org/10.1016/0014-5793(94)80262-9

Arora, A.S., Huang, H.-L., Singh, R., Narui, Y., Suchenko, A., Hatano, T., Heissler, S.M., Balasubramanian, M.K., Chinthalapudi, K., 2023. Structural insights into actin isoforms. eLife 12, e82015. https://doi.org/10.7554/eLife.82015

Bachmann, C., Fischer, L., Walter, U., Reinhard, M., 1999. The EVH2 Domain of the Vasodilator-stimulated Phosphoprotein Mediates Tetramerization, F-actin Binding, and Actin Bundle Formation *. Journal of Biological Chemistry 274, 23549–23557. https://doi.org/10.1074/jbc.274.33.23549

Baghirova, S., Hughes, B.G., Hendzel, M.J., Schulz, R., 2015. Sequential fractionation and isolation of subcellular proteins from tissue or cultured cells. MethodsX 2, 440–445. https://doi.org/10.1016/j.mex.2015.11.001

Bagrodia, S., Taylor, S.J., Jordon, K.A., Van Aelst, L., Cerione, R.A., 1998. A novel regulator of p21-activated kinases. J Biol Chem 273, 23633–23636. https://doi.org/10.1074/jbc.273.37.23633

Bagshaw, C.R., Eccleston, J.F., Eckstein, F., Goody, R.S., Gutfreund, H., Trentham, D.R., 1974. The magnesium ion-dependent adenosine triphosphatase of myosin. Two-step processes of adenosine triphosphate association and adenosine diphosphate dissociation. Biochem J 141, 351–364.

Bagshaw, C.R., Eccleston, J.F., Trentham, D.R., Yates, D.W., Goody, R.S., 1973. Transient Kinetic Studies of the Mg++-dependent ATPase of Myosin and Its Proteolytic Subfragments. Cold Spring Harb Symp Quant Biol 37, 127–135. https://doi.org/10.1101/SQB.1973.037.01.020

Balhara, N., Yadav, R., Ranga, S., Ahuja, P., Tanwar, M., 2024. Understanding the HPV associated cancers: A comprehensive review. Mol Biol Rep 51, 743. https://doi.org/10.1007/s11033-024-09680-6

Bamburg, J. r., Harris, H. e., Weeds, A. g., 1980. Partial purification and characterization of an actin depolymerizing factor from brain. FEBS Letters 121, 178–182. https://doi.org/10.1016/0014-5793(80)81292-0

Basu, A.K., 2018. DNA Damage, Mutagenesis and Cancer. Int J Mol Sci 19, 970. https://doi.org/10.3390/ijms19040970

Belmont, L.D., Orlova, A., Drubin, D.G., Egelman, E.H., 1999. A change in actin conformation associated with filament instability after Pi release. Proc Natl Acad Sci U S A 96, 29–34. https://doi.org/10.1073/pnas.96.1.29

Bergeron, S.E., Zhu, M., Thiem, S.M., Friderici, K.H., Rubenstein, P.A., 2010. Ion-dependent Polymerization Differences between Mammalian β- and γ-Nonmuscle Actin Isoforms. J Biol Chem 285, 16087–16095. https://doi.org/10.1074/jbc.M110.110130

Biesova, Z., Piccoli, C., Wong, W.T., 1997. Isolation and characterization of e3B1, an eps8 binding protein that regulates cell growth. Oncogene 14, 233–241. https://doi.org/10.1038/sj.onc.1200822

Björkegren, C., Rozycki, M., Schutt, C.E., Lindberg, U., Karlsson, R., 1993. Mutagenesis of human profilin locates its poly(L-proline)-binding site to a hydrophobic patch of aromatic amino acids. FEBS Lett 333, 123–126. https://doi.org/10.1016/0014-5793(93)80388-b

Blanchoin, L., Pollard, T.D., 2002. Hydrolysis of ATP by polymerized actin depends on the bound divalent cation but not profilin. Biochemistry 41, 597–602. https://doi.org/10.1021/bi011214b

Blanchoin, L., Pollard, T.D., 1999. Mechanism of interaction of Acanthamoeba actophorin (ADF/Cofilin) with actin filaments. J Biol Chem 274, 15538–15546. https://doi.org/10.1074/jbc.274.22.15538

Borgo, C., D'Amore, C., Sarno, S., Salvi, M., Ruzzene, M., 2021. Protein kinase CK2: a potential therapeutic target for diverse human diseases. Sig Transduct Target Ther 6, 1–20. https://doi.org/10.1038/s41392-021-00567-7

Bork, P., Sander, C., Valencia, A., 1992. An ATPase domain common to prokaryotic cell cycle proteins, sugar kinases, actin, and hsp70 heat shock proteins. Proc Natl Acad Sci U S A 89, 7290–7294. https://doi.org/10.1073/pnas.89.16.7290

Breitsprecher, D., Goode, B.L., 2013. Formins at a glance. J Cell Sci 126, 1–7. https://doi.org/10.1242/jcs.107250

Breitsprecher, D., Kiesewetter, A.K., Linkner, J., Vinzenz, M., Stradal, T.E.B., Small, J.V., Curth, U., Dickinson, R.B., Faix, J., 2011. Molecular mechanism of Ena/VASP-mediated actin-filament elongation. EMBO J 30, 456–467. https://doi.org/10.1038/emboj.2010.348

Brenner, S.L., Korn, E.D., 1981. Stimulation of actin ATPase activity by cytochalasins provides evidence for a new species of monomeric actin. J Biol Chem 256, 8663–8670.

Brown, S.S., Spudich, J.A., 1981. Mechanism of action of cytochalasin: evidence that it binds to actin filament ends. J Cell Biol 88, 487–491. https://doi.org/10.1083/jcb.88.3.487

Bruck, S., Huber, T.B., Ingham, R.J., Kim, K., Niederstrasser, H., Allen, P.M., Pawson, T., Cooper, J.A., Shaw, A.S., 2006. Identification of a Novel Inhibitory Actin-capping Protein Binding Motif in CD2-associated Protein . Journal of Biological Chemistry 281, 19196–19203. https://doi.org/10.1074/jbc.M600166200

Bubb, M.R., Senderowicz, A.M., Sausville, E.A., Duncan, K.L., Korn, E.D., 1994. Jasplakinolide, a cytotoxic natural product, induces actin polymerization and competitively inhibits the binding of phalloidin to F-actin. Journal of Biological Chemistry 269, 14869–14871. https://doi.org/10.1016/S0021-9258(17)36545-6

Bugyi, B., Carlier, M.-F., 2010. Control of actin filament treadmilling in cell motility. Annu Rev Biophys 39, 449–470. https://doi.org/10.1146/annurev-biophys-051309-103849

Buracco, S., Singh, S., Claydon, S., Paschke, P., Tweedy, L., Whitelaw, J., McGarry, L., Thomason, P.A., Insall, R.H., 2022. The Scar/WAVE complex drives normal actin protrusions without the Arp2/3 complex, but proline-rich domains are required. https://doi.org/10.1101/2022.05.14.491902

Burtnick, L.D., Koepf, E.K., Grimes, J., Jones, E.Y., Stuart, D.I., McLaughlin, P.J., Robinson, R.C., 1997. The Crystal Structure of Plasma Gelsolin: Implications for Actin Severing, Capping, and Nucleation. Cell 90, 661–670. https://doi.org/10.1016/S0092-8674(00)80527-9

Cai, L., Makhov, A.M., Bear, J.E., 2007a. F-actin binding is essential for coronin 1B function in vivo. J Cell Sci 120, 1779–1790. https://doi.org/10.1242/jcs.007641

Cai, L., Makhov, A.M., Schafer, D.A., Bear, J.E., 2008. Coronin 1B antagonizes Cortactin and remodels Arp2/3-containing actin branches in lamellipodia. Cell 134, 828–842. https://doi.org/10.1016/j.cell.2008.06.054

Cai, L., Marshall, T.W., Uetrecht, A.C., Schafer, D.A., Bear, J.E., 2007b. Coronin 1B Coordinates Arp2/3 Complex and Cofilin Activities at the Leading Edge. Cell 128, 915–929. https://doi.org/10.1016/j.cell.2007.01.031

Campa, F., Machuy, N., Klein, A., Rudel, T., 2006. A new interaction between Abi-1 and betaPIX involved in PDGF-activated actin cytoskeleton reorganisation. Cell Res 16, 759–770. https://doi.org/10.1038/sj.cr.7310091

Carlier, M.F., Jean, C., Rieger, K.J., Lenfant, M., Pantaloni, D., 1993. Modulation of the interaction between G-actin and thymosin beta 4 by the ATP/ADP ratio: possible implication in the regulation of actin dynamics. Proc Natl Acad Sci U S A 90, 5034–5038.

Carlier, M.-F., Laurent, V., Santolini, J., Melki, R., Didry, D., Xia, G.-X., Hong, Y., Chua, N.-H., Pantaloni, D., 1997. Actin Depolymerizing Factor (ADF/Cofilin) Enhances the Rate of Filament Turnover: Implication in Actin-based Motility. The Journal of Cell Biology 136, 1307–1322. https://doi.org/10.1083/jcb.136.6.1307

Carlier, M.F., Pantaloni, D., 1986. Direct evidence for ADP-inorganic phosphate-F-actin as the major intermediate in ATP-actin polymerization. Rate of dissociation of inorganic phosphate from actin filaments. Biochemistry 25, 7789–7792. https://doi.org/10.1021/bi00372a001

Carlsson, L., Nyström, L.-E., Lindberg, U., Kannan, K.K., Cid-Dresdner, H., Lövgren, S., Jörnvall, H., 1976. Crystallization of a non-muscle actin. Journal of Molecular Biology 105, 353–366. https://doi.org/10.1016/0022-2836(76)90098-X

Carlsson, L., Nyström, L.-E., Sundkvist, I., Markey, F., Lindberg, U., 1977. Actin polymerizability is influenced by profilin, a low molecular weight protein in non-muscle cells. Journal of Molecular Biology 115, 465–483. https://doi.org/10.1016/0022-2836(77)90166-8

Castrillon, D.H., Wasserman, S.A., 1994. Diaphanous is required for cytokinesis in Drosophila and shares domains of similarity with the products of the limb deformity gene. Development 120, 3367–3377. https://doi.org/10.1242/dev.120.12.3367

Castro-Castro, A., Ojeda, V., Barreira, M., Sauzeau, V., Navarro-Lérida, I., Muriel, O., Couceiro, J.R., Pimentel-Muíños, F.X., Del Pozo, M.A., Bustelo, X.R., 2011. Coronin 1A promotes a cytoskeletal-based feedback loop that facilitates Rac1 translocation and activation. EMBO J 30, 3913–3927. https://doi.org/10.1038/emboj.2011.310

Chen, Z., Borek, D., Padrick, S.B., Gomez, T.S., Metlagel, Z., Ismail, A.M., Umetani, J., Billadeau, D.D., Otwinowski, Z., Rosen, M.K., 2010. Structure and control of the actin regulatory WAVE complex. Nature 468, 533–538. https://doi.org/10.1038/nature09623

Choe, H., Burtnick, L.D., Mejillano, M., Yin, H.L., Robinson, R.C., Choe, S., 2002. The calcium activation of gelsolin: insights from the 3A structure of the G4-G6/actin complex. J Mol Biol 324, 691–702. https://doi.org/10.1016/s0022-2836(02)01131-2

Chou, S.Z., Pollard, T.D., 2019. Mechanism of actin polymerization revealed by cryo-EM structures of actin filaments with three different bound nucleotides. Proceedings of the National Academy of Sciences 116, 4265–4274. https://doi.org/10.1073/pnas.1807028115

Cossio, P., Hocky, G.M., 2022. Catching actin proteins in action. Nature 611, 241–243. https://doi.org/10.1038/d41586-022-03343-x

Côté, J.-F., Vuori, K., 2002. Identification of an evolutionarily conserved superfamily of DOCK180-related proteins with guanine nucleotide exchange activity. J Cell Sci 115, 4901–4913. https://doi.org/10.1242/jcs.00219

Coué, M., Brenner, S.L., Spector, I., Korn, E.D., 1987. Inhibition of actin polymerization by latrunculin A. FEBS Letters 213, 316–318. https://doi.org/10.1016/0014-5793(87)81513-2

Courtemanche, N., 2018. Mechanisms of formin-mediated actin assembly and dynamics. Biophys Rev 10, 1553–1569. https://doi.org/10.1007/s12551-018-0468-6

Courtemanche, N., Pollard, T.D., 2013. Interaction of profilin with the barbed end of actin filaments. Biochemistry 52, 6456–6466. https://doi.org/10.1021/bi400682n

Cox, J., Hein, M.Y., Luber, C.A., Paron, I., Nagaraj, N., Mann, M., 2014. Accurate Proteome-wide Label-free Quantification by Delayed Normalization and Maximal Peptide Ratio Extraction, Termed MaxLFQ. Mol Cell Proteomics 13, 2513–2526. https://doi.org/10.1074/mcp.M113.031591

Cox, J., Mann, M., 2008. MaxQuant enables high peptide identification rates, individualized p.p.b.-range mass accuracies and proteome-wide protein quantification. Nat Biotechnol 26, 1367–1372. https://doi.org/10.1038/nbt.1511

Cox, J., Neuhauser, N., Michalski, A., Scheltema, R.A., Olsen, J.V., Mann, M., 2011. Andromeda: A Peptide Search Engine Integrated into the MaxQuant Environment. J. Proteome Res. 10, 1794–1805. https://doi.org/10.1021/pr101065j

Crosby, D., Bhatia, S., Brindle, K.M., Coussens, L.M., Dive, C., Emberton, M., Esener, S., Fitzgerald, R.C., Gambhir, S.S., Kuhn, P., Rebbeck, T.R., Balasubramanian, S., 2022. Early detection of cancer. Science 375, eaay9040. https://doi.org/10.1126/science.aay9040

Cruz, E.M.D.L., Roland, J., McCullough, B.R., Blanchoin, L., Martiel, J.-L., 2010. Origin of Twist-Bend Coupling in Actin Filaments. Biophysical Journal 99, 1852–1860. https://doi.org/10.1016/j.bpj.2010.07.009

Currier, M.A., Stehn, J.R., Swain, A., Chen, D., Hook, J., Eiffe, E., Heaton, A., Brown, D., Nartker, B.A., Eaves, D.W., Kloss, N., Treutlein, H., Zeng, J., Alieva, I.B., Dugina, V.B., Hardeman, E.C., Gunning, P.W., Cripe, T.P., 2017. Identification of Cancer-Targeted Tropomyosin Inhibitors and Their Synergy with Microtubule Drugs. Mol Cancer Ther 16, 1555–1565. https://doi.org/10.1158/1535-7163.MCT-16-0873

Damiano-Guercio, J., Kurzawa, L., Mueller, J., Dimchev, G., Schaks, M., Nemethova, M., Pokrant, T., Brühmann, S., Linkner, J., Blanchoin, L., Sixt, M., Rottner, K., Faix, J., 2020. Loss of Ena/VASP interferes with lamellipodium architecture, motility and integrin-dependent adhesion. Elife 9, e55351. https://doi.org/10.7554/eLife.55351

D'Amore, C., Borgo, C., Sarno, S., Salvi, M., 2020. Role of CK2 inhibitor CX-4945 in anti-cancer combination therapy – potential clinical relevance. Cell Oncol (Dordr) 43, 1003–1016. https://doi.org/10.1007/s13402-020-00566-w

D'Amore, C., Salizzato, V., Borgo, C., Cesaro, L., Pinna, L.A., Salvi, M., 2019. A Journey through the Cytoskeleton with Protein Kinase CK2. Curr Protein Pept Sci 20, 547–562. https://doi.org/10.2174/1389203720666190119124846

de Hostos, E.L., Bradtke, B., Lottspeich, F., Guggenheim, R., Gerisch, G., 1991. Coronin, an actin binding protein of Dictyostelium discoideum localized to cell surface projections, has sequence similarities to G protein beta subunits. The EMBO Journal 10, 4097–4104. https://doi.org/10.1002/j.1460-2075.1991.tb04986.x

De La Cruz, E.M., 2005. Cofilin binding to muscle and non-muscle actin filaments: isoform-dependent cooperative interactions. J Mol Biol 346, 557–564. https://doi.org/10.1016/j.jmb.2004.11.065

De La Cruz, E.M., Gardel, M.L., 2015. Actin Mechanics and Fragmentation*. Journal of Biological Chemistry 290, 17137–17144. https://doi.org/10.1074/jbc.R115.636472

De La Cruz, E.M., Roland, J., McCullough, B.R., Blanchoin, L., Martiel, J.-L., 2010. Origin of Twist-Bend Coupling in Actin Filaments. Biophysical Journal 99, 1852–1860. https://doi.org/10.1016/j.bpj.2010.07.009

Derry, J.M., Ochs, H.D., Francke, U., 1994. Isolation of a novel gene mutated in Wiskott-Aldrich syndrome. Cell 78, 635–644. https://doi.org/10.1016/0092-8674(94)90528-2

Disanza, A., Carlier, M.-F., Stradal, T.E.B., Didry, D., Frittoli, E., Confalonieri, S., Croce, A., Wehland, J., Di Fiore, P.P., Scita, G., 2004. Eps8 controls actin-based motility by capping the barbed ends of actin filaments. Nat Cell Biol 6, 1180–1188. https://doi.org/10.1038/ncb1199

Disanza, A., Mantoani, S., Hertzog, M., Gerboth, S., Frittoli, E., Steffen, A., Berhoerster, K., Kreienkamp, H.-J., Milanesi, F., Di Fiore, P.P., Ciliberto, A., Stradal, T.E.B., Scita, G., 2006. Regulation of cell shape by Cdc42 is mediated by the synergic actin-bundling activity of the Eps8-IRSp53 complex. Nat Cell Biol 8, 1337–1347. https://doi.org/10.1038/ncb1502

Doi, Y., Banba, M., Vertut-Doi, A., 1991. Cysteine-374 of actin resides at the gelsolin contact site in the EGTA-resistant actin-gelsolin complex. Biochemistry 30, 5769–5777. https://doi.org/10.1021/bi00237a020

Dominguez, R., Holmes, K.C., 2011. Actin Structure and Function. Annual Review of Biophysics 40, 169–186. https://doi.org/10.1146/annurev-biophys-042910-155359

Drubin, D.G., Miller, K.G., Botstein, D., 1988. Yeast actin-binding proteins: evidence for a role in morphogenesis. J Cell Biol 107, 2551–2561. https://doi.org/10.1083/jcb.107.6.2551

Dugina, V., Zwaenepoel, I., Gabbiani, G., Clément, S., Chaponnier, C., 2009. Beta and gamma-cytoplasmic actins display distinct distribution and functional diversity. J Cell Sci 122, 2980–2988. https://doi.org/10.1242/jcs.041970

Eckstein, F., 1970. Nucleoside phosphorothioates. J. Am. Chem. Soc. 92, 4718–4723. https://doi.org/10.1021/ja00718a039

Eden, S., Rohatgi, R., Podtelejnikov, A.V., Mann, M., Kirschner, M.W., 2002. Mechanism of regulation of WAVE1-induced actin nucleation by Rac1 and Nck. Nature 418, 790–793. https://doi.org/10.1038/nature00859

Edwards, M., McConnell, P., Schafer, D.A., Cooper, J.A., 2015. CPI motif interaction is necessary for capping protein function in cells. Nat Commun 6, 8415. https://doi.org/10.1038/ncomms9415

Edwards, M., Zwolak, A., Schafer, D.A., Sept, D., Dominguez, R., Cooper, J.A., 2014. Capping protein regulators fine-tune actin assembly dynamics. Nat Rev Mol Cell Biol 15, 677–689. https://doi.org/10.1038/nrm3869

Evangelista, M., Pruyne, D., Amberg, D.C., Boone, C., Bretscher, A., 2002. Formins direct Arp2/3-independent actin filament assembly to polarize cell growth in yeast. Nat Cell Biol 4, 32–41. https://doi.org/10.1038/ncb718

Faix, J., Rottner, K., 2022. Ena/VASP proteins in cell edge protrusion, migration and adhesion. J Cell Sci 135, jcs259226. https://doi.org/10.1242/jcs.259226

Fares, J., Fares, M.Y., Khachfe, H.H., Salhab, H.A., Fares, Y., 2020. Molecular principles of metastasis: a hallmark of cancer revisited. Signal Transduct Target Ther 5, 28. https://doi.org/10.1038/s41392-020-0134-x

Fazioli, F., Minichiello, L., Matoska, V., Castagnino, P., Miki, T., Wong, W.T., Di Fiore, P.P., 1993. Eps8, a substrate for the epidermal growth factor receptor kinase, enhances EGF-dependent mitogenic signals. The EMBO Journal 12, 3799–3808. https://doi.org/10.1002/j.1460-2075.1993.tb06058.x

Feng, S., Chen, J.K., Yu, H., Simon, J.A., Schreiber, S.L., 1994. Two binding orientations for peptides to the Src SH3 domain: development of a general model for SH3-ligand interactions. Science 266, 1241–1247. https://doi.org/10.1126/science.7526465

Ferlay, J., Colombet, M., Soerjomataram, I., Parkin, D.M., Piñeros, M., Znaor, A., Bray, F., 2021. Cancer statistics for the year 2020: An overview. Int J Cancer. https://doi.org/10.1002/ijc.33588

Ferron, F., Rebowski, G., Lee, S.H., Dominguez, R., 2007. Structural basis for the recruitment of profilin–actin complexes during filament elongation by Ena/VASP. The EMBO Journal 26, 4597–4606. https://doi.org/10.1038/sj.emboj.7601874

Forero, C., Wasserman, M., 2000. Isolation and identification of actin-binding proteins in Plasmodium falciparum by affinity chromatography. Mem Inst Oswaldo Cruz 95, 329–337. https://doi.org/10.1590/s0074-02762000000300007

Fujii, T., Iwane, A.H., Yanagida, T., Namba, K., 2010. Direct visualization of secondary structures of F-actin by electron cryomicroscopy. Nature 467, 724–728. https://doi.org/10.1038/nature09372

Fujiwara, I., Zweifel, M.E., Courtemanche, N., Pollard, T.D., 2018. Latrunculin A Accelerates Actin Filament Depolymerization in Addition to Sequestering Actin Monomers. Curr Biol 28, 3183-3192.e2. https://doi.org/10.1016/j.cub.2018.07.082

Funato, Y., Terabayashi, T., Suenaga, N., Seiki, M., Takenawa, T., Miki, H., 2004. IRSp53/Eps8 Complex Is Important for Positive Regulation of Rac and Cancer Cell Motility/Invasiveness. Cancer Research 64, 5237–5244. https://doi.org/10.1158/0008-5472.CAN-04-0327

Gandhi, M., Achard, V., Blanchoin, L., Goode, B.L., 2009. Coronin switches roles in actin disassembly depending on the nucleotide state of actin. Mol Cell 34, 364–374. https://doi.org/10.1016/j.molcel.2009.02.029

Garrett, M.D., Self, A.J., van Oers, C., Hall, A., 1989. Identification of distinct cytoplasmic targets for ras/R-ras and rho regulatory proteins. J Biol Chem 264, 10–13.

Goldschmidt-Clermont, P.J., Furman, M.I., Wachsstock, D., Safer, D., Nachmias, V.T., Pollard, T.D., 1992. The control of actin nucleotide exchange by thymosin beta 4 and profilin. A potential regulatory mechanism for actin polymerization in cells. Mol Biol Cell 3, 1015–1024. https://doi.org/10.1091/mbc.3.9.1015

Goode, B.L., Wong, J.J., Butty, A.-C., Peter, M., McCormack, A.L., Yates, J.R., Drubin, D.G., Barnes, G., 1999. Coronin Promotes the Rapid Assembly and Cross-linking of Actin Filaments and May Link the Actin and Microtubule Cytoskeletons in Yeast. Journal of Cell Biology 144, 83–98. https://doi.org/10.1083/jcb.144.1.83

Goodson, H.V., Jonasson, E.M., 2018. Microtubules and Microtubule-Associated Proteins. Cold Spring Harb Perspect Biol 10, a022608. https://doi.org/10.1101/cshperspect.a022608

Goody, R.S., Eckstein, F., 1971. Thiophosphate analogs of nucleoside di- and triphosphates. J. Am. Chem. Soc. 93, 6252–6257. https://doi.org/10.1021/ja00752a042

Hanahan, D., 2022. Hallmarks of Cancer: New Dimensions. Cancer Discovery 12, 31–46. https://doi.org/10.1158/2159-8290.CD-21-1059

Hanahan, D., Weinberg, R.A., 2011. Hallmarks of Cancer: The Next Generation. Cell 144, 646–674. https://doi.org/10.1016/j.cell.2011.02.013

Hanahan, D., Weinberg, R.A., 2000. The hallmarks of cancer. Cell 100, 57–70. https://doi.org/10.1016/s0092-8674(00)81683-9

Hart, M.J., Eva, A., Evans, T., Aaronson, S.A., Cerione, R.A., 1991. Catalysis of guanine nucleotide exchange on the CDC42Hs protein by the dbl oncogene product. Nature 354, 311–314. https://doi.org/10.1038/354311a0

Hart, M.J., Eva, A., Zangrilli, D., Aaronson, S.A., Evans, T., Cerione, R.A., Zheng, Y., 1994. Cellular transformation and guanine nucleotide exchange activity are catalyzed by a common domain on the dbl oncogene product. J Biol Chem 269, 62–65.

Hatanaka, H., Ogura, K., Moriyama, K., Ichikawa, S., Yahara, I., Inagaki, F., 1996. Tertiary Structure of Destrin and Structural Similarity between Two Actin-Regulating Protein Families. Cell 85, 1047–1055. https://doi.org/10.1016/S0092-8674(00)81305-7

Hayden, S.M., Miller, P.S., Brauweiler, A., Bamburg, J.R., 1993. Analysis of the interactions of actin depolymerizing factor with G- and F-actin. Biochemistry 32, 9994–10004. https://doi.org/10.1021/bi00089a015

Herman, I.M., 1993. Actin isoforms. Curr Opin Cell Biol 5, 48–55. https://doi.org/10.1016/s0955-0674(05)80007-9

Hernandez-Valladares, M., Kim, T., Kannan, B., Tung, A., Aguda, A.H., Larsson, M., Cooper, J.A., Robinson, R.C., 2010. Structural characterization of a capping protein interaction motif defines a family of actin filament regulators. Nat Struct Mol Biol 17, 497–503. https://doi.org/10.1038/nsmb.1792

Herrmann, H., Aebi, U., 2016. Intermediate Filaments: Structure and Assembly. Cold Spring Harb Perspect Biol 8, a018242. https://doi.org/10.1101/cshperspect.a018242

Hertzog, M., Milanesi, F., Hazelwood, L., Disanza, A., Liu, H., Perlade, E., Malabarba, M.G., Pasqualato, S., Maiolica, A., Confalonieri, S., Clainche, C.L., Offenhauser, N., Block, J., Rottner, K., Fiore, P.P.D., Carlier, M.-F., Volkmann, N., Hanein, D., Scita, G., 2010. Molecular Basis for the Dual Function of Eps8 on Actin Dynamics: Bundling and Capping. PLOS Biology 8, e1000387. https://doi.org/10.1371/journal.pbio.1000387

Hocky, G.M., Sindelar, C.V., Cao, W., Voth, G.A., Cruz, E.M.D.L., 2021. Structural basis of fast- and slow-severing actin–cofilactin boundaries. Journal of Biological Chemistry 296. https://doi.org/10.1016/j.jbc.2021.100337

Holmes, K.C., Popp, D., Gebhard, W., Kabsch, W., 1990. Atomic model of the actin filament. Nature 347, 44–49. https://doi.org/10.1038/347044a0

Hoock, T.C., Newcomb, P.M., Herman, I.M., 1991. Beta actin and its mRNA are localized at the plasma membrane and the regions of moving cytoplasm during the cellular response to injury. J Cell Biol 112, 653–664. https://doi.org/10.1083/jcb.112.4.653

Hu, S., Brady, S.R., Kovar, D.R., Staiger, C.J., Clark, G.B., Roux, S.J., Muday, G.K., 2000. Identification of plant actin-binding proteins by F-actin affinity chromatography. The Plant Journal 24, 127–137. https://doi.org/10.1046/j.1365-313x.2000.00852.x

Huehn, A.R., Bibeau, J.P., Schramm, A.C., Cao, W., De La Cruz, E.M., Sindelar, C.V., 2020. Structures of cofilin-induced structural changes reveal local and asymmetric perturbations of actin filaments. Proc. Natl. Acad. Sci. U.S.A. 117, 1478–1484. https://doi.org/10.1073/pnas.1915987117

Humphries, C.L., Balcer, H.I., D'Agostino, J.L., Winsor, B., Drubin, D.G., Barnes, G., Andrews, B.J., Goode, B.L., 2002. Direct regulation of Arp2/3 complex activity and function by the actin binding protein coronin. Journal of Cell Biology 159, 993–1004. https://doi.org/10.1083/jcb.200206113

Im, H., 2011. The Inoue Method for Preparation and Transformation of Competent *E. coli*: "Ultra Competent" Cells. *Bio-101*: e143. DOI: 10.21769/BioProtoc.143.

Isambert, H., Venier, P., Maggs, A.C., Fattoum, A., Kassab, R., Pantaloni, D., Carlier, M.F., 1995. Flexibility of actin filaments derived from thermal fluctuations. Effect of bound nucleotide, phalloidin, and muscle regulatory proteins. J Biol Chem 270, 11437–11444. https://doi.org/10.1074/jbc.270.19.11437

Isenberg, G., Aebi, U., Pollard, T.D., 1980. An actin-binding protein from Acanthamoeba regulates actin filament polymerization and interactions. Nature 288, 455–459. https://doi.org/10.1038/288455a0

Iskratsch, T., Lange, S., Dwyer, J., Kho, A.L., dos Remedios, C., Ehler, E., 2010. Formin follows function: a muscle-specific isoform of FHOD3 is regulated by CK2 phosphorylation and promotes myofibril maintenance. J Cell Biol 191, 1159–1172. https://doi.org/10.1083/jcb.201005060

Ismail, A.M., Padrick, S.B., Chen, B., Umetani, J., Rosen, M.K., 2009. The WAVE regulatory complex is inhibited. Nat Struct Mol Biol 16, 561–563. https://doi.org/10.1038/nsmb.1587

Janmey, P.A., Stossel, T.P., 1987a. Modulation of gelsolin function by phosphatidylinositol 4,5-bisphosphate. Nature 325, 362–364. https://doi.org/10.1038/325362a0

Kabsch, W., Mannherz, H.G., Suck, D., Pai, E.F., Holmes, K.C., 1990. Atomic structure of the actin: DNase I complex. Nature 347, 37–44. https://doi.org/10.1038/347037a0

Kage, F., Winterhoff, M., Dimchev, V., Mueller, J., Thalheim, T., Freise, A., Brühmann, S., Kollasser, J., Block, J., Dimchev, G., Geyer, M., Schnittler, H.-J., Brakebusch, C., Stradal, T.E.B., Carlier, M.-F., Sixt, M., Käs, J., Faix, J., Rottner, K., 2017. FMNL formins boost lamellipodial force generation. Nat Commun 8, 14832. https://doi.org/10.1038/ncomms14832

Kanematsu, Y., Narita, A., Oda, T., Koike, R., Ota, M., Takano, Y., Moritsugu, K., Fujiwara, I., Tanaka, K., Komatsu, H., Nagae, T., Watanabe, N., Iwasa, M., Maéda, Y., Takeda, S., 2022. Structures and mechanisms of actin ATP hydrolysis. Proc Natl Acad Sci U S A 119, e2122641119. https://doi.org/10.1073/pnas.2122641119

Karlsson, T., Songyang, Z., Landgren, E., Lavergne, C., Di Fiore, P.P., Anafi, M., Pawson, T., Cantley, L.C., Claesson-Welsh, L., Welsh, M., 1995. Molecular interactions of the Src homology 2 domain protein Shb with phosphotyrosine residues, tyrosine kinase receptors and Src homology 3 domain proteins. Oncogene 10, 1475–1483.

Katagiri, K., Matsuura, S., 1971. Antitumor activity of cytochalasin D. J Antibiot (Tokyo) 24, 722–723. https://doi.org/10.7164/antibiotics.24.722

Kelleher, J.F., Atkinson, S.J., Pollard, T.D., 1995. Sequences, structural models, and cellular localization of the actin-related proteins Arp2 and Arp3 from Acanthamoeba. J Cell Biol 131, 385–397. https://doi.org/10.1083/jcb.131.2.385

Khanday, F.A., Santhanam, L., Kasuno, K., Yamamori, T., Naqvi, A., Dericco, J., Bugayenko, A., Mattagajasingh, I., Disanza, A., Scita, G., Irani, K., 2006. Sos-mediated activation of rac1 by p66shc. J Cell Biol 172, 817–822. https://doi.org/10.1083/jcb.200506001

Korenbaum, E., Nordberg, P., Björkegren-Sjögren, C., Schutt, C.E., Lindberg, U., Karlsson, R., 1998. The role of profilin in actin polymerization and nucleotide exchange. Biochemistry 37, 9274–9283. https://doi.org/10.1021/bi9803675

Korlach, J., Baird, D.W., Heikal, A.A., Gee, K.R., Hoffman, G.R., Webb, W.W., 2004. Spontaneous nucleotide exchange in low molecular weight GTPases by fluorescently labeled gamma-phosphate-linked GTP analogs. Proc Natl Acad Sci U S A 101, 2800–2805. https://doi.org/10.1073/pnas.0308579100

Korn, E.D., Carlier, M.F., Pantaloni, D., 1987. Actin polymerization and ATP hydrolysis. Science 238, 638–644. https://doi.org/10.1126/science.3672117

Kraynov, V.S., Chamberlain, C., Bokoch, G.M., Schwartz, M.A., Slabaugh, S., Hahn, K.M., 2000. Localized Rac Activation Dynamics Visualized in Living Cells. Science 290, 333–337. https://doi.org/10.1126/science.290.5490.333

Krebs, A., Rothkegel, M., Klar, M., Jockusch, B.M., 2001. Characterization of functional domains of mDia1, a link between the small GTPase Rho and the actin cytoskeleton. Journal of Cell Science 114, 3663–3672. https://doi.org/10.1242/jcs.114.20.3663

Kreider-Letterman, G., Castillo, A., Mahlandt, E.K., Goedhart, J., Rabino, A., Goicoechea, S., Garcia-Mata, R., 2023. ARHGAP17 regulates the spatiotemporal activity of Cdc42 at invadopodia. J Cell Biol 222, e202207020. https://doi.org/10.1083/jcb.202207020

Kudryashov, D.S., Reisler, E., 2013. ATP and ADP actin states. Biopolymers 99, 245–256. https://doi.org/10.1002/bip.22155

Kurochkina, N., Guha, U., 2012. SH3 domains: modules of protein–protein interactions. Biophys Rev 5, 29–39. https://doi.org/10.1007/s12551-012-0081-z

Lamarche, N., Hall, A., 1994. GAPs for rho-related GTPases. Trends in Genetics 10, 436–440. https://doi.org/10.1016/0168-9525(94)90114-7

Lambert, A.W., Pattabiraman, D.R., Weinberg, R.A., 2017a. Emerging Biological Principles of Metastasis. Cell 168, 670–691. https://doi.org/10.1016/j.cell.2016.11.037

Lawson, C.D., Ridley, A.J., 2018. Rho GTPase signaling complexes in cell migration and invasion. J Cell Biol 217, 447–457. https://doi.org/10.1083/jcb.201612069

Lee, S.H., Eom, M., Lee, S.J., Kim, S., Park, H.J., Park, D., 2001. BetaPix-enhanced p38 activation by Cdc42/Rac/PAK/MKK3/6-mediated pathway. Implication in the regulation of membrane ruffling. J Biol Chem 276, 25066–25072. https://doi.org/10.1074/jbc.M010892200

Lettieri, A., Borgo, C., Zanieri, L., D'Amore, C., Oleari, R., Paganoni, A., Pinna, L.A., Cariboni, A., Salvi, M., 2019. Protein Kinase CK2 Subunits Differentially Perturb the Adhesion and Migration of GN11 Cells: A Model of Immature Migrating Neurons. Int J Mol Sci 20, 5951. https://doi.org/10.3390/ijms20235951

Levitsky, D.I., Pivovarova, A.V., Mikhailova, V.V., Nikolaeva, O.P., 2008. Thermal unfolding and aggregation of actin. The FEBS Journal 275, 4280–4295. https://doi.org/10.1111/j.1742-4658.2008.06569.x

Liepiņa, I., Czaplewski, C., Janmey, P., Liwo, A., 2003. Molecular dynamics study of a gelsolin-derived peptide binding to a lipid bilayer containing phosphatidylinositol 4,5-bisphosphate. Biopolymers 71, 49–70. https://doi.org/10.1002/bip.10375

Liu, X., Gao, Y., Lin, X., Li, L., Han, X., Liu, J., 2016. The Coronin Family and Human Disease. Curr Protein Pept Sci 17, 603–611. https://doi.org/10.2174/1389203717666151201192011

Löw, I., Dancker, P., 1976. Effect of cytochalasin B on formation and properties of muscle F-actin. Biochimica et Biophysica Acta (BBA) - Bioenergetics 430, 366–374. https://doi.org/10.1016/0005-2728(76)90092-X

Löw, I., Wieland, Th., 1974. The interaction of phalloidin, some of its derivatives, and of other cyclic peptides with muscle actin as studied by viscosimetry. FEBS Letters 44, 340–343. https://doi.org/10.1016/0014-5793(74)81173-7

Luna, E.J., Wang, Y.L., Voss, E.W., Branton, D., Taylor, D.L., 1982. A stable, high capacity, F-actin affinity column. J Biol Chem 257, 13095–13100.

Machacek, M., Hodgson, L., Welch, C., Elliott, H., Pertz, O., Nalbant, P., Abell, A., Johnson, G.L., Hahn, K.M., Danuser, G., 2009. Coordination of Rho GTPase activities during cell protrusion. Nature 461, 99–103. https://doi.org/10.1038/nature08242

Machesky, L.M., Atkinson, S.J., Ampe, C., Vandekerckhove, J., Pollard, T.D., 1994. Purification of a cortical complex containing two unconventional actins from Acanthamoeba by affinity chromatography on profilin-agarose. J Cell Biol 127, 107–115. https://doi.org/10.1083/jcb.127.1.107

Machesky, L.M., Insall, R.H., 1998. Scar1 and the related Wiskott–Aldrich syndrome protein, WASP, regulate the actin cytoskeleton through the Arp2/3 complex. Current Biology 8, 1347–1356. https://doi.org/10.1016/S0960-9822(98)00015-3

Machesky, L.M., Mullins, R.D., Higgs, H.N., Kaiser, D.A., Blanchoin, L., May, R.C., Hall, M.E., Pollard, T.D., 1999. Scar, a WASp-related protein, activates nucleation of actin filaments by the Arp2/3 complex. Proc Natl Acad Sci U S A 96, 3739–3744. https://doi.org/10.1073/pnas.96.7.3739

Maciver, S.K., Weeds, A.G., 1994. Actophorin preferentially binds monomeric ADP-actin over ATP-bound actin: consequences for cell locomotion. FEBS Lett 347, 251–256. https://doi.org/10.1016/0014-5793(94)00552-4

Maciver, S.K., Zot, H.G., Pollard, T.D., 1991. Characterization of actin filament severing by actophorin from Acanthamoeba castellanii. Journal of Cell Biology 115, 1611–1620. https://doi.org/10.1083/jcb.115.6.1611

Maiti, S., Michelot, A., Gould, C., Blanchoin, L., Sokolova, O., Goode, B.L., 2012. Structure and activity of full-length formin mDia1. Cytoskeleton (Hoboken) 69, 393–405. https://doi.org/10.1002/cm.21033

Manser, E., Loo, T.H., Koh, C.G., Zhao, Z.S., Chen, X.Q., Tan, L., Tan, I., Leung, T., Lim, L., 1998. PAK kinases are directly coupled to the PIX family of

nucleotide exchange factors. Mol Cell 1, 183–192. https://doi.org/10.1016/s1097-2765(00)80019-2

Marei, H., Malliri, A., 2017. GEFs: Dual regulation of Rac1 signaling. Small GTPases 8, 90–99. https://doi.org/10.1080/21541248.2016.1202635

Marschke, R.F., Borad, M.J., McFarland, R.W., Alvarez, R.H., Lim, J.K., Padgett, C.S., Von Hoff, D.D., O'Brien, S.E., Northfelt, D.W., 2011. Findings from the phase I clinical trials of CX-4945, an orally available inhibitor of CK2. JCO 29, 3087–3087. https://doi.org/10.1200/jco.2011.29.15_suppl.3087

Matoskova, B., Wong, W.T., Salcini, A.E., Pelicci, P.G., Fiore, P.P.D., 1995. Constitutive Phosphorylation of eps8 in Tumor Cell Lines: Relevance to Malignant Transformation. Molecular and Cellular Biology. https://doi.org/10.1128/MCB.15.7.3805

McGough, A., Pope, B., Chiu, W., Weeds, A., 1997. Cofilin changes the twist of F-actin: implications for actin filament dynamics and cellular function. J Cell Biol 138, 771–781. https://doi.org/10.1083/jcb.138.4.771

McLaughlin, P.J., Gooch, J.T., Mannherz, H.-G., Weeds, A.G., 1993. Structure of gelsolin segment 1-actin complex and the mechanism of filament severing. Nature 364, 685–692. https://doi.org/10.1038/364685a0

Merino, F., Pospich, S., Funk, J., Wagner, T., Küllmer, F., Arndt, H.-D., Bieling, P., Raunser, S., 2018. Structural transitions of F-actin upon ATP hydrolysis at near-atomic resolution revealed by cryo-EM. Nat Struct Mol Biol 25, 528–537. https://doi.org/10.1038/s41594-018-0074-0

Miki, H, Sasaki, T., Takai, Y., Takenawa, T., 1998. Induction of filopodium formation by a WASP-related actin-depolymerizing protein N-WASP. Nature 391, 93–96. https://doi.org/10.1038/34208

Miki, H., Suetsugu, S., Takenawa, T., 1998. WAVE, a novel WASP-family protein involved in actin reorganization induced by Rac. EMBO J 17, 6932–6941. https://doi.org/10.1093/emboj/17.23.6932

Miki, H., Yamaguchi, H., Suetsugu, S., Takenawa, T., 2000. IRSp53 is an essential intermediate between Rac and WAVE in the regulation of membrane ruffling. Nature 408, 732–735. https://doi.org/10.1038/35047107

Miller, K.G., Alberts, B.M., 1989. F-actin affinity chromatography: technique for isolating previously unidentified actin-binding proteins. Proc Natl Acad Sci U S A 86, 4808–4812.

Miller, K.G., Field, C.M., Alberts, B.M., 1989. Actin-binding proteins from Drosophila embryos: a complex network of interacting proteins detected by F-actin affinity chromatography. J Cell Biol 109, 2963–2975. https://doi.org/10.1083/jcb.109.6.2963

Mockrin, S.C., Korn, E.D., 1980. Acanthamoeba profilin interacts with G-actin to increase the rate of exchange of actin-bound adenosine 5'-triphosphate. Biochemistry 19, 5359–5362. https://doi.org/10.1021/bi00564a033

Mongioví, A.M., Romano, P.R., Panni, S., Mendoza, M., Wong, W.T., Musacchio, A., Cesareni, G., Paolo Di Fiore, P., 1999. A novel peptide–SH3 interaction. The EMBO Journal 18, 5300–5309. https://doi.org/10.1093/emboj/18.19.5300

Moore, P.B., Huxley, H.E., DeRosier, D.J., 1970. Three-dimensional reconstruction of F-actin, thin filaments and decorated thin filaments. J Mol Biol 50, 279–295. https://doi.org/10.1016/0022-2836(70)90192-0

Mounier, N., Sparrow, J.C., 1997. Structural comparisons of muscle and nonmuscle actins give insights into the evolution of their functional differences. J Mol Evol 44, 89–97. https://doi.org/10.1007/pl00006125

Mullins, R.D., Heuser, J.A., Pollard, T.D., 1998. The interaction of Arp2/3 complex with actin: nucleation, high affinity pointed end capping, and formation of branching networks of filaments. Proc Natl Acad Sci U S A 95, 6181–6186. https://doi.org/10.1073/pnas.95.11.6181

Mullins, R.D., Stafford, W.F., Pollard, T.D., 1997. Structure, subunit topology, and actin-binding activity of the Arp2/3 complex from Acanthamoeba. J Cell Biol 136, 331–343. https://doi.org/10.1083/jcb.136.2.331

Nag, S., Ma, Q., Wang, H., Chumnarnsilpa, S., Lee, W.L., Larsson, M., Kannan, B., Hernandez-Valladares, M., Burtnick, L.D., Robinson, R.C., 2009. Ca2+ binding by domain 2 plays a critical role in the activation and stabilization of gelsolin. Proc Natl Acad Sci U S A 106, 13713–13718. https://doi.org/10.1073/pnas.0812374106

Nakagawa, H., Miki, H., Ito, M., Ohashi, K., Takenawa, T., Miyamoto, S., 2001. N-WASP, WAVE and Mena play different roles in the organization of actin cytoskeleton in lamellipodia. J Cell Sci 114, 1555–1565. https://doi.org/10.1242/jcs.114.8.1555

Nakagawa, H., Miki, H., Nozumi, M., Takenawa, T., Miyamoto, S., Wehland, J., Small, J.V., 2003. IRSp53 is colocalised with WAVE2 at the tips of protruding lamellipodia and filopodia independently of Mena. Journal of Cell Science 116, 2577–2583. https://doi.org/10.1242/jcs.00462

Nalbant, P., Hodgson, L., Kraynov, V., Toutchkine, A., Hahn, K.M., 2004. Activation of endogenous Cdc42 visualized in living cells. Science 305, 1615–1619. https://doi.org/10.1126/science.1100367

Namba, Y., Ito, M., Zu, Y., Shigesada, K., Maruyama, K., 1992. Human T cell L-plastin bundles actin filaments in a calcium-dependent manner. J Biochem 112, 503–507. https://doi.org/10.1093/oxfordjournals.jbchem.a123929

Newman, D.J., Cragg, G.M., 2004. Marine Natural Products and Related Compounds in Clinical and Advanced Preclinical Trials. J. Nat. Prod. 67, 1216–1238. https://doi.org/10.1021/np040031y

Nishida, E., Maekawa, S., Sakai, H., 1984. Cofilin, a protein in porcine brain that binds to actin filaments and inhibits their interactions with myosin and tropomyosin. Biochemistry 23, 5307–5313. https://doi.org/10.1021/bi00317a032

Nobes, C.D., Hall, A., 1995. Rho, Rac, and Cdc42 GTPases regulate the assembly of multimolecular focal complexes associated with actin stress fibers, lamellipodia, and filopodia. Cell 81, 53–62. https://doi.org/10.1016/0092-8674(95)90370-4

Oda, T., Iwasa, M., Aihara, T., Maéda, Y., Narita, A., 2009. The nature of the globular- to fibrous-actin transition. Nature 457, 441–445. https://doi.org/10.1038/nature07685

Offenhäuser, N., Borgonovo, A., Disanza, A., Romano, P., Ponzanelli, I., Iannolo, G., Di Fiore, P.P., Scita, G., 2004. The eps8 Family of Proteins Links Growth Factor Stimulation to Actin Reorganization Generating Functional Redundancy in the Ras/Rac Pathway. MBoC 15, 91–98. https://doi.org/10.1091/mbc.e03-06-0427

Ohta, Y., Kousaka, K., Nagata-Ohashi, K., Ohashi, K., Muramoto, A., Shima, Y., Niwa, R., Uemura, T., Mizuno, K., 2003. Differential activities, subcellular distribution and tissue expression patterns of three members of Slingshot family phosphatases that dephosphorylate cofilin. Genes Cells 8, 811–824. https://doi.org/10.1046/j.1365-2443.2003.00678.x

Oosterheert, W., Klink, B.U., Belyy, A., Pospich, S., Raunser, S., 2022. Structural basis of actin filament assembly and aging. Nature 611, 374–379. https://doi.org/10.1038/s41586-022-05241-8

Padrick, S.B., Doolittle, L.K., Brautigam, C.A., King, D.S., Rosen, M.K., 2011. Arp2/3 complex is bound and activated by two WASP proteins. Proceedings of the National Academy of Sciences 108, E472–E479. https://doi.org/10.1073/pnas.1100236108

Pantaloni, D., Carlier, M.F., 1993. How profilin promotes actin filament assembly in the presence of thymosin beta 4. Cell 75, 1007–1014. https://doi.org/10.1016/0092-8674(93)90544-z

Pantaloni, D., Carlier, M.F., Coué, M., Lal, A.A., Brenner, S.L., Korn, E.D., 1984. The critical concentration of actin in the presence of ATP increases with the number concentration of filaments and approaches the critical concentration of actin.ADP. J Biol Chem 259, 6274–6283.

Peck, J., Douglas, G., Wu, C.H., Burbelo, P.D., 2002. Human RhoGAP domain-containing proteins: structure, function and evolutionary relationships. FEBS Lett 528, 27–34. https://doi.org/10.1016/s0014-5793(02)03331-8

Pellegrin, S., Mellor, H., 2005. The Rho Family GTPase Rif Induces Filopodia through mDia2. Current Biology 15, 129–133. https://doi.org/10.1016/j.cub.2005.01.011

Perrin, B.J., Ervasti, J.M., 2010. The actin gene family: Function follows isoform. Cytoskeleton 67, 630–634. https://doi.org/10.1002/cm.20475

Pilla, C., Emanuelli, T., Frassetto, S.S., Battastini, A.M., Dias, R.D., Sarkis, J.J., 1996. ATP diphosphohydrolase activity (apyrase, EC 3.6.1.5) in human blood platelets. Platelets 7, 225–230. https://doi.org/10.3109/09537109609023582

Pollard, T.D., 1986. Rate constants for the reactions of ATP- and ADP-actin with the ends of actin filaments. J Cell Biol 103, 2747–2754.

Pollard, T.D., 2016. Actin and Actin-Binding Proteins. Cold Spring Harb Perspect Biol 8, a018226. https://doi.org/10.1101/cshperspect.a018226

Pollard, T.D., Blanchoin, L., Mullins, R.D., 2000. Molecular Mechanisms Controlling Actin Filament Dynamics in Nonmuscle Cells. Annual Review of Biophysics and Biomolecular Structure 29, 545–576. https://doi.org/10.1146/annurev.biophys.29.1.545

Pollard, T.D., Goldman, R.D., 2018. Overview of the Cytoskeleton from an Evolutionary Perspective. Cold Spring Harb Perspect Biol 10, a030288. https://doi.org/10.1101/cshperspect.a030288

Pollard, T.D., Weeds, A.G., 1984. The rate constant for ATP hydrolysis by polymerized actin. FEBS Lett 170, 94–98. https://doi.org/10.1016/0014-5793(84)81376-9

Pospich, S., Merino, F., Raunser, S., 2020. Structural Effects and Functional Implications of Phalloidin and Jasplakinolide Binding to Actin Filaments. Structure 28, 437-449.e5. https://doi.org/10.1016/j.str.2020.01.014

Provenzano, C., Gallo, R., Carbone, R., Di Fiore, P.P., Falcone, G., Castellani, L., Alemà, S., 1998. Eps8, a Tyrosine Kinase Substrate, Is Recruited to the Cell Cortex and Dynamic F-Actin upon Cytoskeleton Remodeling. Experimental Cell Research 242, 186–200. https://doi.org/10.1006/excr.1998.4095

Pruyne, D., Evangelista, M., Yang, C., Bi, E., Zigmond, S., Bretscher, A., Boone, C., 2002. Role of Formins in Actin Assembly: Nucleation and Barbed-End Association. Science 297, 612–615. https://doi.org/10.1126/science.1072309

Rappsilber, J., Mann, M., Ishihama, Y., 2007. Protocol for micro-purification, enrichment, pre-fractionation and storage of peptides for proteomics using StageTips. Nat Protoc 2, 1896–1906. https://doi.org/10.1038/nprot.2007.261

Raudenská, M., Petrláková, K., Juriňáková, T., Leischner Fialová, J., Fojtů, M., Jakubek, M., Rösel, D., Brábek, J., Masařík, M., 2023. Engine shutdown:

migrastatic strategies and prevention of metastases. Trends in Cancer 9, 293–308. https://doi.org/10.1016/j.trecan.2023.01.001

Ren, R., Mayer, B.J., Cicchetti, P., Baltimore, D., 1993. Identification of a ten-amino acid proline-rich SH3 binding site. Science 259, 1157–1161. https://doi.org/10.1126/science.8438166

Reynolds, M.J., Hachicho, C., Carl, A.G., Gong, R., Alushin, G.M., 2022. Bending forces and nucleotide state jointly regulate F-actin structure. Nature 611, 380–386. https://doi.org/10.1038/s41586-022-05366-w

Richnau, N., Aspenström, P., 2001. RICH, a Rho GTPase-activating Protein Domain-containing Protein Involved in Signaling by Cdc42 and Rac1*. Journal of Biological Chemistry 276, 35060–35070. https://doi.org/10.1074/jbc.M103540200

Ridley, A.J., Comoglio, P.M., Hall, A., 1995. Regulation of scatter factor/hepatocyte growth factor responses by Ras, Rac, and Rho in MDCK cells. Mol Cell Biol 15, 1110–1122. https://doi.org/10.1128/MCB.15.2.1110

Ridley, A.J., Paterson, H.F., Johnston, C.L., Diekmann, D., Hall, A., 1992. The small GTP-binding protein rac regulates growth factor-induced membrane ruffling. Cell 70, 401–410. https://doi.org/10.1016/0092-8674(92)90164-8

Robinson, R.C., Mejillano, M., Le, V.P., Burtnick, L.D., Yin, H.L., Choe, S., 1999. Domain Movement in Gelsolin: A Calcium-Activated Switch. Science 286, 1939–1942. https://doi.org/10.1126/science.286.5446.1939

Robinson, R.C., Turbedsky, K., Kaiser, D.A., Marchand, J.-B., Higgs, H.N., Choe, S., Pollard, T.D., 2001. Crystal Structure of Arp2/3 Complex. Science 294, 1679–1684. https://doi.org/10.1126/science.1066333

Roffers-Agarwal, J., Xanthos, J.B., Miller, J.R., 2005. Regulation of actin cytoskeleton architecture by Eps8 and Abi1. BMC Cell Biol 6, 36. https://doi.org/10.1186/1471-2121-6-36

Rottner, K., Schaks, M., 2019. Assembling actin filaments for protrusion. Current Opinion in Cell Biology, Cell Architecture 56, 53–63. https://doi.org/10.1016/j.ceb.2018.09.004

Rould, M.A., Wan, Q., Joel, P.B., Lowey, S., Trybus, K.M., 2006. Crystal structures of expressed non-polymerizable monomeric actin in the ADP and ATP states. J Biol Chem 281, 31909–31919. https://doi.org/10.1074/jbc.M601973200

Schafer, D.A., Jennings, P.B., Cooper, J.A., 1996. Dynamics of capping protein and actin assembly in vitro: uncapping barbed ends by polyphosphoinositides. J Cell Biol 135, 169–179. https://doi.org/10.1083/jcb.135.1.169

Schirenbeck, A., Bretschneider, T., Arasada, R., Schleicher, M., Faix, J., 2005. The Diaphanous-related formin dDia2 is required for the formation and

maintenance of filopodia. Nat Cell Biol 7, 619–625. https://doi.org/10.1038/ncb1266

Schramm, A.C., Hocky, G.M., Voth, G.A., Blanchoin, L., Martiel, J.-L., De La Cruz, E.M., 2017. Actin Filament Strain Promotes Severing and Cofilin Dissociation. Biophys J 112, 2624–2633. https://doi.org/10.1016/j.bpj.2017.05.016

Schutt, C.E., Myslik, J.C., Rozycki, M.D., Goonesekere, N.C.W., Lindberg, U., 1993. The structure of crystalline profilin-ß-actin. Nature 365, 810–816. https://doi.org/10.1038/365810a0

Scita, G., Confalonieri, S., Lappalainen, P., Suetsugu, S., 2008. IRSp53: crossing the road of membrane and actin dynamics in the formation of membrane protrusions. Trends in Cell Biology 18, 52–60. https://doi.org/10.1016/j.tcb.2007.12.002

Scita, G., Nordstrom, J., Carbone, R., Tenca, P., Giardina, G., Gutkind, S., Bjarnegård, M., Betsholtz, C., Di Fiore, P.P., 1999. EPS8 and E3B1 transduce signals from Ras to Rac. Nature 401, 290–293. https://doi.org/10.1038/45822

Scita, G., Tenca, P., Areces, L.B., Tocchetti, A., Frittoli, E., Giardina, G., Ponzanelli, I., Sini, P., Innocenti, M., Di Fiore, P.P., 2001. An effector region in Eps8 is responsible for the activation of the Rac-specific GEF activity of Sos-1 and for the proper localization of the Rac-based actin-polymerizing machine. Journal of Cell Biology 154, 1031–1044. https://doi.org/10.1083/jcb.200103146

Selden, L.A., Kinosian, H.J., Estes, J.E., Gershman, L.C., 1999. Impact of Profilin on Actin-Bound Nucleotide Exchange and Actin Polymerization Dynamics,. Biochemistry 38, 2769–2778. https://doi.org/10.1021/bi981543c

Selden, L.A., Kinosian, H.J., Newman, J., Lincoln, B., Hurwitz, C., Gershman, L.C., Estes, J.E., 1998. Severing of F-actin by the amino-terminal half of gelsolin suggests internal cooperativity in gelsolin. Biophys J 75, 3092–3100. https://doi.org/10.1016/S0006-3495(98)77750-1

Shestakova, E.A., Singer, R.H., Condeelis, J., 2001. The physiological significance of ß-actin mRNA localization in determining cell polarity and directional motility. Proceedings of the National Academy of Sciences 98, 7045–7050. https://doi.org/10.1073/pnas.121146098

Spector, I., Shochet, N.R., Kashman, Y., Groweiss, A., 1983. Latrunculins: Novel Marine Toxins That Disrupt Microfilament Organization in Cultured Cells. Science 219, 493–495. https://doi.org/10.1126/science.6681676

Stehn, J.R., Haass, N.K., Bonello, T., Desouza, M., Kottyan, G., Treutlein, H., Zeng, J., Nascimento, P.R.B.B., Sequeira, V.B., Butler, T.L., Allanson, M., Fath, T., Hill, T.A., McCluskey, A., Schevzov, G., Palmer, S.J., Hardeman, E.C., Winlaw, D., Reeve, V.E., Dixon, I., Weninger, W., Cripe, T.P., Gunning, P.W.,

2013. A Novel Class of Anticancer Compounds Targets the Actin Cytoskeleton in Tumor Cells. Cancer Research 73, 5169–5182. https://doi.org/10.1158/0008-5472.CAN-12-4501

Stehn, J.R., Schevzov, G., O'Neill, G.M., Gunning, P.W., 2006. Specialisation of the Tropomyosin Composition of Actin Filaments Provides New Potential Targets for Chemotherapy. Current Cancer Drug Targets 6, 245–256.

Straub, F.B., Feuer, G., 1989. Adenosinetriphosphate. The functional group of actin. 1950. Biochim Biophys Acta 1000, 180–195.

Sun, H. Q., Yamamoto, M., Mejillano, M., Yin, H.L., 1999. Gelsolin, a multifunctional actin regulatory protein. J Biol Chem 274, 33179–33182. https://doi.org/10.1074/jbc.274.47.33179

Svitkina, T.M., Borisy, G.G., 1999. Arp2/3 Complex and Actin Depolymerizing Factor/Cofilin in Dendritic Organization and Treadmilling of Actin Filament Array in Lamellipodia. J Cell Biol 145, 1009–1026.

Tilney, L.G., Bonder, E.M., Coluccio, L.M., Mooseker, M.S., 1983. Actin from Thyone sperm assembles on only one end of an actin filament: a behavior regulated by profilin. Journal of Cell Biology 97, 112–124. https://doi.org/10.1083/jcb.97.1.112

Tyanova, S., Temu, T., Sinitcyn, P., Carlson, A., Hein, M.Y., Geiger, T., Mann, M., Cox, J., 2016. The Perseus computational platform for comprehensive analysis of (prote)omics data. Nat Methods 13, 731–740. https://doi.org/10.1038/nmeth.3901

Vandekerckhove, J., Weber, K., 1978. At least six different actins are expressed in a higher mammal: An analysis based on the amino acid sequence of the amino-terminal tryptic peptide. Journal of Molecular Biology 126, 783–802. https://doi.org/10.1016/0022-2836(78)90020-7

Veltman, D.M., Insall, R.H., 2010. WASP family proteins: their evolution and its physiological implications. Mol Biol Cell 21, 2880–2893. https://doi.org/10.1091/mbc.E10-04-0372

Volkmann, N., Derosier, D., Matsudaira, P., Hanein, D., 2001. An atomic model of actin filaments cross-linked by fimbrin and its implications for bundle assembly and function. Journal of Cell Biology 153, 947–956. https://doi.org/10.1083/jcb.153.5.947

Wang, H., Chumnarnsilpa, S., Loonchanta, A., Li, Q., Kuan, Y.-M., Robine, S., Larsson, M., Mihalek, I., Burtnick, L.D., Robinson, R.C., 2009. Helix Straightening as an Activation Mechanism in the Gelsolin Superfamily of Actin Regulatory Proteins. J Biol Chem 284, 21265–21269. https://doi.org/10.1074/jbc.M109.019760

Wang, Y., Stear, J.H., Swain, A., Xu, X., Bryce, N.S., Carnell, M., Alieva, I.B., Dugina, V.B., Cripe, T.P., Stehn, J., Hardeman, E.C., Gunning, P.W., 2020. Drug Targeting the Actin Cytoskeleton Potentiates the Cytotoxicity of Low Dose Vincristine by Abrogating Actin-Mediated Repair of Spindle Defects. Molecular Cancer Research 18, 1074–1087. https://doi.org/10.1158/1541-7786.MCR-19-1122

Watanabe, N., Madaule, P., Reid, T., Ishizaki, T., Watanabe, G., Kakizuka, A., Saito, Y., Nakao, K., Jockusch, B.M., Narumiya, S., 1997. p140mDia, a mammalian homolog of Drosophila diaphanous, is a target protein for Rho small GTPase and is a ligand for profilin. EMBO J 16, 3044–3056. https://doi.org/10.1093/emboj/16.11.3044

Wegner, A., 1976. Head to tail polymerization of actin. J Mol Biol 108, 139–150. https://doi.org/10.1016/s0022-2836(76)80100-3

Wegner, A., Engel, J., 1975. Kinetics of the cooperative association of actin to actin filaments. Biophys Chem 3, 215–225. https://doi.org/10.1016/0301-4622(75)80013-5

Wehland, J., Osborn, M., Weber, K., 1977. Phalloidin-induced actin polymerization in the cytoplasm of cultured cells interferes with cell locomotion and growth. Proc Natl Acad Sci U S A 74, 5613–5617. https://doi.org/10.1073/pnas.74.12.5613

Welch, M.D., Iwamatsu, A., Mitchison, T.J., 1997. Actin polymerization is induced by Arp2/3 protein complex at the surface of Listeria monocytogenes. Nature 385, 265–269. https://doi.org/10.1038/385265a0

Welch, M.D., Rosenblatt, J., Skoble, J., Portnoy, D.A., Mitchison, T.J., 1998. Interaction of human Arp2/3 complex and the Listeria monocytogenes ActA protein in actin filament nucleation. Science 281, 105–108. https://doi.org/10.1126/science.281.5373.105

Wioland, H., Guichard, B., Senju, Y., Myram, S., Lappalainen, P., Jégou, A., Romet-Lemonne, G., 2017. ADF/Cofilin Accelerates Actin Dynamics by Severing Filaments and Promoting Their Depolymerization at Both Ends. Curr Biol 27, 1956-1967.e7. https://doi.org/10.1016/j.cub.2017.05.048

Woodrum, D.T., Rich, S.A., Pollard, T.D., 1975. Evidence for biased bidirectional polymerization of actin filaments using heavy meromyosin prepared by an improved method. Journal of Cell Biology 67, 231–237. https://doi.org/10.1083/jcb.67.1.231

Wuestehube, L.J., Speicher, D.W., Shariff, A., Luna, E.J., 1991. F-actin affinity chromatography of detergent-solubilized plasma membranes: purification and initial characterization of ponticulin from Dictyostelium discoideum. Methods Enzymol 196, 47–65. https://doi.org/10.1016/0076-6879(91)96007-e

Xavier, C.-P., Rastetter, R.H., Blömacher, M., Stumpf, M., Himmel, M., Morgan, R.O., Fernandez, M.-P., Wang, C., Osman, A., Miyata, Y., Gjerset, R.A., Eichinger, L., Hofmann, A., Linder, S., Noegel, A.A., Clemen, C.S., 2012. Phosphorylation of CRN2 by CK2 regulates F-actin and Arp2/3 interaction and inhibits cell migration. Sci Rep 2, 241. https://doi.org/10.1038/srep00241

Yabroff, K.R., Wu, X.-C., Negoita, S., Stevens, J., Coyle, L., Zhao, J., Mumphrey, B.J., Jemal, A., Ward, K.C., 2022. Association of the COVID-19 Pandemic With Patterns of Statewide Cancer Services. J Natl Cancer Inst 114, 907–909. https://doi.org/10.1093/jnci/djab122

Yamagishi, A., Masuda, M., Ohki, T., Onishi, H., Mochizuki, N., 2004. A novel actin bundling/filopodium-forming domain conserved in insulin receptor tyrosine kinase substrate p53 and missing in metastasis protein. J Biol Chem 279, 14929–14936. https://doi.org/10.1074/jbc.M309408200

Yang, C., Czech, L., Gerboth, S., Kojima, S., Scita, G., Svitkina, T., 2007. Novel Roles of Formin mDia2 in Lamellipodia and Filopodia Formation in Motile Cells. PLoS Biol 5, e317. https://doi.org/10.1371/journal.pbio.0050317

Yin, H.L., Stossel, T.P., 1979. Control of cytoplasmic actin gel–sol transformation by gelsolin, a calcium-dependent regulatory protein. Nature 281, 583–586. https://doi.org/10.1038/281583a0

Zheng, Y., Hart, M.J., Shinjo, K., Evans, T., Bender, A., Cerione, R.A., 1993. Biochemical comparisons of the Saccharomyces cerevisiae Bem2 and Bem3 proteins. Delineation of a limit Cdc42 GTPase-activating protein domain. Journal of Biological Chemistry 268, 24629–24634. https://doi.org/10.1016/S0021-9258(19)74512-8

Zigmond, S.H., Evangelista, M., Boone, C., Yang, C., Dar, A.C., Sicheri, F., Forkey, J., Pring, M., 2003. Formin Leaky Cap Allows Elongation in the Presence of Tight Capping Proteins. Current Biology 13, 1820–1823. https://doi.org/10.1016/j.cub.2003.09.057

Zimmet, A., Van Eeuwen, T., Boczkowska, M., Rebowski, G., Murakami, K., Dominguez, R., 2020. Cryo-EM structure of NPF-bound human Arp2/3 complex and activation mechanism. Sci Adv 6, eaaz7651. https://doi.org/10.1126/sciadv.aaz7651

10 Appendices

Table 10-1 Mass spectrometry data from ADP-F-actin only

ADP-F-actin optimisation column			
Protein names	Gene names	Unique peptides	Intensity
Actin, alpha skeletal muscle;Actin, alpha cardiac muscle 1;Actin, gamma-enteric smooth muscle;Actin, aortic smooth muscle	ACTA1;ACTC1;ACTG2;ACTA2	5	2.01E+10
Actin, cytoplasmic 1;Actin, cytoplasmic 1, N-terminally processed	ACTB	2	2.87E+09
Alpha-actinin-4	ACTN4	22	1.56E+09
Filamin-A	FLNA	50	1.45E+09
Angiomotin	AMOT	17	7.88E+08
Protein phosphatase 1 regulatory subunit 12A	PPP1R12A	21	6.77E+08
Plastin-3	PLS3	15	6.43E+08
MARCKS-related protein	MARCKSL1	12	5.53E+08
Transforming protein RhoA;Rho-related GTP-binding protein RhoC	RHOA;RHOC	10	4.46E+08
Eukaryotic translation initiation factor 2 subunit 3;Putative eukaryotic translation initiation factor 2 subunit 3-like protein	EIF2S3;EIF2S3L	9	4.35E+08
Elongation factor 1-alpha 1;Putative elongation factor 1-	EEF1A1;EEF1A1P5;EEF1A2	8	3.91E+08

alpha-like 3;Elongation factor 1-alpha;Elongation factor 1-alpha 2			
EF-hand domain-containing protein D2	EFHD2	11	3.76E+08
Alpha-actinin-1	ACTN1	15	3.72E+08
Drebrin	DBN1	13	3.56E+08
Myristoylated alanine-rich C-kinase substrate	MARCKS	7	3.51E+08
Serine/threonine-protein phosphatase PP1-beta catalytic subunit;Serine/threonine-protein phosphatase;Serine/threonine-protein phosphatase PP1-gamma catalytic subunit;Serine/threonine-protein phosphatase PP1-alpha catalytic subunit	PPP1CB;PPP1CC;PPP1CA	9	3.2E+08
F-actin-capping protein subunit beta	CAPZB	12	3.06E+08
Cleavage and polyadenylation specificity factor subunit 5	NUDT21	5	2.46E+08
Proenkephalin-B;Alpha-neoendorphin;Beta-neoendorphin;Big dynorphin;Dynorphin A(1-17);Dynorphin A(1-13);Dynorphin A(1-8);Leu-enkephalin;Rimorphin;Leumorphin	PDYN	1	2.43E+08
Protein-tyrosine-phosphatase;Receptor-type tyrosine-protein phosphatase kappa	PTPRK	1	2.35E+08

Tumor protein D54	TPD52L2	4	2.19E+08
Developmentally-regulated GTP-binding protein 1	DRG1	9	2.12E+08
Kinesin-1 heavy chain	KIF5B	14	1.95E+08
Tubulin beta chain	TUBB	3	1.87E+08
Eukaryotic translation initiation factor 3 subunit B	EIF3B	6	1.87E+08
Eukaryotic translation initiation factor 3 subunit L	EIF3L	7	1.78E+08
Heat shock cognate 71 kDa protein	HSPA8	9	1.63E+08
Eukaryotic translation initiation factor 3 subunit I	EIF3I	7	1.63E+08
RuvB-like 1	RUVBL1	9	1.57E+08
Signal recognition particle subunit SRP72	SRP72	8	1.47E+08
Zinc finger protein 780B	ZNF780B	1	1.46E+08
POTE ankyrin domain family member J	POTEJ	1	1.43E+08
Histone-binding protein RBBP4	RBBP4	4	1.38E+08
Calmodulin	CALM2;CALM1	3	1.28E+08
Protein arginine N-methyltransferase 5;Protein arginine N-methyltransferase 5, N-terminally processed	PRMT5	7	1.28E+08
	PCDH18	1	1.19E+08
Eukaryotic translation initiation factor 2 subunit 1	EIF2S1	4	1.17E+08
Eukaryotic translation initiation factor 3 subunit G	EIF3G	6	1.12E+08

Importin subunit beta-1	KPNB1	8	1.09E+08
Splicing factor U2AF 65 kDa subunit	U2AF2	5	1.08E+08
Filamin-B	FLNB	8	1.07E+08
Eukaryotic translation initiation factor 4E type 2	EIF4E2	4	1.02E+08

Table 10-2 Mass spectrometry data – all significant hits from "JVM3 – ATPγS"

JVM3 - ATPγS								
Protein names	**Gene names**	**Student's T-test Difference JVM3 (ADP-ATPgS)**	**-Log Student's T-test p-value JVM3 (ADP-ATPgS)**	**Student's T-test Significant JVM3 (ADP-ATPgS)**	**Student's T-test Significant JVM3 (ADP-ATPgS) p-value only**	**Quantified at least 3 times in a group**	**Unique peptides**	**Intensity**
Thymidylate kinase	DTYMK	-7.93	4.89	+	+	+	15	1.66E+09
ATP-citrate synthase	ACLY	-7.72	3.70	+	+	+	31	3.11E+09
Coronin-1C;Coronin	CORO1C	-6.10	3.89	+	+	+	17	5.70E+09
F-actin-capping protein subunit alpha-2	CAPZA2	-5.78	2.41	+	+	+	12	4.99E+09
Glutathione peroxidase;Glutathione peroxidase 1	GPX1	-5.75	4.79	+	+	+	8	3.63E+08
Galectin-3;Galectin	LGALS3	-5.19	2.07	+	+	+	8	5.55E+09
Cysteine and glycine-rich protein 1	CSRP1	-5.10	3.20	+	+	+	8	9.93E+08

Brain-specific angiogenesis inhibitor 1-associated protein 2-like protein 1	BAIAP2L1	-5.09	3.72	+	+	+	10	4.78E+08
Tyrosine-protein kinase ABL1	ABL1	-4.90	2.91	+	+	+	15	6.08E+08
Caldesmon	CALD1	-4.89	3.37	+	+	+	23	2.05E+10
ATP-binding cassette sub-family F member 1	ABCF1	-4.69	2.85	+	+	+	9	3.88E+08
Cleavage stimulation factor subunit 1	CSTF1	-4.22	4.96	+	+	+	5	1.36E+08
Splicing factor 1	SF1	-4.47	1.35		+	+	12	2.17E+09
Fascin	FSCN1	-3.86	2.96		+	+	44	1.35E+11
Epidermal growth factor receptor kinase substrate 8	EPS8	-3.68	2.19		+	+	43	1.65E+10
SLIT-ROBO Rho GTPase-activating protein 2	SRGAP2	-3.60	2.94		+	+	49	1.71E+10
F-actin-capping protein subunit alpha-1	CAPZA1	-3.50	3.46		+	+	12	1.30E+10
Cytospin-B	SPECC1	-3.18	2.28		+	+	6	1.84E+08
Serine/threonine-protein phosphatase;Serine/threonine-protein phosphatase PP1-gamma catalytic subunit	PPP1CC	-2.79	1.33		+	+	3	7.41E+08
60S ribosomal protein L10a	RPL10A	-2.75	1.92		+	+	4	2.96E+08
General transcription factor II-I	GTF2I	-2.58	1.81		+	+	5	8.93E+07
Protein flightless-1 homolog	FLII	-2.54	1.91		+	+	21	1.06E+09
MAP/microtubule affinity-regulating kinase 3	MARK3	-2.28	1.69		+	+	3	5.74E+07
WD repeat-containing protein 1	WDR1	-2.12	1.33		+	+	14	1.58E+09
Vimentin	VIM	-2.10	1.58		+	+	16	1.95E+09

Microtubule-associated protein;Microtubule-associated protein 4	MAP4	-1.85	1.68		+	+	20	5.86E+08
Leucine-rich repeat flightless-interacting protein 1	LRRFIP1	-1.50	2.67		+	+	15	1.20E+09
Serine/threonine-protein phosphatase PP1-beta catalytic subunit;Serine/threonine-protein phosphatase	PPP1CB	-1.43	2.01		+	+	8	4.89E+09
Pre-mRNA-splicing factor RBM22	RBM22	-1.32	2.20		+	+	12	5.12E+08
Non-POU domain-containing octamer-binding protein	NONO	-1.31	1.48		+	+	10	9.61E+08
5-3 exoribonuclease 2	XRN2	-1.31	1.52		+	+	20	1.55E+09
A-kinase anchor protein 2	AKAP2	-1.16	1.64		+	+	36	2.00E+10
Tight junction protein ZO-2	TJP2	-1.03	1.74		+	+	63	4.07E+10
Serine/threonine-protein kinase MARK2	MARK2	-1.00	1.48		+	+	16	7.54E+08
Formin-like protein 1	FMNL1	-0.71	1.43		+	+	10	5.34E+08
T-complex protein 1 subunit beta	CCT2	-0.71	2.51		+	+	10	4.68E+08
LIM domain and actin-binding protein 1	LIMA1	-0.68	1.54		+	+	20	2.77E+09
Myotubularin	MTM1	-0.57	1.48		+	+	5	1.50E+08
Tropomyosin alpha-4 chain	TPM4	0.92	1.74		+	+	5	3.59E+09
Filamin-B	FLNB	1.24	1.78		+	+	127	3.83E+11
Kinesin-like protein KIF13B;Kinesin-like protein	KIF13B	2.27	1.82		+	+	3	3.34E+07

Chromosome transmission fidelity protein 8 homolog isoform 2	CHTF8	2.98	3.31		+	+	3	8.32E+07

Table 10-3 Mass spectrometry data – all significant hits from "PDAC – ATPγS"

PDAC - ATPγS								
Protein names	**Gene names**	**Student's T-test Difference PDAC2 (ADP-ATPgS)**	**-Log Student's T-test p-value PDAC2 (ADP-ATPgS)**	**Student's T-test Significant PDAC2 (ADP-ATPgS)**	**Student's T-test Significant PDAC2 (ADP-ATPgS) p-value only**	**Quantified at least 3 times in a group**	**Unique peptides**	**Intensity**
Absent in melanoma 1 protein	AIM1	-7.79	4.23	+	+	+	5	1.46E+09
T-complex protein 1 subunit eta	CCT7	-7.70	4.25	+	+	+	5	1.17E+09
Protein SET;Protein SETSIP	SET;SETSIP	-7.52	4.54	+	+	+	15	6.14E+08
Galectin-3;Galectin	LGALS3	-7.19	3.61	+	+	+	8	5.55E+09
Ribonucleoprotein PTB-binding 1	RAVER1	-6.66	8.06	+	+	+	8	4.12E+08
Ras-related protein Rab-39A;Ras-related protein Rab-6A;Ras-related protein Rab-6B	RAB39A;RAB6B;RAB6A	-6.34	2.99	+	+	+	20	5.86E+08
RNA-binding protein FUS	FUS	-6.10	5.33	+	+	+	7	3.99E+08
Leucine-rich repeat flightless-interacting protein 1	LRRFIP1	-5.93	3.28	+	+	+	2	9.76E+08
Pleckstrin homology domain-containing family G member 3	PLEKHG3	-5.84	3.29	+	+	+	6	1.15E+09

Prothymosin alpha;Prothymosin alpha, N-terminally processed;Thymosin alpha-1	PTMA	-5.43	3.46	+	+	+	15	8.04E+08
40S ribosomal protein S12	RPS12	-5.40	2.86	+	+	+	3	5.79E+08
60S ribosomal protein L5	RPL5	-5.29	3.80	+	+	+	5	1.92E+08
Calponin-3;Calponin	CNN3	-5.17	3.59	+	+	+	3	1.58E+08
CCR4-NOT transcription complex subunit 1	CNOT1	-5.11	3.27	+	+	+	10	5.34E+08
DNA polymerase;DNA polymerase delta catalytic subunit	POLD1	-4.95	4.68	+	+	+	8	1.61E+08
Coronin-1A;Coronin	CORO1A	-4.93	2.46	+	+	+	3	1.78E+08
Caspase-14;Caspase-14 subunit p17, mature form;Caspase-14 subunit p10, mature form;Caspase-14 subunit p20, intermediate form;Caspase-14 subunit p8, intermediate form	CASP14	-4.91	3.33	+	+	+	2	2.86E+08
Serine/arginine-rich splicing factor 3	SRSF3	-4.80	3.36	+	+	+	3	7.30E+07
DnaJ homolog subfamily A member 1	DNAJA1	-4.66	4.01	+	+	+	4	1.15E+08
Uncharacterized protein KIAA1211-like	KIAA1211L	-4.66	3.78	+	+	+	3	1.52E+08
Polyadenylate-binding protein 1;Polyadenylate-binding protein;Polyadenylate-binding protein 3	PABPC1;PABPC3	-4.63	3.39	+	+	+	6	1.66E+08
Cleavage and polyadenylation specificity factor subunit 5	NUDT21	-4.62	2.94	+	+	+	9	1.40E+08
Testin	TES	-4.52	3.32	+	+	+	4	1.67E+08
40S ribosomal protein S18	RPS18	-4.51	2.74	+	+	+	5	8.88E+07
mRNA export factor	RAE1	-4.42	4.57	+	+	+	6	1.39E+08

Probable cytosolic iron-sulfur protein assembly protein CIAO1	CIAO1	-4.26	2.24	+	+	+	2	9.44E+07
Polymerase delta-interacting protein 3	POLDIP3	-4.17	3.59	+	+	+	5	7.65E+07
Adenosylhomocysteinase	AHCY	-4.04	2.86	+	+	+	13	8.39E+08
60S ribosomal protein L37a	RPL37A	-4.01	4.43	+	+	+	20	1.55E+09
Oligophrenin-1	OPHN1	-3.95	2.82	+	+	+	2	9.36E+07
Histone-binding protein RBBP4	RBBP4	-3.68	3.91	+	+	+	3	8.62E+07
Transforming protein RhoA	RHOA	-3.62	1.90	+	+	+	2	1.04E+08
Microtubule-associated protein;Microtubule-associated protein 4	MAP4	-3.34	1.94	+	+	+	5	8.93E+07
Rho guanine nucleotide exchange factor 1	ARHGEF1	-3.34	3.84	+	+	+	3	5.34E+07
Ribosomal protein L15;60S ribosomal protein L15	RPL15	-3.34	3.52	+	+	+	5	1.01E+08
Calpain-1 catalytic subunit	CAPN1	-3.25	1.94	+	+	+	5	3.04E+08
Splicing factor, proline- and glutamine-rich	SFPQ	-3.17	3.54	+	+	+	3	4.36E+07
60 kDa heat shock protein, mitochondrial	HSPD1	-3.10	2.24	+	+	+	18	3.88E+09
14-3-3 protein gamma;14-3-3 protein gamma, N-terminally processed	YWHAG	-3.03	5.37	+	+	+	4	2.55E+07
Arginase-1	ARG1	-2.94	5.84	+	+	+	6	9.85E+07
SH3KBP1-binding protein 1	SHKBP1	-2.92	1.94	+	+	+	2	3.98E+07
Tensin-2	TNS2	-2.84	2.32	+	+	+	2	8.72E+07
60S acidic ribosomal protein P1	RPLP1	-2.40	2.58	+	+	+	3	3.69E+07
40S ribosomal protein S17	RPS17	-2.37	3.60	+	+	+	16	3.18E+09

Rho-related GTP-binding protein RhoG	RHOG	-2.30	3.19	+	+	+	1	3.41E+07
Actin-binding protein anillin	ANLN	-2.29	3.35	+	+	+	4	3.93E+07
Caldesmon	CALD1	-2.25	2.84	+	+	+	23	2.05E+10
14-3-3 protein eta	YWHAH	-2.08	2.22	+	+	+	6	1.46E+09
LIM domain and actin-binding protein 1	LIMA1	-2.07	2.59	+	+	+	14	1.58E+09
Involucrin	IVL	-1.91	3.12	+	+	+	3	1.81E+07
F-actin-capping protein subunit alpha-2	CAPZA2	-1.82	3.38	+	+	+	12	4.99E+09
Cleavage stimulation factor subunit 1	CSTF1	-1.80	2.97	+	+	+	12	2.17E+09
Protein phosphatase 1 regulatory subunit 12B	sm-M20;PPP1R12B	-1.74	3.22	+	+	+	24	6.71E+09
A-kinase anchor protein 2	AKAP2	-1.71	2.23	+	+	+	19	1.50E+09
ATP-dependent RNA helicase DDX3Y	DDX3Y	-1.71	2.66	+	+	+	3	5.10E+08
Tropomyosin alpha-4 chain	TPM4	-1.71	2.22	+	+	+	20	4.35E+10
Septin-10	SEPT10	-1.69	4.52	+	+	+	7	4.34E+08
Serine/threonine-protein phosphatase PP1-alpha catalytic subunit;Serine/threonine-protein phosphatase	PPP1CA	-1.68	2.58	+	+	+	2	2.74E+07
Tubulin beta chain	TUBB	-1.64	2.66	+	+	+	55	6.67E+09
Ras GTPase-activating-like protein IQGAP1	IQGAP1	-1.58	3.98	+	+	+	11	8.83E+09
Rho GDP-dissociation inhibitor 1	ARHGDIA	-1.51	2.44	+	+	+	11	3.13E+09
Actin-binding LIM protein 1	ABLIM1	-1.50	2.42	+	+	+	14	2.82E+09
Small nuclear ribonucleoprotein Sm D2	SNRPD2	-1.49	2.65	+	+	+	31	5.11E+09
Citron Rho-interacting kinase	CIT	-1.41	2.25	+	+	+	12	8.05E+08

F-actin-capping protein subunit alpha-1	CAPZA1	-1.41	2.21	+	+	+	12	1.30E+10
60S ribosomal protein L31	RPL31	-1.33	3.39	+	+	+	3	1.79E+08
Phosphoserine aminotransferase	PSAT1	-1.21	2.58	+	+	+	3	5.82E+08
EH domain-binding protein 1	EHBP1	-1.04	2.12	+	+	+	7	2.88E+08
Unconventional myosin-VI	MYO6	-0.98	2.47	+	+	+	8	3.16E+08
Eukaryotic translation initiation factor 6	EIF6	-0.93	2.26	+	+	+	36	2.00E+10
60S ribosomal protein L4	RPL4	-0.86	2.21	+	+	+	6	4.06E+08
Septin-8	SEPT8	-0.84	2.26	+	+	+	6	6.48E+08
Tubulin alpha-1C chain	TUBA1C	0.74	2.47	+	+	+	173	9.97E+11
Fascin	FSCN1	0.77	2.24	+	+	+	44	1.35E+11
Protein-glutamine gamma-glutamyltransferase E;Protein-glutamine gamma-glutamyltransferase E 50 kDa catalytic chain;Protein-glutamine gamma-glutamyltransferase E 27 kDa non-catalytic chain	TGM3	1.17	2.99	+	+	+	127	3.83E+11
Dihydropyrimidinase-related protein 3	DPYSL3	1.58	2.53	+	+	+	33	2.71E+10
Protein FAM107B	FAM107B	2.79	2.57	+	+	+	5	1.13E+08
Nucleophosmin	NPM1	5.04	3.40	+	+	+	3	2.12E+08
General transcription factor II-I	GTF2I	-1.67	2.77	+		+	3	9.59E+07
Actin, cytoplasmic 2 (Fragment)	ACTG1	-4.54	1.38		+	+	6	3.18E+08
Beta-2-microglobulin;Beta-2-microglobulin form pI 5.3	B2M	-4.36	1.43		+	+	3	3.21E+08
ATP-citrate synthase	ACLY	-4.34	1.33		+	+	31	3.11E+09
Sorting nexin-5	SNX5	-4.23	1.62		+	+	7	2.99E+08

Eukaryotic translation initiation factor 3 subunit B	EIF3B	-3.91	1.49		+	+	2	1.47E+08
Serine/threonine-protein phosphatase;Serine/threonine-protein phosphatase PP1-gamma catalytic subunit	PPP1CC	-3.74	1.36		+	+	6	1.84E+08
Pyruvate kinase PKM;Pyruvate kinase	PKM	-3.68	1.32		+	+	7	2.05E+08
Early endosome antigen 1	EEA1	-3.48	1.49		+	+	2	2.91E+08
Ras-related protein Rab-8B	RAB8B	-3.38	1.44		+	+	4	1.07E+08
Eukaryotic translation initiation factor 4B	EIF4B	-3.20	1.31		+	+	4	9.96E+07
Vacuolar protein sorting-associated protein 45	VPS45	-3.16	1.31		+	+	5	3.51E+08
40S ribosomal protein S2	RPS2	-2.90	1.66		+	+	1	2.35E+08
Rho GTPase-activating protein 15	ARHGAP15	-2.32	1.87		+	+	3	2.24E+07
Eukaryotic translation initiation factor 3 subunit F	EIF3F	-2.28	1.32		+	+	4	7.38E+07
Activated RNA polymerase II transcriptional coactivator p15	SUB1	-2.15	1.68		+	+	9	1.30E+09
Annexin A1;Annexin	ANXA1	-2.13	1.76		+	+	13	9.28E+08
Serine/threonine-protein kinase N2	PKN2	-2.08	1.85		+	+	18	2.95E+08
Poly(rC)-binding protein 1	PCBP1	-2.03	1.86		+	+	13	5.65E+08
Serine/threonine-protein phosphatase PP1-beta catalytic subunit;Serine/threonine-protein phosphatase	PPP1CB	-1.81	1.34		+	+	21	1.06E+09
CAD protein;Glutamine-dependent carbamoyl-phosphate synthase;Aspartate carbamoyltransferase;Dihydroorotase	CAD	-1.54	1.88		+	+	8	2.75E+09

Serine-threonine kinase receptor-associated protein	STRAP	-1.31	1.52		+	+	10	2.67E+09
Histone H4	HIST1H4A	-1.24	1.35		+	+	6	4.19E+08
Transcription elongation factor B polypeptide 1	TCEB1	-1.17	1.78		+	+	10	4.00E+08
MARCKS-related protein	MARCKSL1	-1.10	1.62		+	+	3	3.00E+08
40S ribosomal protein S15a	RPS15A	-1.03	1.82		+	+	6	8.24E+09
Tyrosine-protein kinase ABL1	ABL1	-1.00	1.81		+	+	15	6.08E+08
Coronin-1C;Coronin	CORO1C	-0.99	1.62		+	+	17	5.70E+09
CD2-associated protein	CD2AP	-0.97	1.86		+	+	16	9.74E+08
Myosin-9	MYH9	-0.88	1.64		+	+	7	3.53E+08
Epidermal growth factor receptor kinase substrate 8	EPS8	-0.86	2.11		+	+	43	1.65E+10
Nucleosome assembly protein 1-like 1	NAP1L1	-0.83	1.97		+	+	10	7.43E+08
60S ribosomal protein L22	RPL22	-0.82	1.39		+	+	9	1.58E+09
Protein RCC2	RCC2	-0.76	2.00		+	+	4	5.14E+08
60S ribosomal protein L9	RPL9	-0.74	2.04		+	+	5	2.46E+08
Vacuolar protein sorting-associated protein 26B	VPS26B	-0.73	1.95		+	+	8	1.89E+08
Myosin light chain kinase, smooth muscle;Myosin light chain kinase, smooth muscle, deglutamylated form	MYLK	-0.72	1.36		+	+	11	1.21E+09
WD repeat-containing protein 1	WDR1	-0.71	1.84		+	+	15	7.75E+08
Cystatin-A;Cystatin-A, N-terminally processed	CSTA	-0.70	1.32		+	+	1	3.40E+08
U1 small nuclear ribonucleoprotein C	SNRPC	-0.58	1.67		+	+	8	2.92E+08
THO complex subunit 4	ALYREF	-0.57	2.29		+	+	16	7.18E+08

Rho guanine nucleotide exchange factor 7;Rho guanine nucleotide exchange factor 6	ARHGEF7;ARHGEF6	-0.50	1.64		+	+	6	2.24E+08
Protein S100-A8;Protein S100-A8, N-terminally processed	S100A8	-0.47	1.40		+	+	4	1.24E+08
40S ribosomal protein S5;40S ribosomal protein S5, N-terminally processed	RPS5	-0.36	1.36		+	+	17	1.81E+09
Filamin-A	FLNA	0.43	1.49		+	+	5	3.59E+09
AP-3 complex subunit sigma-1	AP3S1	0.49	1.46		+	+	10	2.53E+09
Desmocollin-1	DSC1	0.50	1.44		+	+	4	3.81E+08
Nuclease-sensitive element-binding protein 1	YBX1	0.56	1.76		+	+	2	1.10E+10
ADP-ribosylation factor GTPase-activating protein 3	ARFGAP3	0.65	1.35		+	+	6	5.92E+08
Eukaryotic initiation factor 4A-I	EIF4A1	1.95	1.62		+	+	35	2.98E+09

Table 10-4 Mass spectrometry data – all significant hits from "JVM3 – Jasplakinolide"

JVM3 - Jasplakinolide

Protein names	Gene names	Student's T-test Difference JVM3-ADP_JVM3-Jas	-Log Student's T-test p-value JVM3-ADP_JVM3-Jas	Student's T-test Significant JVM3-ADP_JVM3-Jas	Student's T-test Significant JVM3-ADP_JVM3-Jas p-value only	Quant 3 times in JVM3	Unique peptides	Intensity
Ig kappa chain V-I region HK102	IGKV1-5	-8.36	5.06	+	+	+	4	30.93
Macrophage migration inhibitory factor	MIF	-5.87	4.03	+	+	+	2	30.70
Acidic leucine-rich nuclear phosphoprotein 32 family member A	ANP32A	-4.47	2.66	+	+	+	6	27.77
40S ribosomal protein S25	RPS25	-3.42	2.58	+	+	+	4	26.48
Protein LSM12 homolog	LSM12	-3.41	2.08	+	+	+	5	29.12
Embryonic stem cell-specific 5-hydroxymethylcytosine-binding protein	HMCES	-3.25	4.00	+	+	+	12	27.35
Mitochondrial fission 1 protein	FIS1	-3.24	3.72	+	+	+	4	26.27
DENN domain-containing protein 1A	DENND1A	-3.13	2.34	+	+	+	7	25.84
General transcription factor IIF subunit 1	GTF2F1	-3.13	2.59	+	+	+	8	26.28
Gamma-adducin	ADD3	-3.12	1.32	+	+	+	14	27.88
Ig kappa chain C region	IGKC	-2.84	3.20	+	+	+	7	30.58
Neutrophil cytosol factor 2	NCF2	-2.64	2.78	+	+	+	11	27.48
Pre-mRNA-splicing factor RBM22	RBM22	-2.60	2.65	+	+	+	7	24.83
Cysteine and glycine-rich protein 1	CSRP1	-2.44	4.28	+	+	+	9	31.24

Rho guanine nucleotide exchange factor 7	ARHGEF7	-2.31	2.65	+	+	+	12	27.40
Activated RNA polymerase II transcriptional coactivator p15	SUB1	-2.28	1.66	+	+	+	16	34.53
CUGBP Elav-like family member 2	CELF2	-2.23	2.56	+	+	+	5	24.62
Zinc finger CCCH-type antiviral protein 1-like	ZC3HAV1L	-2.22	1.74	+	+	+	4	25.71
Nuclease-sensitive element-binding protein 1	YBX1	-2.20	2.06	+	+	+	7	28.02
S-adenosylmethionine synthase isoform type-2	MAT2A	-2.20	2.10	+	+	+	6	29.45
Eukaryotic translation initiation factor 3 subunit H	EIF3H	-2.19	3.36	+	+	+	4	25.99
Ubiquilin-1	UBQLN1	-2.19	1.41	+	+	+	7	27.65
Interferon regulatory factor 2-binding protein 2	IRF2BP2	-2.15	1.88	+	+	+	9	28.12
RNA-binding protein FUS	FUS	-2.10	3.00	+	+	+	12	31.41
Cdc42 effector protein 4	CDC42EP4	-2.07	2.34	+	+	+	7	26.53
Protein FAM195B	FAM195B	-1.98	3.15	+	+	+	6	28.57
Vimentin	VIM	-1.96	3.00	+	+	+	16	28.85
Zinc finger Ran-binding domain-containing protein 2	ZRANB2	-1.96	2.05	+	+	+	4	24.95
Actin, cytoplasmic 2;Actin, cytoplasmic 2, N-terminally processed	ACTG1	-1.92	1.68	+	+	+	2	35.79
Probable cytosolic iron-sulfur protein assembly protein CIAO1	CIAO1	-1.88	1.63	+	+	+	4	26.55
Eukaryotic translation initiation factor 3 subunit I	EIF3I	-1.85	1.72	+	+	+	9	27.60

Brain-specific angiogenesis inhibitor 1-associated protein 2-like protein 1	BAIAP2L1	-1.82	2.23	+	+	+	18	30.16
Ubiquitin-like protein 4A	UBL4A	-1.80	2.53	+	+	+	6	26.07
Actin, cytoplasmic 1;Actin, cytoplasmic 1, N-terminally processed	ACTB	-1.79	3.03	+	+	+	2	35.52
26S proteasome non-ATPase regulatory subunit 6	PSMD6	-1.77	1.83	+	+	+	15	28.44
Protein RCC2	RCC2	-1.66	1.54	+	+	+	15	29.35
Formin-binding protein 1	FNBP1	-1.66	1.87	+	+	+	6	26.39
Survival of motor neuron-related-splicing factor 30	SMNDC1	-1.66	1.92	+	+	+	2	23.99
Protein LSM14 homolog A	LSM14A	-1.66	1.94	+	+	+	9	28.63
Leucine-rich repeat flightless-interacting protein 1	LRRFIP1	-1.63	2.03	+	+	+	8	25.47
Phosphatidylinositol 3,4,5-trisphosphate 5-phosphatase 2	INPPL1	-1.59	2.15	+	+	+	19	28.12
Caspase-4;Caspase-4 subunit 1;Caspase-4 subunit 2	CASP4	-1.56	2.46	+	+	+	15	29.29
Charged multivesicular body protein 1a	CHMP1A	-1.56	1.69	+	+	+	3	24.41
Arf-GAP with coiled-coil, ANK repeat and PH domain-containing protein 1	ACAP1	-1.53	1.47	+	+	+	4	25.53
Suppressor of G2 allele of SKP1 homolog	SUGT1	-1.53	2.03	+	+	+	6	26.12
Shootin-1	KIAA1598	-1.52	2.62	+	+	+	7	24.58
Protein FAM107B	FAM107B	-1.52	1.91	+	+	+	2	32.90
Calpain-1 catalytic subunit	CAPN1	-1.51	3.39	+	+	+	23	29.25
Ras-related protein Rab-7a	RAB7A	-1.49	2.07	+	+	+	14	29.49
Ras-related protein Rab-5C	RAB5C	-1.41	1.96	+	+	+	5	26.03

Tumor protein D54	TPD52L2	-1.39	2.59	+	+	+	4	30.64
Transmembrane protein 263	TMEM263	-1.39	2.12	+	+	+	6	29.89
Serine/threonine-protein kinase 10	STK10	-1.37	1.73	+	+	+	13	28.00
Suprabasin	SBSN	-1.37	1.82	+	+	+	6	27.78
Ras-related protein Rap-1A	RAP1A	-1.36	1.61	+	+	+	2	25.29
Tumor protein D52	TPD52	-1.34	2.69	+	+	+	18	33.14
Tyrosine-protein phosphatase non-receptor type 6	PTPN6	-1.33	1.85	+	+	+	11	25.66
Ras-related protein Rab-8B	RAB8B	-1.33	1.52	+	+	+	5	30.20
F-actin-capping protein subunit alpha-1	CAPZA1	-1.31	3.13	+	+	+	16	33.82
Splicing factor 1	SF1	-1.28	1.57	+	+	+	9	27.64
Heat shock protein beta-1	HSPB1	-1.26	2.42	+	+	+	10	30.02
F-actin-capping protein subunit beta	CAPZB	-1.25	1.82	+	+	+	6	30.94
Ataxin-2-like protein	ATXN2L	-1.24	2.50	+	+	+	35	32.24
Protein SEC13 homolog	SEC13	-1.22	2.58	+	+	+	13	31.62
Phosphatase and actin regulator 2	PHACTR2	-1.21	1.55	+	+	+	4	24.58
Ras-related protein Rab-8A	RAB8A	-1.20	2.54	+	+	+	6	32.53
Spartin	SPG20	-1.20	3.18	+	+	+	20	31.26
Exosome complex component MTR3	EXOSC6	-1.19	1.70	+	+	+	4	25.57
Tubulin beta-8 chain	TUBB8	-1.19	2.27	+	+	+	2	30.01
Rho GTPase-activating protein 17	ARHGAP17	-1.16	1.98	+	+	+	32	30.86
Eukaryotic translation initiation factor 6	EIF6	-1.14	2.23	+	+	+	6	26.84
Endophilin-A2	SH3GL1	-1.14	1.82	+	+	+	20	29.77

Tubulin beta-4B chain;Tubulin beta-4A chain	TUBB4B;TUBB4A	-1.13	1.71	+	+	+	4	31.73
Lymphocyte cytosolic protein 2	LCP2	-1.13	2.57	+	+	+	12	29.11
Myosin light chain 6B	MYL6B	-1.11	2.56	+	+	+	6	28.04
Protein phosphatase Slingshot homolog 1	SSH1	-1.10	2.42	+	+	+	8	25.43
Neutrophil cytosol factor 1;Putative neutrophil cytosol factor 1B;Putative neutrophil cytosol factor 1C	NCF1;NCF1B;NCF1C	-1.10	2.24	+	+	+	5	29.12
Signal recognition particle 14 kDa protein	SRP14	-1.08	2.68	+	+	+	2	26.99
Vasodilator-stimulated phosphoprotein	VASP	-1.08	1.89	+	+	+	28	35.42
Wiskott-Aldrich syndrome protein	WAS	-1.07	1.74	+	+	+	23	34.03
F-actin-capping protein subunit alpha-2	CAPZA2	-1.07	1.87	+	+	+	13	31.35
ATP-dependent RNA helicase DDX1	DDX1	-1.05	1.67	+	+	+	13	27.24
Tubulin beta chain	TUBB	-1.04	1.82	+	+	+	6	32.78
Arf-GAP with Rho-GAP domain, ANK repeat and PH domain-containing protein 1	ARAP1	-1.02	2.42	+	+	+	35	30.67
RNA-binding protein EWS	EWSR1	-1.02	2.03	+	+	+	8	30.93
60S ribosomal protein L18a	RPL18A	-1.01	2.40	+	+	+	3	26.48
Guanine nucleotide-binding protein subunit beta-2-like 1;Guanine nucleotide-binding protein subunit beta-2-like 1, N-terminally processed	GNB2L1	-0.99	1.50	+	+	+	17	31.38

ADP-ribosylation factor 1;ADP-ribosylation factor 3	ARF1;ARF3	-0.98	2.21	+	+	+	7	31.28
Peroxisomal multifunctional enzyme type 2;(3R)-hydroxyacyl-CoA dehydrogenase;Enoyl-CoA hydratase 2	HSD17B4	-0.97	1.50	+	+	+	11	27.29
PRKC apoptosis WT1 regulator protein	PAWR	-0.96	1.50	+	+	+	14	30.47
Probable ATP-dependent RNA helicase DDX6	DDX6	-0.95	2.06	+	+	+	26	32.39
Prothymosin alpha;Prothymosin alpha, N-terminally processed;Thymosin alpha-1	PTMA	-0.95	1.46	+	+	+	7	30.25
Coatomer subunit delta	ARCN1	-0.91	1.64	+	+	+	8	27.53
Ribonucleoprotein PTB-binding 1	RAVER1	-0.90	1.63	+	+	+	9	27.62
Interferon-stimulated gene 20 kDa protein	ISG20	-0.89	1.54	+	+	+	4	24.22
40S ribosomal protein S19	RPS19	-0.88	2.20	+	+	+	7	29.56
Protein transport protein Sec23B	SEC23B	-0.88	1.58	+	+	+	11	27.47
Voltage-gated potassium channel subunit beta-2	KCNAB2	-0.87	2.06	+	+	+	18	30.99
Coronin-1A	CORO1A	-0.87	2.34	+	+	+	20	31.44
Fascin	FSCN1	-0.87	3.37	+	+	+	65	39.25
Clathrin interactor 1	CLINT1	-0.84	2.56	+	+	+	12	29.68
Phosphatidylinositol 3,4,5-trisphosphate 5-phosphatase 1	INPP5D	-0.83	1.85	+	+	+	60	32.80
TBC1 domain family member 5	TBC1D5	-0.82	1.69	+	+	+	25	30.54
Nck-associated protein 1-like	NCKAP1L	-0.81	1.71	+	+	+	4	25.93
Calmodulin-3	CALM3	-0.78	1.74	+	+	+	16	35.00

DnaJ homolog subfamily A member 2	DNAJA2	-0.72	2.60	+	+	+	12	29.60
B-cell linker protein	BLNK	-0.71	1.75	+	+	+	16	30.77
AP-2 complex subunit beta	AP2B1	-0.70	2.48	+	+	+	11	28.57
U6 snRNA-associated Sm-like protein LSm5	LSM5	-0.68	2.47	+	+	+	1	28.54
Neuroblast differentiation-associated protein AHNAK	AHNAK	-0.64	2.03	+	+	+	406	38.61
Elongation factor 1-alpha 1;Putative elongation factor 1-alpha-like 3	EEF1A1;EEF1A1P5	-0.60	1.96	+	+	+	26	34.73
Ras-related C3 botulinum toxin substrate 1;Ras-related C3 botulinum toxin substrate 3	RAC1;RAC3	-0.59	2.77	+	+	+	5	33.08
40S ribosomal protein S12	RPS12	-0.33	3.20	+	+	+	7	30.38
Vacuolar protein sorting-associated protein VTA1 homolog	VTA1	0.69	2.42	+	+	+	9	30.99
Thioredoxin-like protein 1	TXNL1	0.91	1.87	+	+	+	9	29.11
Protein disulfide-isomerase A6	PDIA6	0.93	1.69	+	+	+	10	29.81
Transgelin-2	TAGLN2	0.95	1.64	+	+	+	14	32.46
Ras-related C3 botulinum toxin substrate 2	RAC2	0.97	1.91	+	+	+	5	33.05
60S ribosomal protein L11	RPL11	0.97	1.50	+	+	+	2	27.98
Prefoldin subunit 2	PFDN2	1.21	1.81	+	+	+	5	30.13
Prefoldin subunit 1	PFDN1	1.36	1.89	+	+	+	4	28.74
Alpha-actinin-4	ACTN4	1.44	1.78	+	+	+	47	34.73
60S ribosomal protein L23a	RPL23A	1.45	2.91	+	+	+	4	28.38
Prefoldin subunit 5	PFDN5	1.53	3.00	+	+	+	7	29.14
40S ribosomal protein S17	RPS17	1.84	1.60	+	+	+	3	27.16

BolA-like protein 2	BOLA2	1.85	2.94	+	+	+	4	27.54
Ras GTPase-activating-like protein IQGAP1	IQGAP1	2.05	1.70	+	+	+	45	31.18
Trafficking protein particle complex subunit 12	TRAPPC12	2.10	1.93	+	+	+	5	27.69
26S protease regulatory subunit 4	PSMC1	2.43	2.65	+	+	+	9	28.13
Thymosin beta-4;Hematopoietic system regulatory peptide	TMSB4X	2.51	3.49	+	+	+	5	28.77
60S ribosomal protein L14	RPL14	2.53	2.75	+	+	+	3	28.65
40S ribosomal protein S2	RPS2	2.55	1.41	+	+	+	7	28.45
Coatomer subunit epsilon	COPE	2.61	2.56	+	+	+	5	27.89
Rho GTPase-activating protein 9	ARHGAP9	3.06	2.87	+	+	+	18	31.04
Putative heat shock protein HSP 90-beta 2	HSP90AB2P	3.29	2.76	+	+	+	1	28.74
LIM and SH3 domain protein 1	LASP1	-3.62	1.25	+		+	13	29.86
General transcription factor IIF subunit 2	GTF2F2	-2.17	1.25	+		+	6	26.22
U6 snRNA-associated Sm-like protein LSm1	LSM1	-1.23	1.32		+	+	4	28.78
Ubiquitin carboxyl-terminal hydrolase 14	USP14	-0.93	1.35		+	+	4	25.99
DnaJ homolog subfamily A member 1	DNAJA1	-0.90	1.34		+	+	8	29.17
SAM and SH3 domain-containing protein 3	SASH3	-0.88	1.34		+	+	10	29.09
Proteasome subunit beta type-3	PSMB3	-0.78	1.32		+	+	6	27.41
Cellular nucleic acid-binding protein	CNBP	-0.71	1.61		+	+	5	28.23
CapZ-interacting protein	RCSD1	-0.70	1.31		+	+	15	31.02
40S ribosomal protein SA	RPSA	-0.70	1.40		+	+	11	30.82

Nascent polypeptide-associated complex subunit alpha;Nascent polypeptide-associated complex subunit alpha, muscle-specific form	NACA	-0.66	1.42		+	+	4	29.17
Lymphocyte-specific protein 1	LSP1	-0.64	1.43		+	+	27	34.94
Phosphatase and actin regulator 4	PHACTR4	-0.63	1.45		+	+	8	27.63
Heterogeneous nuclear ribonucleoprotein D0	HNRNPD	-0.56	1.69		+	+	5	27.80
Cell division control protein 42 homolog	CDC42	-0.52	1.40		+	+	2	30.24
UPF0568 protein C14orf166	C14orf166	-0.51	1.48		+	+	8	28.08
Pro-interleukin-16;Interleukin-16	IL16	-0.50	1.78		+	+	15	29.23

Table 10-5 Mass spectrometry data – all significant hits from"PDAC – Jasplakinolide"

PDAC - Jasplakinolide								
Protein names	**Gene names**	**Student's T-test Difference PDAC-ADP_PDAC-Jas**	**-Log Student's T-test p-value PDAC-ADP_PDAC-Jas**	**Student's T-test Significant PDAC-ADP_PDAC-Jas**	**Student's T-test Significant PDAC-ADP_PDAC-Jas p-value only**	**Quant 3 times in PDAC**	**Unique peptides**	**Intensity**
SH2 domain-containing protein 3C	SH2D3C	-4.71	2.91	+	+	+	2	29.25
LIM and SH3 domain protein 1	LASP1	-3.82	1.67	+	+	+	13	29.86
RNA-binding protein FUS	FUS	-3.31	2.36	+	+	+	12	31.41

Septin-7	SEPT7	-3.27	2.55	+	+	+	18	31.86
Striatin-3	STRN3	-2.99	2.05	+	+	+	6	27.40
C-1-tetrahydrofolate synthase, cytoplasmic;Methylenetetrahydrofolate dehydrogenase;Methenyltetrahydrofolate cyclohydrolase;Formyltetrahydrofolate synthetase;C-1-tetrahydrofolate synthase, cytoplasmic, N-terminally processed	MTHFD1	-2.94	2.65	+	+	+	37	32.01
Unconventional myosin-Ie	MYO1E	-2.80	1.74	+	+	+	10	27.72
Abelson tyrosine-protein kinase 2	ABL2	-2.75	2.33	+	+	+	7	27.90
WAS/WASL-interacting protein family member 1	WIPF1	-2.48	2.18	+	+	+	23	33.60
Twinfilin-1	TWF1	-2.28	1.63	+	+	+	9	29.11
AP-2 complex subunit beta	AP2B1	-1.96	2.50	+	+	+	11	28.57
Rho GTPase-activating protein 5	ARHGAP5	-1.93	2.59	+	+	+	31	29.38
Rho guanine nucleotide exchange factor 1	ARHGEF1	-1.88	2.39	+	+	+	37	32.09
Protein phosphatase 1 regulatory subunit 12A	PPP1R12A	-1.87	1.93	+	+	+	45	32.97
Cysteine and glycine-rich protein 1	CSRP1	-1.86	1.88	+	+	+	9	31.24
40S ribosomal protein S10;Putative 40S ribosomal protein S10-like	RPS10;RPS10P5	-1.81	1.82	+	+	+	5	29.91
Pleckstrin homology domain-containing family G member 3	PLEKHG3	-1.70	2.34	+	+	+	7	27.52
Ataxin-2-like protein	ATXN2L	-1.70	1.93	+	+	+	35	32.24
Arf-GAP with SH3 domain, ANK repeat and PH domain-containing protein 1	ASAP1	-1.67	2.63	+	+	+	9	26.91
Probable ATP-dependent RNA helicase DDX6	DDX6	-1.66	2.32	+	+	+	26	32.39
Insulin receptor substrate 2	IRS2	-1.63	2.46	+	+	+	7	27.37

Polyadenylate-binding protein 1	PABPC1	-1.22	1.86	+	+	+	16	31.33
Septin-9	SEPT9	-1.20	1.85	+	+	+	28	31.49
PDZ and LIM domain protein 5	PDLIM5	-1.12	2.49	+	+	+	25	31.91
Fascin	FSCN1	-1.03	2.33	+	+	+	65	39.25
Vacuolar protein sorting-associated protein 26B	VPS26B	1.36	1.90	+	+	+	3	26.44
Dynamin-1	DNM1	-3.01	1.35		+	+	13	28.00
ADP-ribosylation factor GTPase-activating protein 2	ARFGAP2	-2.65	1.43		+	+	22	32.48
Breakpoint cluster region protein	BCR	-2.54	1.46		+	+	17	27.79
Rho GTPase-activating protein 17	ARHGAP17	-2.50	1.30		+	+	32	30.86
Twinfilin-2	TWF2	-2.26	1.50		+	+	13	30.02
Src substrate cortactin	CTTN	-2.07	1.33		+	+	17	30.78
Sorbin and SH3 domain-containing protein 2	SORBS2	-1.74	1.39		+	+	9	27.02
Casein kinase II subunit beta	CSNK2B	-1.60	1.57		+	+	5	26.78
Tensin-2	TNS2	-1.58	1.68		+	+	13	27.99
Calcium/calmodulin-dependent protein kinase type II subunit delta	CAMK2D	-1.54	1.38		+	+	15	30.32
Rho guanine nucleotide exchange factor 7	ARHGEF7	-1.52	1.42		+	+	12	27.40
Protein LSM12 homolog	LSM12	-1.51	1.47		+	+	5	29.12
Epidermal growth factor receptor kinase substrate 8-like protein 2	EPS8L2	-1.47	1.73		+	+	5	26.39
Ankycorbin	RAI14	-1.40	1.58		+	+	10	27.68
Adenylyl cyclase-associated protein 1	CAP1	-1.39	1.36		+	+	24	31.11
Rho GTPase-activating protein 35	ARHGAP35	-1.33	1.71		+	+	36	30.72
Arf-GAP with Rho-GAP domain, ANK repeat and PH domain-containing protein 1	ARAP1	-1.33	1.59		+	+	35	30.67

ADP-ribosylation factor 5	ARF5	-1.17	1.36		+	+	5	27.25
Unconventional myosin-XVIIIa	MYO18A	-1.10	1.64		+	+	64	33.24
Actin-related protein 2/3 complex subunit 2	ARPC2	-1.04	1.31		+	+	27	34.09
F-actin-capping protein subunit alpha-2	CAPZA2	-1.04	1.88		+	+	13	31.35
Brain-specific angiogenesis inhibitor 1-associated protein 2	BAIAP2	-0.92	1.91		+	+	15	28.66
CD2-associated protein	CD2AP	-0.91	1.35		+	+	42	33.81
ADP-ribosylation factor 1;ADP-ribosylation factor 3	ARF1;ARF3	-0.88	1.61		+	+	7	31.28
Actin-related protein 2	ACTR2	-0.85	1.66		+	+	19	33.79
Protein enabled homolog	ENAH	-0.80	2.11		+	+	9	27.86
FH1/FH2 domain-containing protein 1	FHOD1	-0.74	1.31		+	+	50	33.19
Actin-related protein 2/3 complex subunit 1B	ARPC1B	-0.74	1.64		+	+	22	34.04
Actin-related protein 2/3 complex subunit 4	ARPC4	-0.66	1.34		+	+	11	33.51
Transcription elongation factor B polypeptide 1	TCEB1	-0.63	1.37		+	+	6	28.45

Table 10-6 Copyright permissions

Journal	Article	Cited as	Figure in the article	Figure in this thesis	Modification made	Copyright permission
Nature Structural Molecular Biology	Structural transitions of F-actin upon ATP hydrolysis at near-atomic resolution revealed by cryo-EM	Merino et al., 2018	Figure 6a	Figure 8-1	Half of panel 6a was used	Creative commons Attribution license CC BY 4.0 – free to adapt and reuse* https://creativecommons.org/licenses/by/4.0/
BioRxiv	The Scar/WAVE complex drives normal actin protrusions without the Arp2/3 complex, but proline-rich domains are required	Buracco et al., 2022	Figure 1&5	Figure 8-2,Figure 8-3 and Figure 8-4	Figure 1A,F&G used; Figure 5E&G used	Creative commons Attribution license CC BY 4.0 – free to adapt and reuse* https://creativecommons.org/licenses/by/4.0/

*This is an open access article distributed under the terms of the Creative Commons CC-BY 4.0 license, which permits unrestricted use, distribution, and reproduction in any medium, provided the original work is properly cited. It is not required to obtain permission to reuse this article. https://creativecommons.org/licenses/by/4.0/